DOE/JPL-954344-78/1
DISTRIBUTION CATEGORY UC-63B

WEB-DENDRITIC GROWTH

R. B. Hilborn, Jr., Program Manager, 803-777-4195
University of South Carolina
College of Engineering
Columbia, S. C. 29208

Final Report

October 1975 - August 1977

Prepared by:

R. B. Hilborn, Jr., J. W. Faust, Jr., Curtis Rhodes

Under JPL Contract Number: 954344
(Subcontract under NASA Contract NAS7-100)

This work was performed for the Jet Propulsion Laboratory, California Institute of Technology, under NASA Contract NAS7-100 for the U. S. Department of Energy (DOE), Division of Solar Energy.

The JPL Low-Cost Silicon Array Project is funded by DOE and forms part of the Solar Photovoltaic Conversion Program to initiate a major effort toward the development of low-cost solar arrays.

NEW TECHNOLOGY

No reportable items of new technology have been identified.

ACKNOWLEDGEMENT

Appreciation is expressed for the assistance of the following personnel on this project:

D. Jolley
Y. Tung
G. Summer
G. Keisler
J. Peeples
D. Paradis
J. Lin
C. Chandler
M. Guerrein
M. Harrill

ABSTRACT

This final report gives the results of work performed by the University of South Carolina to develop methods of producing large areas of silicon ribbon by the web-dendritic method. A prototype web-dendritic growth machine, on hand at the beginning of the contract, was assembled and activated. A program for investigating the role of the various machine design parameters on the growth of web-dendritic ribbon was carried out during the duration of the contract. The development of the machine proceeded to the point where ribbons could be reproducibly grown up to lengths of 1 meter, with widths increasing linearly from a minimum, at the initiating seed button, up to 1 cm. at the point of termination of growth.

Considerable thermal data was collected and evaluations were made of actual seeding and growth for variations in a large number of parameters affecting heat loss. From this we found for achieving suitable growth that the mechanical system should be very rigid and stable, and the tolerances and specifications of the quartz crucibles must be far tighter than normal quartz tolerances. The widening rates of the ribbons were found to be a function of the temperature gradient rather than the temperature differences alone. A twin spacing in the seed of 3μ - 2μ was found to be unfavorable for growth; whereas spacing of .9μ - 2μ and 8μ - 2μ were favorable. It was found, however, that the spacing of 8μ - 2μ sets an upper limit of 4 cm/min on the maximum achievable rate.

Extensive thermal modeling studies were carried out to investigate the effect of furnace design parameters on the temperature distributions in melt and the growth of the dendritic-web ribbon. From this study it was found that the pull rate of the ribbon is strongly dependent on the temperature of the top thermal shield, the spacing between this shield and the melt, and the thickness of the growing web.

FINAL REPORT - TABLE OF CONTENTS

FINAL REPORT - TABLE OF CONTENTS (Cont'd)

LIST OF FIGURES

LIST OF FIGURES (cont'd)

LIST OF FIGURES (Cont'd)

LIST OF FIGURES (Cont'd)

LIST OF TABLES

LIST OF TABLES (Cont'd).

ALPHABITICAL LIST OF ABBREVIATIONS

Abbreviation	Meaning	Figure Number
AH	after heaters	32,47
BH	bottom heat shield	42
BT	bow tie	44., C-5
CP	coil position - from top of heat shield to top of coil	33
DB	dog bone	8
DBe	dumb bell	43
LDBe	long dumb bell	35
LDBeW	long wide dumb bell	35
LDBeWM1	modification 1 of Fig. 17	35
LDBeWM2	modification 2 of Fig. 17	36
LDBeXW	long extra wide dumb bell	35
LSDBN	long straight narrow dog bone	C-7
MSS	medium straight slot	C-4
NBT	narrow bow tie	C-9
NSS	narrow straight slot	25
OM	optical microscopy	
REM	replica electron microscopy	
S	distance between surface of melt and heat shield	33
SDB	straight side dog bone	29
SDBN	straight narrow dog bone	C-7
SEM	scanning electron microscopy	
SS	straight side susceptor	12
SSDB	short straight dog-bone	C-3
SS	straight slot	7
TC	thermocouple	
TDB	tapered dog bone	3
TG	temperature gradient	
TS	taper sided susceptor	11
TSP	taper susceptor with ports	17
TSPO	taper susceptor with oval ports	17
WSS	wide straight slot	24

1. SUMMARY

A. Web Growth - the primary objectives of this project were:

(1) Reactivate and modify an existing web-dendrite machine to pull web and provide a capability of varying process control parameters.

(2) Pull as a minimum, web based on experience of 1965.

(3) Operate the web-dendrite machine to support the thermal modeling studies and obtain a better understanding of the web-dendritic growth process and its limitations.

(4) Characterize the web grown.

(5) Investigate mechanical stability.

(6) Investigate and define thermal stability.

Approach Objective (1) was met by calling on past experience and on experience gained as we set up and used the equipment, and trained the operators.

Objective (2) and (3) were met by (a) studying and correcting mechanical problems that caused damaging vibrations or sudden jarring, (b) studying the horizontal and vertical thermal gradients and optimizing conditions to give suitable isotherms for web growth, (c) perfecting the seeding technique and methods of making changes in temperature and pull speed to sustain growth, and (d) varying the r.f. heat transfer by changing the shape of the susceptor and the number, thickness and opening in the top heat shields, and the use of after heaters. We also examined the heat loss down the pedestal.

Objective (4) was met by evaluating the following parameters: (a) thickness, (b) width, (c) length, (d) surface finish, (e) twin spacings, (f) resistivity, and (g) perfection.

Objective (5) was met by visual observations while a number of parameters were varied one at a time and by measurement of the mechanical vibration spectra during the initial phases.

Finally,Objective (6) was met by making very precise (1/4°) thermocouple measurements throughout the melt while varying a number of parameters.

B. Thermal Modeling of Web growth

The primary objectives of this part of the project were:

(1) To develop a mathematical model of the web-dendritic growth to predict the furnace design parameters which effect the growth of the web.

(2) To develop a mathematical model to predict the temperature distribution in the melt, crucible, susceptor and thermal shield. The model will be used to determine the effect of slot geometry and susceptor geometry on the temperature distribution in the melt.

Approach

Objective (1) was met by the development of a one-dimensional heat transfer model of the web and meniscus. The rate of heat transport of the latent heat of crystallization from the liquid-solid interface of the web determines the rate of growth. Heat is transported in the web and meniscus by conduction and convection; heat is exchanged at the surfaces with the environment by radiation and convection.

Meniscus geometry was calculated and the effect of joining angle on the meniscus height and shape were determined.

Radiation heat transfer between the thermal shield and web was included in the model. The angle factor between the thermal shield and web was determined.

To meet objective (2) a finite difference heat transfer model was developed for the melt, susceptor, crucible, and thermal shield. Convection was neglected in the melt thus heat is transferred in the melt by conduction. Heat transfer in the quartz crucible is by radiation and convection. Radiation accounts for the most of the heat transfer at the surfaces. Heat transfer between the melt surface and the thermal shield is primarily due to radiation.

Because of the rectangular slot geometry, heat transfer in non-axiosymmetric thus a three dimensional heat transfer model was required.

Analysis of the effect of the radiation ports in the susceptor requires the use of a three-dimensional heat transfer model.

2. INTRODUCTION

At the time of initiation of this project, fall 1975, the "millstone-around-the neck" of the solar cell industry was the high cost of production of solar cells. This kept the fairly well developed space technology from being given serious application to meet terrestiral energy needs of the world. With the recent awareness by the general public of the inevitably limited supply of cheap fossil fuels, it became apparent that an investigation should be made into the feasibility of making commercially competitive solar cells.

A considerable portion of the cost of producing the conventional silicon solar cells is tied up in the production of the single crystal silicon in sheet form for use in fabricating the cells. The standard process for producing the sheet silicon for solar cells used for spare applications was to slice wafers from ingots grown by the Czochralski process and then laboriously prepare the sliced wafers by polishing and etching until they had the required surface perfection to be suitable for use. An alternate process for producing silicon in sheet form had been invented at the Westinghouse Corporation in 1965 which appeared to show some promise in reducing the cost of producing the silicon sheet. This process was called the Web-dendritic process and it produced flat crystalline ribbons approximately 2 cms. wide and up to several meters in length, having acceptably perfect flat polished surfaces as grown. It was felt that the elimination of the process steps necessary for preparing the surfaces of solar cell wafers from the Czochralski grown crystals, would

result in a considerable reduction in the cost of solar cells. Relatively little was known, outside of Westinghouse, of the web process and in fact it had been abandoned by Westinghouse also. No growth facilities existed in operating condition in 1975.

It was in response to the obvious need that the University of South Carolina prepared the work reported herein to the Jet Propulsion Laboratory, which had been given the prime contract to develop silicon solar cells for terrestrial applications.

It was proposed that a growth facility already existing on the campus be activated and used to investigate the feasibility of producing sheet silicon by the web-dendritic process of adequate quality for solar cell purposes at a cost which would make solar cells commercially competitive energy sources.

The program was broken up into two distinct yet mutually supporting areas of research, namely: the growth of web-dendritic ribbon and the computer modeling of the growth system and process for the development of improved, less costly growth facilities having improved throughout. The following pages constitute the report on the results of this investigation which ran from October 1975 to September 1977.

3. THEORETICAL THERMAL ANALYSIS

3.1. Thermal Modeling of Ribbon Solidification

3.1.1 Introduction

This investigation focuses on the heat transport in the web and meniscus during the growth of silicon ribbon (see Figure 1). Previous experimental studies indicate that the maximum pull rate of the web-dendritic ribbon growth is limited by the web rather than the edge dendrites. Single silicon dendrites have been grown at rates of approixmately 20 cm/min while silicon web-dendritic ribbon growth rates are normally less than 5 cm/min. There does not appear to be any reason that the two edge dendrites cannot grow as rapidly as single dendrites. Thus, it is concluded that the web-dendritic ribbon growth is limited by the solidification rate of the web. The rate of heat transport of the latent heat of crystallization from the liquid-solid interface of the web determines the rate at which the ribbon grows. Heat is transported in the web and meniscus by conduction and convection; heat is exchanged at the surfaces with the environment by radiation and convection.

An analytical model of the web growth is developed and numerical results are presented for the growth of silicon ribbon. The furnace design as well as meniscus and web geometry are shown to determine the maximum attainable pull rate. Parameters that are of most importance are the web thickness, meniscus joining angle, thermal shield temperature, and the spacing between the thermal shield and melt surface.

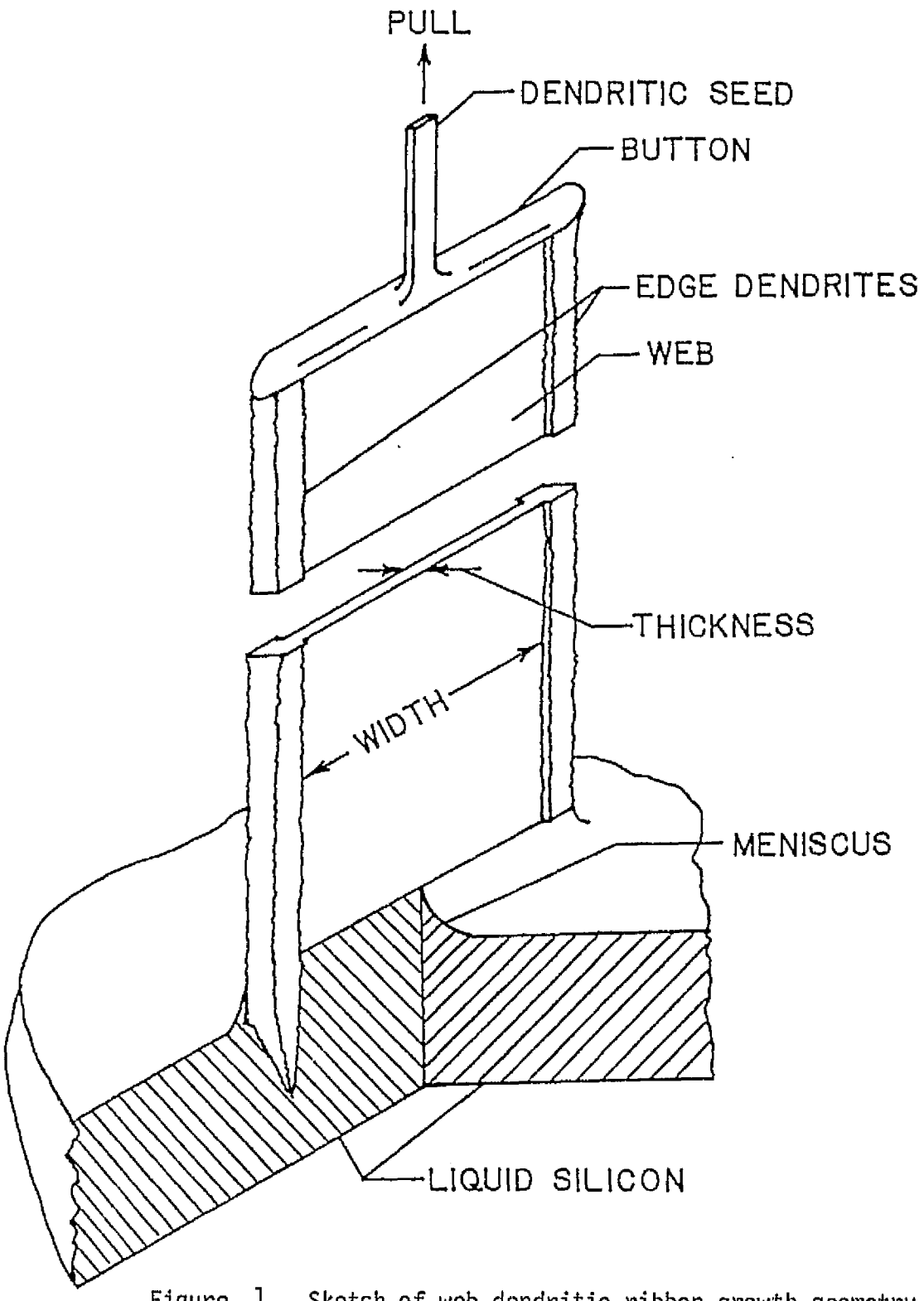

Figure 1. Sketch of web-dendritic ribbon growth geometry.

3.1.2. Heat Transport in the Meniscus and Web

The transport of heat in the region of the liquid-solid interface determines the rate at which latent heat of crystallization is removed from the liquid-solid interface. Figure 2 shows the cross-section of the meniscus, web, and thermal shield of a web dendritic ribbon growth furnace. The web is withdrawn through a slot in the molybdenum thermal shield covering the melt. The melt is contained in a fused quartz crucible which is fitted into a molybdenum susceptor. Heat is supplied to the furnace by induction heating the molybdenum susceptor by an r.f. field.

The purpose of the thermal shield is to reduce heat losses from the upper melt surface so that temperature gradients within the melt can be minimized. Because of radiation from the thermal shield, the shield assists in obtaining the correct temperature gradient in the web.

The temperature gradient along the length (or z-direction) shown in Figure 2 is of primary importance. Since web width greater than approximately 5 cm are of commercial importance, temperature variation across the width will be small compared to that in the z-direction. Temperature variations across the thickness is also small since the web thickness is usually in the range of 0.1 to 0.2 mm. At the base of the meniscus, the thickness increases significantly but since temperature gradients are small in that region, the two-dimensional heat conduction is insignificant. Consequently, one-dimensional steady-state heat transport can be assumed in the web and meniscus. Because the web and meniscus melt are moving in the z-direction, both convective and conduction transport mechanisms are present. The material is opaque, therefore, radiation in the solid and liquid can be neglected. Convective and radiation heat exchange with the surrounding environment occurs at the surfaces of the web.

Harrill [2] derived the governing differential equation for the temperature variation in web and meniscus. The differential equation for the meniscus differs slightly from that of the web because the variation of meniscus thickness is a function of z. The temperature variation in the web is given by,

$$\frac{d^2T}{dz^2} + \frac{\rho_s C_p V}{k_s}\frac{dT}{dz} - \frac{2h}{k_s t_s}(T-T_a) - \frac{2(W-\alpha H)}{k_s t_s} = 0 \qquad (1)$$

The symbols used in Equation (1) are as follows:

- T - Temperature
- ρ - density
- Cp - specific heat
- h - surface convective heat transfer coefficient
- V - ribbon pull rate
- k - thermal conductivity coefficient
- t - thickness
- W - emissive power of surface
- H - total irradiation of surface
- α - radiation absorption coefficient

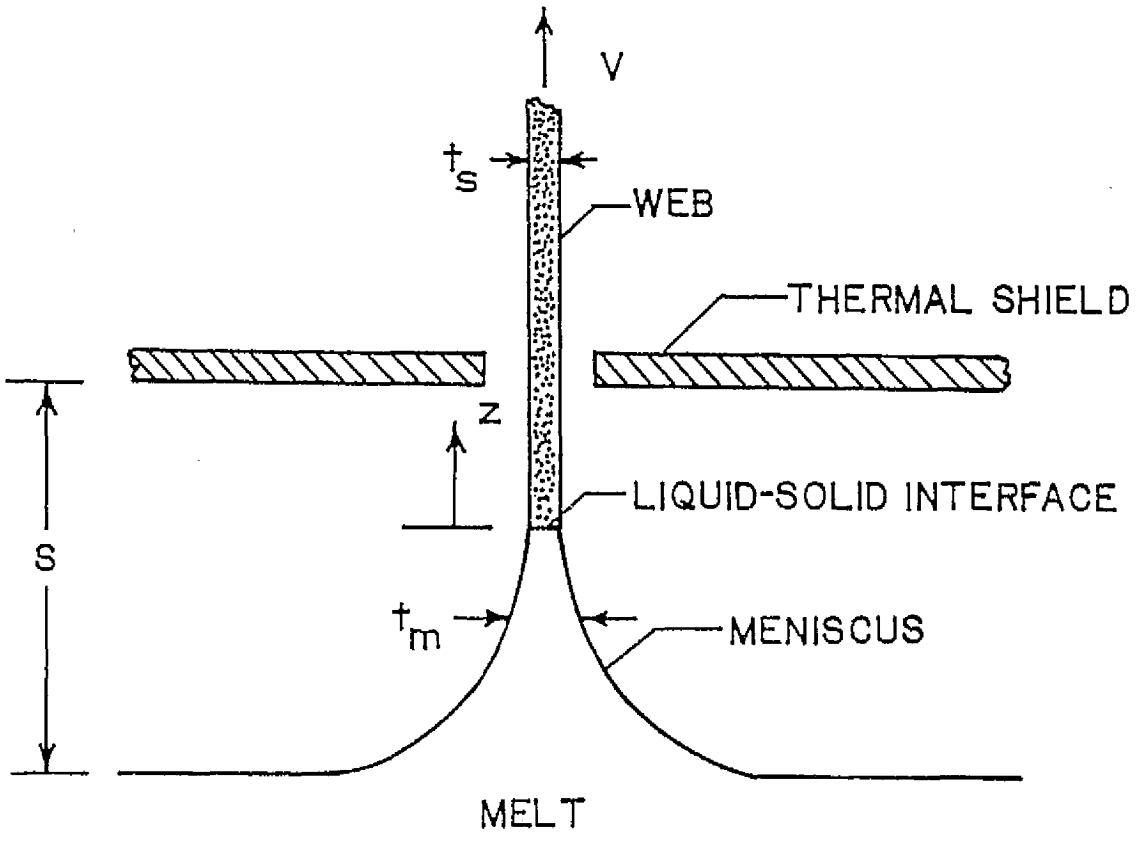

Figure 2. Cross-section of furnace showing melt, meniscus, web and thermal shield.

Subscripts:

a - atmosphere
s - solid

The first term of equation (1) accounts for heat conduction in the web. Constant thermal conductivity is assumed since calculations performed to determine the effect of thermal conductivity variation with temperature, have indicated that the assumption of a constant conductivity introduced an error of less than 5 percent [2].

The second and third terms of equation (1) are the convective transport of the web which results from web motion and the convective exchange with the surrounding environment (argon) respectively. The last term is the radiation exchange at the surface of the web. The surface emission, W, given by

$$W = \varepsilon\sigma T^4 \tag{2}$$

where ε and σ are the emissivity of the surface and Stefan-Boltzmann constant, respectively. The radiation absorbed from the surroundings is the total irradiation H multiplied by the absorptance α. The surfaces are assumed gray; therefore, α and ε are equal.

The governing differential equation for the temperature in the meniscus is [3],

$$\frac{d^2T}{dz^2} + \left(\frac{1}{t_m} \frac{dt}{dz} + \frac{\rho_s C_p t_s V}{k_m t_m} \right) \frac{dT}{dz} - \frac{2h}{k_m t_m} (T-T_a) - \frac{2(W-\alpha H)}{k_m t_m} = 0 \tag{3}$$

where the subscript, m, refers to the melt. Note that equation (1) and (3) are identical except for the second term. The first term in the parenthesis is the additional conduction term for a variable meniscus thickness, t_m. The velocity of the melt in the meniscus is also a function of z and has been factored into the second term in the parenthesis by using the mass conservation principle.

Latent heat of crystallization is released at the liquid-solid interface. Assuming that the temperature is continuous across the liquid-solid interface, the latent heat is conducted into the meniscus and web. Thus, at z = 0 we find,

$$\rho_s L_f V - k_s \left.\frac{dT}{dz}\right|_s + k_m \left.\frac{dT}{dz}\right|_m = 0 \tag{4}$$

where L_f is the latent heat of crystallization and $\left.\frac{dT}{dz}\right|_s$ and $\left.\frac{dT}{dz}\right|_m$ are the temperature gradients in the web and meniscus, respectively, at z = o.

Solutions to the differential equations must satisfy boundary conditions imposed by the system. In this case, there are three temperatures that are maintained; first the temperature at the base of the meniscus is equal to the crucible melt temperature. Since the growing tips of the dendrites are submerged, the melt entering the base of the meniscus is supercooled.

A second boundary condition is at the liquid-solid interface. Because the web solidifies in a mechanism similar to Czochralski growth, the temperature of the liquid-solid interface is at the silicon melting temperature. The third boundary condition is above the thermal shield where the temperature of the web approaches equilibrium with the surrounding furnace atmosphere at a large distance from the thermal shield. The temperature gradient in the z-direction becomes negligible and the first and second terms of equation (1) can be neglected yielding,

$$h(T-T_a) + W - \alpha H = 0 \qquad (5)$$

Equation (5) then is used to determine the equilibrium temperature on the web at a distance above the thermal shield.

Because equations (1) and (3) are second order, only two of the boundary conditions are normally needed to obtain a unique solution. However, the differential equations contain unknown parameters V, t_c, and t_m whose values must be choosen specifically to satisfy the third boundary condition. For a given meniscus and web geometry, the boundary conditions can be satisfied for only a particular V. Thus, one boundary condition determines unknown parmeters contained in the differential equation.

3.1.3. Heat Transfer at the Web and Meniscus Surface

The convective heat transfer coefficient h on the surface of the meniscus and web results from the cooling effect of the surrounding argon. The flow rate of the argon is small; so that the flow of the argon on the surfaces is primarily due to either bouyancy or natural convection. Thus h was determined assuming natural convection from a vertical surface [2] and is 3.45 W/m.^{o}C. The magnitude of the convective heat transfer from the surface is found to be much less than radiation and could be neglected without significant error.

The net radiation heat transfer at the surface is the difference between emission W and absorption H. Because W is described by equation (2), at this point we need only discuss H. In the region below the thermal shield, the meniscus and web are irradiated by the horizontal melt surface and the bottom surface of the thermal shield as seen in Figure 2. The radiation received from each surface is determined by the radiation leaving the surface and the angle factor. Below the thermal shield Harrill [2] showed that

$$H = \frac{\sigma}{2\left(\frac{1}{\varepsilon_1} + \frac{1}{\varepsilon_2} - 1\right)} \left[T_1^4\left(\frac{2}{\varepsilon_2} - 1\right) + T_2^4\left(\frac{2}{\varepsilon_1} - 1\right)\right] \qquad (6)$$

where surface (1) and (2) are the thermal shield and horizontal melt surfaces, respectively.

The web surface extending above the thermal shield is irradiated primarily from the upper surface of the thermal shield since the temperature of the surrounding surfaces is relatively low. The magnitude of H is thus greatly reduced at the thermal shield because there is no contribution from the melt surface. In addition H reduces with distance above the thermal shield due to the reduction in angle factor between the thermal shield surface and the web surface. An expression for H is derived in Appendix I and is given by

$$H = \frac{\varepsilon_1 T_1^4}{\pi} - \left[\frac{xR}{x^2+R^2} + \tan^{-1}\left(\frac{R}{x}\right)\right] \qquad (7)$$

where x is the distance from the thermal shield surface to an element of area on the web and R is the radius of the thermal shield. It is seen that $x = z - (s-h_o)$. The subscript (1) in equation (7) refers to the thermal shield.

3.1.4. Meniscus Geometry

The thickness of the meniscus t_m and meniscus height needed in equation (3) are determined by the meniscus geometry. Because the width of the web is large relative to the height, the meniscus is two-dimensional. Batchelor [3] presents the solution to the Euler-Laplace equation for the meniscus on an infinite flat plate which is also applicable to the present problem. The meniscus is attached to a solid web as shown in Figure 3. The joining angle is the angle between the meniscus surface and the vertical axis at the juncture of the meniscus with the solid web. In Figure 3, the web thickness is shown uniform so that the web surface is vertical. If web thickness is increasing or decreasing, the web surface is no longer vertical. Negative values of θ are to the left of the vertical axis and positive values are to the right. Neglecting dynamic effects, meniscus height h_o [3] is given by

$$h_o = K\sqrt{2(1-\sin\theta)} \qquad (8)$$

where

$$K = \sqrt{\gamma/\rho_m g} \qquad (9)$$

and γ is the surface tension, ρ_m is density and g acceleration of gravity. In equation (8) it is seen that meniscus height decreases while θ increases. The meniscus is given by

$$y/K = \cosh^{-1}\frac{2K}{z'} - \cosh^{-1}\frac{2K}{h_o} + \left(4 - \frac{h_o}{K^2}\right)^{1/2} - \left(4 - \frac{z'}{K^2}\right)^{1/2} \qquad (10)$$

where y and z' are the horizontal and vertical coordinates of the meniscus surface with the origin located as shown in Figure 3.

Figure 4 shows silicon menisci joining angles of -10°, 0°, 10° that were determined using equations (8) through (10). Silicon properties used in the calculations are contained in Table 1 and the acceleration of gravity is 980 cm/sec^2. For negative values of θ, it is seen that necking occurs

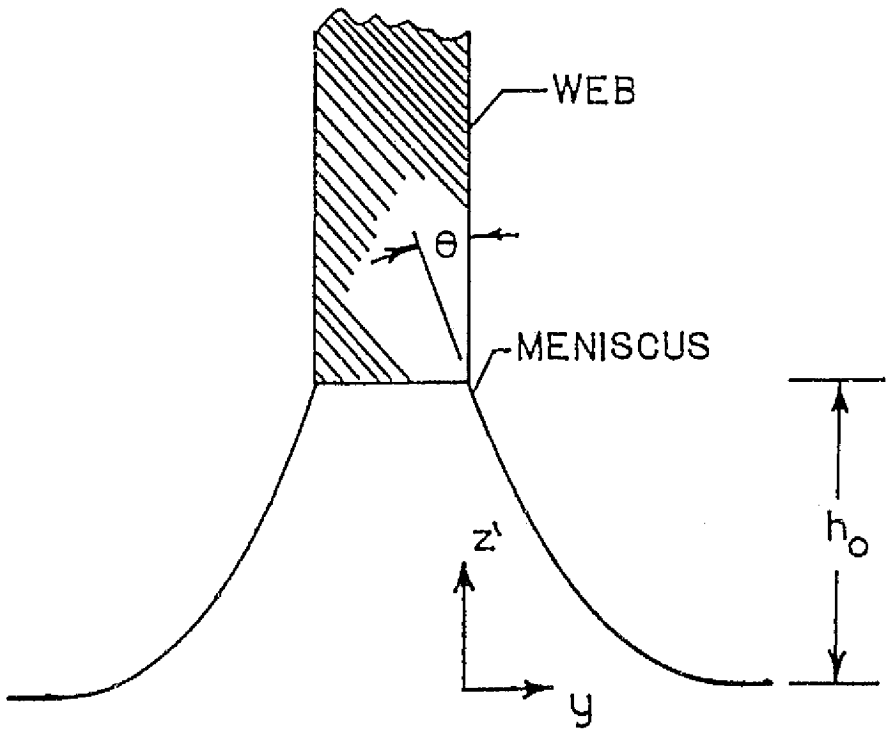

Figure 3. Meniscus geometry. The joining angle, θ, is the angle between the vertical axis and meniscus tangent at the junction. The height of the meniscus is h_o.

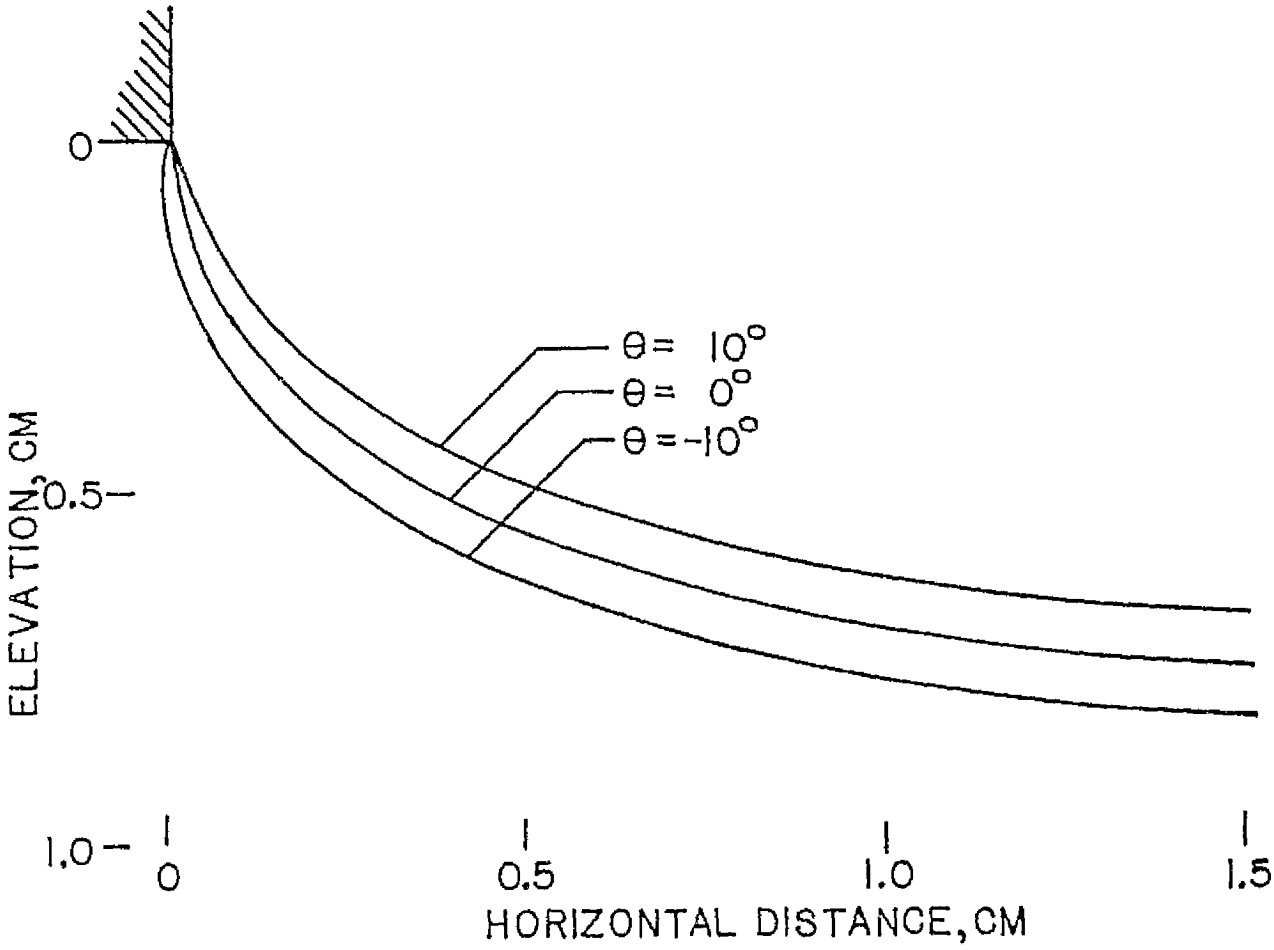

Figure 4. Shape of the meniscus for silicon melt with joining angle, θ, of -10°, 0°, and 10°. Meniscus height is seen to increase as θ decreases. Necking of the meniscus is seen to occur for $\theta<0°$.

Table 1. THERMOPHYSICAL PROPERTIES OF SILICON

Property	Units	State	
		Molten	Solid
Thermal conductivity coefficient	w/m-°C	60	22
Specific heat	KJ/Kg - °C	2.60	2.60
Density	g/cm^3	2.53	2.30
Emissivity		0.22	0.3
Surface Energy	Erg/cm^2	720	
Latent heat of Crystallization	kJ/Kg	1800	

occurs below the liquid-solid interface. Since necking occurs for negative values of θ , values of θ less than approximately - 10° results in separation of the melt from the web causing a disruption of growth. As θ increases, the meniscus thickness increases and h_o is decreased.

3.1.5. Numerical Results for the Growth of Silicon Ribbon

Numerical results for the heat transfer model were obtained for the growth of silicon ribbon. Thermophysical properties of silicon used in the analysis are contained in Table 1. Integration of the differential equations was carried out using the IBM CSMP3 (Continuous System Modeling Program III) [4] on an IBM 370 computer. A variable-step Runge-Kutta integration routine was used which varied the step size to maintain accuracy of the numerical integrations. Provision for including functional relations such as t_m and H are built into the CSMP3 program and greatly simplify problem input. The thermal shield radius R in equation (7) was assumed equal to 5.0 cm and its temperature is assumed uniform. An emissivity of 0.37 was assumed for both the top and bottom surfaces of the thermal shield [5].

Figures 5 and 6 show the temperatures calculated in the meniscus and web respectively for web thicknesses of 0.10 mm and 0.20 mm web thickness. A thermal shield temperature T_1 of 1300°C was choosen and the spacing between the thermal shield and melt surface is 1.0 cm. These are representative values for current furnace experiments. The effect of these variables on the growth characteristics is discussed later.

Experimental measurements performed by Surek and Chalmers [6] indicates that the web of uniform thickness is obtained for $\theta = 11°$. At larger values the web increases in thickness while at smaller values the thickness decreases.

In Figure 5 and 6 a joining angle of 11° is assumed. As mentioned earlier the liquid-solid interface is at the melting temperature which is approximately 1412°C for silicon. It was assumed that the melt is supercooled 5°C, thus the temperature of the meniscus is 1407°C. In Figure 5 the base of the meniscus is at the crucible melt temperature of 1407°C and the liquid-solid interface is at 1412°C. It is seen that the minimum temperature is reached when the meniscus temperature is slightly lower than that at the base as a result of heat losses from the meniscus surface. Heat is conducted from both the crucible melt and the liquid-solid interface and radiated by the meniscus surface.

Figure 6 shows the web temperature as a function of distance from the liquid-solid interface. The sharp decrease in temperature results from the lower thermal conductivity of the web in comparison to the melt in the meniscus (Table 1). Because the thermal shield is approximately 0.3 cm above the liquid-solid interface a slight increase in the slope of the curves is observed at that position. This increase is the result of the decrease in H at the thermal shield as shown in Figure 7. The large decrease in H shown in Figure 6 at 1.0 cm from the melt surface is the position of the thermal shield.

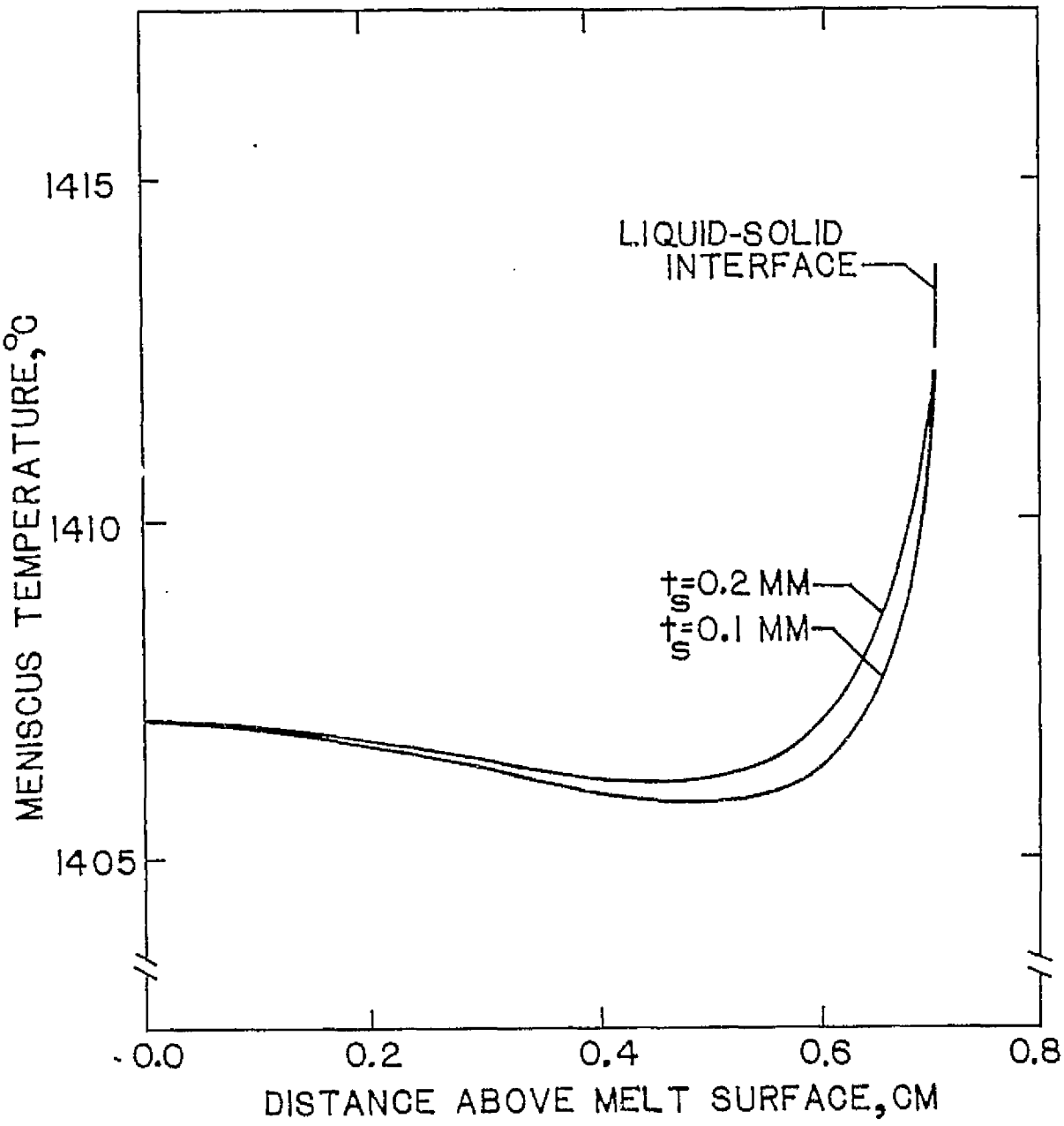

Figure 5. Temperature of the meniscus for web thickness of 0.1 and 0.2 mm. The thermal shield temperature is 1300°C and θ = 11°. Silicon melt temperature is 1407°C and the liquid-solid interface temperature is 1412°C.

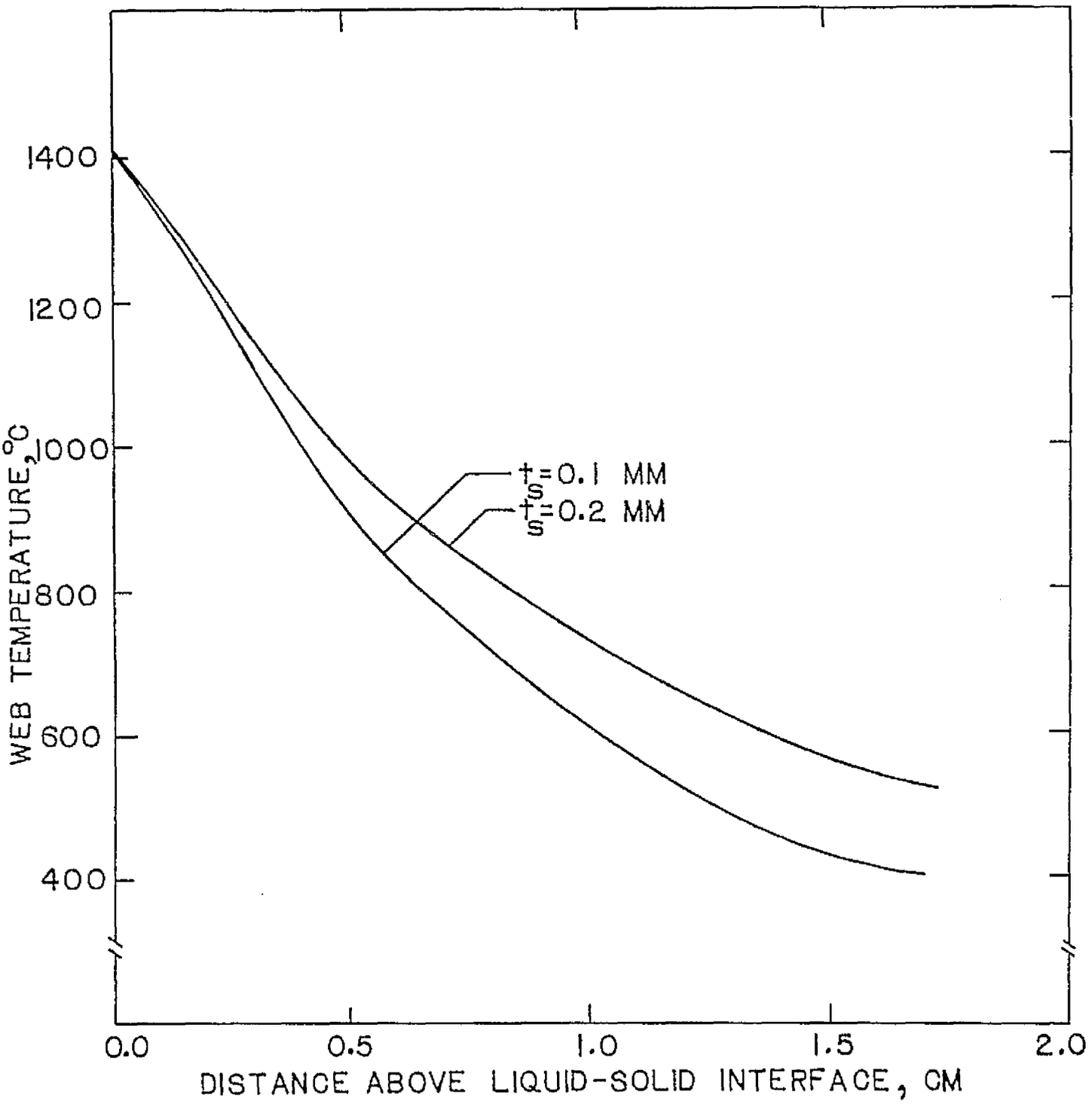

Figure 6. Temperature of web for web thickness of 0.1 and 0.2 mm. The thermal shield temperature is 1300°C and θ = 11°.

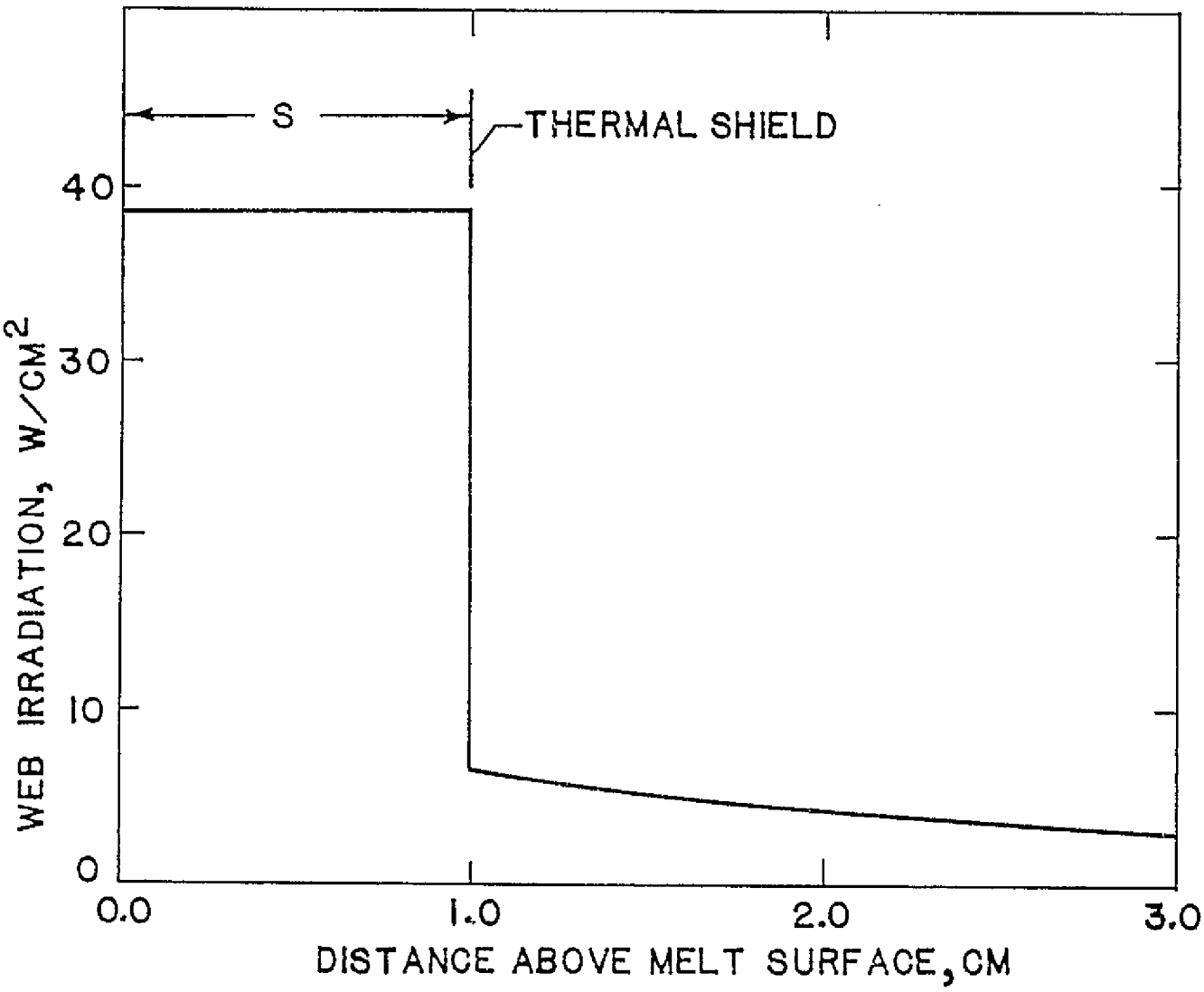

Figure 7. Irradiation H of meniscus and web surface. Thermal shield is 1.0 cm from melt and has a temperature of 1300°C.

The effect of θ on the calculated pull rate is shown, Figure 8, for web thicknesses of 0.10 mm, 0.15 mm, and 0.20 mm. It is seen that the pull rate is greater for the thinner web and the pull rate is also higher for smaller θ. The higher pull rate is due to the greater meniscus height which results in a larger surface area for radiating heat. When θ becomes negative, necking occurs in the meniscus and causes a decrease in the thermal conductance of latent heat from the liquid-solid interface. In Figure 8 it is seen that the maximum pull rate occurs at approximately $\theta = -5°$ and smaller values of θ have a lower pull rate. Values of S and T_1 are 1.0 cm and 1300°C, respectively.

Assuming a uniform web thickness is obtained at $\theta = 11°$, Figure 8 predicts pull rates of approximately 3.6, 4.0, and 4.5 cm/min for web thicknesses of 0.20, 0.15, and 0.10 mm web thicknesses respectively. It appears that the growth is stable because equilibrium conditions are restored after perterbating the pull rate. If the pull rate is suddenly increased after equilibrium conditions have been established, θ will decrease along the constant web thickness curve to the increased velocity. It is seen in Figure 7 that θ is now smaller than for uniform web thickness; the web thickness grows thinner and at the same time θ increases. When θ reaches 11°, equilibrium conditions are restored at faster pull rate and thinner web thickness.

Extreme changes in pull rate, however, can lead to growth failure. A large increase in pull rate will cause separation of the web from the melt. For example, Figure 8, if the web is initially being pulled at a uniform web thickness of 0.15 mm and pull rate is increased from the pull rate of 4.0 to a value greater than approximately 4.3 cm/min, separation occurs since θ cannot be decreased sufficiently to obtain a higher pull rate at the 0.15 mm thickness. Large decreases in the pull rate may lead to melt wetting of the side of the web, causing additional dendrites, or "thirds", to initiate in the web region. This would render the web useless from an economic standpoint.

The results presented in Figure 8 are for a thermal shield temperature of 1300°C and a spacing between the thermal shield and melt surface of 1.0 cm. The thermal shield temperature can be varied in the furnace by raising or lowering the induction coils. Although the optimum thermal shield temperature has not been established, the effect of its temperature on the pull rate was determined and results are shown in Figure 9 . As expected, the pull rate decreases as the thermal shield temperature increases. Increasing the thermal shield temperature from 1300°C to 1350°C results in a decrease in the pull rate of approximately 10 percent. Since the thermal shield temperature has a significant effect on pull rate, it is important to design the furnace for operation at the minimum possible thermal shield temperatures.

In Figure 10 it is seen that the pull rate is highest for the smallest spacing between the thermal shield and the melt surface. Since H is greater for the web and the meniscus surface under the thermal shield, minimizing this space reduces the total irradiation. If the web and meniscus surface receive less radiation from the surroundings, net heat loss to the surroundings is increased. Consequently the latent heat is more rapidly lost from the interface so that pull rate can be increased.

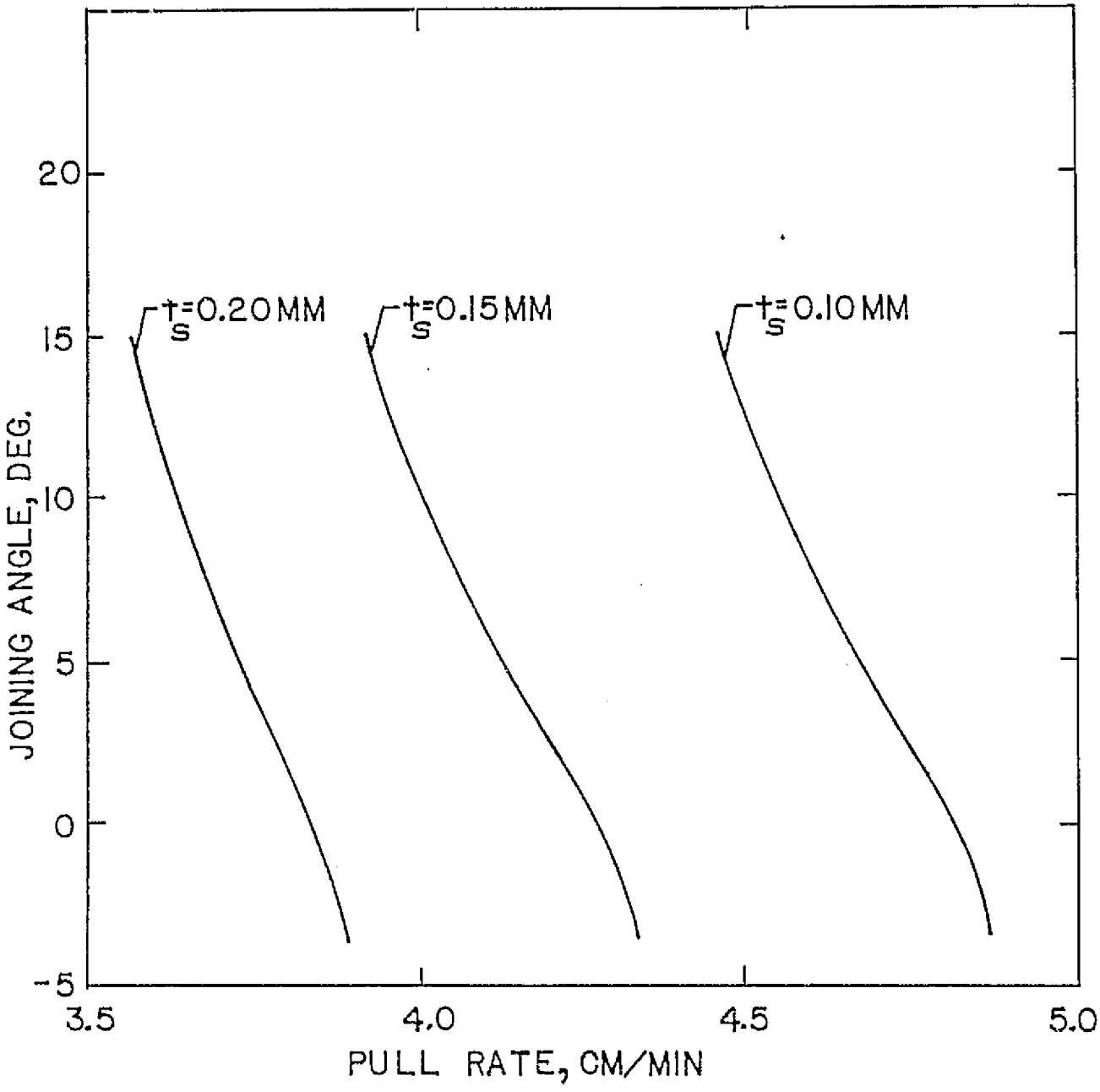

Figure 8. Joining angle θ as a function of pull rate V for web thickness of 0.10, 0.15, and 0.20 mm. Thermal shield temperature is 1300°C and spacing between thermal shield and melt is 1.0 cm.

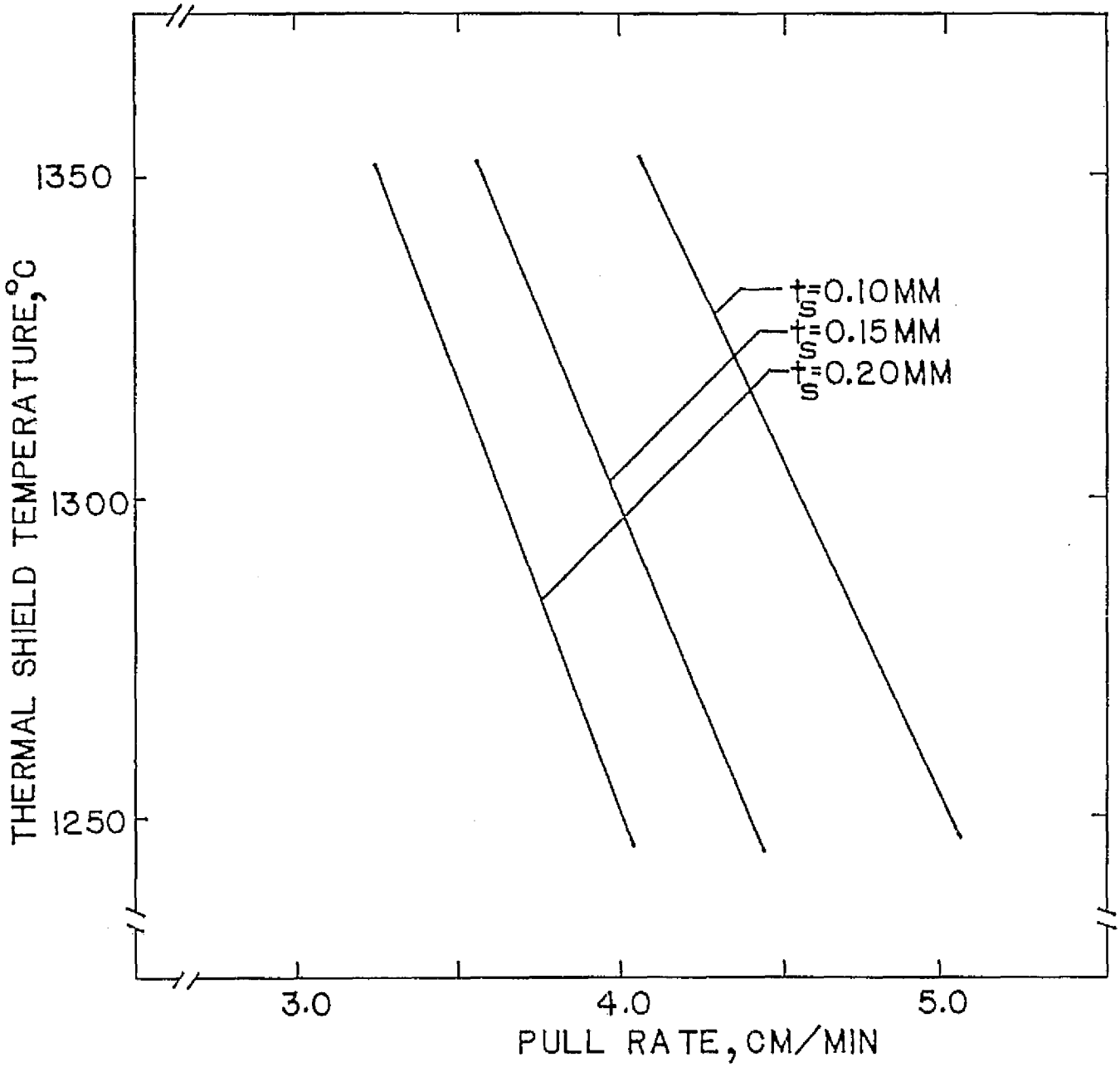

Figure 9. Dependence of pull rate on thermal shield temperature for web thickness of 0.10, 0.15, 0.20 mm. Spacing between thermal shield and melt is 1.0 cm and joining angle is 11°.

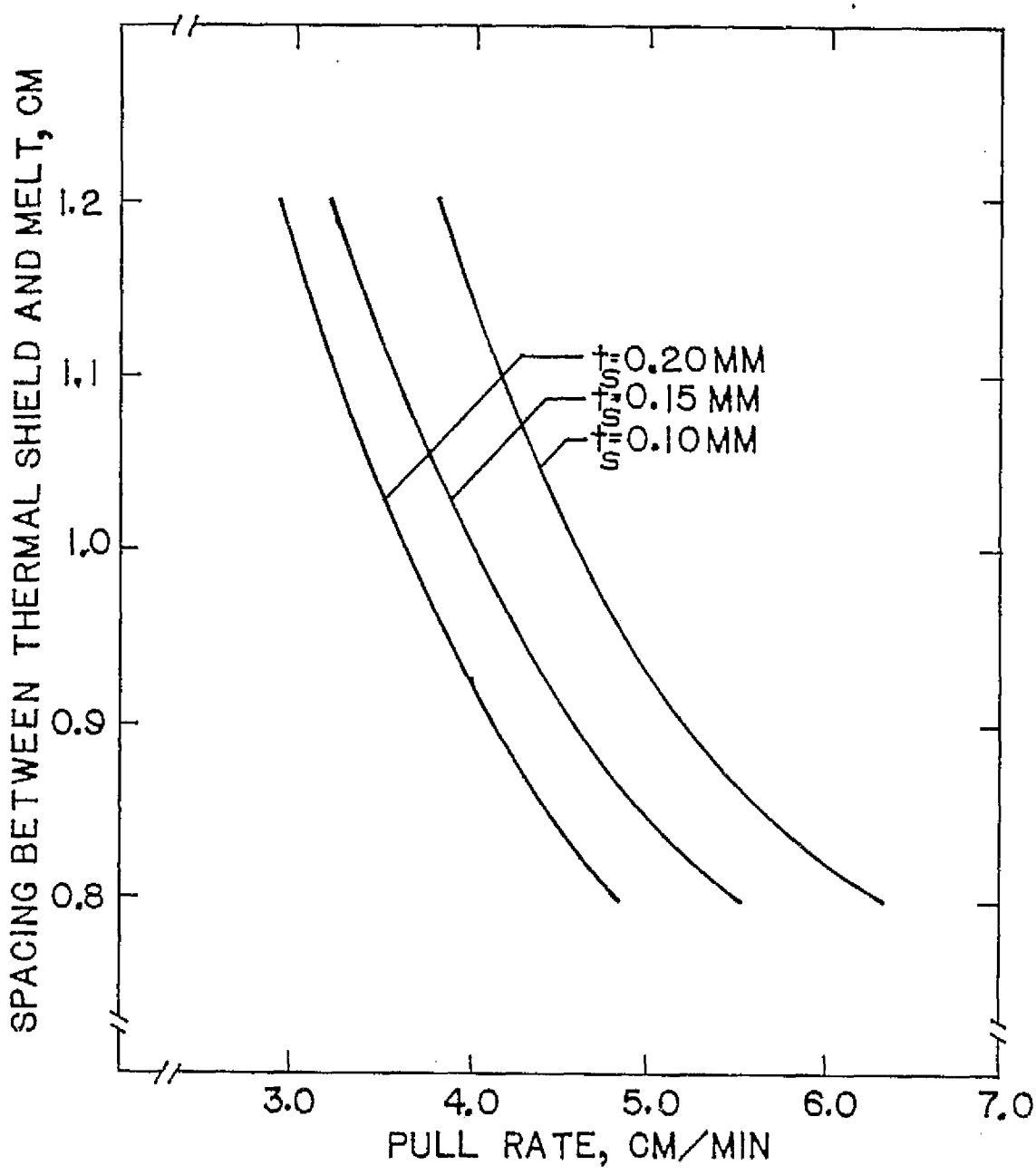

Figure 10. Dependence of pull rate on spacing between thermal shield and melt for web thicknesses of 0.10, 0.15, and 0.10 mm. Thermal shield temperature is 1300°C and joining angle is 11°.

As a result of the variations of pull rate with spacing shown in Figure 10, a gradual decrease in pull rate will be required as the melt level in the crucible is lowered unless thermal compensation is performed by other means. By continuously replinishing the silicon in the crucible to maintain a constant level, the pull rate can be maintained constant.

3.1.6. Discussion

An analytical model of the web-dendritic ribbon growth was developed and numerical results were obtained using the model for silicon. The furnace design at the University of South Carolina was used in the study. Detailed comparisons of the analytical results with experimental data were not performed since experimental data of sufficient detail to make these comparisons was not available. However, general agreement has been obtained with experimental results. For example, pull rates are generally in the range from 3-5 cm/min as is expected from the analytical predictions.

The furnace parameters that have the greatest effect on the pull rate have been identified. To improve pull rates appreciably will require modification of furnace design to increase the heat losses from the web and meniscus surface in the region of the liquid-solid interface.

The physical properties used in the numerical calculation are contained in Tables 1 and 2. Measurements contained in the literature differ widely and therefore some judgement must be exercised in choosing the properties. This is particularly true of the emissivity of solid silicon where values as high as 0.6 have been measured. Increased emissivity values of the web will result in higher pull rates. Thus the curves presented in Figure 8 - 10 will be shifted to the right. However, a higher molybdenum emissivity than that listed in Table 2 will result in a lower pull rate due to the increased radiation transport to the meniscus and web. A parametric study would be needed to determine the effect of these parameters on predicted results. However, the maximum effect is not expected to exceed approximately 10%.

3.2 Furnace Temperature Analysis

3.2.1. Introduction

The furnace temperature distribution was investigated using LION-4 [1] which is a finite difference thermal program. The program is capable of solving three-dimensional conduction steady and non-steady heat transfer problems with convection and radiation boundary conditions. The effect of furnace design parameters such as susceptor geometry, slot geometry and radiation ports on the steady state temperature was investigated.

Temperature distributions were calculated for the two susceptor designs used in the experimental growth and studies, Figures 11 and 12. Calculations were performed for the tapered susceptor with and without the radiation ports in order to determine the effect of the ports on the melt temperature distribution.

Table 2. THERMOPHYSICAL PROPERTIES OF SELECTED MATERIALS

Material	Emissivity	Thermal Conductivity $\frac{watts}{m^{\circ} K}$
Molybdenum	0.37	86.5
Silicon Melt	0.22	60.0
Quartz	--	11.9
Alumina	0.0	4.62

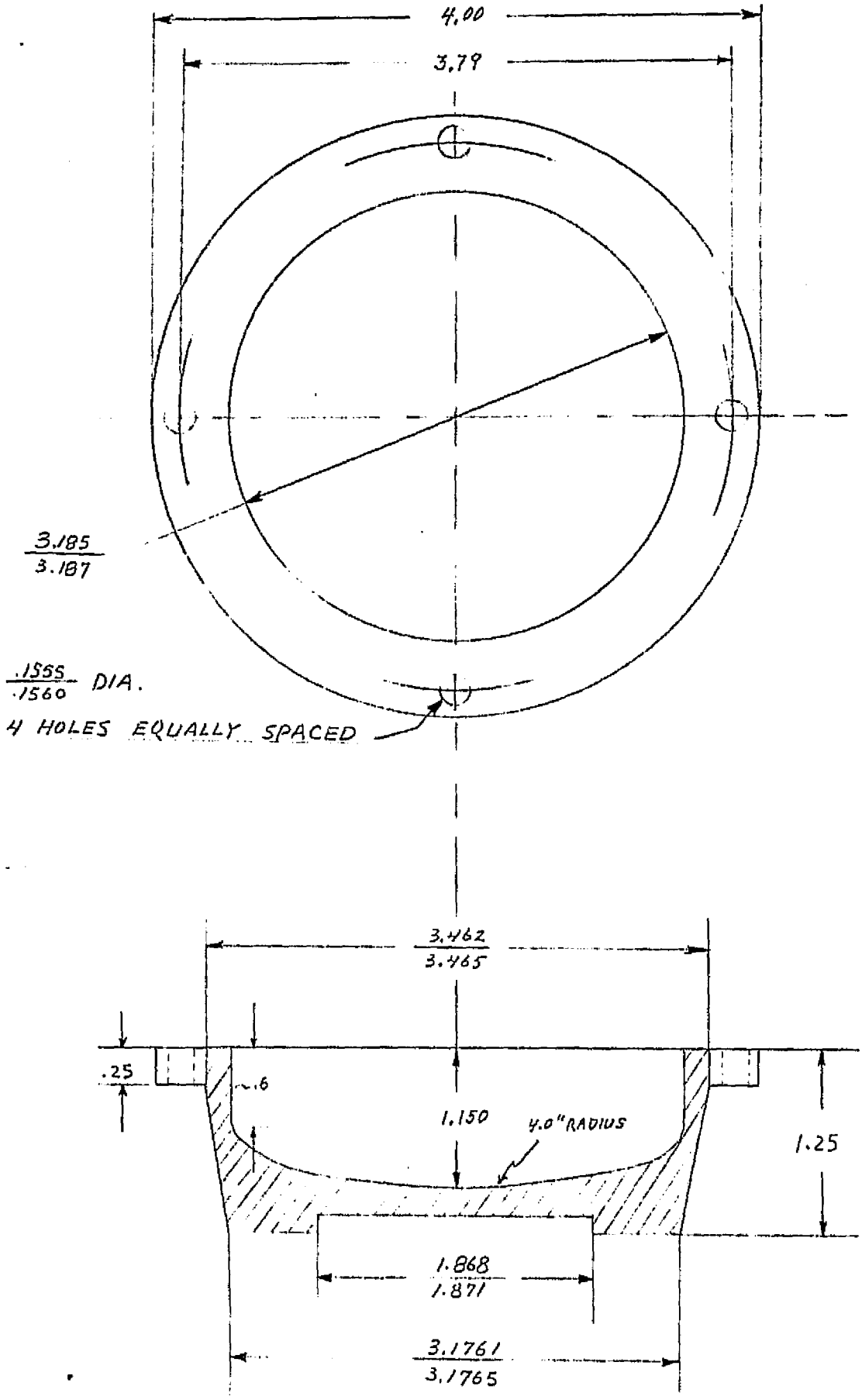

Figure 11. Taper sided (TS) susceptor.

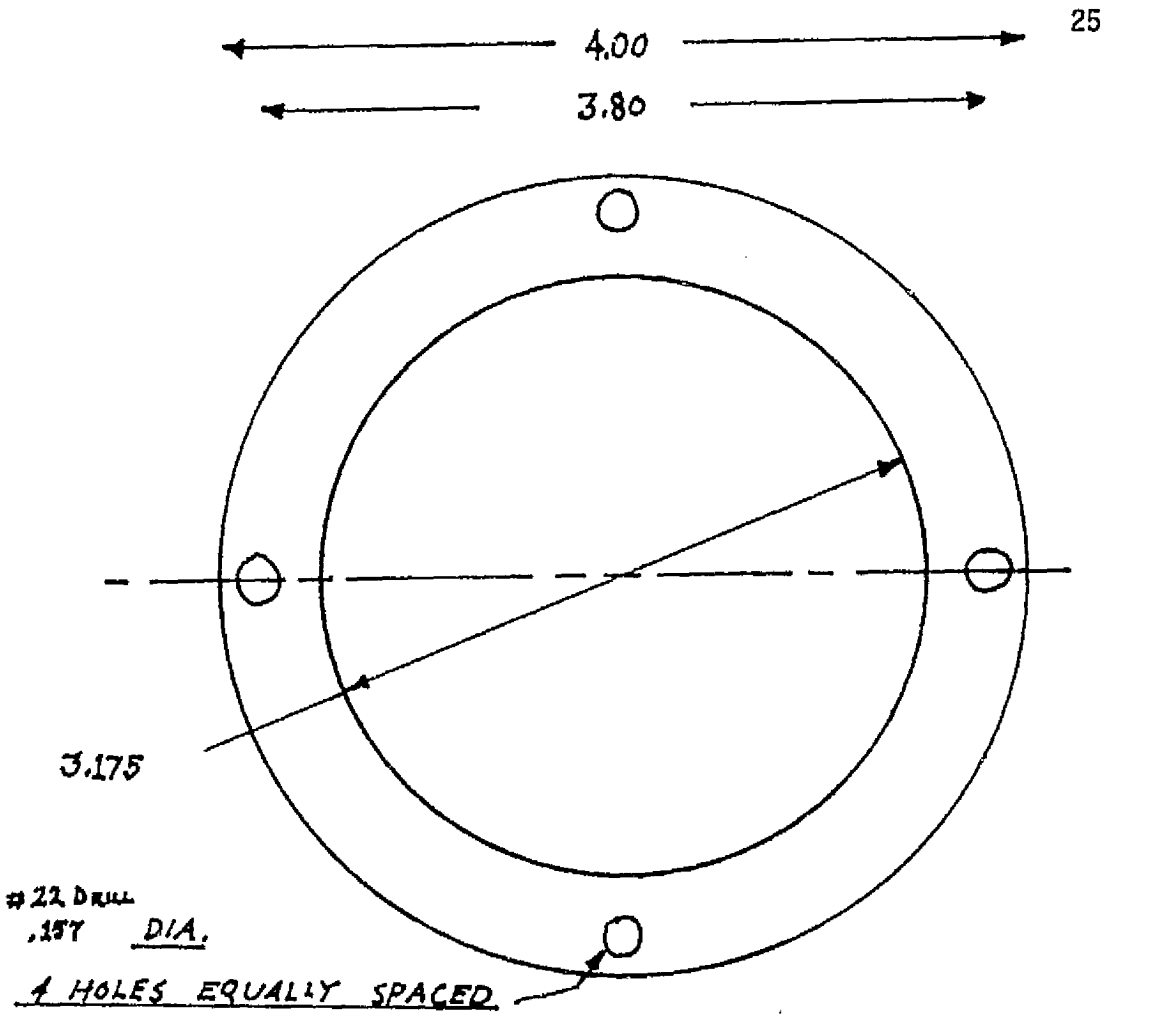

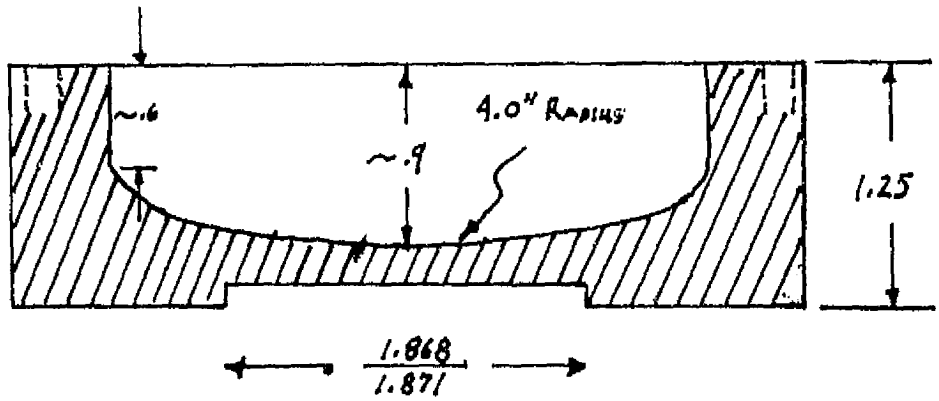

Figure 12. Straight sided (SS) susceptor.

Because heat radiated by the melt escapes through the slot, the temperature of the melt in the region of the slot is effected by the slot geometry. Ribbon growth occurs in the region of the melt slot, therefore, geometry affects the growth characteristics.

3.2.2 Heat Transport in the Furnace

Heat is supplied to the furnace by induction heating from an r.f. generator having a frequency of 290 KHz. The skin depth in molybdenum at this frequency is approximately 0.6 mm. The heat generation is primarily in the surface of the susceptor adjacent to the induction coils. In the straight side susceptor design the heat generation is approximately uniform

in the annular surface facing the coils. With the tapered susceptor the intensity of the field at the lip is considerably higher than that in the conical surface; thus the major portion of the heat is generated in the thin surface of the lip.

Although only a small fraction of the total generation occurs in the thermal shield, this heat generation has an appreciable effect on its temperature. Because the thermal shield is 1.5 mm thick the generation in the upper surface is a significant fraction of the total generation in the thermal shield.

Figure 13 shows the induction field geometry which was obtained using a conducting paper analog. It is seen that the field lines curve over the thermal shield which results in generation in the shield. The heating in the thermal shield is reduced by lowering the induction coils.

Heat transfer from the susceptor atmosphere is by convection and radiation. Convective heat transfer to the argon was shown to be negligible compared to radiation. Heat transfer between the silicon melt and the thermal shield is primarily by radiation. The radiation transport is approximated by assuming that the an element of area on the surface of the melt exchanges radiation with only an element of area on the thermal shield located vertically above the element. Heat radiation exchange to surrounding surfaces is small because of the small spacing between the thermal shield and melt surface. The net radiation heat flux between an area dA_1 on the melt surface and an area dA_2 on the thermal shield was calculated using the relation

$$q_{1-2} = \frac{\sigma(T_1^4 - T_2^4)}{\frac{1}{\varepsilon_1} + \frac{1}{\varepsilon_2} - 1} \qquad (1)$$

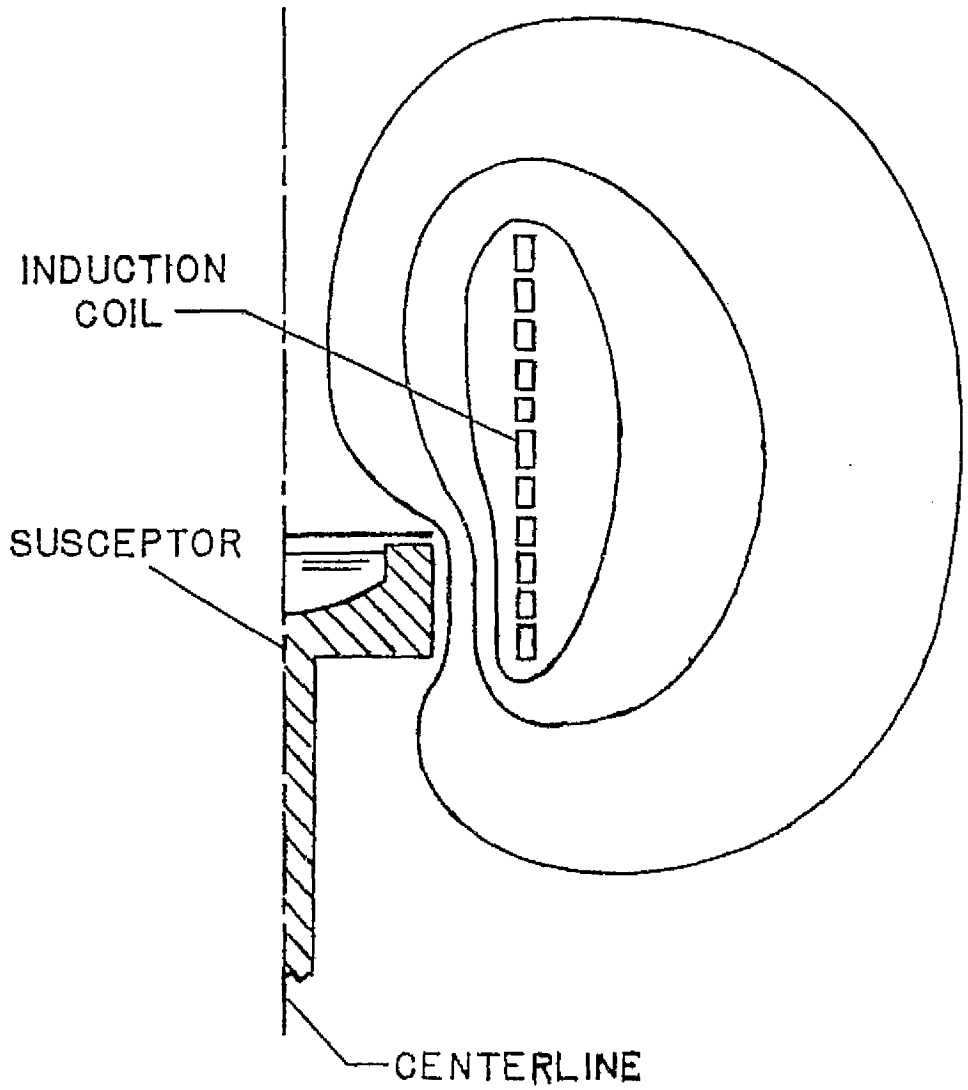

Figure 13. Induction field geometry in furnace. Most of heat generation is in the annular surface of susceptor adjacent to induction coils.

where q_{1-2} is the net heat flux from the melt to the thermal shield, α is the Stefan-Boltzmann constant, and ε is the emissivity of the surfaces. Subscripts (1) and (2) refer to the melt surface and thermal shield respectively. Because the surface temperature of the melt and thermal shield temperature, T_1 and T_2 respectively, are functions of the locations of dA_1 and dA_2, q_{1-2} will depend on the location of the elements of area.

Thermal properties used in the calculations are listed in Table 2. Heat transfer in the melt is assumed by conduction: bouyancy and surface tension driven convection is assumed negligible. Further study is needed to determine the accuracy of this assumption particularly in furnace designs where the temperature differences are large.

Heat transfer through the quartz crucible is by conduction and radiation. At the operating temperature of the furnace the quartz is transparent to approximately 80% of the radiation energy emitted by the susceptor and melt. Heat transfer through the quartz is primarily by heat conduction: radiation accounts for approximately 20% of the heat transfer.

3.2.3. Two-Dimensional Temperature Distribution

Figure 14 shows a section of the furnace with the nodal distribution used to calculate the temperature distribution in the straight sided susceptor. The left boundary of the figure is the central axis of the furnace. A similar nodal geometry was used for the tapered susceptor. The depth of the nodes was increased with radial distance from the center of the furnace to account for the circular geometry. The furnace is supported by a cylindrical alumina cylinder and has a single molybdenum thermal shield inside the cylinder.

Because this model is two-dimensional, the temperature distribution in the melt has been approximated. A three-dimensional heat transfer model was developed for studying the effect of the slot geometry and is discussed in the section which follows.

Figure 15 shows the isotherms in the furnace with a straight sided susceptor design. The melt temperature is approximately 45°C lower at the center than that of the edge, the melt temperature increases with depth. The outside surface temperature of the crucible is approximately uniform because the r.f. heating is uniform along the outer surface of the susceptor. The higher temperature near the top of the susceptor results from the radiation shielding afforded by the thermal shield.

The thermal shield temperature is approximately 200°C lower at the center than that at the edge. This decrease is the result of radiation losses to the environment from the upper surface and the high concentration of induction heating in the edge of the shield.

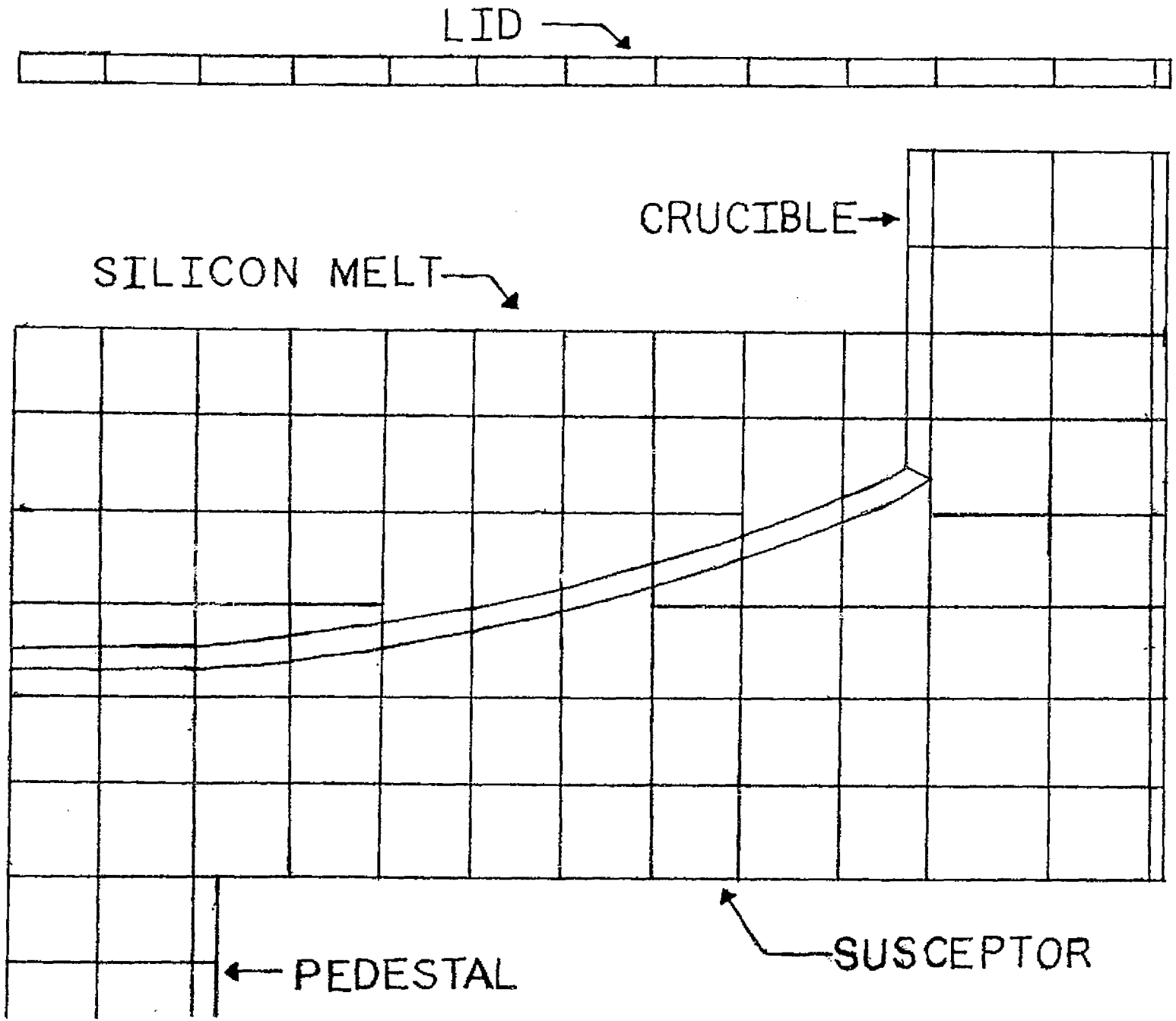

Figure 14. Nodal geometry for two-dimensional heat transfer model.

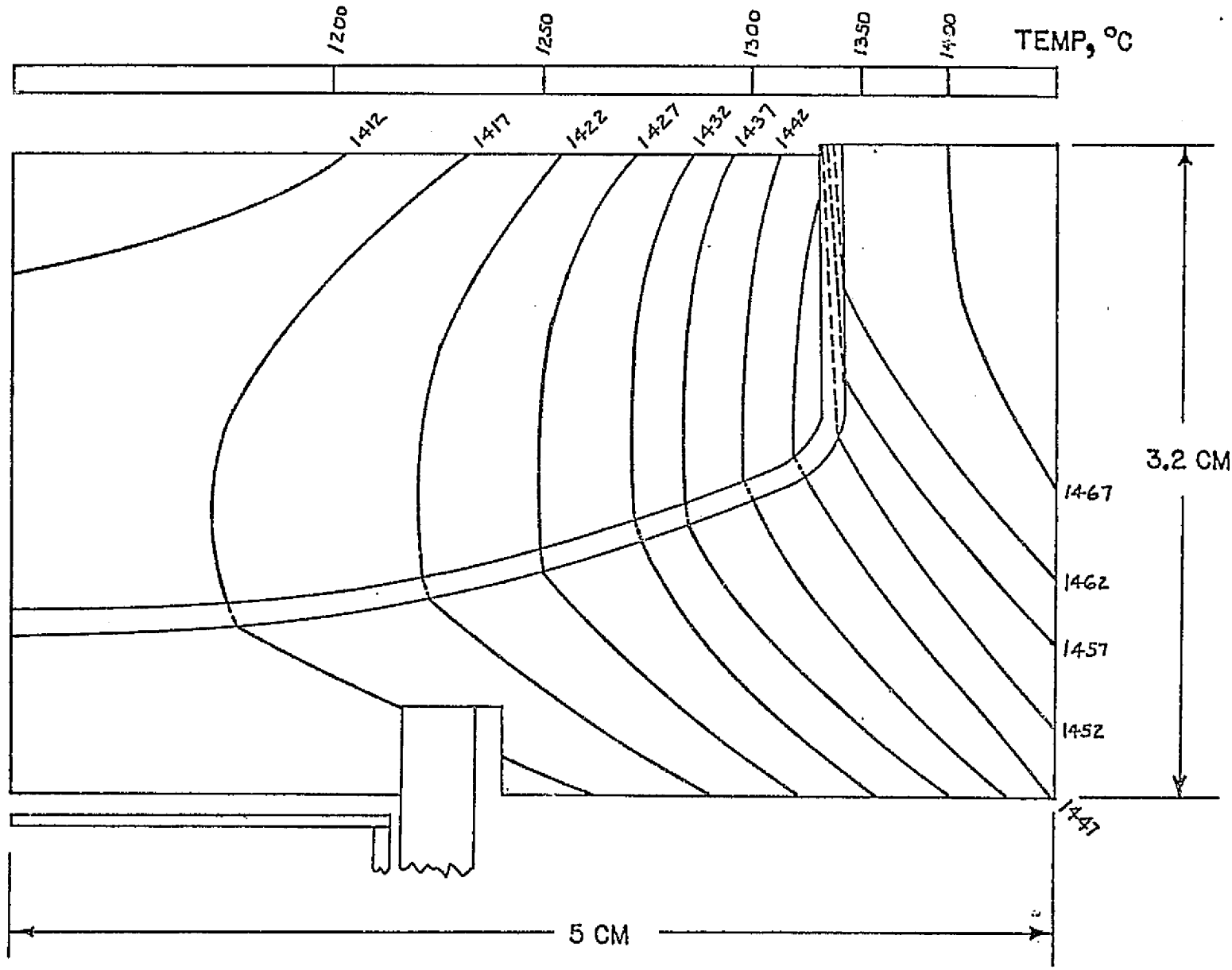

Figure 15. Isotherms determined for straight side susceptor.

Figure 16 shows the isotherms in the furnace with the tapered susceptor design. The lip temperature reaches a temperature of approximately 1650°C because of the high heat generation in this region. As a consequence of the high concentrations of heat generation near the top of the susceptor, the melt surface temperature is higher at the top than at the bottom. By comparing Figures 15 and 16 it is seen that the radial temperature gradient is considerably greater than that for the straight sided susceptor design.

The high radial temperature for the tapered susceptor may be the reason that the web widths that were obtained with it were small. It seems likely that greater widths are attained with the straight side susceptor than with the tapered design.

A technique that has been considered as a possible means of improving the temperature distribution is that of placing radiation ports in the bottom as shown in Figure 17. A three-dimensional model was developed to investigate the effect of the radiation ports. Figure 18 shows the effect radiation ports on the isotherms for a section taken along the center of the radiation ports. The solid lines are the isotherms with the radiation ports, thus it is seen that the thermal model predicts that the radiation ports effect only the melt temperature in the region of the radiation port. Rather than reducing temperature in the melt as was originally anticipated the model predicts that the melt temperature is increased slightly. The reason for the increase in temperature results from the fact that the bottom of the susceptor is at a lower temperature than the melt and therefore heat is conducted from the melt to the susceptor. Conduction serves a more effective heat sink than radiation, thus the model predicts a decrease in the heat losses at the ports rather than increasing heat losses.

Experimental data seems to contradict the analytical results which cannot be explained at the present time. Some improvement in ribbon growth has been experienced when the ports are used, thus apparently the thermal effect is greater than indicated by the thermal model. Further study of this anomaly is needed.

3.2.4. Effect of Slot Geometry on the Melt Temperature

A three-dimensional heat transfer model was developed for the region of the melt in the vicinity of the slot in the thermal shield. Figure 19 is a top and side view of the nodal geometry. Because of thermal symmetry, the temperatures were determined for only the one-quarter of the melt region effected by the slot as shown in Figure 19. Because the three-dimensional effects only occur in the melt, only the melt was included in the model. The boundary conditions were obtained from the two dimensional calculations. This approach reduced considerably the computer time that would be required had the entire furnace been modeled three-dimensionally. It does not appear that the accuracy was significantly decreased.

Figure 20 shows the isotherms on the surface of the melt for rectangular slot 6.48 cm long by 0.955 cm wide using the straight side susceptor. As would be expected the isotherms are elongated in the direction of the slot. Reductions of the temperature is highly desirable in order to encourage widening of the ribbon.

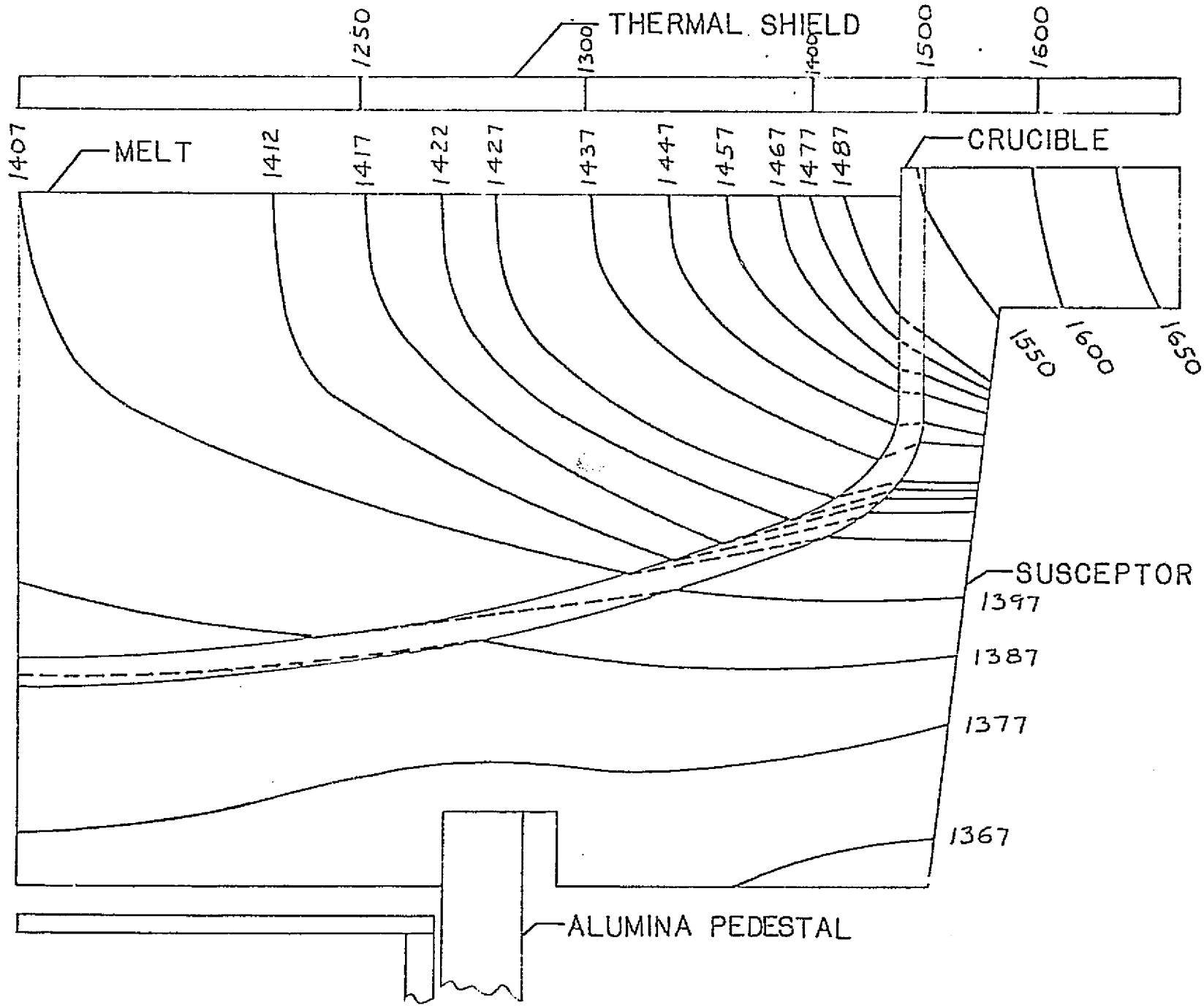

Figure 16. Isotherm for a tapered susceptor design.

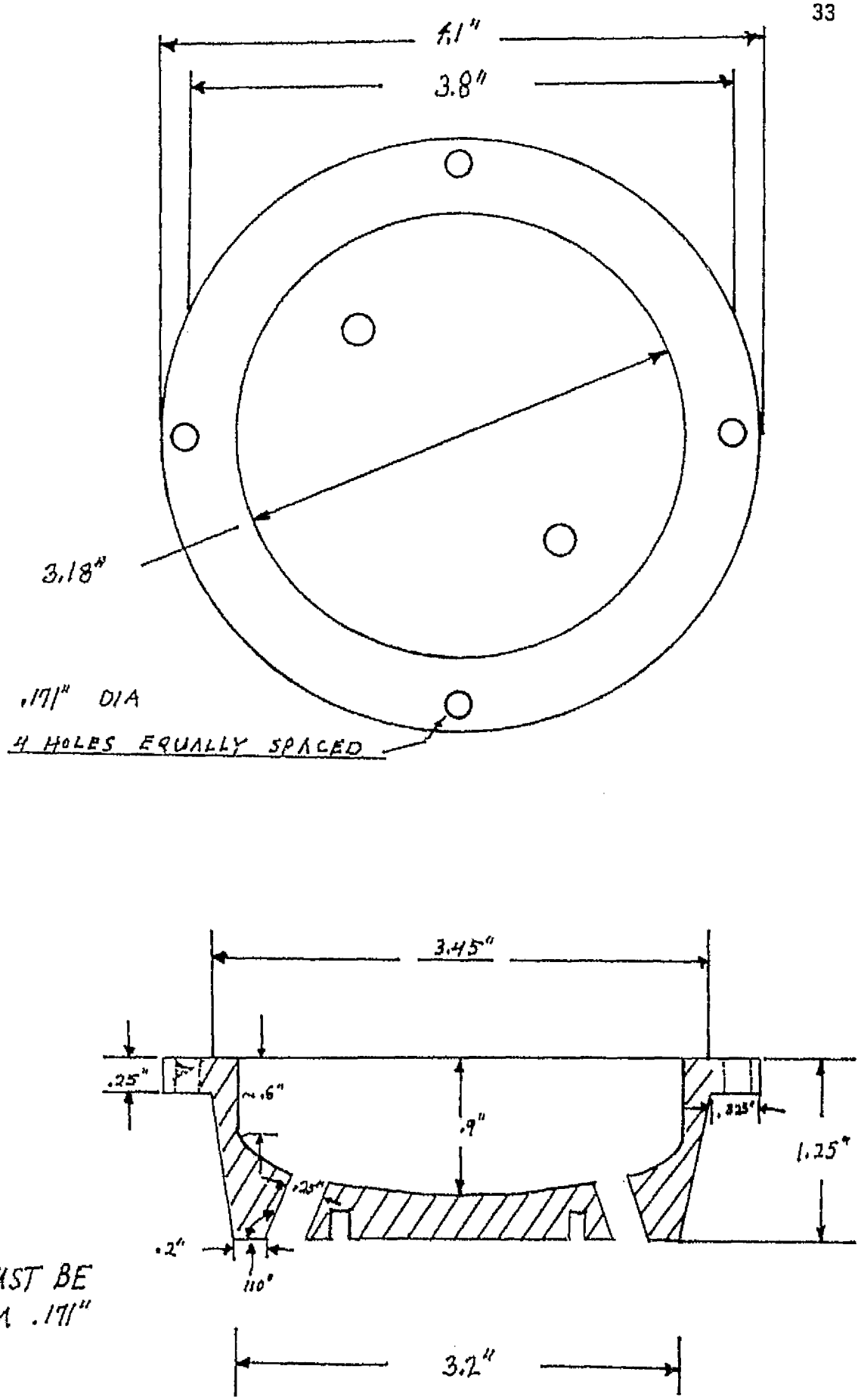

Figure 17. Tapered susceptor with radiation ports (TSP).

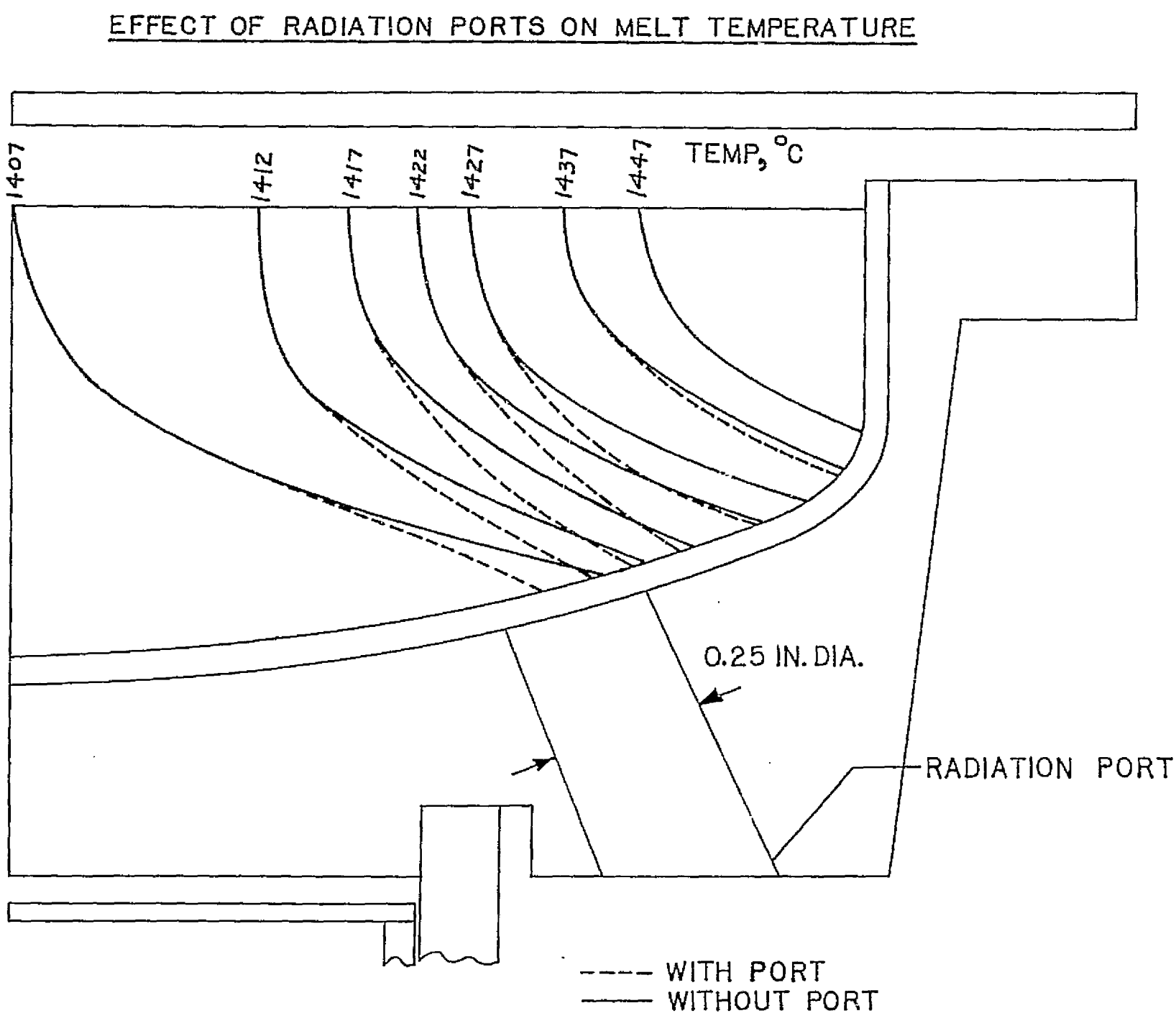

Figure 18. Effect of radiation ports on melt temperature

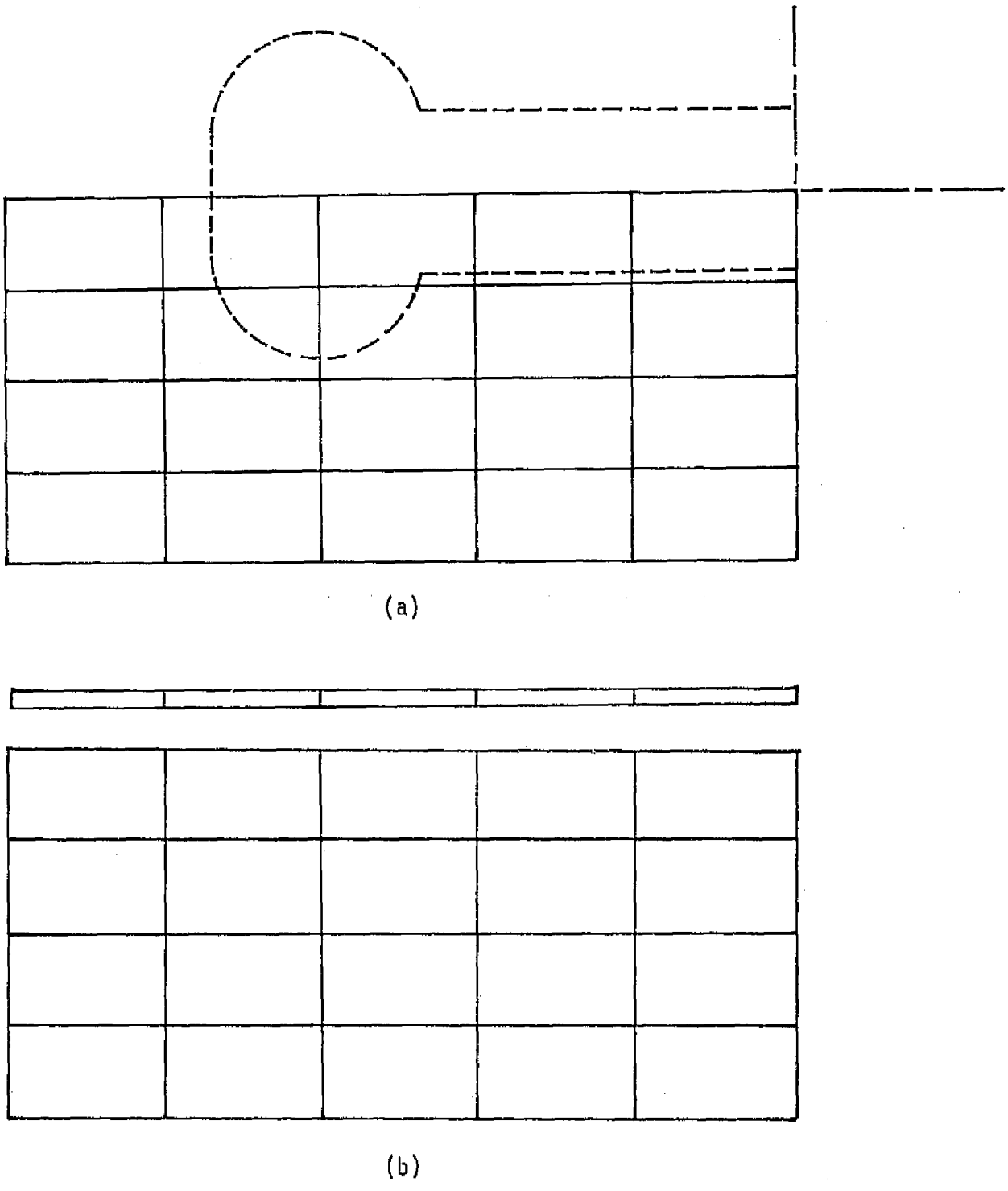

Figure 19. Three-dimensional model geometry of thermal model to determine temperature distribution in the region of the thermal shield slot. (a) Top view showing typical slot geometry (b) side view of thermal shield and depth into melt.

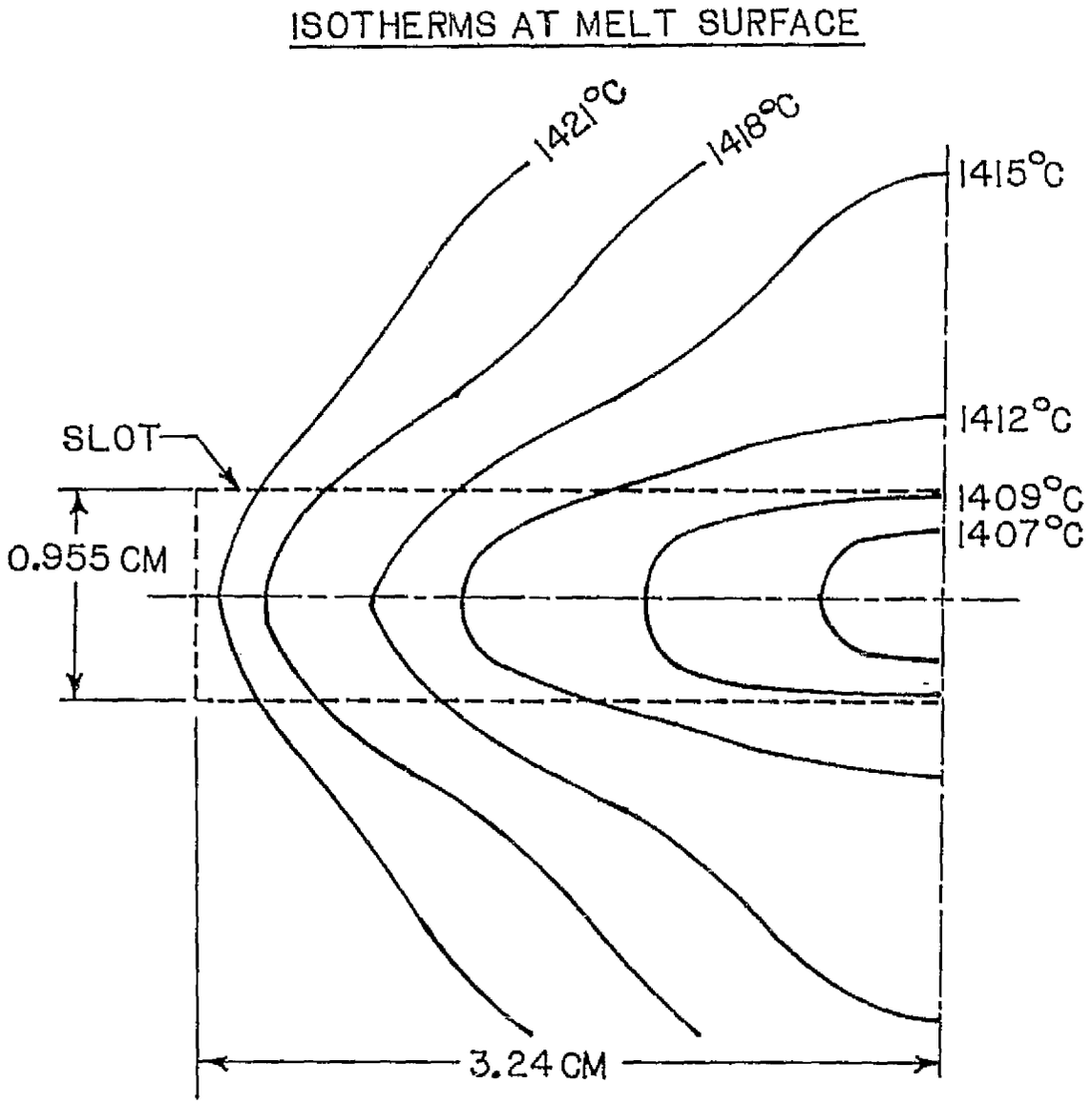

Figure 20. Isotherms at surface of melt for 0.955 cm x 6.48 cm rectangular slot

Figure 21 is a plot of isotherms calculated for a dog-bone slot obtained by increasing the width of the slot to 1.91 cm over approximately one-half its length. Further reduction of the temperature gradient is obtained which is accompanied by a decrease in the temperature gradient in the direction perpendicular to the slot. The increased temperature uniformity is more desirable since it reduces the likelihood of the ribbon encountering a high temperature melt. Thus the dog-bone slot provides a more favorable temperature condition than that of the rectangular slot.

3.2.5 Effect of Silicon and Molybdenum Emissivities on Temperature Distributions

As mentioned earlier the emissivity coefficients of silicon contained in the literature have considerable scatter. Thus, the emissivity values in Table 1 and 2 could have considerable error. Although the effect has not been investigated, generally increased emissivities cause increased temperature gradients and vice versa. The radial melt temperature gradients shown in Figures 15, 16 and 18, for example would increase if higher emissivities were used.

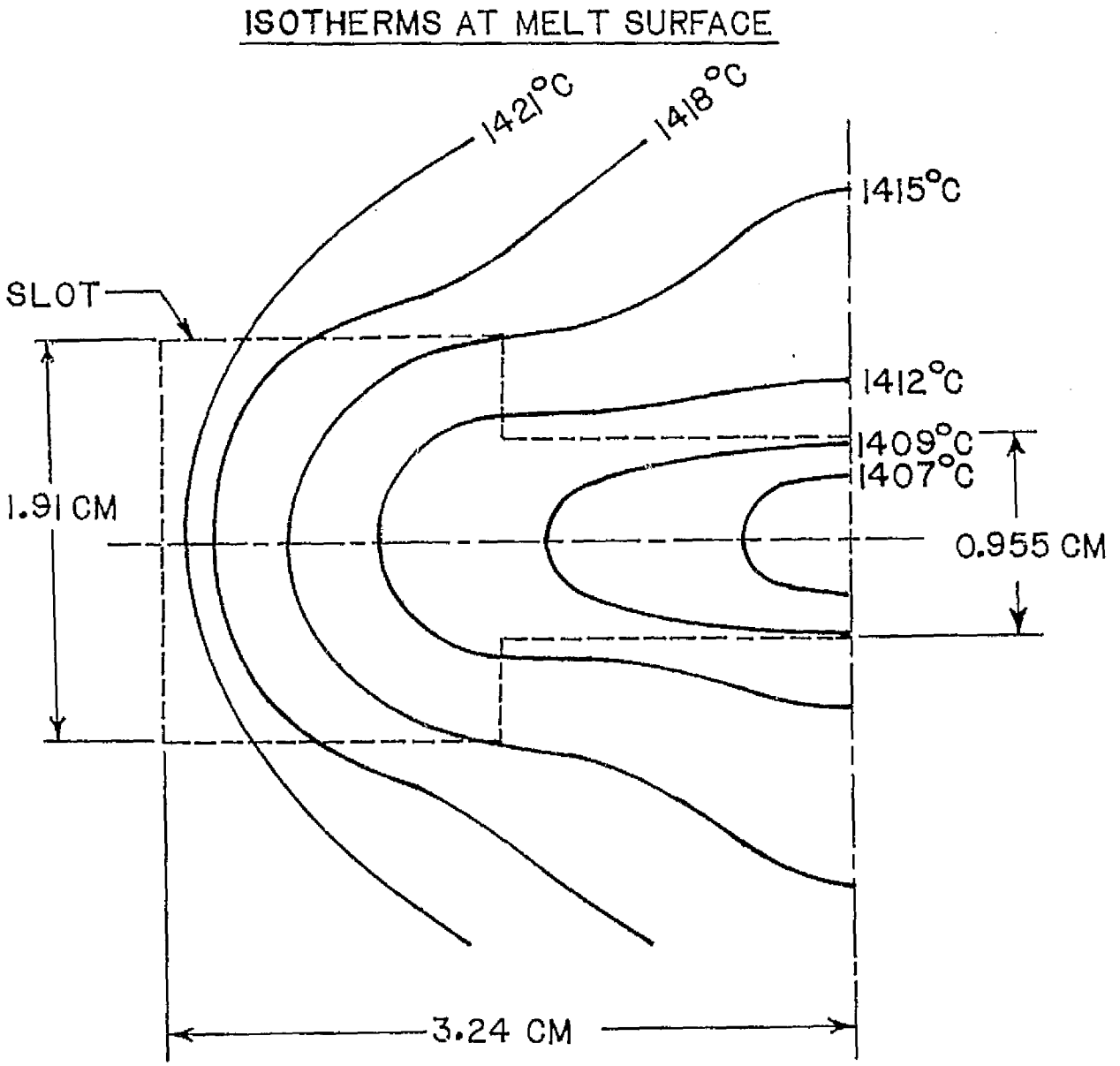

Figure 21. Isotherms at surface of melt for dog-bone slot 6.48 cm long.

4. Experimental Observations

4.1 Set up Web Furnace

This Task Element was approximately 90% complete at the start of the contract. The laboratory had been completed and the furnace and generator put in place, wired, and plumbed in; also it had been ascertained that both the generator and furnace were workable. Gas controls for the protection of the system and for the leveling and shock vibration mounting system, temperature sensing and controls for generator/furnace and pulling needed to be completed before an actual test run could be made. These were accomplished in the allotted time.

The four posts which acted as the legs of the furnace table were equipped with a servo-level Vibration Isolation System made by the Barry Controls Division of Barry Wright Corp. Nitrogen gas was used to activate the system. Initially the system was used mainly for leveling but also in the anticipation that it would keep out unwanted vibrations. Later in the contract period, after several months of pulling experience, it was found that the system appeared to be more of a hindrance than a help. Whenever the table top was touched, vibrations were set up in the melt. A guard rail was attached to the floor on the side where the person who operates the tape and web controls stood. This helped as far as touching the table top was concerned. It became evident that touching the controls on the furnace, or any part of the furnace, caused the melt to vibrate. To ascertain whether any vibrations in the room actually could cause vibrations in the melt if the isolation system were not used, the acoustic vibrations in the laboratory were measured with the result that all vibrations detected in the room over a period of several days, were found to be below the cutoff frequency of the isolation system. Thus, for our laboratory, all we were getting from our Isolation System was leveling. We then stopped using the isolation system and leveled the table with the leveling screws on the table legs. Before using an isolation system, it is suggested that a frequency study be made in the room where the web puller is located, and not be used unless necessary. Vibrations contribute to premature pull-out during web growth.

A manifold to hold four argon tanks was constructed to allow one, two, three, or four tanks to be used through a single pressure regulator valve. Two tanks were used at a time with the other two kept in reserve. The pressure regulator valve was adjusted to give 120 psi. The gas to the furnace passed through a flow regulator; this was adjusted to 50 cfh during the time the furnace was being brought up to temperature. When the silicon had melted, the flow was reduced to 35 cfh. The two tanks would last 6 to 8 hours before it was necessary to switch tanks. After two mishaps and several "close calls", a low pressure warning buzzer was installed on the manifold to sound off when the pressure reached 100 psi - this gave ample time to switch tanks.

The purity of the argon is of prime concern. Standard tank argon was found to contain too much oxygen causing considerable SiO formation. Higher purity argon was obtained in tanks for a slightly higher price. These tanks were carefully cared for by the Liquidair Corp. and filled first from the first half of storage tanks of liquid argon. This proved very satisfactory giving minimal SiO generation. Two bottles of ultrapure argon (each costing 5 times that of the "higher purity" argon) were tried. No improvement over the "higher purity" argon was found; thus the very expensive ultrapure argon was not used. After 4 to 6 hours of operation SiO would usually build up on the edges of the heat shield opening to an extent that it interfered with web pulling. SiO touching the web as it emerged from the heat shield was one cause of the web going poly and/or third dendrite formation. For the first year of the contract, when the SiO built up too much, it would be knocked down into the melt, and the melt temperature raised until it disappeared. Since this operation was time consuming, it was desired to have a technique to remove the oxide that did not necessitate knocking into the melt. A "vacuum cleaner" was devised that worked perfectly. It consisted of a long quartz tube, 1/8" in diameter, (actually a piece of tubing used to make the protective tubes for the thermocouple) attached to an aspirator by a long piece of plastic tubing. This worked so well that it became our usual practice to remove the SiO long before it became a problem.

The biggest problem that was encountered in this task was the r.f. generator. Actually it posed a problem periodically for practically all of the contract causing us to lose approximately 5 months of the first year through actual down time or having to repeat work done to be sure that the generator had not interfered with the results obtained just before the generator quit. When we had obtained the generator, it came with an extra unattached condenser. When the generator was set up, according to the instruction manual, it ran at approximately 400 kHz. The generator was controlled by an Ircon Optical Pyrometer sited on the susceptor. The output fed into a digital readout and into an Ircon Modline 3 mode proportional temperature controller. An interfacing circuit was designed and constructed to match the output of the Ircon control circuit to the magamp of the r.f. generator. The r.f. generator appeared at first to be operating satisfactorily; however, these tests were not run at full power. Attempts to heat a susceptor to 1500°C failed. At elevated temperatures, there was a lot of arcing which either kicked out the generator around 1000 to 1200°C or caused us to reduce power to avoid a generator shutdown. Furthermore the voltage fluctuated at higher power. The generator was carefully checked over after several telephone consultations with the Lindberg engineers. Finally a repairman, with knowledge in this series of generators, was called in. He said that the generator was functioning properly but the magamp control was unstable. The magamp control was removed from the circuit, and an H. P. 6299A DC power supply was purchased to drive the generator. A new electronic interface circuit, Figure 22, was designed to match the output of the Ircon controller to the input of the D.C. power supply. After a few days, however, arcing again occurred so that it was not possible to raise the power high enough to melt silicon. The problem was finally solved by adding another tank capacitor in parallel with the existing one, and melting of silicon was finally achieved.

CONTROLLER TO GENERATOR INTERFACE CIRCUIT

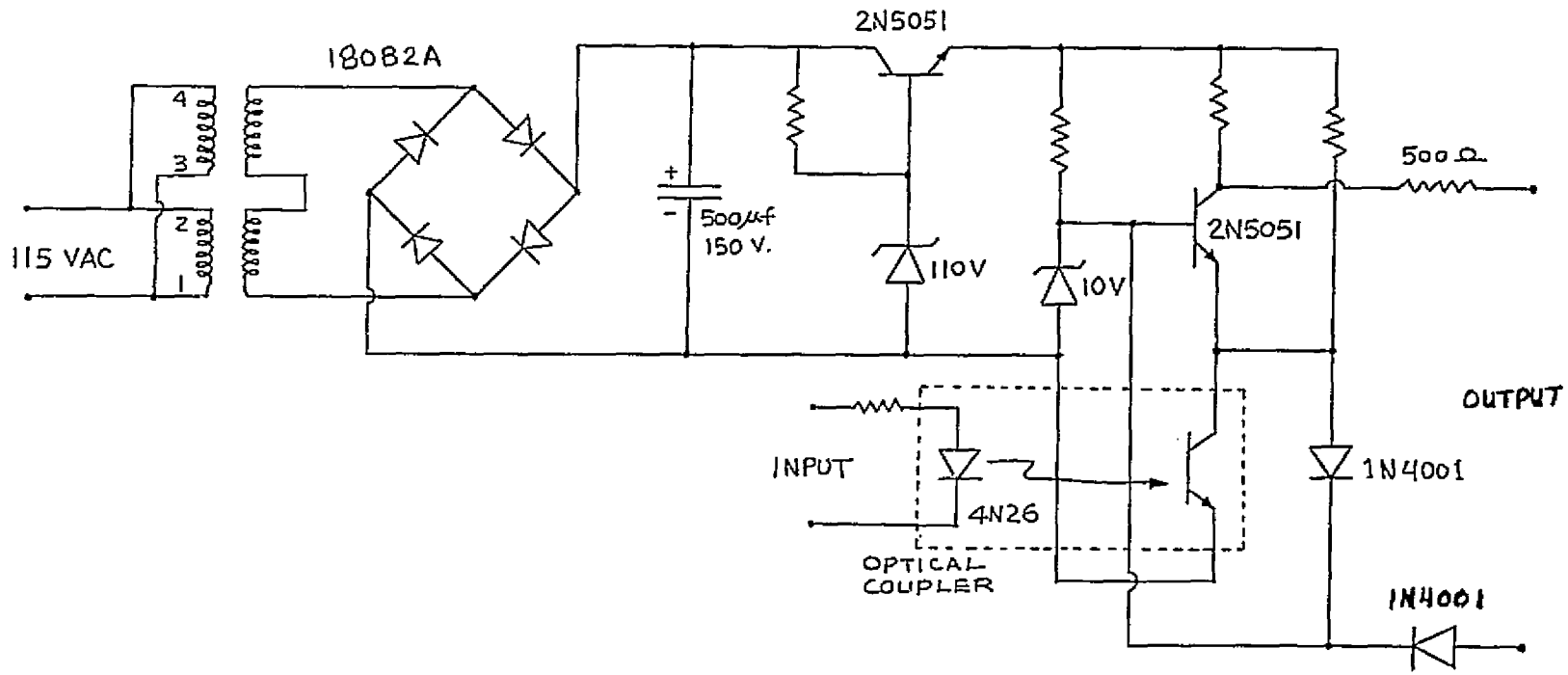

Figure 22. Controller to Generator.

The generator and furnace were cooled with city water; however, several times the water pressure dropped during a melt causing the generator to shut down. A closed loop distilled water system cooled by a heat exchanger utilizing the building's closed loop chilled water line was designed, built and installed. Unfortunately 6 months elapsed before the system was finally completed and installed. Just before it could be installed, the city water temperature rose causing a catastrophic generator failure. This caused problems, periodically, that were not definitely pinpointed until the contract was almost completed.

The r.f. work coil that came with the furnace had 11 turns of copper tubing with a rectangular cross-section of 3/8" x 1/4". The coil was 5" tall and had a diameter of 6". The coil was rigidly mounted on a platform that could be raised and lowered. It soon became evident that x-y horizontal movements were necessary to center the thermal symmetry each day. Two other coils were used in the final four months as will be taken up in Section 4.2. It became evident that the original coil was too long; the same number of turns were required in a shorter space to concentrate the heat more. The new coil was also 6" in diameter but was made out of 1/4" copper tubing and was 3 3/4" tall. The spacing was maintained by four strips of silastic run up the sides and forced into the spacing between the coils. The final coil was made of 1/4" copper tubing with a closer spacing to the turns and a larger diameter to give more leeway in adjusting the center of thermal symmetry. The coil height was 3 1/4" and the diameter 6 1/2".

The quartz envelope of the furnace consisted of GE quartz tubing 135 mm O.D. To allow more x-y motion of the coil, the envelope was replaced with quartz tubing 130 mm OD.

Several different types, shapes, and sizes of susceptors were examined to determine the best combination. Each susceptor was initially placed in the vertical center of the work coil and the taps on the tank coil were varied to find an optimum, if indeed there was one. These susceptors were:

1. carbon, 3.25" in diameter and 3.625" tall with straight sides. Although the voltage was low (7.5 Kv), the plate current limit (2 amps) was exceeded before the susceptor reached 1200°C.

2. Carbon, 2.375" in diameter and 2.27" tall with straight sides. With this susceptor the plate voltage was higher (10.7 Kv) and the plate current was lower (1.88 amps); however, a maximum temperature of only 1470°C was obtained. Since the generator was being pushed to its maximum to get this temperature, and only a small silicon charge could be used, this susceptor was discarded.

3. Molybdenum, 4" diameter and 1 1/4" deep with a lip and tapered sides as shown in Figure 11. This susceptor with a straight slotted heat shield gave the first complete melt without straining the generator (approx. 8.5 Kv plate voltage and 1.6 amp plate current).

4. Molybdenum, 2.625" in diameter and 2.15" tall. With maximum plate current (11.Kv), the susceptor never rose above 1100°C. This susceptor was too small for our setup.

The temperature of the melt was monitored by sighting on the bottom of the susceptor with the Ircon optical pyrometer. Ideally it would be desireable to monitor the temperature at the growing interface; however, no suitable technique for this has been devised. Temperatures were taken on the bottom of the susceptor. These readings were lower than the actual temperature at the surface of the melt. On the tapered susceptor with the lip, the optical pyrometer was later sighted on the under part of the lip with the idea that the response would be quicker since most of the coupling was taking place on the lip. Using the button formation as a criterion, it was found that there was little or no difference between the response time at the two sites. It was also found that the temperatures on the lip approached that of the maximum of our digital readout. For these reasons, all sighting was done on the bottom of the susceptors. The response time was measured with thermocouples much later and confirmed these findings. Additionally, results of thermal modeling showed that there should be no difference in the response time for using either location for the control temperature monitor.

The drawing of the crucible used throughout this work is shown in Figure 23. The volume of the crucible is 85 cc. Thus the maximum charge of silicon that the crucible can hold is 198 gms. This value can only be achieved by shaping a solid piece of silicon to fit the crucible. The initial silicon charges used to carry out the studies in this task were approximately 100 grams. After these studies indicated that the work on the furnace and generator, required of this task, was completed, a charge of 160 gms of silicon was melted as a final check on the furnace and generator. This is the maximum charge that can be put in with a slice of silicon (75 cm in diameter) without shaping the slice to the contour of the crucible. Much of the studies reported in section 3.2 were made with charges between 90 and 125 gms. The size of the charge was based on the calculations given in Appendix B.

During the entire course of the contract a number of heat shields of different designs were used. Descriptions of them will be given in the appropriate places throughout this section. The heat shield used for the initial thermal probing of the melt in this task is shown in Figure 24. This shield had too large an opening. The second shield used had a smaller opening as shown in Figure 25.

The heat shield is held above the susceptor by 4 tantalum pins as shown in Figure 26. The susceptor sat on a Molybdenum pedestal, also shown in the figure. The plate at the base of the pedestal, in Figure 26, is a diffuser plate made of molybdenum, a drawing of which is given in Figure 27. The main purpose of the diffuser plate was to hold an inner quartz cylinder. Since the 4" susceptor was found to couple the best, the inner cylinder was not used and thus the diffuser plate was abandoned.

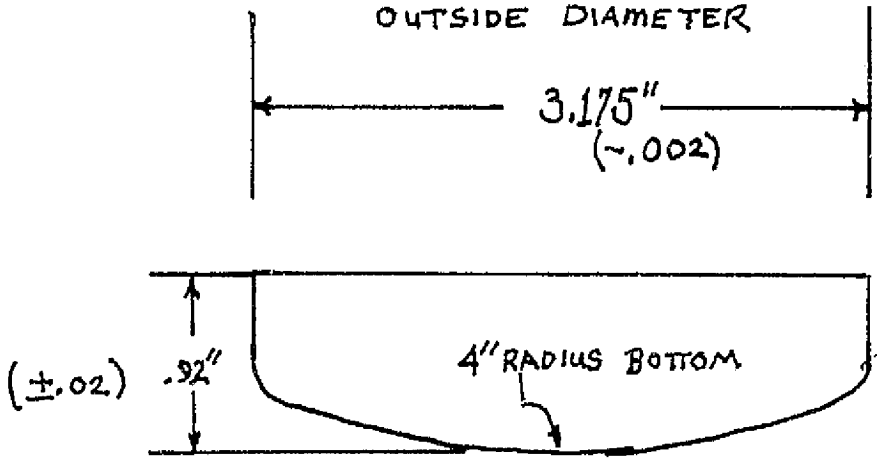

Figure 23. Details of Quartz crucible.

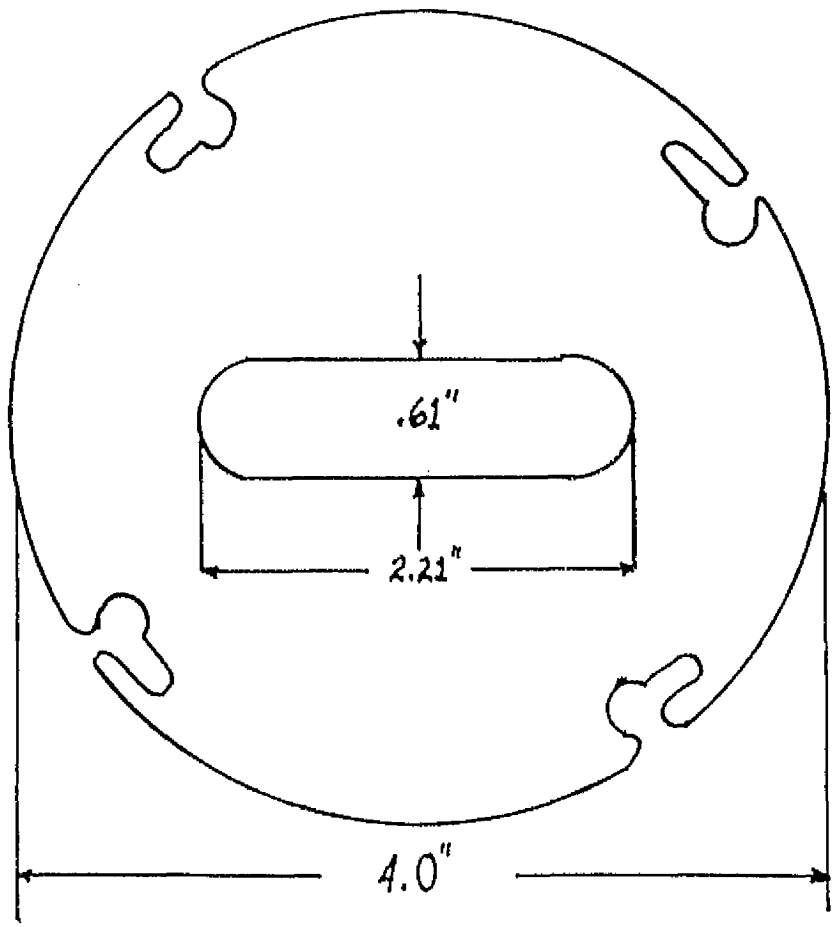

Figure 24. Wide straight sided (WSS) heat shield.

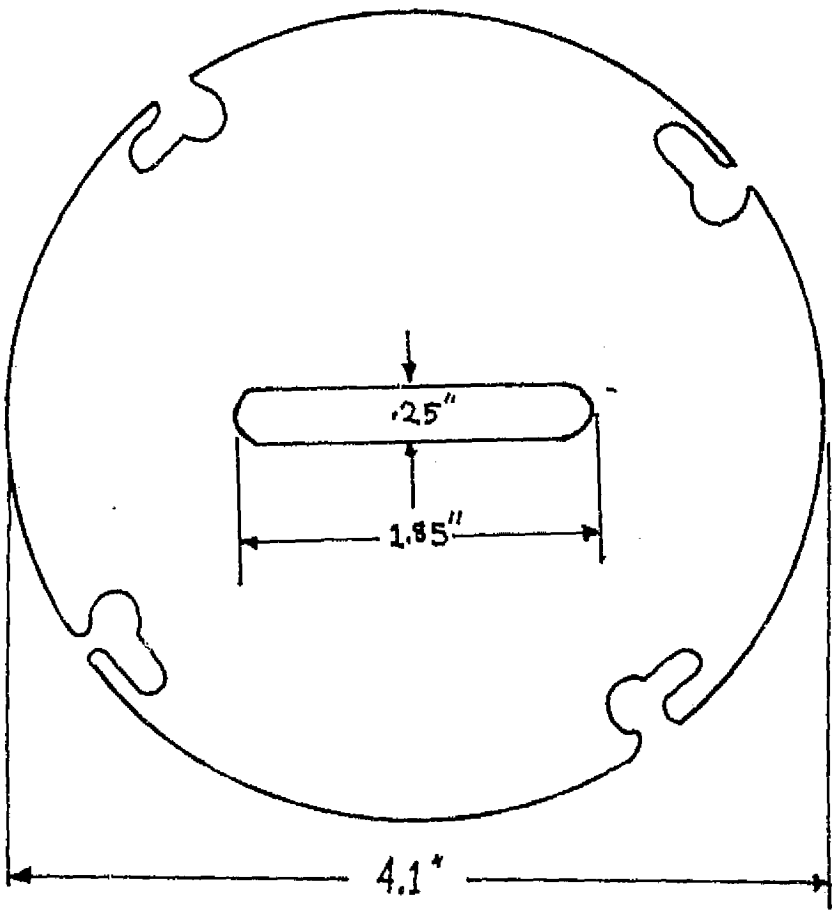

Figure 25. Narrow straight sided (NSS) heat shield.

NSS6 = 60 mil thick
NSS4 = 40 mil thick
NSS2 = 20 mil thick

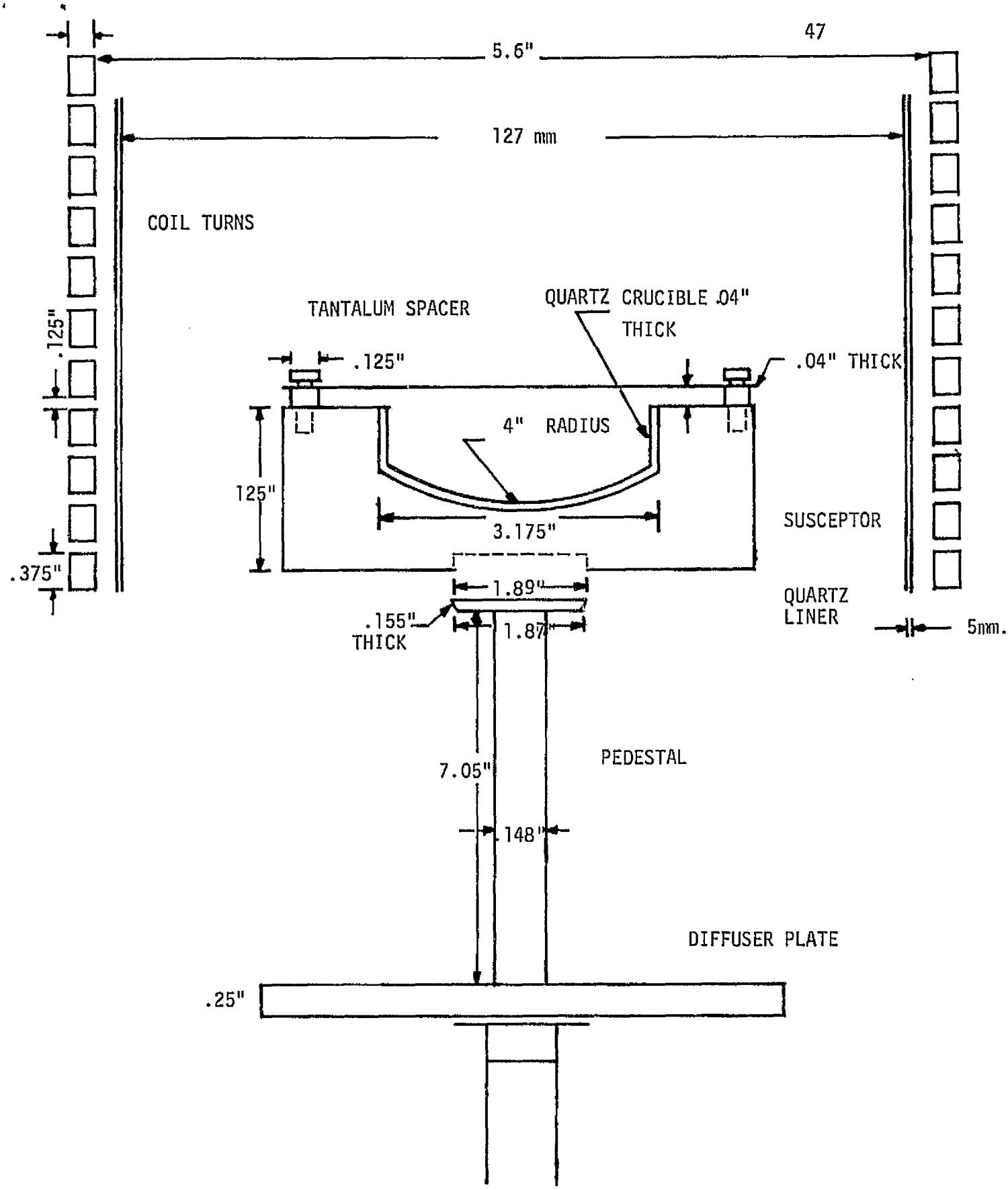

Figure 26. Initial arrangement of susceptor and pedestal in RF coil.

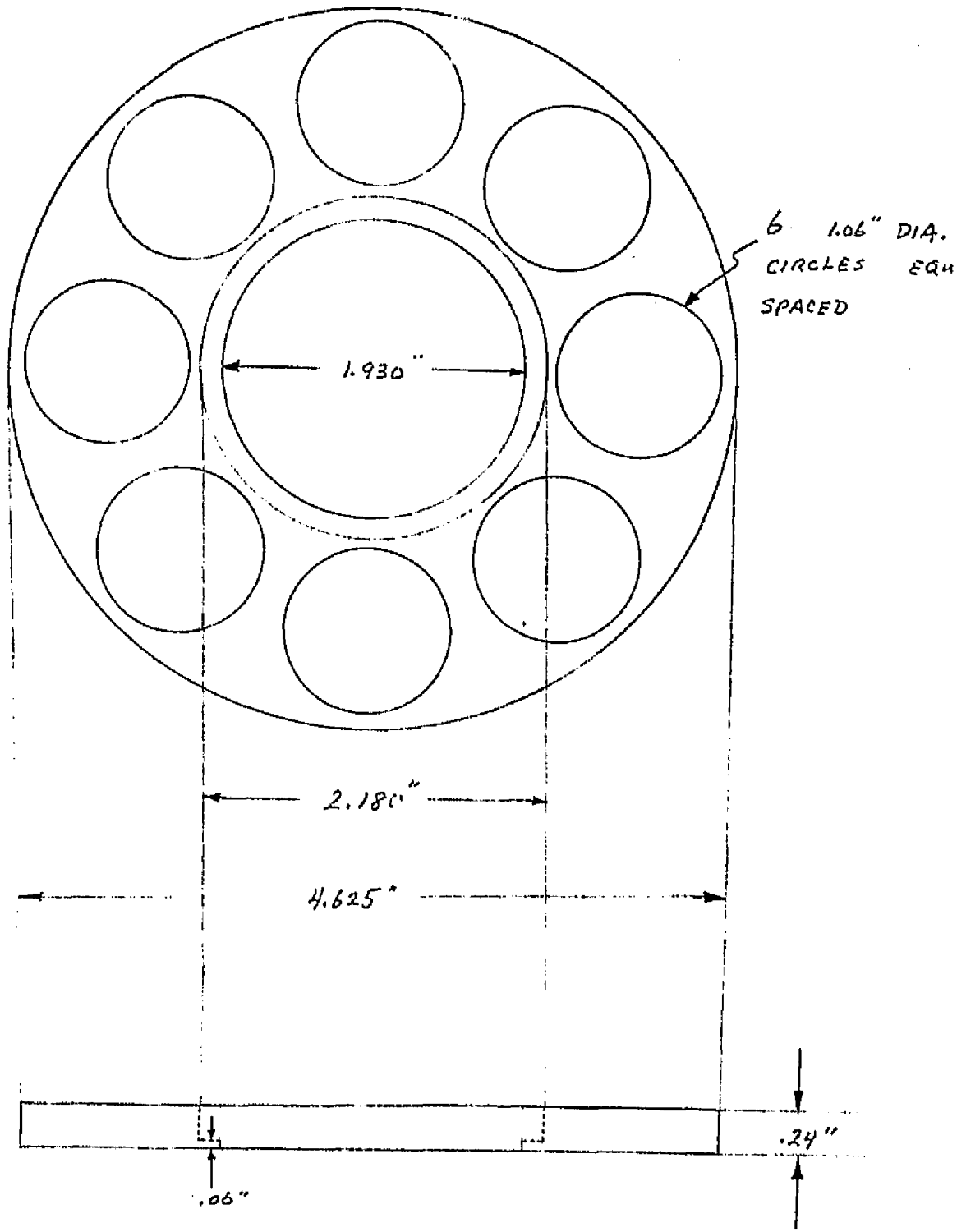

Figure 27. Molybdenum diffuser plate.

The pulling mechanism consisted of a steel tape attached, with nylon screws, to a take-up reel, 36" in diameter, upon which the webs or dendrites were wound during pulling. The seed was attached to the free end of the tape. Initially the seed on the tape was held by a stainless steel wire. Later chucks were designed and used as will be described in Section 4.2.3.2. The take-up reel was driven by a Servo-Tec variable speed motor through a Metron 600 to 1 reduction gear and an 8" drive wheel. The pull rate was measured for various settings over the range of the variac. The curve is given in Figure C-1 of Appendix C along with curves for modifications made during the contract. These modifications will be taken up in Section 4.2.

Proof that the furnace and generator were operational and ready for pulling dendritic web was obtained when 102 gms of Si were melted and 4 1/2 inches of small diameter Czochralaski ingot were grown. This run also showed, as did all runs after that, that the center of thermal symmetry was close to the geometric center of the crucible.

The furnace operation procedures used initially are given in Table D-1 of Appendix D.

4.2 Pull Nominal Web based on 1965

4.2.1 Dendrites

Once the web furnace had been proven operational, it was necessary to have the correct susceptor-heat shield setup and their placement in the r. f. field to give favorable vertical and horizontal temperature gradients for dendritic growth. Also the operators had to gain experience in seeding and growth of dendrites and webs. Although actual values of the temperature gradients must be measured with a thermocouple, one can find relative information on the thermal gradients at the surface by probing the melt with a seed and observing the shape, rate of growth, and symmetry of the buttons and wings formed. Information on the vertical gradients can be obtained by observing the growth behavior of dendrites being pulled at or near the geometric center. Probing the melt with a dendrite seed was used here to attain conditions for web growth. Later, especially starting in July of 1976, thermcouple data was taken for a "fine adjust", (i.e., more critical comparisions between set-ups).

The taper sided susceptor (TS, Figure 11) with the wide straight slot heat shield (WSS, Figure 24) had been used to prove the system operational as reported in Section 4.1 and thus was used at the start of obtaining conditions for dendritic growth. We did not vary the design of the susceptor but stayed with the TS susceptor. The initial runs with the wide straight sided heat shield gave rounded buttons that pulled free of the melt suggesting that the surface temperature was too cold. Thus a heat shield with a narrow straight sided slot (NSS, Figure 25) was made and used. This shield did overcome the "cool" surface temperature of the wide slotted one; however, it was difficult to get dendrites, and when they were grown it was not possible to sustain growth. The longest dendrite grown with this shield was 10 cm. During this period, the main concentration on shaping the thermal conditions was on the vertical temperature gradient (i.e. surface of melt to bottom of melt). The vertical temperature gradient study was done by raising

and lowering the r.f. coil. The coil position, CP, was varied from 5.45 cm to 10.45 cm (these values are the distance between the top of the coil and the top of the susceptor). This meant that since the coil that we were using was 13.2 cm high (see Section 4.1), and the susceptor is 3.18 cm high, the coil extended 7.75 and 2.75 cm respectively below the bottom of the susceptor. When the CP was around 10.45 cm, the bottom of the susceptor "saw" more of the outside; thus the temperature gradient (TG) was largest. This position was found to be not good because (a) if the surface temperature was correct for dendrites to grow, the vertical gradient was too high, and the dendrites would tend to freeze to the bottom, and (b) if the surface temperature was adjusted to give a reasonable TG, ice formed on the surface when the temperature was dropped to give the ΔT necessary for growth. On the other hand if the CP was in the vicinity of 5.45 cm, the TG was too low as a result of the bottom of the susceptor being more in the center of the coil. This was not good either because (a) if the temperature was adjusted (i.e. lowered) to give a reasonable ΔT, the surface would be too cold resulting in ice formation, and (b) if the temperature was not adjusted buttons formed would pull out with no dendritic growth. The optimum CP for this susceptor/heat shield appeared to be in the neighborhood of 8.45 cm.

The difficulty in obtaining dendritic growth with this setup caused us to measure the temperatures. At this stage we felt that measurement of the temperature of the surface of the melt, the heat shield, and the bottom of the susceptor by optical pyrometry would give us the information we desired. As can be seen in Figure 28 and in Table 3, the position in the area of a CP of 6 to 9 cm appears to be about right. Comparison of temperature readings across the narrow and wide straight slotted heat shields suggested that we were wrong in our initial assessment of the wide slotted heat shield. If we had varied the CP over the wider range before going to the narrow slot, we possibly would have gotten good dendrites earlier. This information lead us to go back to the wide shield where we were able to sustain dendritic growth for 50 cm at a CP of 8.45 cm.

From this time on until the end of the dendritic portion of this task, we kept the susceptor/heat shield set up the same and at the same CP and concentrated on seeding techniques and pulling dendrites. This was necessary (a) to check out our pulling and guidance system in actual pulling, (b) to build up a good supply of seed material, and (c) to train our operators in seeding and growth. The "transient seeding" technique was used. The procedure for this technique consists of:

1. Find growth temperature. The growth temperature is taken as the temperature at which a button begins to grow.

2. Raise the melt temperature 15 to 20° above the growth temperature. Dip seed into the melt to melt off end.

3. Reset temperature controller for the "growth temperature".

4. As temperature of melt drops, the seed is dipped into the melt at 5 to 7° above the "growth temperature" to the seed.

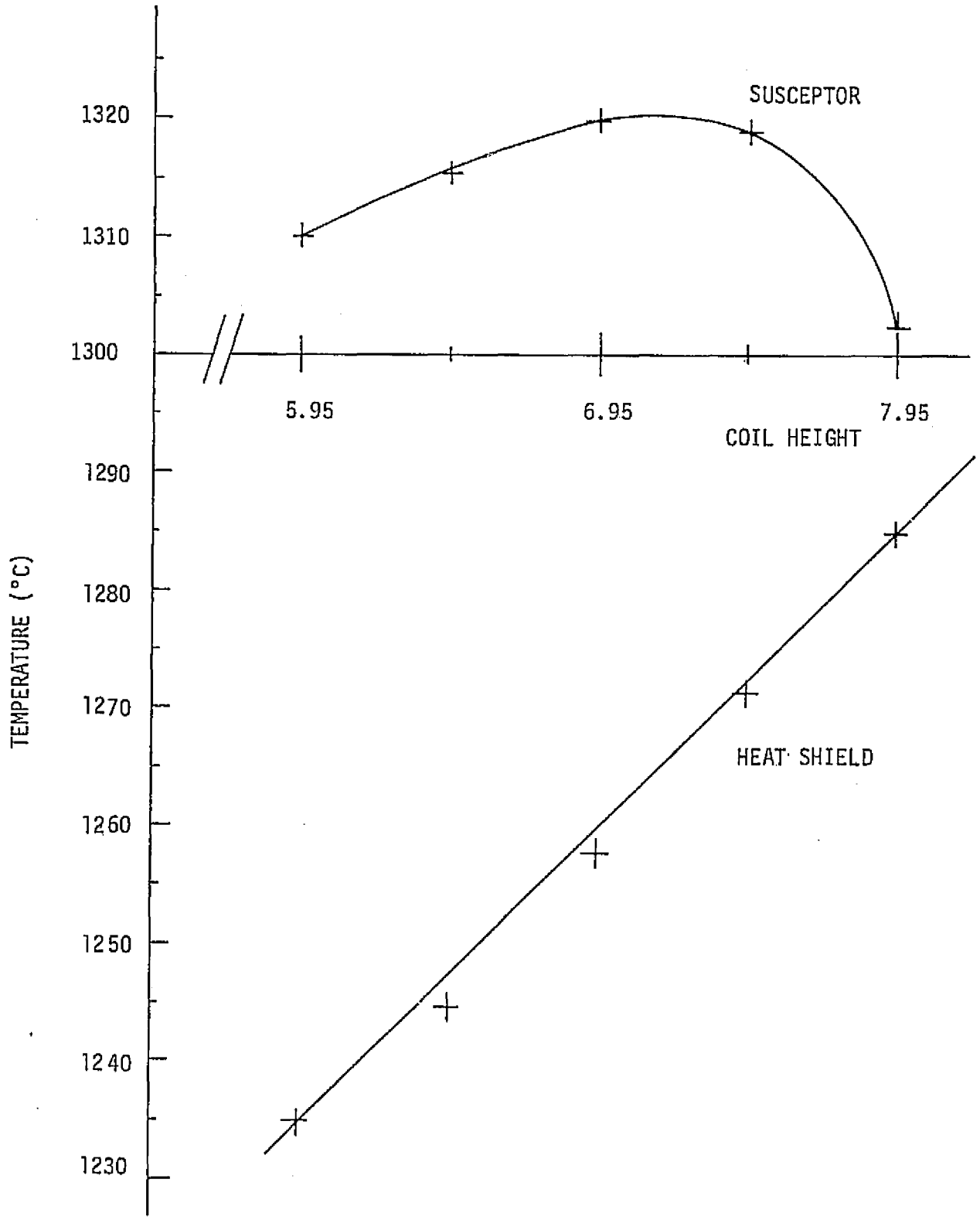

Figure 28. Heat shield and susceptor temperatures in coil height. Temperature readings were taken on the bottom heat shield at a distance of 1/3 the shield diameter from the center.

Table 3. TEMPERATURE DIFFERENCE BETWEEN HEAT SHIELD AND SUSCEPTOR BOTTOM AS A FUNCTION OF COIL POSITION

Coil Position* (cm)	Temperature Difference (°C)
5.95	73
6.45	69
6.95	65
7.45	51
7.95	22
8.45	41
8.95	22

Note*: Distance between the top of the coil and the top of the susceptor.

The transient seeding technique was used initially because of (a) the difficulty in setting temperatures, (b) the apparent fluctuation while trying to hold the melt at a constant temperature, and (c) the under or over shooting of the temperature after the temperature was changed. This technique was used while we were tracking down the causes of the temperature variations and then while we were constructing an interface.

The technique was successful for seeding, but in itself lacked reproducibility. Also it was very difficult to sustain growth of web.

5. As melt temperature drops further, button growth begins. When wings form on button, pulling is started at 80 - 100% on the speed controller (this corresponds to 6 to 7 cm per min.).

6. As soon as the button starts to rise, decrease pull speed to that for web growth unless it is desired to pull only dendrites - in which case do not change the pull rate.

During these runs, a number of things that had to be changed before we could hope to achieve web growth became evident. (1) It was found that buttons could get caught on the guide fingers which had only fine control and no way to swing them out of the way quickly as the buttons were pulled up. The control rods holding the fingers were modified to give a fast swing in addition to the fine control. (2) Several buttons caught on the chimney. This was eliminated by splitting the chimney about 1½ inches from the end and belling it out. This had the further advantage in that the chimney could then act as another guide if necessary. (3) Another problem was control of the temperature. We had been operating the furnace by manual control using the Ircon controller only for reading the temperature of the susceptor. This mode of operating was too slow and did not allow precise temperature control. Thus an electronic interface was designed that would enable the automatic controls of the Ircon controller to be used. On the first run using the interface we grew 50 cms. of very narrow web. On our next run we were able to "sustain" growth and pulled a piece of web 45 cms. long, and a dendrite 1.2 meters long.

We also found in this stage the importance of having the end of the seed, that goes into the melt, very narrow.

4.2.2 Webs

The webs mentioned above were not only very narrow but also they had not formed from the initial button but from a button formed on one of the dendrites that grew from the initial button. The second phase of this task then was to perfect the conditions favorable for growth of webs with the 1965 specifications. This called for a more careful and detailed look at not only the vertical TG but also the horizontal TG. To this end, in addition to the position of the coil relative to the melt (i.e., designated as CP), the shape of the susceptor and the shape of the opening in the heat shield were studied. Also two ways of affecting vertical heat loss were examined - (a) thermal insulation between the susceptor and the pedestal, and (b) after heaters on the heat shield. Each change generally meant varying the CP to optimize it for the new setup; this usually took a week. Initially the setup that was used was the one with which we had gotten the web, mentioned in 4.2.1, namely the tapered sided susceptor (TS, Figure 11) and the heat shield with the wide straight slot (WSS, Figure 24). Since we

had looked strongly at the vertical TG in Section 4.2.1 and since the web grown at the end of that stage was very narrow, it was decided to investigate the horizontal TG by changing the slot opening in the heat shield to lower the horizontal TG and induce the edge dendrites to spread apart. The first change involved putting holes at the ends of a narrow straight slot to form a "dog-bone" (SDB, Figure 29). As expected, the horizontal TG was flattened out; however, no improvement was seen in web widening. Comparison of the straight sided slot to the Dog-bone slot from thermal calculations bear out our finding as can be seen in Section 3.2.3. It appeared that the straight part of the slot was too long, at least for the present webs. In an attempt to correct this, a taper was put in the dog-bone (TDB, Figure 30). This did not seem to help. We were still having difficulties with the vertical TG. All indications were that, although we were in a favorable CP, the gradient was still too large.

Looking then at the susceptor, it was apparent that most of the r.f. coupling was taking place at the lip of the tapered susceptor and that most of the heat at the bottom came from conduction. Thus a large vertical ΔT may be expected and attempts to rectify this by CP would be tricky. We then tried a straight sided susceptor (SS, Figure 12) with the thought that r.f. coupling would take place evenly up and down the sides resulting in more heat generation at the bottom and thus a lower vertical TG. These thoughts were borne out in heat transfer studies (Section 3.2). It was quite evident that the vertical TG had been drastically lowered, in that the coil had to be raised 1 to 2 cm to get growth. The next attempt to lower the vertical TG was to retard the heat loss from the susceptor to the pedestal by use of Al_2O_3 spacers between the susceptor and the pedestal. Optical pyrometer data was taken on this setup, Figure 31, which showed that to be the case. Since the Al_2O_3 spacer is not a complete thermal insulator, two thicknesses were tried; however, one spacer broke before this setup could be evaluated. Another method to lower the vertical TG was to use afterheaters, Figure 32, on the heat shield. The idea here was to retard the loss of heat from the opening in the heat shield and to keep the web hotter after it had left the heat shield, and thus reduce the heat loss by conduction up the web. Thermal modeling of the ribbon will be found in Section 3.1. It was found that these afterheaters were too long and too tall. Their height made it impossible to view the button growth in the most crucial stage. Furthermore SiO built up on them badly, interfering with growth, and was loose and had a tendancy to drop into the melt.

In all of the changes made in this stage (i.e. from 2 Feb. to 28 April 1976), some webs were grown. These were invariably multidendrite webs, or webs that grew from buttons formed on one of the grown dendrites. Finally toward the end we were getting good buttons with 2 dendrites, but the web fell out before it could solidify. The attack on this problem will be taken up next in Section 4.2.3. We were also losing webs and dendrites through jerking and vibrations. Some of this was caused by accidental jarring by the operator when adjusting the pull tape or control figures and part was mechanical and thermal. We noticed that the center of thermal symmetry

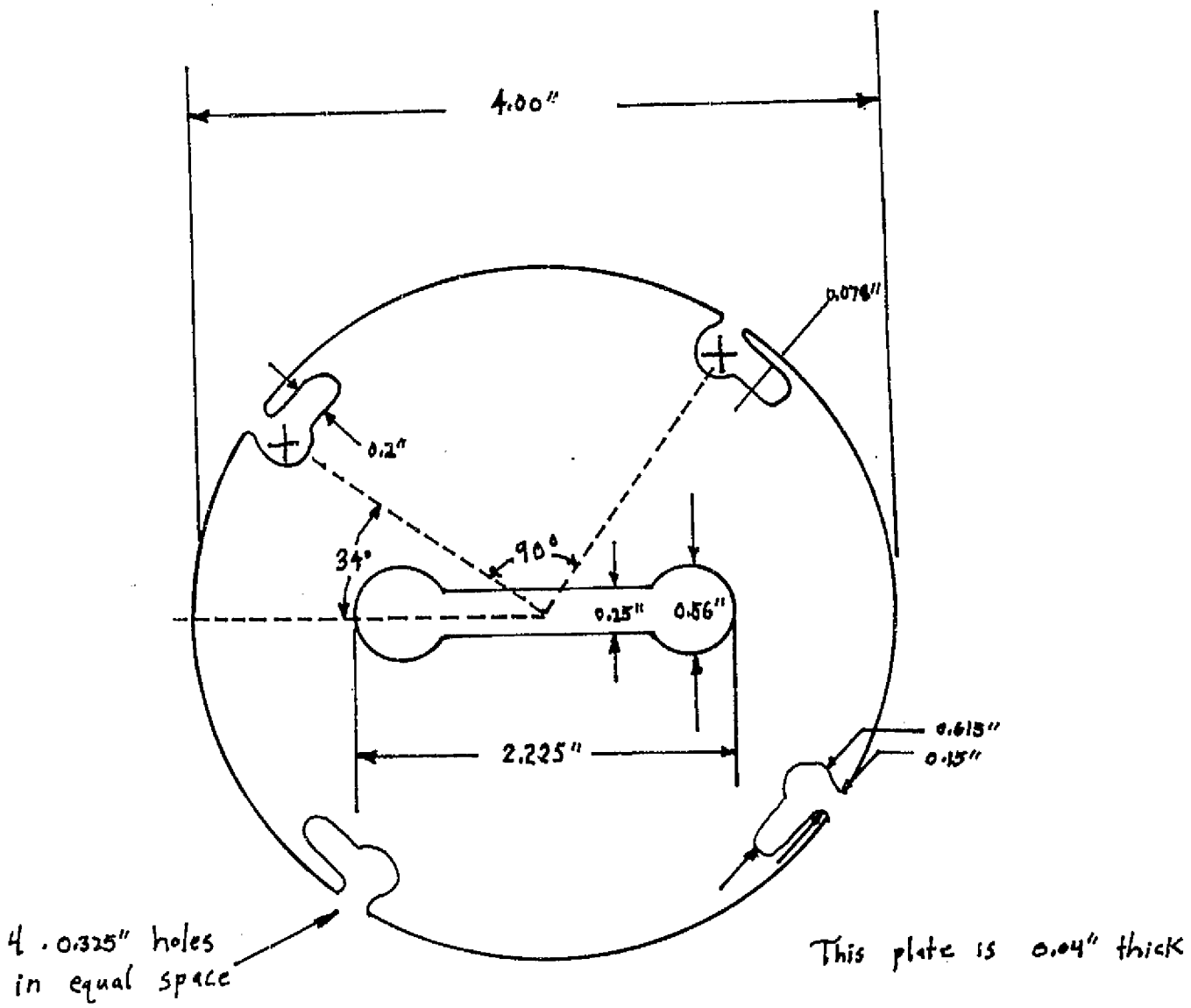

Figure 29. Straight dog-bone (SDB) heat shield.

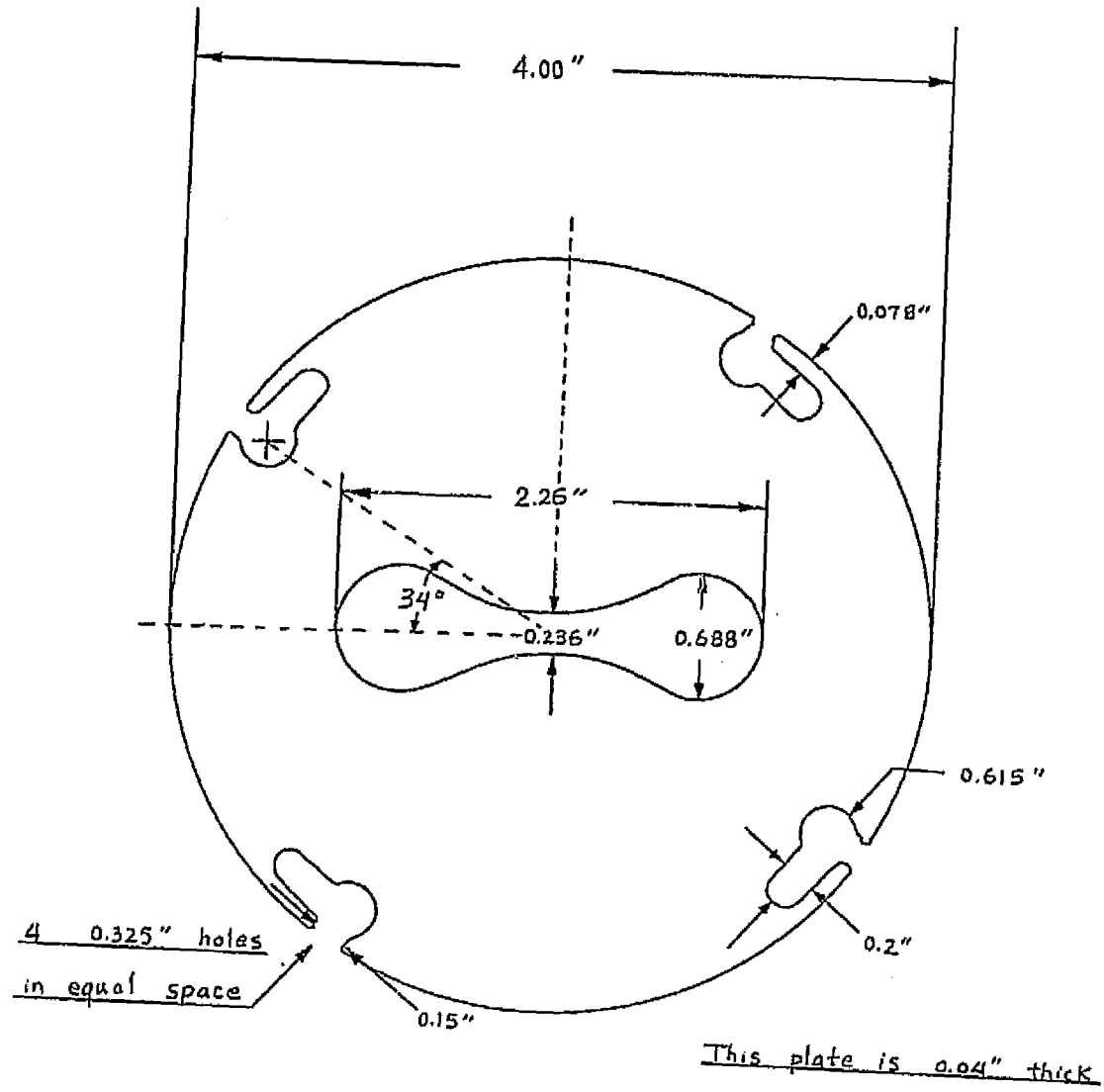

Figure 30. Tapered dog-bone (TDB) heat shield.

4" STRAIGHT SIDED SUSCEPTOR

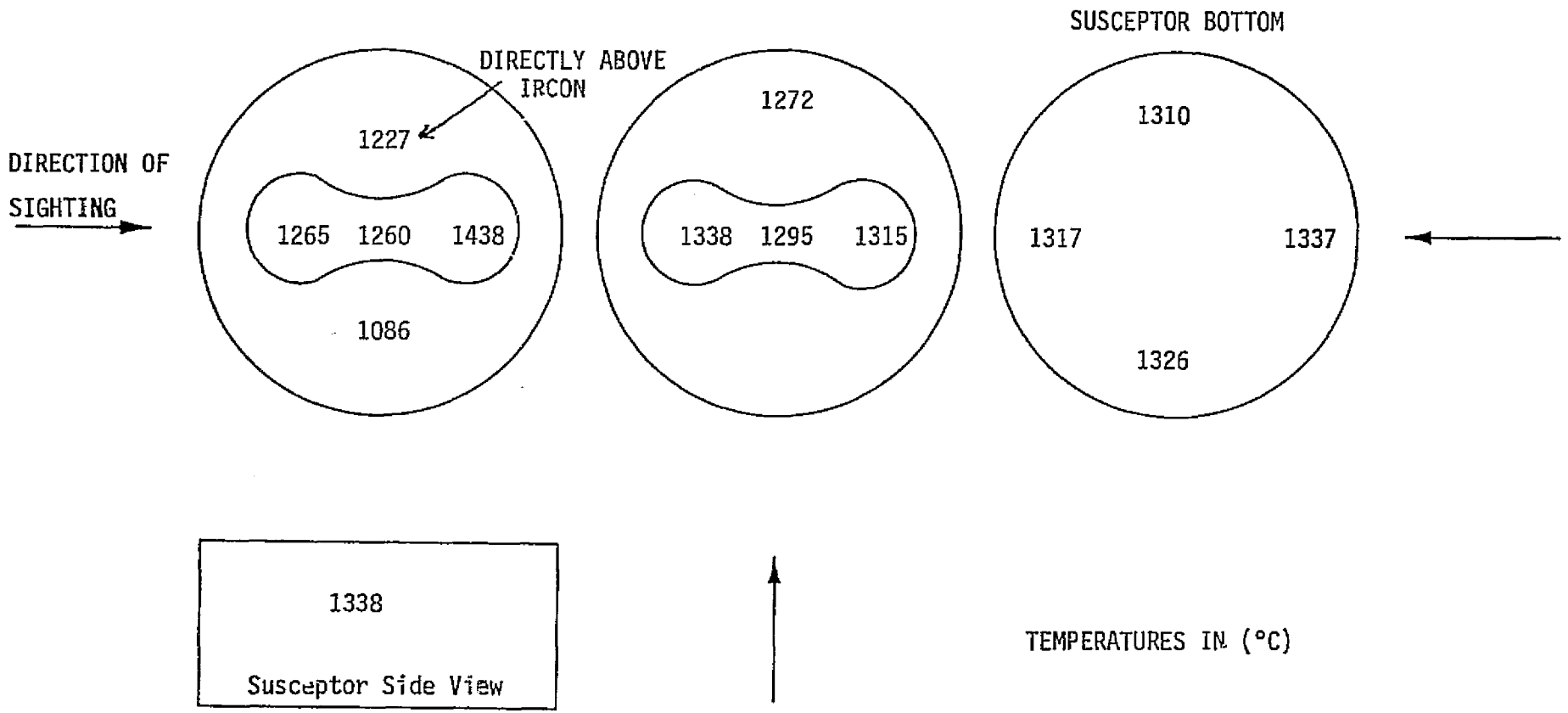

Figure B1. Optical pyrometer data taken on SDB/SS with Al_2O_3 spacer on pedestal. Readings were taken at locations indicated by temperature readings.

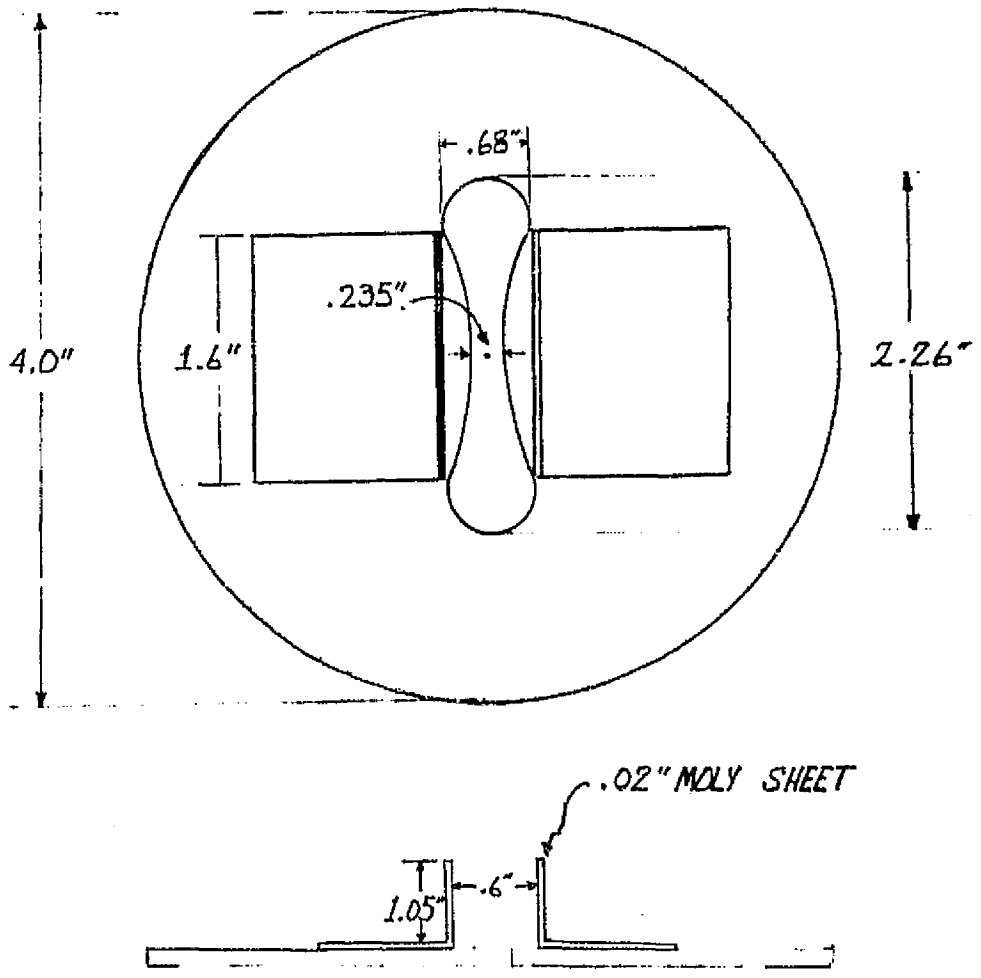

Figure 32. Afterheater arrangement.

was invariably to the left of the geometric center. In the case of the taper sided susceptor, part of the problem was found to be that a piece of the molybdenum lip had chipped out around one hole for the tantalum pins that held the heat shields. A new susceptor was made. Thermal symmetry, however, was also to the left on the TS susceptor. It became obvious that an x-y movement for the coil was vital. One was built and used. We had also noticed that the coil was not fixed rigidly enough in the mount and would occasionally twist - especially when we raised and lowered the coil drastically. Thus when the x-y motion was installed, the coil mount was altered to hold the coil rigidly in place.

Another thermal problem was control of the temperature; we were getting fluctuations. Part of the problem was that our temperature meter could not be read with enough accuracy. Replacing it with a digital readout solved the problem. At the same time we replaced it, we reset the controls on the Ircon controller more precisely. Early in this stage, we had trouble with the melt pulling to the front of the crucible so badly that we could see the bottom of the crucible at the back. Tilting the table with the vibration isolation legs appeared to be of some help; however, sandblasting the inside of the crucible eliminated the problem. Thus sandblasting was incorporated into our loading routine.

The drive wheel for the take-up reel that we had used up to the start of this stage had been 8" in diameter. This gave pull rates from 3 to 14 cm/min well within the pull rates for dendrites but above the range for webs. We had used this, however, since this was the desired range for webs for our goal. It became evident, however, that we would have to work first with slower pull rates. Thus a 4" drive wheel was made and installed. This gave us a pull rate range from 2 to 6 cm/min, see Figure C-1 in Appendix C which covered the top of the web and bottom of the dendrite ranges.

During this stage, primitive dendrites were grown to obtain seeds with other twin spacings. This will be taken up in the following section.

4.2.3 Web Fallout

Although the studies reported in Section 4.2.2 led to web, the web was narrow and invariably grew from a button that had grown on one of the two growing dendrites rather than starting directly from the button that grew on the seed. The silicon that had been pulled up with the initial button dropped free, for the most part, before it could solidify into a web. This led us to believe that the space between the surface of the melt and the bottom of the heat shield, or the heat shield itself, was too hot. Thus, in addition to continuing the studies to improve the vertical and horizontal temperature gradients, our attention was turned to the heat shield and the space above the melt.

4.2.3.1 Thermal Aspects

4.2.3.1.1. Parameters Affecting Temperatures Above Melt

Figure 33 shows the various parameters investigated during the course of these studies to control the temperature between the surface of the melt and the heat shield. The effect of ε, the emissivity of the underside of the top heat shield, was reported in Section 4.2.2. Some effect had been expected - see for example equation 1 in Section 3.2.2; however, the effect was much greater than we had anticipated. The effect of the other parameters are given below:

1. Crucibles: The shape, height, wall thickness, and variation in the wall thickness of the crucible are all very important. The second batch of crucibles that we ordered were too tall, so much so that when placed in the susceptor they touched the heat shield. This situation appeared to keep the region above the melt too hot in that we had to change the CP by 3 cm to correct for it, and then had difficulty in controlling growth. It was necessary to shorten the crucibles by 1/8" to get normal results. We have reported the shift in the center of thermal symmetry from time-to-time. This was shown to occur whenever we had a crucible that did not fit snugly and evenly in the cavity of the susceptor, F in Figure 23, (this was by no means the only cause of shifts in thermal symmetry - others have been mentioned already or will be mentioned later in this report). We also found that if the wall thickness of our crucibles exceeded 50 mils we were not able to melt the silicon. Finally, we found a direct correlation to wall thickness variation, t_v, and the center of thermal symmetry. Thus it is exceedingly important to have very tight specifications on the crucibles; far more exacting than for other melt growth techniques and more exacting than was considered for web growth in the 1960's.

2. Open space between heat shield and susceptor: As mentioned above, the tall crucible blocked the loss of heat from this opening. To get the surface of the melt at a lower temperature for growth, it was necessary to lower the susceptor in the coil because we were working below the center of the coil at that time. Toward the end of the work for this section, we found it necessary to work with the susceptor above the center of the coil as will be described in the paragraph on C.P. (coil position). When we first moved to the top of the coil, we experienced icing from the periphery of the melt. In an effort to overcome this, the four tantalum pins that held the heat shield above the susceptor were replaced with a solid annular molybdenum ring in an effort to retard heat loss from the opening. The result was the same as in the case of the opening being closed by a tall crucible. Heat was indeed held in; however, since we were working toward the top of the coil, it was necessary to raise the susceptor in the coil to obtain a lower surface temperature. This in turn caused icing. Thus it seems quite obvious that for the system shown in Figure 33, there must be an open space between the heat shield and the susceptor.

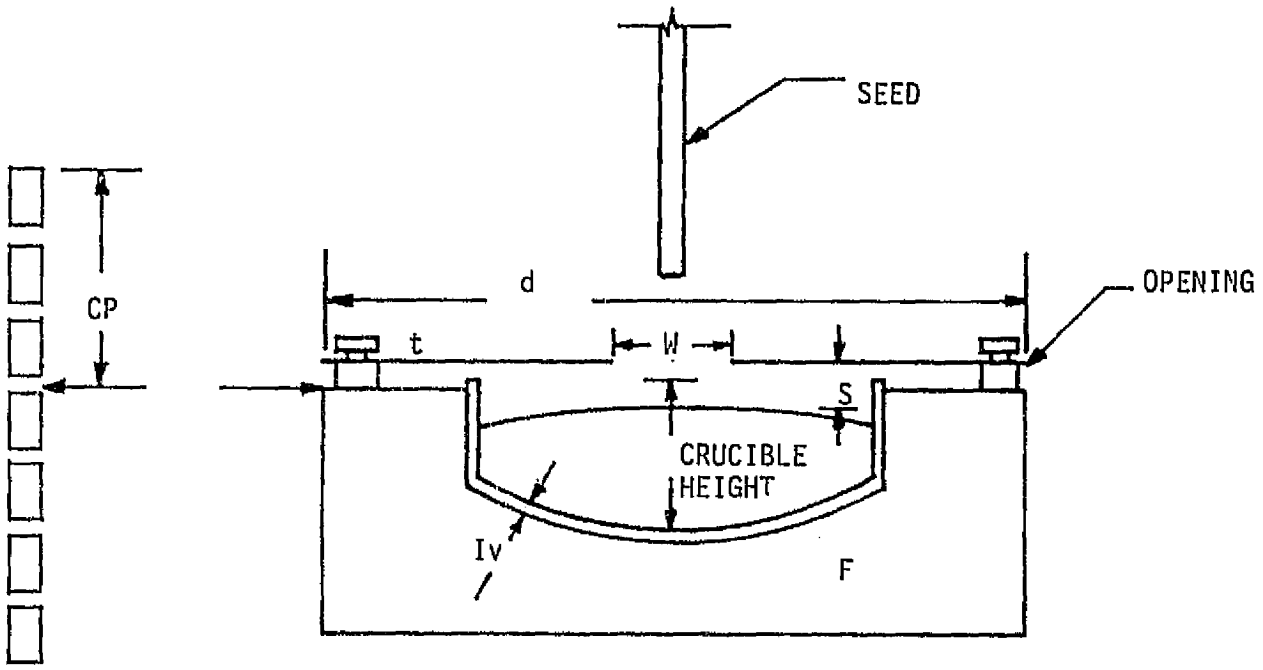

Figure 33. Parameters involved with temperature of the space between the surface of the melt and the bottom of the heat shield.

3. Coil Position (CP): We have already discussed, and will continue to discuss, the effects of changes in CP in our studies since it is the easiest and most direct way of changing the temperature of the surface of the melt. During the first eight months of pulling, the susceptor was varied in the bottom half of the coil. Initially we had the susceptor in the center of the coil and found that the vertical temperature gradient (TG) was uniform (see Section 4.2.4.) When the coil was aised, it was possible to change the vertical TG and the surface temperature enough for growth. On the other hand, lowering the coil, even to the maximum (this still left the top of the susceptor several centimeters from the top of the coil), did not appear to help. Thus we worked in the bottom half of the coil.

It was not until we added two inches to the pedestal that we could get the top of the susceptor up high enough in the coil to show that working near the top of the coil gave us much better control over the melt surface temperature and the vertical TG than working in the lower half of the coil. The effect of the coil position on the temperature of the heat shield, and the temperature of the space between the heat shield and the surface of the melt (as evidenced by the temperature difference between the surface of the melt and the top of the heat shield above it) was seen from the optical pyrometer data. For example Table 4 shows the top heat shield to be approximately 200° cooler at the edges and approximately 100° cooler in the center when the susceptor is raised 2 cm from a CP (i.e., distance between top of the susceptor to the top of the coil) of 7.05 cm. Raising the susceptor also gave a less drastic gradient from the edge of the heat shield to the center; CP 5.05 cm gradient was 90°, CP 7.05 cm was 230°. The temperature difference between the surface of the melt and the top of the heat shield can be illustrated by Figure 34 where the heat shield to melt TG was 106° at a CP of 3.55 cm. Raising the susceptor in the coil one cm, increased the TG to 139°; and raising 1/4 cm more, increased the TG to 161°.

4. Height of heat shield above melt, S: It was felt that if the level of the melt was high enough, it would be possible to pull the button through the heat shield where the molten silicon could solidify into web before it fell under its own weight. To test this, 164 gms of silicon were used. Also the heat shield was placed directly on the susceptor. This put S at approximately .4 to .5 cm rather than 1.4 cm that we generally had used. This appeared not to help; in fact the buttons were poor. In view of the discussion in 3. above, it now appears that our negative results were the result of not having an open space between the susceptor and the heatshield.

In Section 3.1.5, it was reported that the thermal modeling studies predict a relationship between the pull rate and S; as S increases the pull rate decreases. Our studies did not confirm this, but our studies were only preliminary, and it is felt that more experimental work in this area should be done. In one of our studies to see the effect of S on the temperature above the melt, a heat shield (NSS, Figure 25) that had bowed in the center was used with a 100 gm melt. For this size melt, S was approximately 1.4 cm; however, with the shield concave upward S in the center region was approximately 1.8 cm and with the shield concave downward, S was approximately 1.0

Table 4. THE EFFECT OF COIL POSITION ON THE TEMPERATURE OF VARIOUS LOCATIONS ON THE TOP HEAT SHIELD[1] AND THE SIDE OF THE SUSCEPTOR MEASURED WITH AN OPTICAL PYROMETER.

Position on Heat Shield or Susceptor Wall[2]	Temperatures (°C) for coil Positions (cm)	
	7.05	5.05
1	1338	1187
2	1143	1065
3	1160	1071
4	1316	1115
5	1393	1160
6	1304	1168
7	--	1154
8	--	1221
T	1254	1282
M	1299	1281
B	1307	1326
H	--	1332

Notes: 1. Heat shield LDBeW (Figure 17) was above an LDBeW shield 1/4" thick. The SS (Figure 12) susceptor sat on the Al_2O_3 pedestal with one Mo bottom shield.

2. Measurements were made at points indicated by numbers or letters on the sketches.

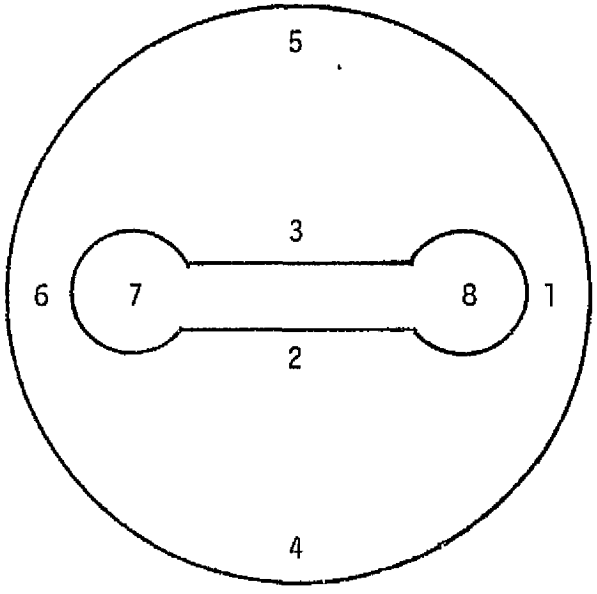

Heat Shield (Top)

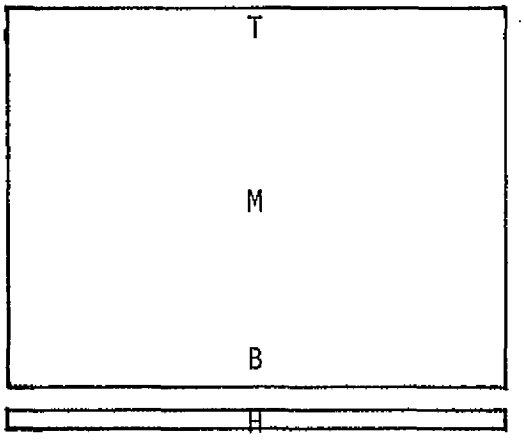

Side View of Susceptor and Bottom Heat Shield.

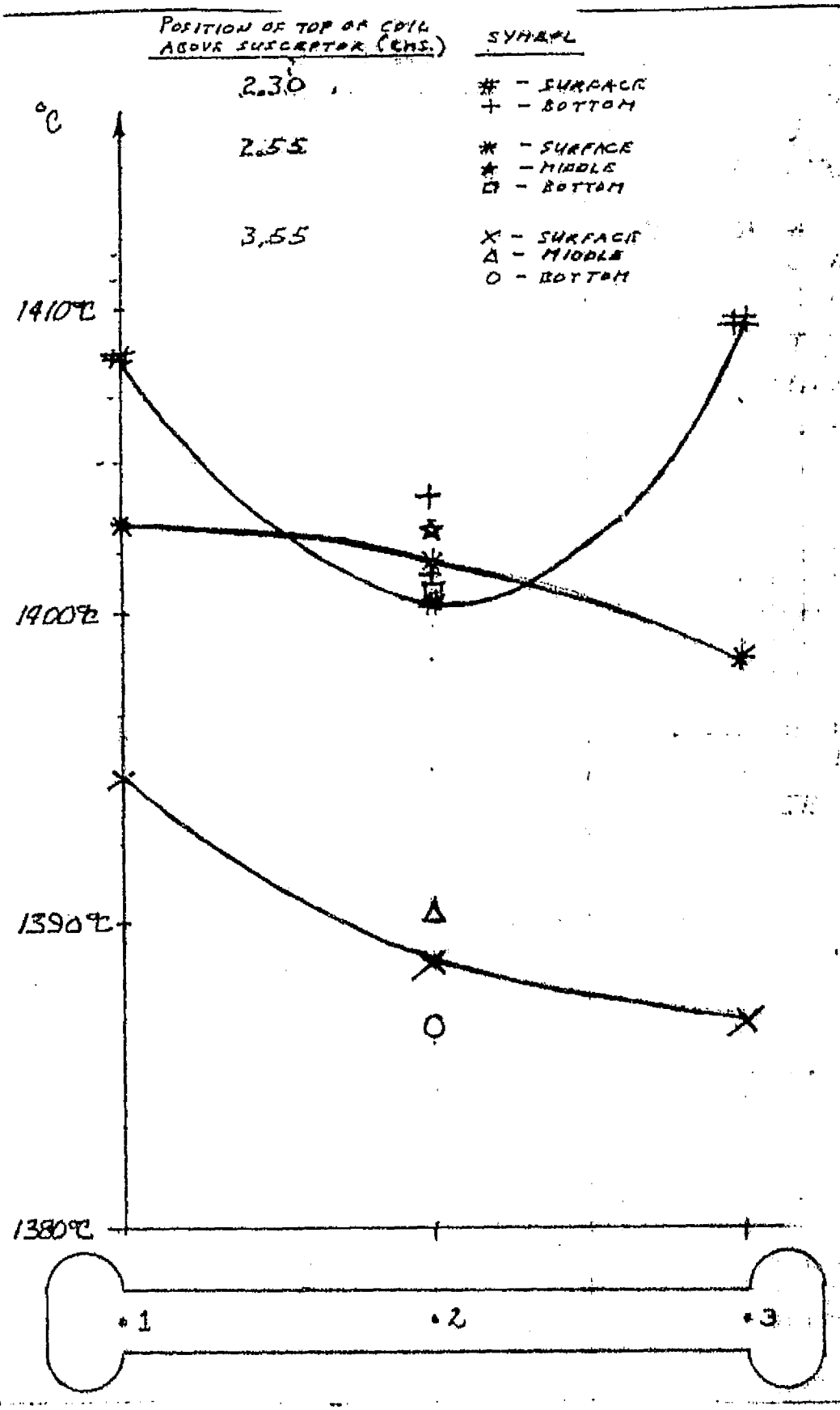

SET-UP: .06" X 4" TOP SHIELD LDBeW
1.25" X 4" SUSCEPTOR SS
.025" X 3.85" BOTTOM SHIELD MOLY
CERAMIC PEDESTAL

Figure 34. Thermal profiles in melt for various coil positions.

cm. Although we can say nothing from our pulling data about the effect of S on the pull rate, it is quite obvious that there was an effect on the temperature. For S ≈ 1.0 cm, the vertical TG was too great, necessitating lowering the coil from .2 to .4 cm below that necessary for S ≈ 1.8 cm. Since we were working in the region below the center of the coil, lowering the coil results in a decrease in the vertical TG.

5. Ar flow: In the thermal modeling, Section 3.2.2, it was reported that the contribution of convective heat flow to the Argon was so much less than radiation losses that it could be neglected. Thus it is not surprising that varying the Ar flow rate from 25 to 50 cph gave no effect on surface temperature. It did, however, have an effect on the oxide build-up. The 50 cfh is definitely recommended for purging the system during melting. Flow rates between 25 to 35 cfh, however, are recommended after the charge for the day has melted.

6. Seed: Although the desire to remove heat from the button to encourage the molten silicon drawn up between the dendrites to solidify would suggest having seeds with large cross-sections, this is definitely not what is wanted during seeding. The larger the cross-section of the seed, the more heat is conducted up it from the melt. Thus a large seed gives a greater radial ΔT than desired, resulting in a larger button, if not an irregular button, which in turn gives erratic growth. The cross-section of the seed should be as small as possible; not only does this help control the ΔT but also keeps the button small, and aspect ratio large which has been found necessary for good yields of web.

7. Heat Shields: The finish of the heat shield in regards to ϵ has already been taken up. The role of the width (W) of the opening on the heat shield to the temperature of the surface of the melt and the temperature above the surface of the melt was alluded to in Section 4.2.1. It was pointed out there that heat was retained when a narrow straight slot (NSS) was substituted for a wide one (WSS). The width of the opening in the heat shield, however, is intimately associated with the length and shape. Since the opening (width, length, and shape) in the heat shield is used primarily to shape the surface isotherms, the width effect will be taken up in another part of this section. Three other factors that could influence the temperature of the heat shield, and thus the temperature between the heat shield and the surface of the melt, were investigated; these were:

a. Diameter (d) of the heat shield: All heat shields had been cut to the same diameter as the susceptor - namely 4". It was quite evident, from the color shading of the shields, that the periphery of the shield was coupling with the r.f. This was borne out by optical pyrometer data. It was found that, for the same type of shield opening, the 4" diameter shield had a higher TG between shield and melt than did the 3.885" diameter shield (the temperature of the melt surface in each case was approximately the same).

b. Thickness (t) of the heat shield: The first shields that we used at the beginning of the contract, see Section 4.2.1, were 40 mils thick. It was found, however, that after a few days the shields began to bow and after a week or two were too bowed for use. Thus all shields after that were made from 60 mil thick sheet - these held their shape on prolonged usage. Since only the periphery of the shield receives heat through coupling with the r.f., the center of the shield receives its heat from conduction through the sheet and from radiation from the melt. In our studies to reduce the temperature in the interior of the shield, we looked again at thinner shields as a way to reduce coupling at the perifery and conduction across the shield. Shields made from 40, and even 20, mil thick sheet did not, however, show any noticeable change, over the 60 mil shields, in our seeding and growth; although there did appear to be a slight decrease in temperature by visual observation. We did, however, run into the bowing problem with the 40 and 20 mil thick shields. It was particularly bad with the 20 mil thick shields which lasted only a run or two. Looking, however, at thicker shields, we found that using a 60 mil thick shield, the TG from the periphery to the opening of the heat shield was approximately 190°, while a 1/4" thick shield with a 60 mil shield above it, see Table 4, the TG was only 90°. Thus the thicker undershield lessens the temperature drop to the opening. It should be pointed out that the temperature drop across a 45 mil shield was predicted to be 270° from the thermal modeling studies (Section 3.1). This is far greater than any drop found experimentally for any configuration.

c. Number of top heat shields: The effect of two top heat shields on the temperature above the melt was investigated. To test this heat shield LDBeW (Figure 35) was used in the regular position, a heat shield with a larger opening LDBeWM2 (Figure 36) was positioned 1/8" above it. This arrangement gave no improvement. Then two heat shields - both LDBeW - were used, but again we found no improvement. Later two heat shields with the LDBeW opening were used - the one nearest the melt was 1/4" thick and the one above it 60 mils. Runs were also made using only one or the other of these shields. The thermal data one should compare for the effect of these shields on the shield temperature and the temperature of the space between the top heat shield and the surface of the melt, are just that temperature difference. The data is given here in Table D-2 of Appendix D. The heat shield to melt TG is measured with an optical pyrometer and thus one can expect, and finds, variations in the data; however, there is enough difference to be able to compare the effects of the shields. Examining this data at the same CP, one can see that the TG for the 1/4" thick shield alone is less than that for the 60 mil thick shield alone as would be expected from our discussion on the thickness of the heat shields where we compared the temperature across the heat shields from the perifery to the center. Thus the thicker 1/4" shield is hotter at the center giving the expected low TG. This more uniform temperature across the 1/4" shield, then lessens the temperature drop at the center of the 60 mil shield when they are used together and gives an intermediate TG as can be seen in Table D-2, the 1/4" shield and the two

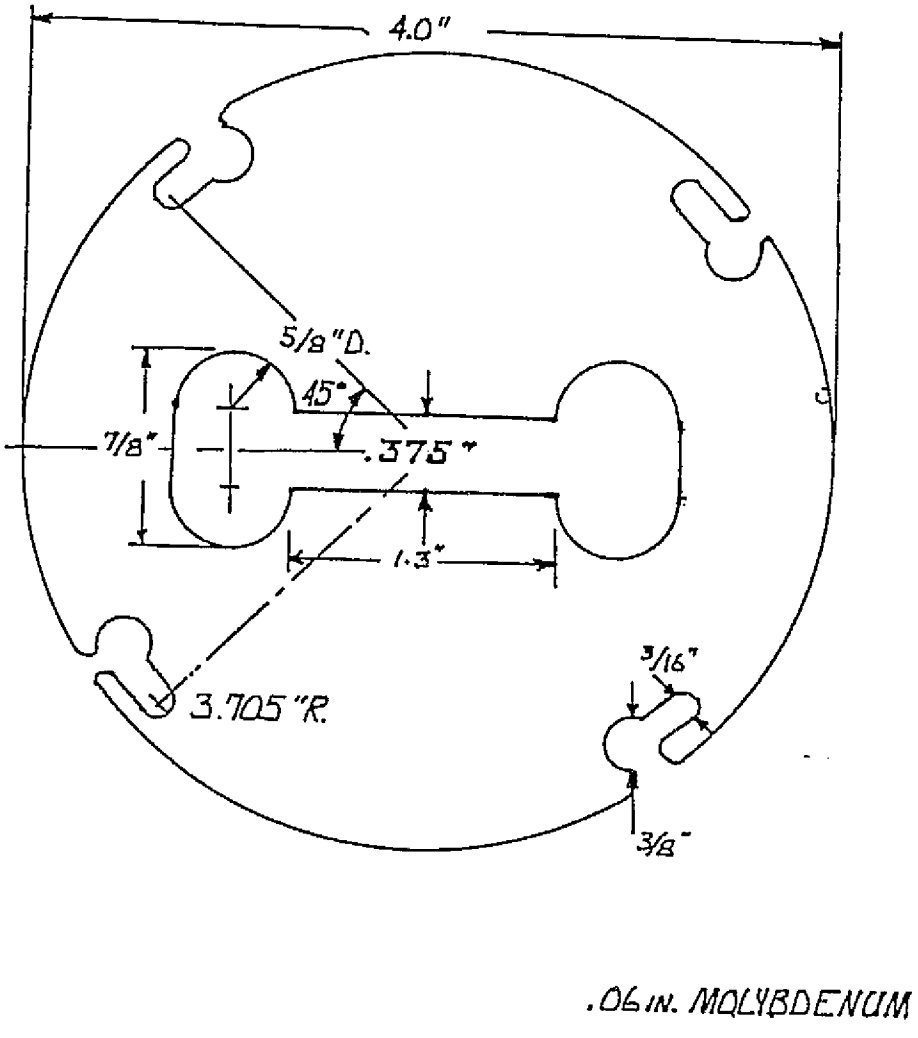

Figure. 35. Long dumbbell with wide slot (LDBeW) heat shield.

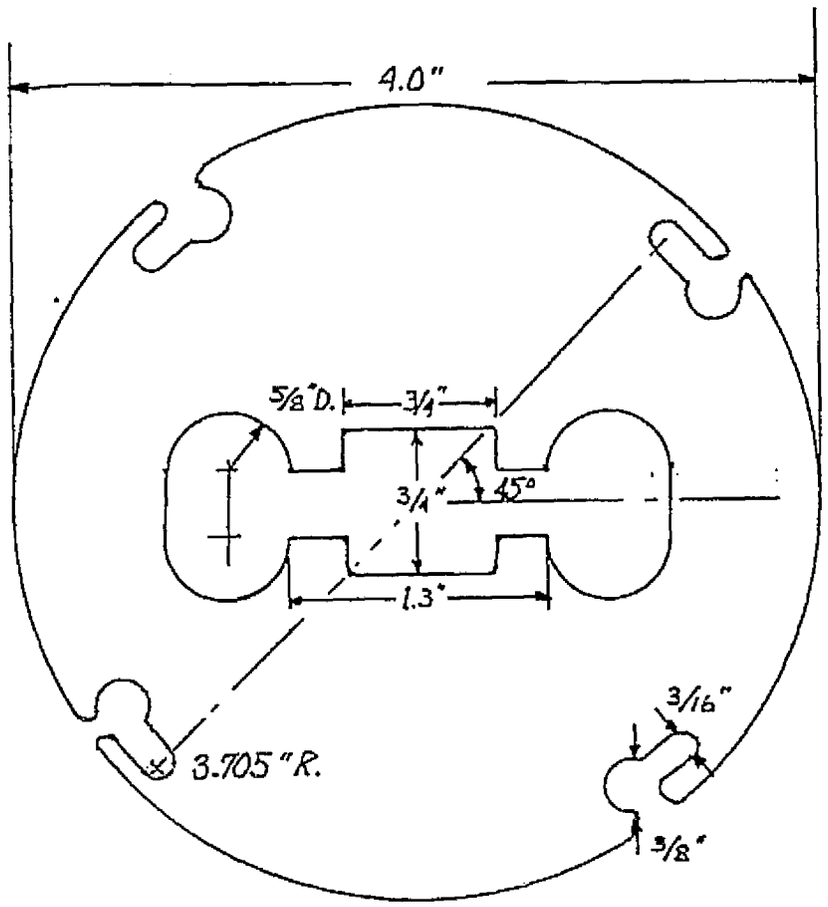

Figure 36. Modification 2 of LDBeW heat shield. LDBeWM2

together give a very small temperature gradient across the slot in the melt. It was for these reasons and the fact that we had no improvement in seeding or pulling web that we discontinued work on the number and thickness of the top shields. At the end of this phase of the investigation we had settled on one top shield, 60 mils thick, and studied the changes caused by different openings.

4.2.3.1.2 Shape of Thermal Gradients

The shape of the thermal gradients - both horizontal and vertical - are vital to the successful growth of web while the horizontal gradients are far more important in the widening process. Figure 37a, shows the desired temperature isotherm across a melt for a growing web. This gradient, if present initially would only be of use if one could seed directly from a web of the desired width - something that has not been possible to do, as yet - at least routinely. The correct growth isotherm results from the proper balance between an initial isotherm such as Figure 37b, and the heat given off from the solidification of the button and the growing web as shown in isotherms, c through e. Isotherm e, is the practical realization of the desired isotherm. As can be seen in Figure 37b, the desired starting isotherm has a ΔT of from 3 to 7°. The growing button puts heat into the center of the isotherm and on pulling we get the situation in Figure 37c. The large cool regions to either side of the growing web encourage the edge dendrites to spread apart as shown in Figure 37d. Then when the planned width is reached, Figure 37e, the desired isotherm, Figure 37a, is very closely approximated, and growth continues with no further increase in width.

Figure 38 illustrates what can happen if the temperature gradient is too steep. We stress the steepness of the gradient rather than the ΔT, for a ΔT that is good for one heat shield opening may not be good for a different one. This is illustrated in Figure 38a by the dashed isotherm A ---A; for this isotherm the ΔT is the same as that used in Figure 37 but with a heat shield opening of 1/2 the length. As can be seen, the gradient is as steep as the one we have illustrated. For too steep a gradient, seeding takes place too rapidly and one obtains a primitive growth mass (see Section 4.2.1) or an irregularly shaped button. A steep gradient can result in seeding; however, the buttons form very quickly making the growth difficult to control. Furthermore the edge dendrites tend to grow too deeply into the melt. These two combine to make it difficult and in some cases impossible, to maintain the "pockets" B in Figure 38b, that induce widening. Thus the edge dendrites will not grow apart giving a constant width, or if the edge dendrites are deep enough into the melt, they will grow inward seeking the cooler center below the surface resulting in web narrowing as illustrated in Figure 38c. Although this type of gradient was present when the ΔT was too large for a given heat shield opening, it was quite often encountered unintentionally using the transient seeding technique described in Section 4.2.2. The correct isotherms in the melt

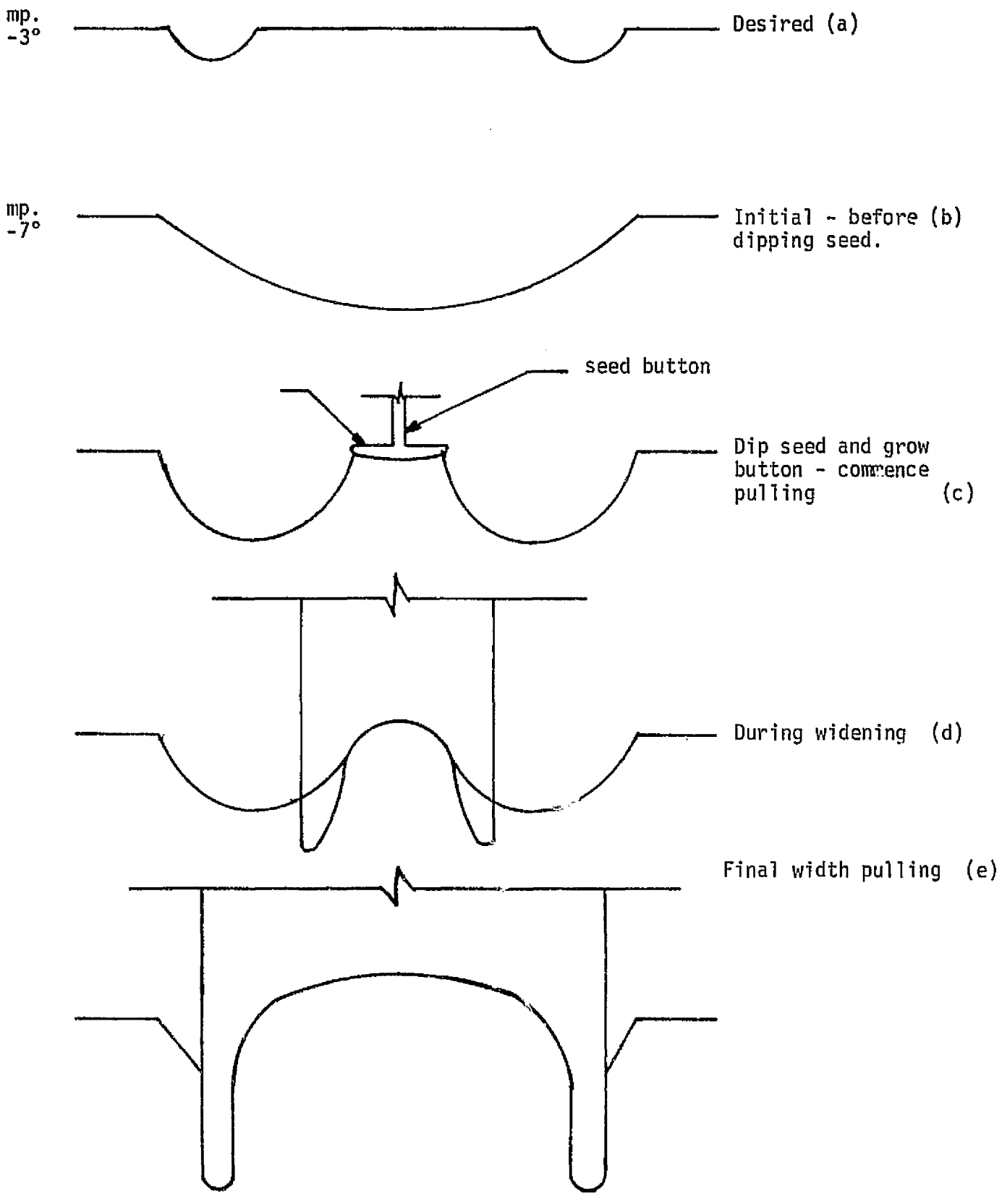

Figure 37. Schematic of Isotherms across melt.

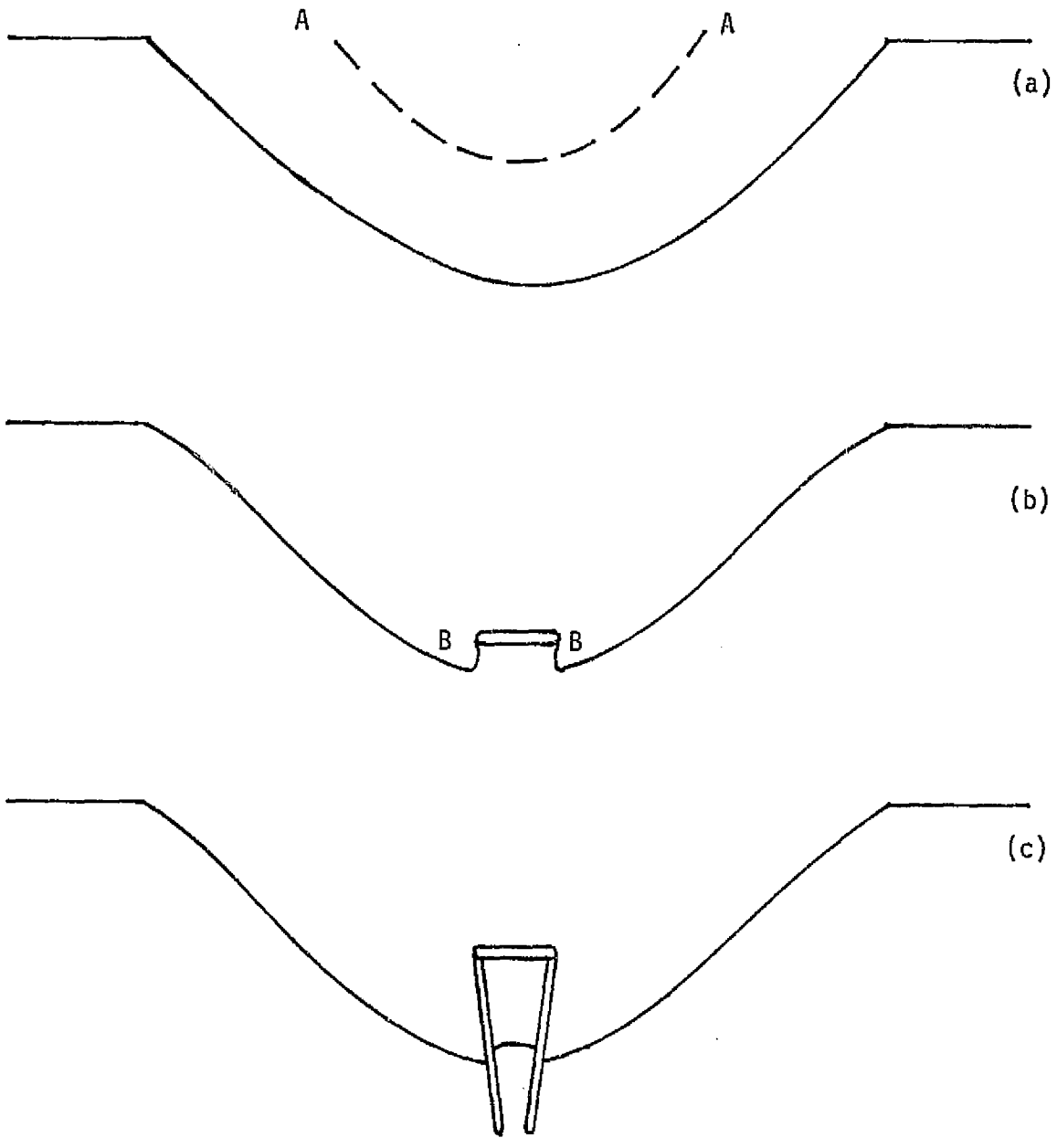

Figure 38. Schematic of isotherms for too steep a temperature gradient.

can be obtained by finding the proper relation between the vertical and horizontal temperature gradients. The changes made during this phase of the investigation to obtain the desired isotherms are given below. For the most part, the effect of changes were assessed from the way in which the buttons and webs grew; however, numerous times throughout this part of the investigation thermal data was taken to understand better the isotherms in the melt.

4.2.3.1.3 Temperature Measurement Techniques

All of the temperature data reported in Section 4.2.2 was taken with an optical pyrometer (Pyrometer Inst. Co. Model 95) that had been checked against a Leeds and Northrup optical pyrometer (Model 8621). This type of instrument is not as accurate as thermocouples for the following reasons: (a) necessity of sighting through the quartz furance wall whose optical transmission continually changes during a run (fortunately the change is usually not enough to cause a problem, especially over a short period, i.e., one or two hours), (b) difficulty in sighting on the exact spot again, (c) possible variation in emissivity of the surface being sighted, and (d) accuracy in matching the color of the filament to the surface. It does, however, have the advantage that temperatures can be taken during pulling. For this reason it was used to get temperatures on the surface of the melt, heat shield and susceptor each time a change in the susceptor/heat shield setup was made. Temperature data within the melt, however, is necessary to study the effect of a change within the melt or to get readings across the surface of the melt in fine detail. Such data can only be obtained by using Thermocouples. Thermocouples were made up from Pt - Pt 10% Rh run through single bore quartz tubing .06 in diameter. This was placed inside a quartz protective tube .125" in diameter and sealed at one end. The emf was measured using a digital microvolt meter. The first thermocouple had a straight end

and was used with an LDBwWM2 heat shield on an SS susceptor which rested on a Mo pedestal with no bottom heat shields. The melt charge was 50 gms. The thermocouple data is given in Table D-3 in Appendix D. Here it can be seen that the TG from the "surface" of the melt (just below the surface) to the bottom is 45°. This in itself is not too unreasonable for such an open heat shield; however, the data showed a problem in that (a) the highest temperature reading, on the bottom, is 100° below the melting point of silicon and (b) the readings in 7 surface positions indicate an essentially isothermal surface 150° below the melting point of silicon These results indicated that

we were not getting true results because too much heat was being conducted up the quartz tubing. To see if this was caused by the straight thermocouple or by the small melt charge, the measurements were repeated with twice the silicon - i.e., a 100 gm charge. The data is given in Table D-4 of Appendix D. Here one can see more realistic temperatures at the bottom of the melt. The temperatures across the bottom are more uniform than predicted in the Thermal Modeling Section. The TG across the melt approximately .5 cm below the surface is not only relatively large but also approximately 100° below the melting point of silicon. This indicates that the straight thermocouple is conducting too much heat from the regions within .5 centimeters of the surface. In an effort to get realistic readings, the ends of the thermocouple TC, were bent to make approximately 1/4" of the TC parallel to the surface. Table D-5 of Appendix D gives the data obtained using this new TC. Here one can see that the readings are consistent with the melting point of silicon. Thus all measurements thereafter, were made using bent TC's.

4.2.3.1.4 Vertical Temperature Gradients

The vertical TG can be shaped by manipulating the heat loss from the top and the bottom of the susceptor. The factors that influence the heat losses are shown in Figure 39. The fact that the argon atmosphere has a negligible effect on the heat loss compared to radiation was shown in Section 3.2.2 and it was reported in the discussion on the temperature above the melt that this was found to be correct experimentally. The factors involved in heat loss from the top are: the dimensions of the seed (i.e., thickness and width), the radiation loss from the grown web, and the heat shield - number, diameter, thickness and opening. The coil, number of turns, height, diameter, and of course CP (position of the susceptor in the coil) affect the heat input and as such the heat loss from not only the top but also the bottom. The factors that affect heat loss from the bottom are the susceptor, shape and size; pedestal, type of material, and spacers, and bottom heat shields, number, type, and thickness. These are taken up individually below.

4.2.3.1.4.1 The R.F. Coil: During this phase of our investigation, two coils were used. These coils contained 11 turns. Full details on the makeup of these coils is given in Section 4.1 - "Set Up Web Furnace". The taller coil (13.2 cm high) was used initially and throughout most of this phase. Problems of coupling with the top and bottom heat shield along with the high power rating necessary to melt the silicon, and the desire to give us more control over the vertical TG, led us to make a new coil with smaller diameter copper tubing and closer spacing between turns to give a shorter coil - 9.53 cm. An attempt was made to use a coil with a lesser number of turns; however, this turned out to be impractical.

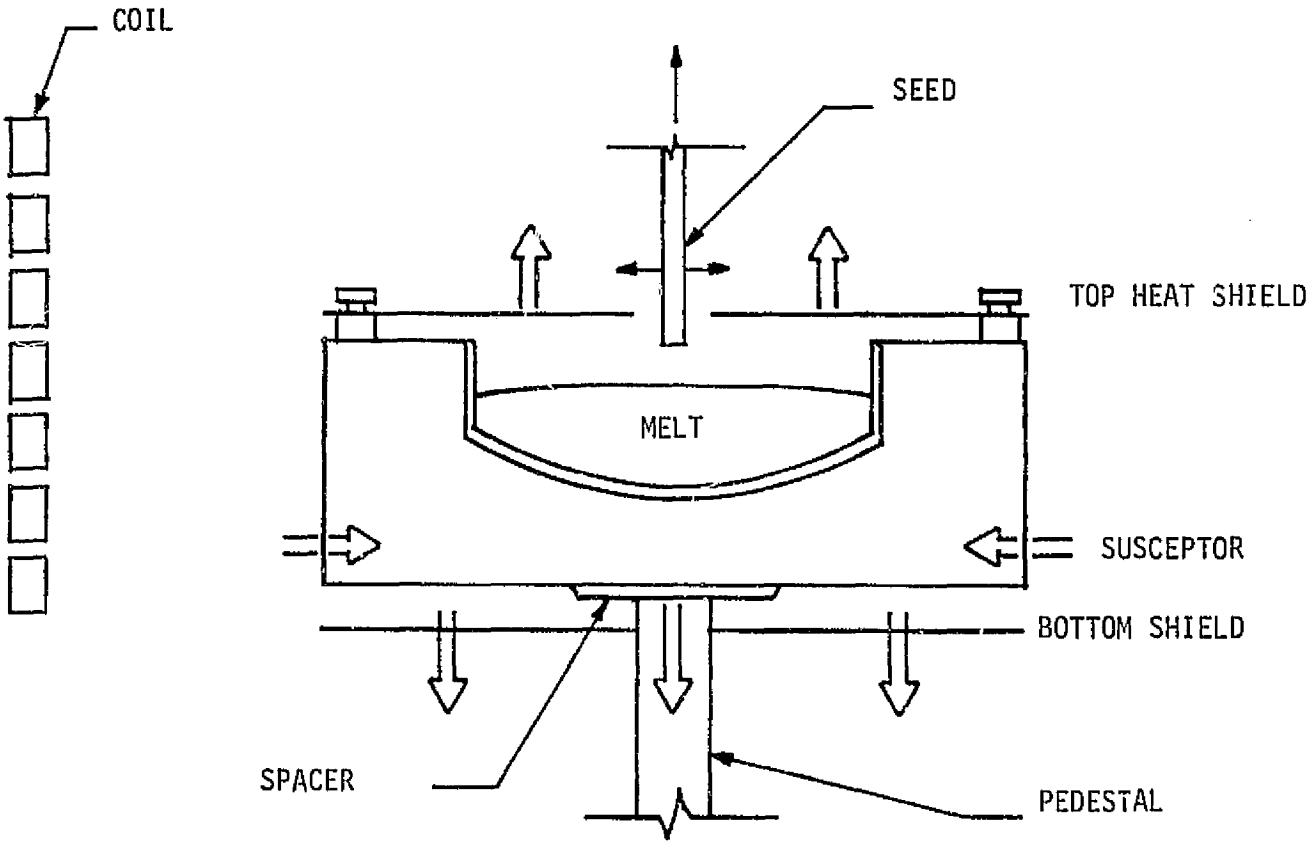

Figure 39. Heat losses involved in vertical temperature gradients.

The effect of the position of the coil (CP), the distance between the top of the coil and the top of the susceptor, on the temperature of the heat shield was discussed in some detail in the part on the temperature of the space between the heat shield and the surface of the melt. Its effect on the temperature gradient into the melt was only briefly discussed in Section 4.2.2. In this phase of the investigation, thermocouples were made up and data taken within the melt at several heights and several locations across the slot in the heat shields. Comparing the temperature reading at the top, middle, and bottom of the melt it can be seen that the gradients can be changed as desired by changing the CP. For example in Figure 40 with the CP of 4.05 cm., the top of the melt and the middle were at approximately the same temperature and 3° hotter than the bottom of the melt. With a CP of 3.70 cm, the top was 13° cooler than the middle and bottom which were at approximately the same temperature. Changing the CP to 3.55 cm left the top cool - it was 5° cooler than the bottom of the melt; however, the middle was now hotter than both the top and the bottom. There were numerous examples, involving changing between cool top, medium center, hot bottom; cool top, hot center, medium bottom; medium top, cool center, hot bottom; etc., by moving the CP. There are also examples where a change in CP did not result in a change in the sequence - see Figure 41 where the sequence did not change on changing the CP by 0.3 cm, but the temperature between top and bottom was changed.

4.2.3.1.4.2 Susceptor: The diameter and the type of material used in the susceptor were discussed in Section 4.1. The effect of the shape of the susceptor was taken up in Section 4.2.2 where it was shown that a straight sided susceptor (Figure 12) drastically reduced the vertical TG over that of the taper sided susceptor (Figure 11). This fact coupled with the thought that the straight sided susceptor should give the widest material (Thermal Modeling studies, Sec. 3.2.3) caused us to use the straight sided susceptor throughout this stage of the investigation. This fact was reconfirmed by thermal data coupled with web pulling during this stage of the investigation. It was necessary to lower the tapered sided susceptor into the coil almost 3 cm below that for the straight sided susceptor. In an effort to reduce further the heat loss through the bottom, a new susceptor was made that was 2.5" high, rather than 1.25". This gave a thickness below the crucible of 1.50" of Mo rather than our usual .25". That it did not decrease the heat loss out the bottom was evidenced by the fact that it was necessary to lower the susceptor until the bottom was almost below the bottom turn of the coil. Further the large mass of the susceptor caused the controller to over- and undershoot its set point by 5 to 7°, causing difficulty in getting dendrites to grow on the buttons, and causing "drop-out" of the web from these buttons that did get dendrites. Throughout the course of this phase of the investigation, a number of top heat shields were used with these susceptors. The various susceptor/heat shield combinations are given in Table 5.

4.2.3.1.4.3 Pedestal: The susceptor was supported on a molybdenum pedestal as reported in Section 4.1. Quite a bit of heat was conducted down the pedestal. In an effort to reduce the conduction loss down the pedestal, one Al_2O_3 wafer .025" thick was placed between the pedestal and the susceptor and later two spacers. These results were inconclusive. They were again tried in conjunction with bottom heat shields. The thermal results will be incorporated with the discussion of the bottom heat shields. The final effort on the pedestal was to do away with molybdenum and replace it with an Al_2O_3 pedestal

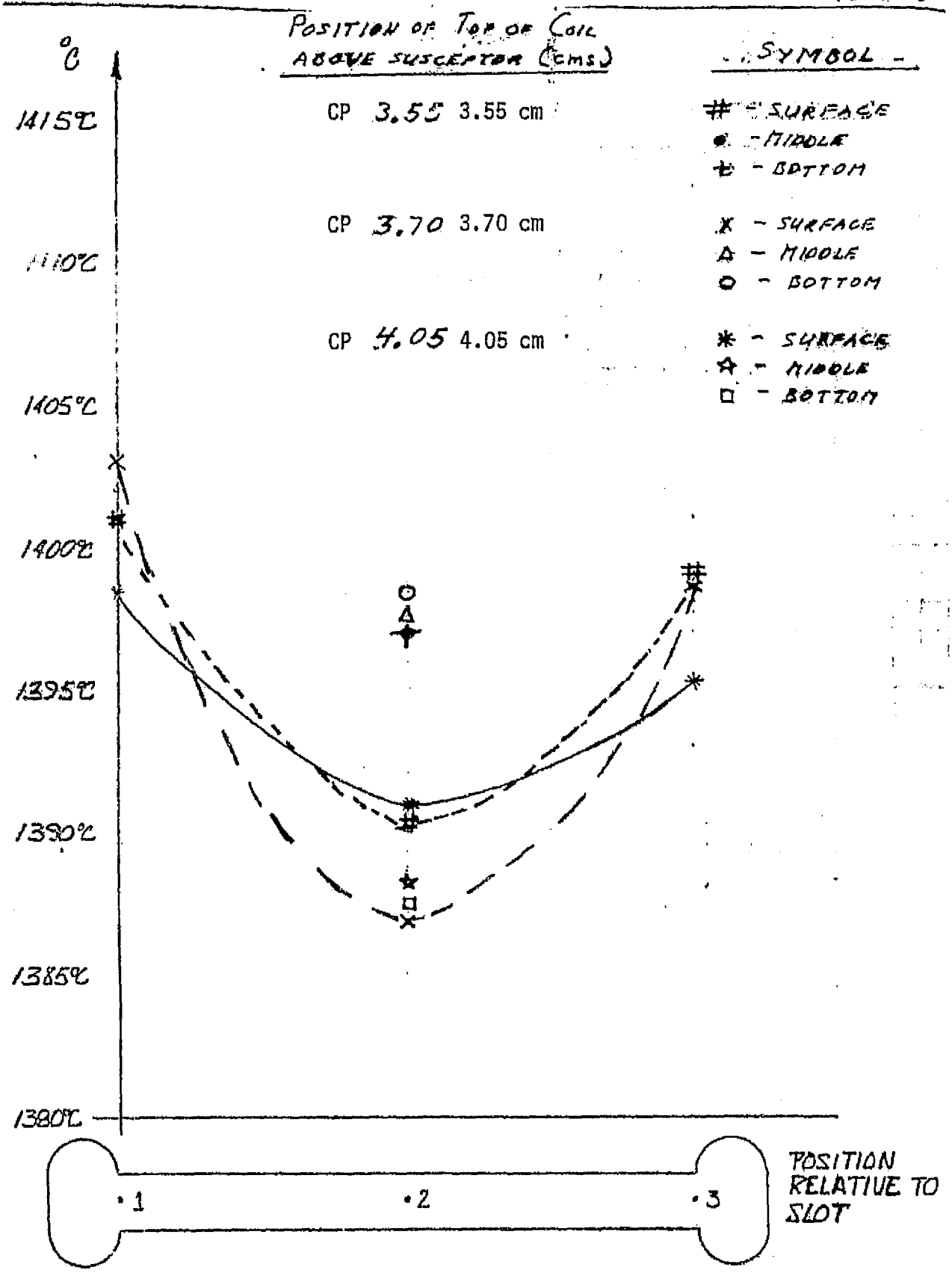

Figure 40. Thermal Profiles in Melt for Various Coil Positions

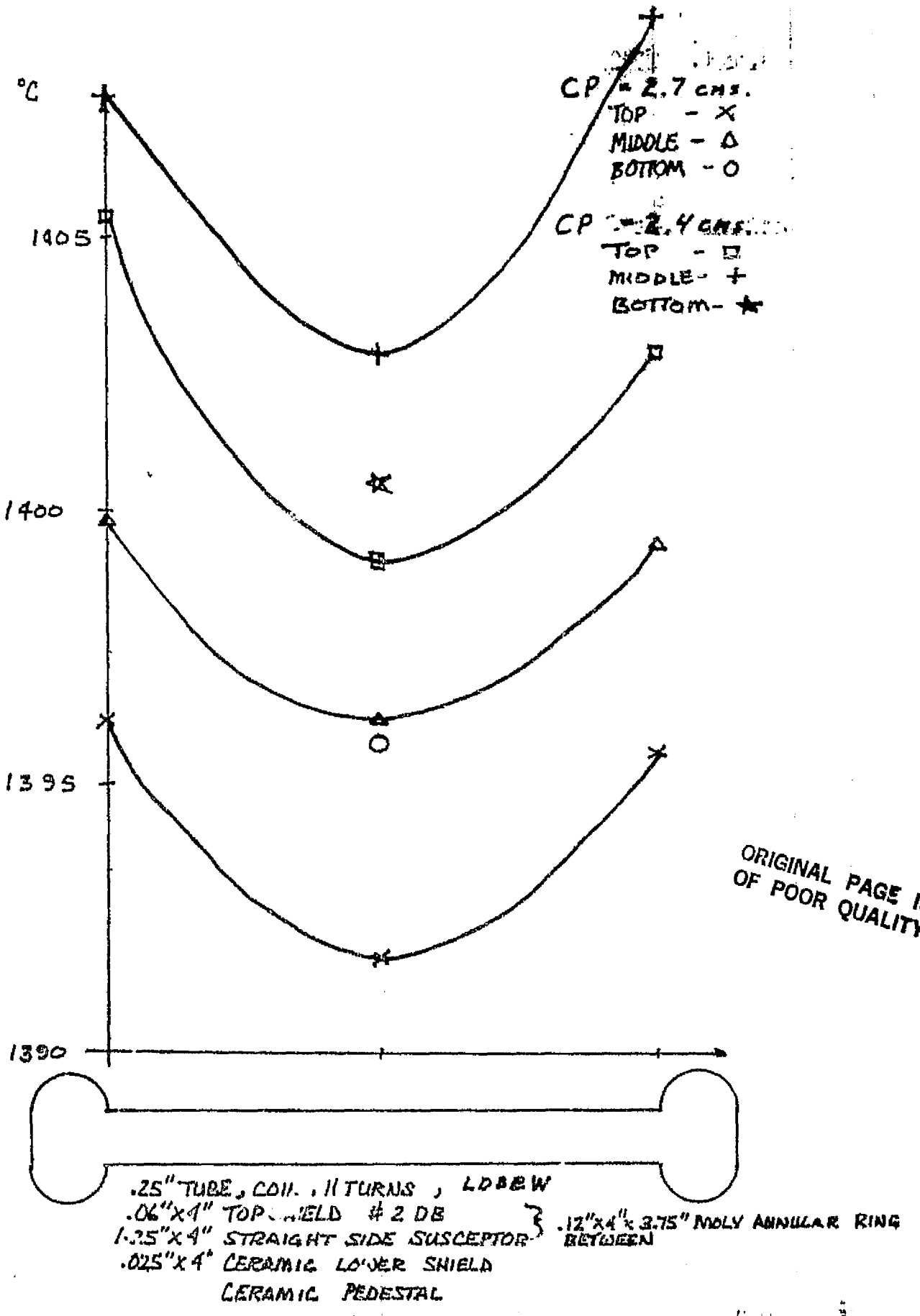

Figure 41. Thermal profiles in melt for various coil position.

Table 5. HEAT SHIELD SUSCEPTOR ARRANGEMENTS USED IN SECTION 3.2.1.3.

Heat Shield[1]		Susceptor[2]	
Designation	Figure Number	SS	TS
TDB	30	4-30-76[3]	
LDBe	32	5-12-76	5-17-76
LDBeW	35	6-28-76	11-16-76
LDBeWM1	35	7-16-76	
LDBeWM2	36	7-20-76	8-6-76
NSS	38	8-2-76	8-24-76
WDB	40	8-12-76	
NSSM1	39	8-11-76	
SR	44	9-13-76	
LDBeW1/4	33	11-5-76	
LDBeXW	5	1-4-77	

Notes:
1. Meaning of Designations are given in list of abbreviations.
2. SS Figure 12, straight sided susceptor.
   TS Figure 11 taper sided susceptor.
3. Dates signify first time the arrangement was used.
4. Results of these arrangements are given in the text.

(see Figire C-2 in Appendix C). The Al_2O_3 pedestal was not used without bottom heat shields during this phase of the investigation, thus nothing can be said of its action alone, at present. It is quite evident, however, that the Al_2O_3 pedestal did even out the bottom temperature gradients. It was found necessary to ground the susceptor when the Al_2O_3 pedestal was used to eliminate thermionic emission. A 20 mil tungsten wire hooked around one of the pins and the base was found to be a sufficient ground.

4.2.3.1.4.4 Bottom Heat Shields: The first attempt to control heat loss from the bottom of the susceptor by heat shields employed the diffuser plate (Figure 27) placed on the Mo pedestal one inch below the susceptor. The r.f., however, coupled so strongly to the 1/4" thick molybdenum plate that it was impossible to melt the Si charge. A bottom shield was designed (Figure 42) and made from 40 mil molybdenum. This was placed 1/16" below the susceptor on the molybdenum pedestal. It did, indeed, cause a reduction in heat loss resulting in a more uniform temperature across the bottom of the melt. Two molybdenum shields were then used but this arrangement made little difference compared to one heat shield in the temperature gradient across the bottom of the melt. It did, however, allow the use of lower power from the generator. Three heat shields were used to gain information for the Thermal Analysis Section that indicated it would be better. Three shields, however, gave no improvement. An attempt was made to reduce the r.f. coupling to the bottom shield by making it 3/8" in diameter. This did have an effect but did not appear to be beneficial.

The Al_2O_3 pedestal (Figure C-2) was used in place of the molybdenum pedestal shown in Figure 26 first with 4 molybdenum bottom heat shields. Later two bottom Mo shields were used and finally only one bottom shield was used. It was found that 4 heat shields gave a temperature difference from the top to the bottom of the susceptor of 44°, Table 4, while 2 heat shields, Table 6, at the same CP, gave a temperature difference of 74°. The difference between 4,2 and 1 heat shields gave little practical difference; thus one shield was settled upon for ease of set-up. In an effort to see the effect of the coupling of the r.f. to the heat shield, shields were made from Al_2O_3. As in the case of the molybdenum shields, a second heat shield does give a greater reduction in the heat loss from the bottom. One could, however, see little difference between the Al_2O_3 shields which cannot couple, and the Mo shields that can couple.

4.2.3.1.4.5 Seed: The role of heat conduction up the seed and its effect on the vertical TG have already been discussed in conjunction with the temperature between the top shield and the melt earlier in this section.

4.2.3.1.5 Horizontal Temperature Gradients

4.2.3.1.5.1 Top Heat Shields: Earlier in this section the effects of the diameter, thickness, and number of the heat shields on the temperature of the heat shields, the TG between the top of the heat shield and the melt, and the gradients across the melt were discussed. It was pointed out that the size and shape of the opening in the heat shield was used mainly to shape the surface isotherms in the melt and would be taken up in this part of the section. In Section 4.2.2 we discussed the first investigations on shaping the isotherms - that of cutting "large" holes at the ends of the narrow straight slot to form a dog-bone and of tapering the slot opening to form a tapered dog-bone (TDB). In this phase of the investigation, we used 10 other shapes in addition to the TDB shield. The heat shields and the suscep-

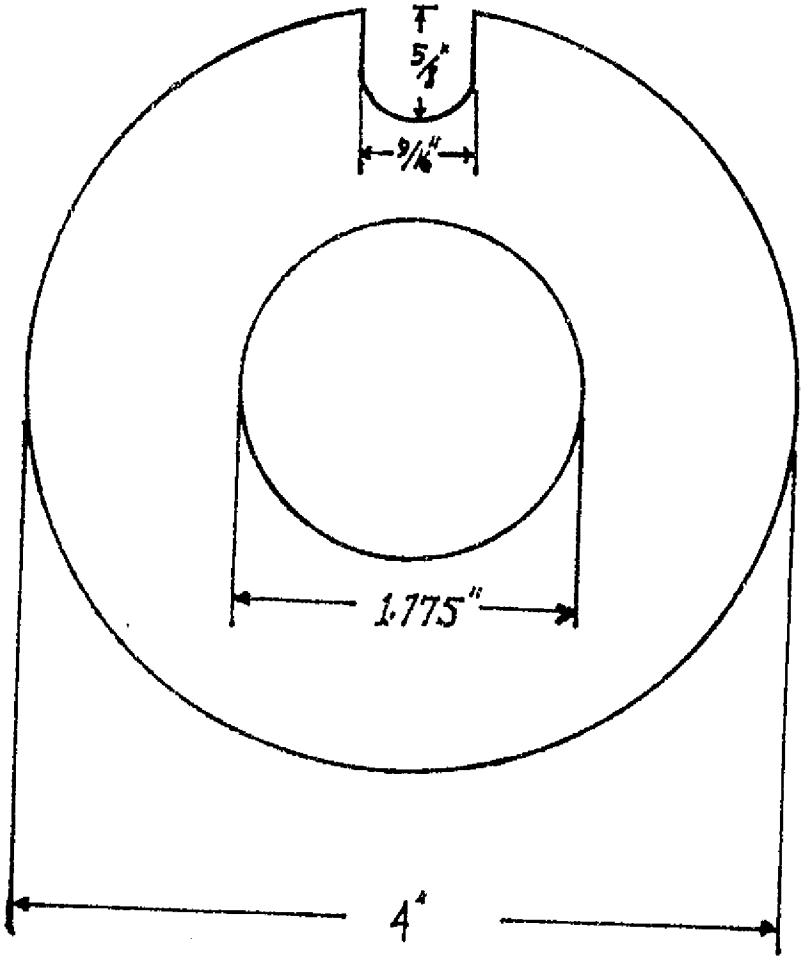

Figure 42. Bottom heat shield (BH).

Table 6. TEMPERATURES AT VARIOUS POSITIONS IN THE MELT AND ON SUSCEPTOR WALL.

Position [1]	Temperature (°C)
1	1307
2	1296
3	1188
4	1232
5	1171
6	1126
T	1286
M	1327
B	1360
H	1366

Note: 1. Measurements made at locations indicated in sketches below.

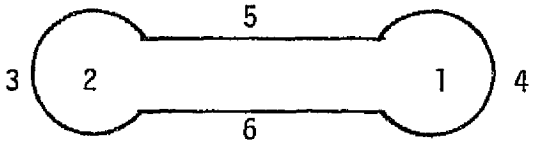

Slot in top heat shield.

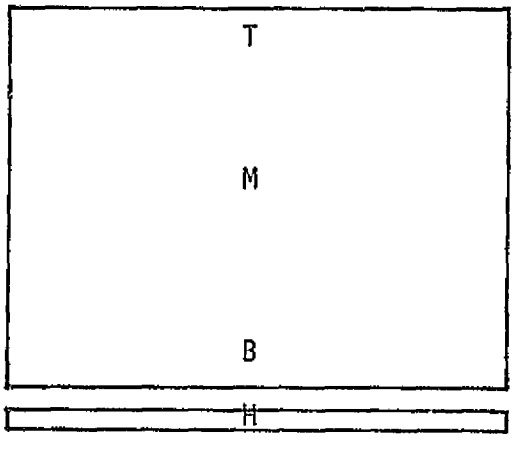

Side view of susceptor and bottom heat shield.

tor with which they were used are given in Table 5 along with the run in which it was first used. Toward the latter part of this phase of the investigation, thermal modeling studies were applied to thermal gradients on the surface of the melt for four different shapes of openings simulating the straight slot (Figure 20, Section 3.2.4), the dog-bone (Figure 21, Section 3.2.4), the dumbell (Figure 43) and the Bow Tie (Figure 44) which will be taken up in Section 4.2.4. The temperatures at the same distance in inches from the center of the slot towards the end of the slot were taken from these figures and listed in Table 7 for easy comparison. As can be seen the values of the temperature at any given distance from the center are essentially the same for all four, as pointed out in the discussion of Figures 20 and 21 in Section 3.2.4. By comparing the figures, however, one can see that there are differences in the temperature gradients.

Actual values of the temperature across the slots are given in Table D-2 in Appendix D for one and two heat shields with the LDBeW (Figure 35) opening in Table 8 for several other shields. Examining these tables and the figures with the thermal data, it can be seen that the measured values do not show great differences and are, for the most part, quite similar to those found in the Thermal Modeling studies. This is further made evident by Figure 45. The points are the actual experimental data and the solid lines are curves with the lowest point fixed on the experimental point at the center. Two things can be seen on a careful study of the experimental data: (1) a difference - however slight - can be seen between some shields, and (2) the difference in temperatures along the slot depend on the position of the susceptor in the r.f. coil (i.e., CP).

In shaping the isotherms, the temperature gradient along the centerline of the slot (i.e., left to right, L-R) is not, however, the only gradient to be considered; the front to back (F-B) is very important to control button shape and thickness of the web. The figures giving the isotherms for the four simulated heat shields calculated from Thermal Modeling (Figures 20,21, 43, and 44) indicated that the temperature difference between the centerline of the heat shield slot and that under the heat shield to the front and back was approximately 5° in all four cases. Table 9 compares experimental data taken on three different shields. Here one can see that for all but the heat shield with the widest (i.e. width of a slot is the front-to-back distance) the temperatures just under the heat shield are 4° to 8° hotter than in the slot; the wider shield has a value of 15° to 20°. One can also see that these gradients are becoming less step in the melt, as one would expect.

As was mentioned above, one can see on careful examination and comparison of the temperature gradient that there does appear to be differences at least between several of the heat shields. One should also notice that although the thermocouple data taken here was recorded from a digital microvoltmeter, the apparent fluctuations in the temperature could be as high as 50 to 100 microvolts. At these temperatures, a voltage of 12 microvolts is equal to 1°. For this reason, one cannot rely on temperature data alone to chose an optimum setup: the growth of buttons and dendrites is far more sensitive to temperatures and temperature gradients than are thermocouple readings. In all cases but especially in those cases where

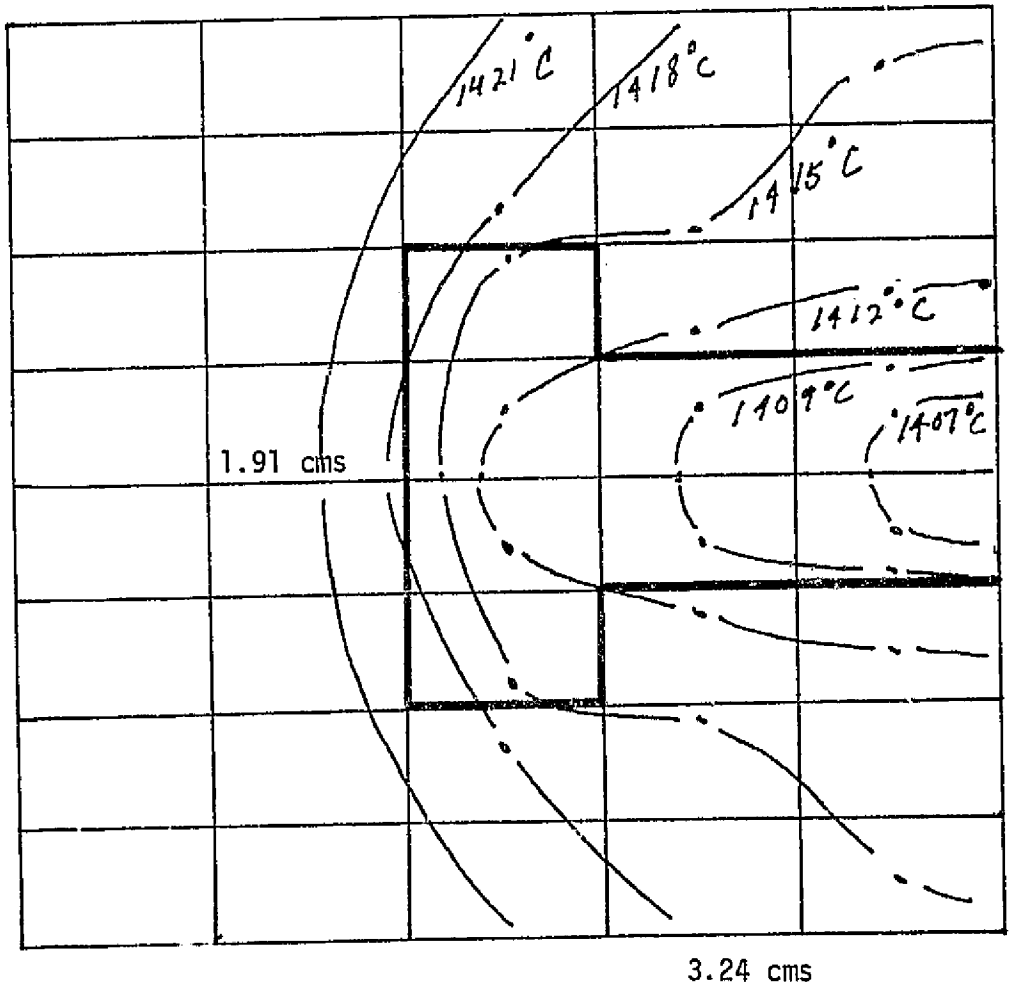

Figure 43. Computer generated temperature profiles for dog-bone slot on surface of melt.

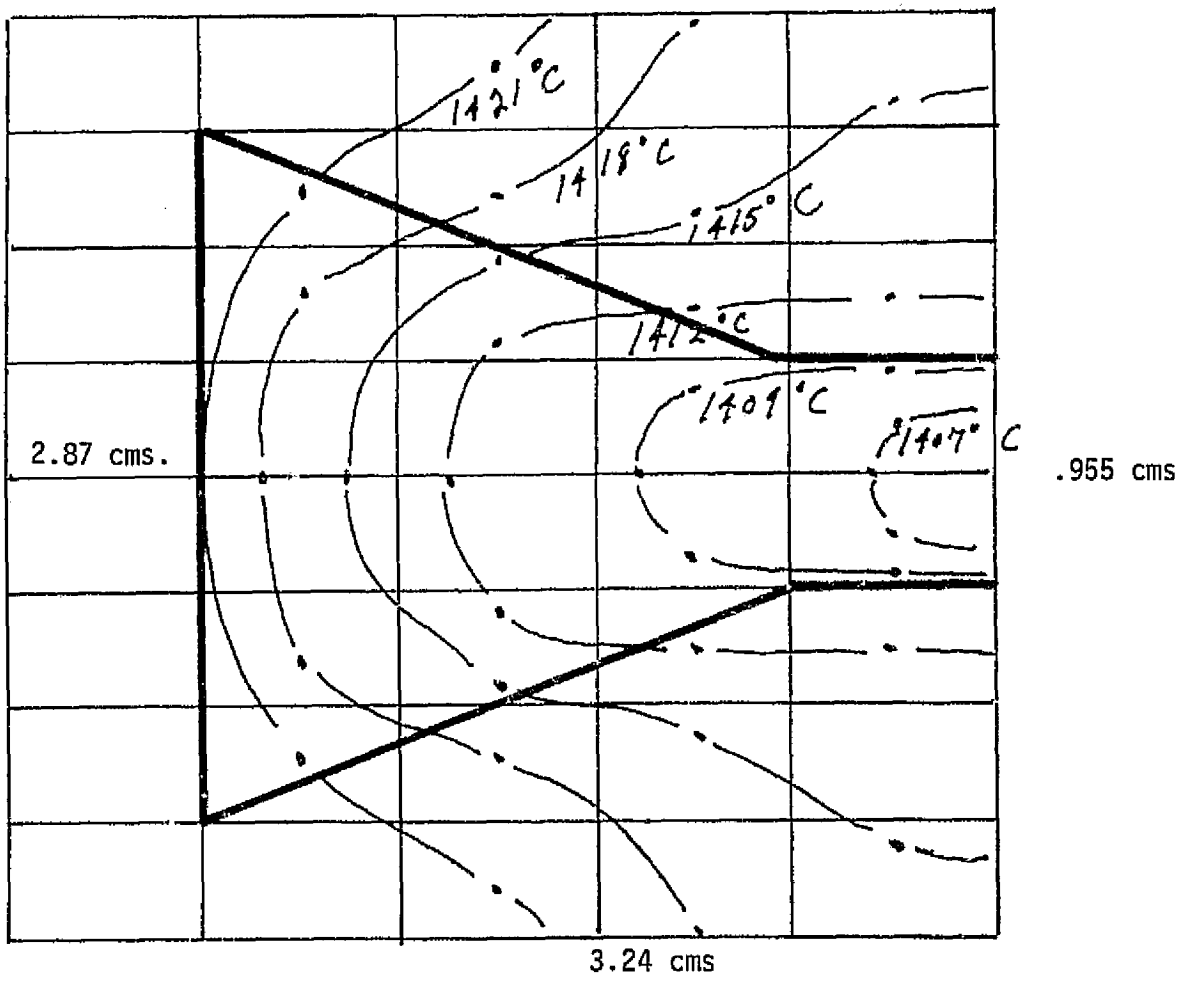

Figure 44. Computer generated temperature profiles for bow-tie slot on Surface of Melt.

Table 7. TEMPERATURES ALONG SLOT OBTAINED FROM THERMAL MODELING STUDIES

Distance from center (inches)	Shape of Slot[1]			
	SS	DB	DBe	BT
	Temperatures (°C)			
.169	1407	1407	1407	1407
.481	1408.8	1408.5	1408.7	1408.2
.794	1412	1410.9	1411.9	1410.8
.963	(1415)	(1413.6)	(1417)	1413.5)
1.107	1417.7	1416.4	1422	1416.3
1.276	1421	1421		1421

Notes: 1. Slot abreviations. SS, straight slot; DB, Dog-bone; DBe, Dumbbell; and BT, Bow-Tie.

Table 8. MEASURED TEMPERATURES ALONG SLOTS IN HEAT SHIELDS

Run	Top	Bottom	Ped	CP	LS	M	RS	heat shield to melt
7-27-76	LDBeWM2[2]	None	M	8.95	1423	1406	1440	--
1-12-77	LDBeXW	1A	A	1.10	1402	1395	1401	137
	"	1A	A	.60	1387	1378	1387	175
	"	1A	A	.10	1402	1398	1402	175
8-26-76	NSS	1M	M	9.45	1383	1383	1391	--
1-14-77	LDBeW	1A	A	.90	1396	1393	1396	162
	"	1A	A	.60	1405	1399	1402	173

Notes: 1. Abbreviations. CP, coil position (cm); LS, left side; M, middle; RS, right side; M, Molydenum pedestal; A, Al_2O_3 pedestal.
2. Heat shield abbreviation given in table of abbreviation.
3. Temperature (°C).

C-2

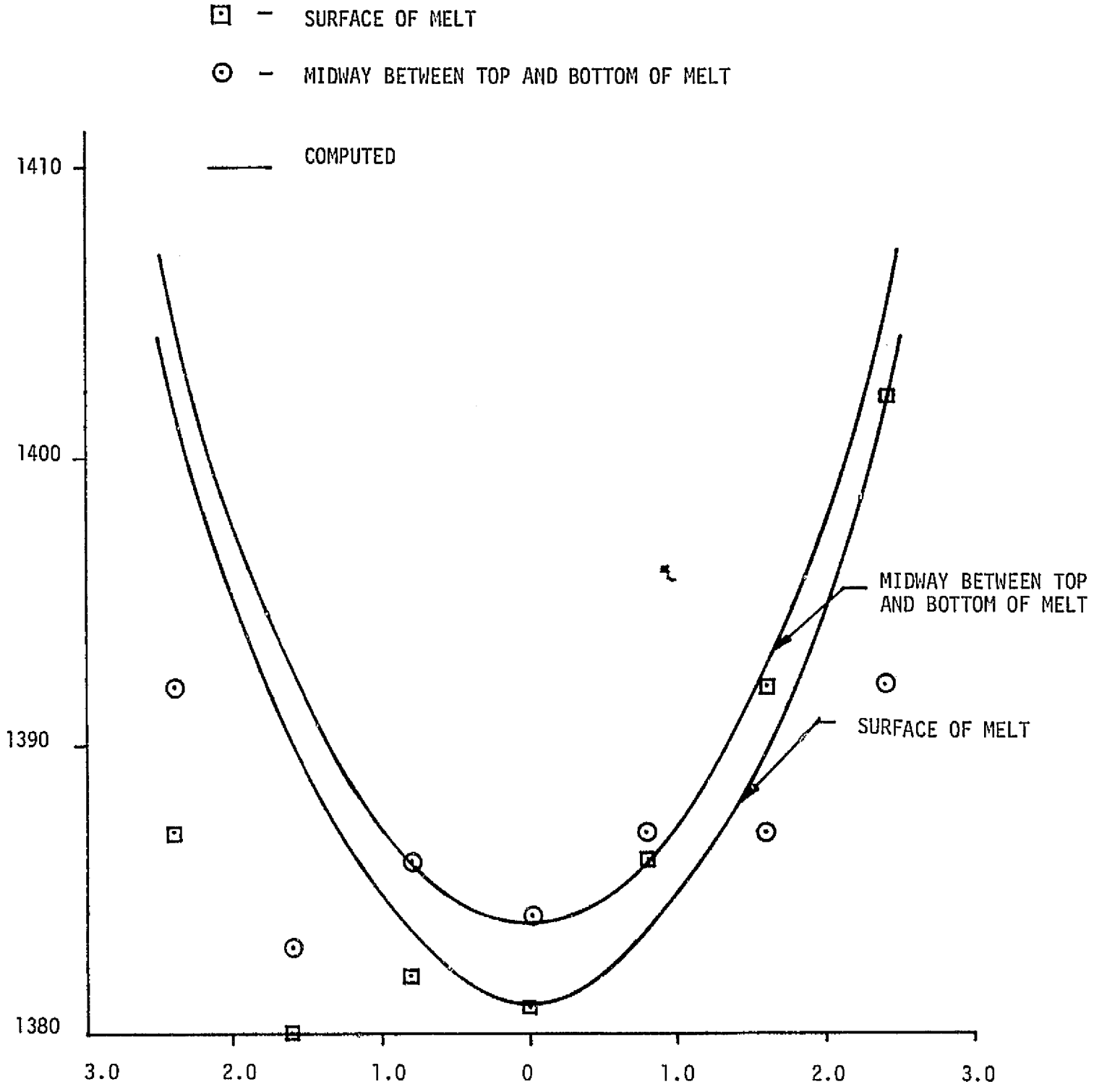

Figure 45. Measured and computed temperature profiles in crucible.

Table 9. TEMPERATURES IN THE X-Y PLANE AT DIFFERENT DISTANCES BELOW THE SURFACE OF THE MELT.

Run	Heat Shield	CP[1](cm)	Position Across Slot			Position Front to Back			Position in Melt
			LS	M	RS	B	M	F	
7-27-76	LDBeWM2[2]	8.95	1423	1406	1440	1423	1406	1423	C
						1431	1418	1423	RS
8-26-76	NSS[3]	9.45	1383	1383	1391	1390	1384	1392	SN
			1386	1386	1391	1386	1386	1382	1/2
			1393	1390	1393	1386	1390	1387	B
10-21-76	LDBeW[4]	3.55	1401	1397	1397	1401	1397	1403	LS
						1400	1395	1400	RS
		3.05	1393	1390	1391	1386	1386	1392	LS
						1396	1391	1392	RS
		2.55	1397	1390	1397	1392	1392	1398	LS
						1392	--	1397	RS

Notes:
1. Abbreviations: CP, coil position; LS, left side of slot; M, middle of slot; RS, right side of slot; B, under heat shield to back; F, under heat shield to front; c, centerline; Su, near the surface; 1/2, midway between surface and bottom of melt; B, bottom of melt.
2. LDBeWM2 (Fig. 36) on a molybdenum pedestal. No bottom shield.
3. NSS (Fig. c-8) on a molybdenum pedestal with one molybdenum bottom shield and an Al_2O_3 + pacer between the susceptor and the pedestal.
4. LDBew (Fig. 35) on Al_2O_3 pedestal with one molydenum bottom shield.

there appears to be no difference from thermal data, one should observe the ease (or difficulty) in seeding, the shape of the buttons during their growth and upon pulling. For example (a) if the temperature at the surface is too hot the buttons will be rounded rather than faceted, (b) if the temperature is too cool the button will be irregular and in some cases have twin lamellae being initiated and wings growing at odd angles, (c) if the temperature is close to being correct but is still on the hot side, the button may be well faceted; however, on pulling it will pull free and be smooth on the bottom rather than pulling into dendrites and (d) if the temperature is close to being correct but is on the cool side, the button may be well faceted, but on pulling one obtains three or more dendrites. Examples of these are found in Table 10 which gives the aspect ratios (i.e., width to length) of the buttons for various heat shields (Table 5) used in this section and at different CP's. Here one can see that the most desirable aspect ratios are from 1/2 to 1/5. Aspect ratios less than this (i.e., 1/1, 2/3/ etc.) and greater than this (i.e., 1/7, 1/8, etc.) usually do not give good results. One can see that the long narrow slots favor good aspect ratios.

4.2.3.1.5.2 Seeds: The effect of the size of the seed on the temperature of the melt was taken up earlier. The seed also plays a vital roll in the aspect ratios of the buttons and in the seeding itself which is vitally connected to the discussion just completed. The seeds should be thin; if they are too thick the width of the button will be thicker than desired and the button will then be too large. The number, spacing and continuity of the twin planes across the button are very important. The necessity of having three closely spaced twin planes is well known in the literature and was evident several times during the course of the work. The necessity of having the twin configuration continuous across the cross-section of the seed is also well known; failure to do so can result in the button forming no wings (NW) or wings on one side only (1D) possibly some of the buttons reported in Table 10 could be the result of this. The effect of the spacing of the three twin planes on the growth of silicon dendrites (and thus web) had never been investigated as it was for Germanium. For Ge it was found that twin spacings above 10μ and below .5μ were not favorable and that optimum spacing between two of the three twins was 1.7μ with the third twin being .5μ away from either of these two.

4.2.3.2 Mechanical and Growth Aspects

This phase of the investigation was directed toward the thermal aspects in an effort to retain the web for a sufficient time between the two edge dendrites until it could solidify, and to encourage widening. We had noted problems of premature pull-out not only of web but also of dendrites and picking up "third" dendrites (i.e., one or more extra dendrites either within the web or to the outside of the edge dendrites). Although much of this was

Table 10. BUTTON ASPECT RATIOS FOR SELECTED HEAT SHIELD - SUSCEPTOR COMBINATIONS

Run	Heat Shield	Susceptor	CP[1] (cm)	Aspect Ratios, W/L[1]
6-22-76	LDBE[2]	TS[3]	6.25	1/2; NW[1]
			6.0	2/3; 1/3; 1/4; ND
			6.50	1/1; NW; 3 - 2/3; ND
6-24-76	LDBe	SS[3]	8.95	2 - 2/3; 1/3; ND
			9.20	2/3; 1/3; 1/4; ND
			8.85	2/3 (web)
			8.55	1/3; 1/2 (web fell)
				2/3; 1/2 ND
6-28-76	LDBeW	SS	8.45	1/3; 2 - 1/2; ID; MD[1]; 3- 1/2 (web fell)
			8.35	2/3; 1 W
7-19-76-	LDBeWM1	SS	8.65	2 - 1/2; 3 - 1/3; 2 - ID; 2 - NW; 1/2 (web fell)
7-20-76	LDBeWM2	SS	8.65	2 - 1/1; NW
8-2-76	NSS	SS	8.70	1/1 distorted; 2 - 1/3; 2 - 1/2; 2 - ID
8-2-76	NSS	SS	8.70	1/1 distorted; 2 - 1/3; 2 - 1/2; 2 - ID
8-4-76	NSS	SS	8.70	1/2 (web fell)
			8.95	1/3; 1/4; 1/5 (Gen malfunctioning)
8-5-76	NSS	SS	9.55	1 - 2/3; MD
8-9-76	NSS (3.85")	SS	9.45	2/3 (web fell);1/3; 2 - 1/2; MD
			9.15	1/2; MD + ice
			9.65	2/3; 1/2; MD
8-25-76	NSS	TS	7.55	1/3; ND
9-17-76	LDBeW	SS	7.45	1/2 (lost web) D too wide
			7.25	2/3; 1/2 (lost web) D too wide
			6.85	1/2 (short D); 2/3 (lost web)
1-4-77	LDBeXW	SS	.60	2 - 1/3; button and wing to right
			.10	1/2(web fell)1/1.5 (thick web)
			.0	1/2; 1/4 (web fell)
			- .40	1/4 (web fell)
1-13-77			.60	2 - 1/3 (web fell)
1-14-77	LDBeW	SS	1.10	1/2; 1/3; 1/4; 2D; 1/2; 1/2.5 (web fell)

Notes:
1. Abbreviations: CP, coil position; W/L, width/length; NW, no web; ND, no dendrites; MD, multidentrites.
2. Heat Shields: LDBe, similar to Fig. 35, but not as wide; LDBeW, Fig. 35; LDBeWM1, similar to Fig. 36, but center not opened as much; LDBeWM2, Fig. 36; NSS, Fig.25; LDBeXW, similar to Fig. 35, only wider.
3. Susceptors: TS, taper sided; SS, straight sided.

ascribed to incorrect thermal conditions, some of it was quite obviously the result of mechanical or non-thermal problems. Perhaps one of the biggest non-thermal problems was the generator itself. During this phase of the investigation (approximately 8 1/2 months), the generator was down a total of approximately 2 1/2 months for various reasons - including over one month for a cooling water system that had been ordered 6 months prior to the breakdown. The generator problems, however, have been taken up earlier (Section 4.1) and will not be repeated here. It should be pointed out, however, that the 2 1/2 month down time was not the only time lost as a result of generator breakdown. On a number of occasions the generator "acted up" for a day or two before breaking down, putting the studies made during those times in question; it was thus necessary to rerun such data to see if the results had been influenced by the generator problem or by the changes we had made. Other problems found and corrected were:

(1) Inadvertant jarring of the furnace by the operator: This was greatly decreased by rearranging the positions of the controls and by the addition of a guard rail rigidly attached to the floor to support the operator when it was necessary for him to reach above the furnace.

(2) Slipping of the drive wheel against the take-up reel: The rubber strip on the drive wheel loosened up. Attempts to stop the slipping by using epoxy to hold the rubber band on the wheel resulted only in a temporary solution. It was necessary to fabricate a new 4" drive wheel that employed standard sized O-rings to provide the friction.

(3) X-Y motion of the coil: The necessity of being able to move the coil in a horizontal x-y motion so that the center of thermal symmetry could be made to coincide with the geometric center has already been discussed. During this phase, it was found, however, that sometimes it was not possible to adjust the coil enough because of arcing when the coil was moved too close to the quartz funance wall. Part of this was due to contamination that builds up on the walls in the neighborhood of the coils over an extended period of time. This effect could be greatly reduced by cleaning the inside of the furnace walls with $HF-HNO_3$ solution or eliminated by using a new tube. Occasionally it was found that this was not sufficient. It was necessary to use a smaller diameter tube for the furnace envelope. We had been using a tube 135 mm in diameter but found that a tube 130 mm in diameter could be used. This change helped greatly in positioning the center of thermal symmetry.

(4) Positioning of susceptor: In line with the preceding, it was also found necessary to be sure that the susceptor and shields were always replaced on the pedestal in the same sense. Care was always taken to be sure that the susceptor was correctly seated on the pedestal.

(5) Seed holders: The seed holder that had been used in the last phase (Sec. 4.2.2) began to give us troubles in that the seeds would quite often fall out. Also it was difficult to align the seed properly such that it would be perpendicular to the melt. The seed holder shown in Figure 46 was designed and installed. It solved the problems that we were having at the time.

(6) A two inch drive wheel was made and used near the end because we felt that we should drop our pull rate below the 2 cm/min limit of the 4" drive wheel during the period while the molten sheet was solidifying into web. The pull rate curves for the 2" drive wheel are given in C-1 of Appendix C.

The above mentioned thermal and mechanical changes made during this phase helped greatly in obtaining our goal for that phase - namely getting two dendrite web to grow from buttons that were grown on the seeds. Three changes in procedure, however, should be mainly credited with the attainment of our goal.

1. Changes in temperature and pull rate: We found that abrupt changes of 1° or more in the temperature during pulling invariably led to the web falling free at the start or to the web and edge dendrites pulling free at any time after the web had solidified. This was especially true when we were using the transient seeding technique. In a like manner abrupt increases in the pull rate led to the formation of "third" dendrites in the web portion or to the outside of either edge dendrite. The latter effect was enhanced if the web was growing in an asymmetric temperature gradient.

2. Seeding technique: We had been using the "Transient Seeding" technique as described in Section 4.2.1. This technique had given us problems in overshooting the temperature as we have already mentioned. The interface allows us to control the temperature automatically so that the "Stationary Seeding" technique could be used. The procedure for the technique consists of:

   (a) Find melting point of melt. This is accomplished by dipping a seed into the melt and adjusting the temperature until the seed neither melts nor grows. A seed etched to a point gives a more accurate melting point. Note: Be sure that the seed is clean. Once the m.p. has been found, it is best to check it by etching the seed and lowering it into the melt again.

SEED HOLDER

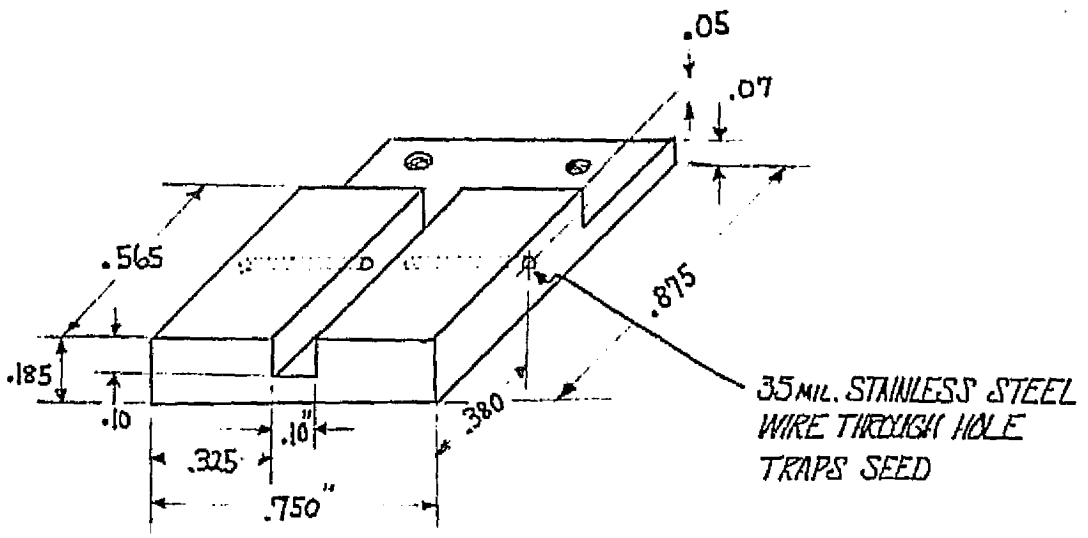

Figure 46. Seed holder.

GK 7/30/76

(b) Set desired ΔT on the temperature controller (can be any where from 2-25°. Actually we used 5 - 10°).

(c) As the melt temperature drops to the new value, a button begins to grow. When wings just first appear pulling is commenced at 70% of speed controller (this corresponds to 5 cm/min). As the button reaches the surface of the melt, the speed controller is reduced almost to zero and the temperature is raised to give a ΔT of from 2 -5°.

(d) After the web has solidified the pull rate is slowly increased to the desired velocity for web growth (2 -5 cm/min.).

Temperature and pull speeds are adjusted during the pull as needed. Note: Changes should be small at any one time.

3. Pull rate: When we first used the stationary seeding technique, the pull rate after the button cleared the surface of the melt had been reduced to 10% rather than the "almost zero" given in (c) above. This proved to be too fast, and it was not until we went to this "almost zero" rate until the web solidified did we get reproducable web from the initial seed.

4.2.4 Sustaining Web Growth

The goal for that phase of the work reported in Section 4.2.3 was to be able to grow good two dendrite web from the button grown initially on the seed and do so reproducibly. This goal was reached; however, we found a problem in sustaining growth. Invariably the two dendrite web would pull free from the melt or develop "thirds". The goals for the final phase of the contract, then, was to study the problem of pull outs and thirds as well as to study widening rates to get information on width and pull rates of web. To keep the number of parameters that we vary to a minimum, we set upon a standard furnace configuration so that all parameters except those that pertain to the goals of this phase of the investigation were kept constant.

The most promising furnace configuration was chosen from temperature profile data and from observations of button formation, dendrite and web growth. This configuration consisted of (a) the tapered molybdenum susceptor (TS. Figure 56) set on the alumina pedestal (Figure C-2 of Appendix C), (b) since we found that two top shields gave us no improvement, in fact if anything they hurt us, we standardized on one top shield made from 60 mil molybdenum, (c) no bottom shields, since they appeared not to be of any help with the TS susceptor, (d) the 130 mm diameter quartz envelope, and (e) the r.f. coil 15.24 cm in diameter that was made from 1/4" copper tubing (the coil height = 9.53 cm). Although our studies indicated little effect of the size of the silicon charge on button formation and ribbon growth, a 150 gram charge was adopted as the standard for this phase of the work.

4.2.4.1 Mechanical Aspects

Premature pull-out of the ribbon from the melt appears to become increasingly

more of a problem as the width of the ribbons are increased. Several modifications were incorporated into the puller that helped considerably in preventing premature pull-out of the web. During these experiments it was found that there was insufficient fine temperature control to enable the operator to reproducibly set melt temperatures from run to run, and during the same run, with sufficient accuracy to carry out the experiments. A fine tuning, 10 turn, potentiometer was installed on the controller which gave the operator sufficient reproducible control enabling him to make much finer adjustments to the melt temperature during the run. An additional change which was of considerable help was the incorporation of an 8 inch drive wheel with a new quieter motor and a new gear box on the ribbon take-up reel. This gave greater control on the pull rates over the range of pull speeds found most appropriate for pulling the ribbons, i.e., 1-5 cms/min. The pull speeds attainable with the 3 inch drive wheel, with a new motor and the 8 inch wheel with new motor and gear box are shown in Figure C-1 of Appendix C. Some difficulty was encountered due to mechanical vibration introduced when the seed holder and take-up ribbons were wound up onto the take-up reel. This was improved by fabrication of a slimmer seed holder and the addition of mechanical guides to feed the steel tape onto the take-up reel. Other changes made were:

1. Aligned old motor and gear box.
2. Put on new motor and controller and aligned carefully with old gear box.
3. Put on new gear box with new motor.
4. Made new aligning jig on chimney. This allows lateral movement of the tape to control lateral position in the slot rather than shifting reel which can cause jerking.
5. Moved spindle so that 3' takeup reel was firmly on spindle. Tuned up 3' reel.(It was warped slightly).
6. Put stop on reel support to keep tape from wandering to right and rubbing against wheel which causes jerking. This guide is necessary when tape gets out of chimney.
7. Beveled top and bottom edges of seed holder to reduce sudden movement when seed holder goes over fingers and also into chimney.
8. Made a new thin seed holder.
9. Tried a new type tape - last 12" made up of 4" pieces held together by small ring - it didn't work.

10. Worked to smooth action of fingers.

11. Reduced gas flow to 35 cfh.

12. Took reading on frequency of vibrations in room and furnace.

4.2.4.2 Thermal Aspects and Web Widening

We mentioned at the start of this section that we standardized on a furnace configuration so that we could devote our time to shaping the isotherm in the melt to set up conditions favorable to web widening. This required then mainly working with the top heat shield. In the last phase, Section 4.2.3, we reported that more than one top heat shield actually hurt us in our widening rates; thus our standardization on one heat shield. Very early in this phase we found that we did not need to have a bottom heat shield, especially with the tapered susceptor; thus we stopped using one.

The last heat shield variation we had used in the previous phase was the LDBeXW. This had given too much cooling at the center. We decided to work first with a variation of this shield that was not as wide - namely, the LDBeW - which had not been tried with the tapered susceptor (TS). The various shield and susceptor setups used in this phase are given in Table 11. Before using the LDBeW with the TS, however, we used it with the straight sided susceptor (SS). The results that we got with the LDBeW/SS setup were the same as before. The LDBeW/TS setup gave us our best results. The aspect ratios of the buttons were better, i.e., more of the 1/2, 1/3 and higher as can be seen in Table 12. We were, however, not getting the improvements in widening rates that we desired. We then went to a short straight sided dog-bone (SSDB), Figure C-3 in Appendix C. This gave us good aspect ratios (see Table 12), our longest web up to that time, and the widening rates seemed to be better; however, the length of the slot (see Figure C-3) limited the final width of the web. Besides shaping the openings of the heat shield, the use of ports in the bottom of the susceptor affects the isotherms in the melt and may be used to encourage widening. In the first attempt 1/4" holes were cut in the susceptor as shown in Figure 17. This susceptor was designated TSP. So that we were seeing the effect of the ports only, a medium length straight slot (MSS, Figure C-4) was used. Growth in this setup was similar to growth in a susceptor with no ports - indicating that the openings were too small. The ports were opened to 3/8" diameter. The growth showed that the ports were giving an effect. Later a susceptor was made with oval ports (3/8" x 1/2") TSPO, Figure 17). This size ports gave too much cooling and was abandoned. Before studying the effects of shaped slotted heat shields, after heaters (AH, Figure 47) were used with MSS. These after heaters were not as tall nor as wide as the ones reported in Section 4.2.2. The effect of the after heaters was questionable, and since they still gave bad SiO build-up, they were set aside.

Since we were not getting the desired widening effects with straight slotted shields, we designed an opening that would give a gradual increase in width to each end; it was designated the "bowtie" (BT, Figure C-5). This

Table 11. HEAT SHIELD/SUSCEPTOR ARRANGEMENTS USED IN SECTION 3.2.1.4

Heat Shield[1]	Susceptor[2]			
	TS	TSP	TSPO	SS
LDBeW	1-25-77[3]	2-18-77		1-14-77
LDBeXW	2-4-77			1-4-77
MSS		2-18-77		
MSS + AH		2-19-77		
BT		2-23-77		
TDB		2-24-77		
NBT		2-28-77		
SSDB	2-10-77	3-1-77		
SDBN	3-7-77	3-3-77	3-16-77	
SDBN+AH		3-17-77		
LSDBN		3-13-77		
LSDBN+AH		3-21-77		

Notes:
1. Heat Shields: LDBeW, Fig. 17; LDBeXW, same as Fig. 17 only wider; MSS, same as Fig. 5 only wider; AH, Fig. 34; BT, Fig. 35; TDB, Fig. 11; SSDB, Fig. 8; SDBN, similar to Fig. 37 only distance between openings is .75"; LSDBN, Fig. 37.
2. Susceptors: TS, taper sided; TSP, taper sided with ports; TSPO, taper sided with oval ports; SS, straight sided.
3. Dates give the first time the arrangement was used.
4. Results of these measurements are given in the text.

Table 12. ASPECT RATIOS OF BUTTONS FROM SELECTED HEAT SHIELD-SUSCEPTOR COMBINATIONS

Run	Heat Shield	Susceptor	Aspect Ratios, W/L[1]
1-17-77	LDBeW[2]	SS[3]	20-1/2; 5-1/3; 4-2/3; 2-1/5
1-25-77	LDBeW	SS	7-1.2; 9-1/3; 2-1/1; 1-2/3
2-4-77	LDBeXW	TS	15-1/2; 3-1/3; 1-14
2-10-77	SSDB	TS	13-1/2; 5-1/3; 1-1/4
2-18-77	MSS/TSP1/4		3-bad; 2-1/1; 5-1/2
2-19-77	MSS/TSP3/8	AH	4-bad; 1-2/3; 3-1/2; 3-1/3
2-23-77	BT	TSP	1-1/1; 7-1/2; 10-1/3; 6-1/4; 4-1/5; 3-1/6; 1-1/7
2-24-77	TDB	TSP	2-1/2; 7-1/3; 1-1/4; 1-15
2-28-77	NBT	TSP	2-1/1; 8-1/2; 2-2/3; 7-1/3; 1-1/2; 2-1/6
3-1-77	SSDB	TSP	2-1/1; 3-1/2; 5-1/3; 3-1/4; 2-1/6; 1-1/7
3-3-77	SDBN	TSP	6-1/2; 9-1/3; 4-1/4
3-17-77	SDBN+AH	TSP	2-1/1; 6-1/2; 7-1/3; 1-1/4
3-13-77	LSDBN	TSP	3-1/1; 18-1/2; 6-1/3
3-21-77	LSDBN+AH	TSP	6-1/2; 2-1/3

Notes:
1. Width/Length.
2. Heat Shields: LDBeW, Fig. 17; LDBeXW, similar to Fig. 17, only wider slot; SSDB, Fig. 8; MSS, similar to Fig. 5 only wider; BT, Fig. 35; TDB, Fig. 11; NBT, Fig. 39; SDBN, similar to Fig. 37 only distance between openings is .75"; LSDBN, Fig. 37; AH, Fig. 34.
3. Susceptors: SS, straight sided; TS, taper sided; TSP, taper sided with ports.

AFTER SHIELDS

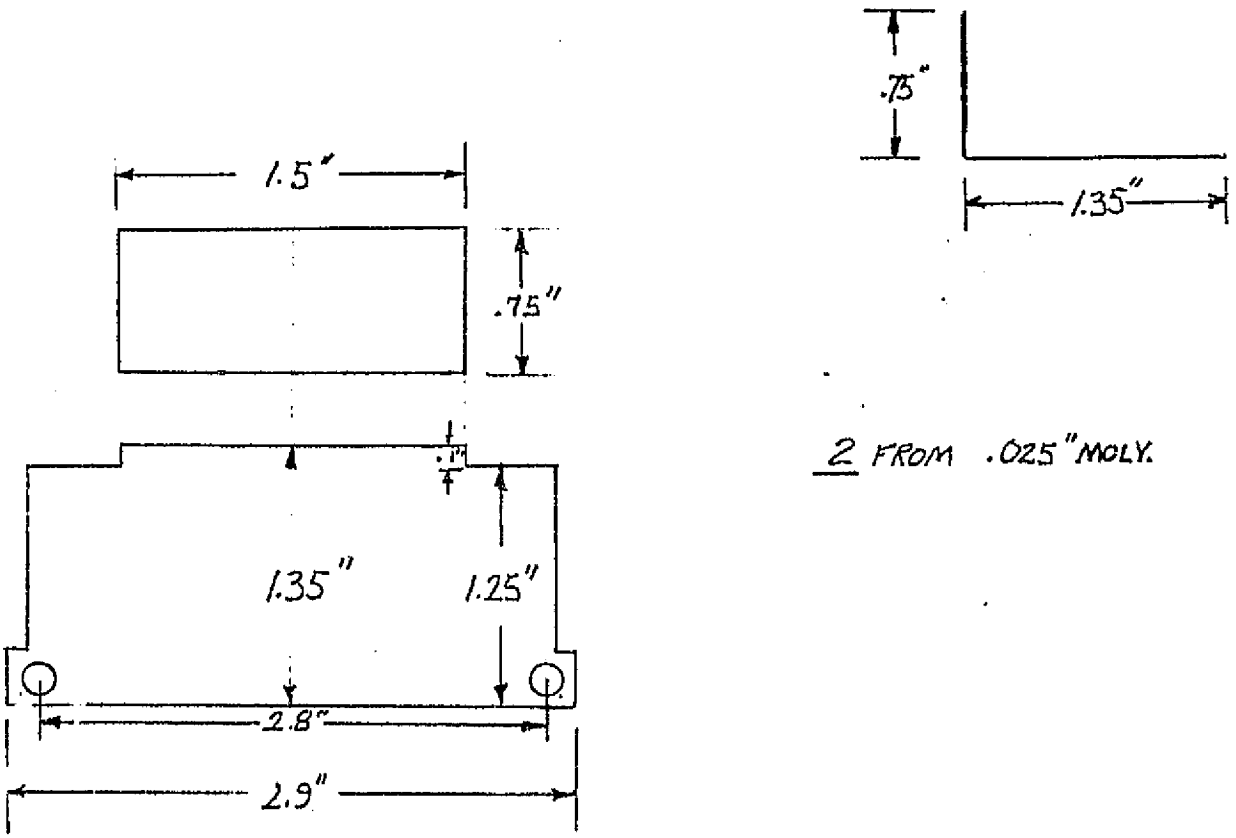

Figure 47. After heaters (AH)

looked promising, but the width of the opening appeared too large. The changes in widths and lengths of the opening in "dog bone" and "bow tie" type openings are given in Table 11. By studying the aspect ratios (Table 12) and widening rates (Table D-6) in Appendix D, one can see that the after heaters did not help in the widening rates. We do believe that they will be helpful in the perfection of wide web - more work should be done on this.

Looking at the widening rate data, it can be seen that there is some correlation between the thickness of the web and the widening rate. As a rule the thicker the web, the higher the widening rate. It seems quite obvious that there must be a "trade-off" on the widening rate. Where that "trade-off" is, our data does not allow us to say. We feel that rather than a large widening rate, (which is conducive to thirds), one should have a small sustained rate. In reality, seeding should be done using webs themselves as seeds. This was tried several times in this phase of the work. The results were encouraging enough to warrant further studies.

4.3 Growth of Primitive Dendrites

During this phase of the investigation, primitive dendrites were grown to give us a supply of various twin spacings, by dipping a seed into a supercooled melt. The seed may be any piece of silicon, single crystal, polycrystal, or a piece of dendrite. The idea is to have the melt so supercooled that rapid growth takes place on the seed in the form of growth mass. The growth being so rapid that growth mistakes are made in the form of many twin planes - silicon has a strong tendancy for twinning. Many of these twins will be parallel, and some of these will be close enough together to allow the growth of primitive dendrites upon rapidly pulling the growth mass from the melt. These primitive dendrites varying from an inch to several inches are then broken off, and their twin spacings catalogued.

Our first attempts to pull primitive dendrites involved the use of the wide straight slotted heat shield (Figure 24). For this shield, all primitive growth masses were too large to get through the opening. A heat shield with a large circular opening was made, Figure 48. With it we were able to pull large-growth masses. The growth masses contained approximately ten primitive dendrites. The data on the twin spacings measured from the various growth masses are given in Table 13.

From these, we chose two primitive dendrites, one whose two lamellae were almost of equal width (3μ, 2μ) and one in which one lamella is much larger than the other (8μ, 2μ). From these primitives, dendrites were grown for use as seed materials. The effect of the twin plane spacing on buttons (ease of formation and growth), wings (ease of formation and growth), and webs (growth) were assessed. These studies showed that there was very little difference in the aspect ratios of the buttons that were formed from seeds with twin spacings (a) 8-2μ; (b) 0.9-2μ; and (c) 3-2μ. Originally it was thought that the more favorable twin spacing would have the bigger aspect ratio (i.e. bigger refer, to the denominator). It was found, however, that the 3-2μ seeds caused a great deal of difficulty in seeding and as such are not favorable. As far as ease of seeding is concerned the 8-2μ and 0.9-2μ seeds appeared to be similar, with the 8-2μ seeds showing a slight "edge" on ease of seeding. During the latter part of the next phase (Section 4.2.4) seeds with the 8-2μ twin spacing were used in an attempt to encourage

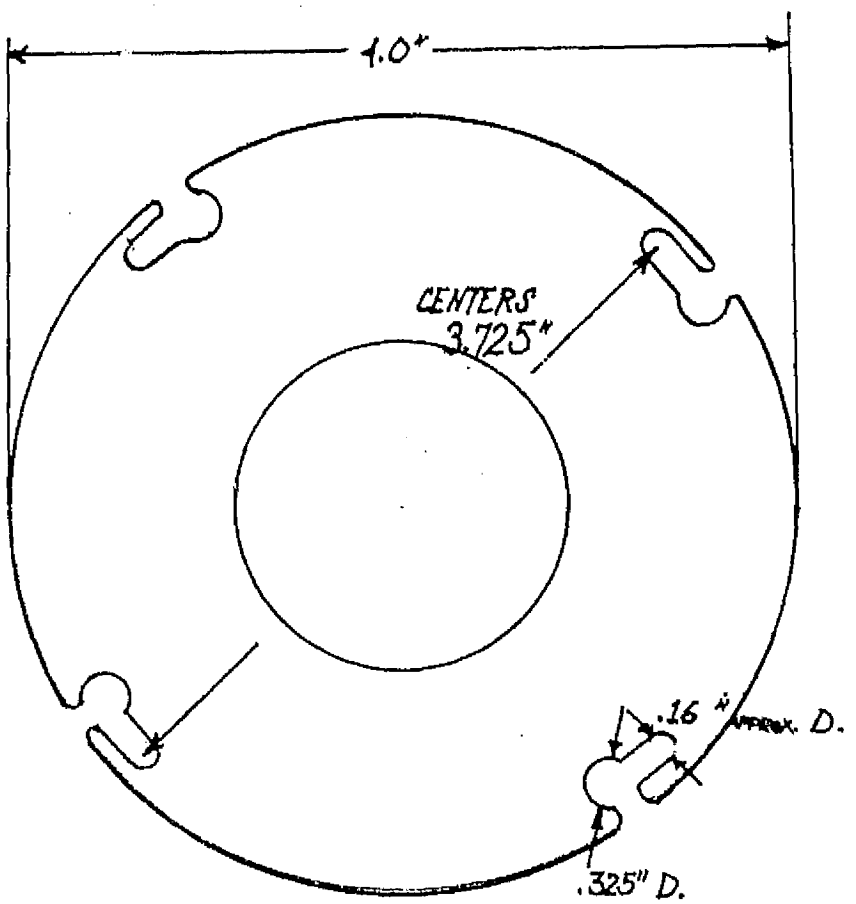

Figure 48. Circular heat shield for primitive growth.

DMJ 5/20/76

Table 13. TABLE OF TWIN SPACINGS FROM PRIMITIVE DENDRITE PULLS

Number of Twin Planes	Twin Plane Spacings (μm)			
	A[1]	B	C	D
5	0.4	0.4	0.1	1.9
4	1.6	2.4	1.0	
	8.0	2.0	10.0	
	19.2	1.0	8.8	
3	2.0	1.0		
	4.0	1.0		
	4.4	2.0		
	8.0	2.0		
	1.9	0.8		
	8.8	1.0		
	0.8	0.6		
	8.5	0.3		
2	14.0			
	12.0			
	9.4			
	7.0			
	6.4			

Notes: 1. Letters refer to lamellae as shown in Table 33.

widening of the web. It was found, however, that when dendrites and web having the 8-2μ twin spacings were pulled at speeds greater than 4 cm/min branching occurred. Dendrites and web having the 0.9-2μ spacing, on the other hand, could be pulled at rates exceeding 10 cm/min without branching. It thus appears that the optimum spacing would be .9 to 2μ for one lamella and between 3 and 8μ for the second lamella. This would put the optimum possibly the same as for Ge, although there is no reason to believe that they should be the same.

4.4 Summer Extension

The goals set for the next phase were:(1) to study the mechanical stability of web growth, and (2) to investigate the thermal conditions in the melt by careful and extensive thermocouple probing.

4.4.1 Mechanical and Thermal Stability: During all previous phases of this work problems in the mechanical stability of our system were investigated as they arose and appropriate changes made. These have all been reported in the other sections of this report. Toward the end of the last phase, a complilation of the causes for termination of two-dendrite web was made to guide our work in this phase. This is given in Table 14. As a result of this the following aspects of the furnace were studied and changes made:

1. The mechanical vibrations present on the floor of the laboratory were measured and compared with the vibration spectra on the growth table. Very low level, low frequency (≈3 hz) was found present throughout the room, i.e., on the floor and growth table. The air-table vibration isolator on the growth table had little or no effect on this low frequency vibration. The vibration spectra observed on the table did not change during actual pulling of dendritic-web ribbon. These results indicate that the ripples frequently seen on molten silicon surface do not originate from mechanical vibrations introduced during the pulling.

2. A new set of high and low control fingers for adjusting the ribbon position in the crucible were fabricated and installed.

3. Reduced mechanical play in all finger controls on top furance plate.

4. Designed and fabricated a new tape system.

Table 14. CAUSES FOR TERMINATION OF 2 DENDRITE WEB

I. Drop away from button

(a) melt too hot, (b) pull speed too fast, (c) button too wide.

II. Pull out

(a) melt got too hot (i.e., we increased the temperature too much,
(b) web not kept in center - one dendrite got much smaller than the other because it was in a hotter area.
(c) pulled too rapidly for temperature.
(d) melt vibrated violently.
(e) tape rubbed against wheel causing sudden jerk, or operator caused a sudden jerk.
(f) pull tape rubbed against the guide or reel caused a jerk.
(g) position of molten charge in crucible.
(h) edge dendrites much thicker than web.
(i) oxide forming "curtain" on one opening of dog-bone.

III. Third dendrite in web

(a) melt got too cold in web portion - did not go up in temperature enough or soon enough.
(b) fillet region too thick and/or too wide (a temperature and pull rate problem).
(c) web touched heat shield - this invariably results in web turning poly and soon thereafter a third starts. Turns poly because touching heat shield is an unwanted heat sink.
(d) button too wide.
(e) oxide drops in melt and attaches to web portion.
(f) pull tape rubbing against guide or reel.

IV. Third on outside of edge dendrites

(a) usually at start, the center of lateral symmetry is way off, or else seed put in off-center.
(b) web gets off-center, and one dendrite sees a much cooler region.
(c) oxide drops in melt and attaches to outside of either edge dendrites.

5. The ribbon take-up reel was trimmed up for roundness.

6. Installed a teflon lower tape guide with a concentric level to decrease wander of tape during pulling.

7. A concave groove was machined in the cloth tape guide to keep the tape from wandering from side to side during pulling.

8. A one inch slot was machined in the take-up reel so that the head of the screw holding the cloth tape would not protrude above the surface of the reel bed. (A protruding screw head had caused breakage of a ribbon in the past as it was being wound onto the reel.)

9. A support was fabricated and installed to keep the r.f. coil rigid and level.

10. An improved friction brake to keep a uniform tension on the cloth tape storage reel was designed and fabricated.

11. A new base was designed and installed for the pedestal so that the entire pedestal column and susceptor could be re-centered each time a new charge is introduced to the crucible. This insured the placement of the charge in the thermal center of symmetry for each run.

The following items were performed in preparation to making improvements in the thermal stability of the growth facility:

1. Fabricated a new 6 1/2" diameter r.f. coil to allow greater latitude in controlling the center of thermal symmetry in the melt.

2. The pedestal support was re-machined to give better geometric symmetry.

3. Polished the ends of the alumina pedestal so that they were flat and parallel to permit better geometric symmetry.

4. A gauge was designed and fabricated to check the geometric symmetry of the furnace components.

The following general changes were made in the system to improve reliability:

1. A low Ar pressure warning buzzer was installed.

2. Improved the electrical isolation of the generator filament transformers to reduce risk of generator breakdown.

3. A new heat exchanger plate was installed on the generator cooling water system to reduce the cooling water temperatures.

4.4.2 Thermocouple Studies

The thermocouple data reported in Sections 4.2.3 and 4.2.4 were taken by measuring directly the emf of the Pt - Pt 10% Rh thermocouple (TC) with a digital microvoltmeter. With this set up, we encountered fluctuations of from 10 to 50 microvolts - and occasionally even higher. This of course limited our accuracy since 12 microvolts equalled 1 degree. This accuracy was, however, acceptable for those studies. In the present studies, we wanted to be able to measure accurately temperature differences of 1/2° or less. To get this accuracy it was necessary to eliminate or greatly reduce the fluctuation and to use a voltage to buck-out all but a small amount of the emf generated by the thermocouple. For temperature differences between two points of the melt, we could of course buck one TC against another. For individual measurements, however, it was necessary to use an exceedingly stable DC voltage that could be varied. It was felt that the required stability of the voltage source could not be readily obtained from commercial D. C. power supplies. Thus a power supply was made from a 1 1/2 volt Hobby battery with a large resistor and a 10 turn potentiometer in series as shown in Figure C-6. This proved to be exceedingly stable.

The original idea was to make five readings simultaneously at the center and at four spots symmetrically placed toward the edges of the melt. A special water cooled top plate for the furnace was fabricated which contained appropriate openings for the thermocouple probes. A 4 channel Sanborn recorder was obtained for this purpose. This proved highly impractical, however, as a full scale of 12 to 36 microvolts was required to get the desired accuracy. This meant that temperature differences of over 3° required either a scale change or a change in the bucking voltage. Either one added too great an uncertainty in the readings. Next a Honeywell Electronik 19 TC recorder along with a 5 position thermocouple switch was purchased from the Omega Corporation in an effort to make the five readings sequentially and record them on one recorder. A box was constructed to hold the bucking voltage source, connectors for the 5 thermocouples, and connectors for external monitoring. This, however, proved unmanageable in that each thermocouple required a different bucking voltage to keep it on the chart. We found that the most accurate way was to use a single thermocouple, connected directly to the bucking power supply and the recorder, and move it to the desired position in the melt. The Honeywell recorder was used exclusively after the Sanborn continued to breakdown.

Considerable difficulty had been experienced in what we thought was pick-up of the r.f. noise. Shields made from molybdenum tubing appeared to help. Frequency measurements of the noise showed, however, that it could not be r.f. We went to direct connection to reduce noise in our signal. At first we were getting quite a bit of noise and "temperature" fluctuations. In an effort to reduce this, every conceivable thing that could remotely contribute to noise and "temperature" fluctuations was varied while the thermocouple was at a set temperature. The items varied were:

(a) Argon flow. Changing the flow between 25 and 50 cfh had no effect on either the noise or the temperature.

(b) Air currents. The door was opened and closed, the hood exhaust fan, furnace exhaust fan, and air conditioner were turned off and on. None of these had any effect on the noise. The only one of these to affect the temperature was opening and closing the door. Opening the door caused an increase of approximately 1°C.

(c) R. F. pickup. The r.f. was turned off momentarily. Although temperature dropped, the noise on the chart line did not change.

(d) Connections. All connections were examined and wires "wiggled". Those causing noise were tightened or remade until this case was eliminated. It is still necessary to check these periodically. The junction box was found to be a particularly bad source of contact noise. Since we had found that one thermocouple was best, we eliminated the junction box and directly connected the thermocouple to the recorder. Omega type NMP miniature thermocouple connectors were used. An Omega electronic ice point thermocouple connector was tried but had no effect in eliminating noise.

(e) Automatic temperature controller. The interface circuit that converts the signal from the automatic temperature controller to match the input required for the D.C. power supply, which controls the generator, was re-wired to reduce the fluctuation in its output. To see if the automatic controller and/or the interface circuit might be causing the noise or "temperature" fluctuations, the following were done:

(i) The furnace was manually controlled from the automatic control panel (this operation went through the interface circuit).

(ii) The furnace was manually operated from the D.C. power supply (i.e., the automatic control and the interface circuit were disconnected). Analysis of the results showed that neither the interface nor the automatic controller were contributing to the noise or fluctuations.

(f) Position of thermocouple in furnace. Temperatures were monitored at various positions and depths in the melt, and also in cavities in the susceptor. It was found that when the thermocouple was near the surface (within 4 mm) or near the edges the noise increased. It was also noiser when the thermocouples were placed in holes in the lip of the susceptor.

(g) Shielding. In June before the preceding was done, it was felt that shielding the thermocouple and all wires to the recorder would be necessary. Molybdenum tubing was used to shield the thermocouple, all connectors were shielded as were the wires. When these were first used, they appeared to help. After we had eliminated all possible source of noise, we found that shielding was not necessary.

(h) Motion of melt. We looked at the motion of the melt as a source of noise. The frequency of normal movement, however, did not correspond to the frequency of the noise. Also on days when there was essentially no movement to the melt, there was little change in the noise. There was one day when the motion of the melt became quite violent toward the end of the day. At that time, the noise had increased to 1 - 1.4°C.

These studies resulted in a recording with noise below .5°C usuaally it was around .25°C. With the coil at our pulling height (i.e., 2.5 mm above the top of the heat shield) and the temperature at 1450°C, according to the optical pyrometer, the temperature varied only $\pm$ .6°C, over a 15 minute period.

Studies were then started on the probing. The tapered sided susceptor (TS) was used in conjunction with the dog-bone (LSDBN), Figure C-7, heat shield. The coil was moved horizontally, and the temperature was measured across the slot. For measurements involving moving the coil in the x-y plane, the thermocouple or thermocouples are held stationary in the desired position (positions) until all readings are taken for that particular position. Then if necessary the TC and/or the CP are changed to another position. This is continued until all desired positions have been measured. It was not possible to adjust the center of thermal symmetry. The left side was always colder even though the coil was almost against the glass on that side. It was noticed that the lip of the left side had a chip in it. The next day the susceptor was rotated 180° so that the chip was on the right side. It was again not possible to adjust the center of thermal symmetry, only this time the right side remained colder. A new tapered susceptor (TS) was made. When this was used, it was possible to balance the thermal symmetry - see Table 15. A straight sided susceptor (SS) was also run with the dog-bone heat shield, as shown in Table 16. The effect on the temperature from front to back shifts of the coil for the LSDBN/TS was also investigated and the data given in Table 17. In these tables, it can be seen that the center of thermal symmetry was satisfactorily adjusted by x and y shifts of the coil.

Table 15. THE EFFECT ON TEMPERATURE ACROSS THE SLOT FOR HORIZONTAL COIL CHANGES

Thermocouple Position in Slot*					Coil Position (cm)	
1	2	3	4	5	L-R [1]	F-B [2]
**						
5.3	1.8	.9	2.9	7.6	3.87	5.57
7.2		2.7		7.6	4.30	5.57
rotated susceptor and coil 180° to above						
1.0		.6		2.2	3.75	5.57
5.3				7.4	4.31	5.57
4.6				6.4	4.86	5.57
4.2	2.0	2.0	2.4	4.2	5.22	5.57
5.4				4.4	5.57	5.57

Notes: The LSDBN/TS arrangement was used. The coil was 2.5 mm above the top of the heat shield, and the thermocouple was .44 cm above the bottom of the crucible.

* Numbers shown indicate position of measurement.

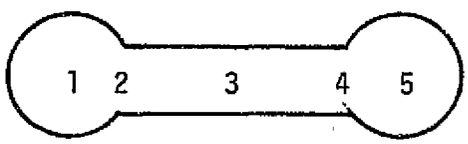

** Relative temperatures (°C).

1. Left-Right Coil Movement
   Scale reading. Center Reading: 4.00 cms.
   Higher values indicate off center to left.

2. Front-Back Coil Movement
   Scale reading. Center reading: 5.57 cm.

Table 16. THE EFFECT ON TEMPERATURE ACROSS THE SLOT FOR HORIZONTAL COIL CHANGES

	TC position in slot *					
	1	2	3	4	5	Action
**	8	4.8	6.4	7.2	10.7	initial
	8.8	7.2	6.6	8.5	8.2	moved coil to adjust
	9.4	7.7		8-8.5	9.7	T increased
	10.9				8.5	coil moved closer to (1)
	8.2				10.4	coil moved closer to (5)

Notes: The LSDBN/SS arrangement was used. The coil was 2.5 mm above the top of the heat shield, and the thermocouple was .44 cm above the bottom of the crucible.

*Numbers in figure show position of measurement

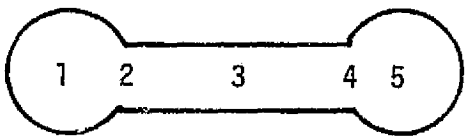

** Relative temperatures (°C).

Table 17. THE EFFECT ON TEMPERATURE FOR HORIZONTAL COIL CHANGE

Thermocouple Position		Horizontal Coil Position (cm)	
Front[1]	Back[1]	F-B[2]	L-R[2]
* 26.2	18.8	7.0	3.74
27	20.8	7.5	3.74
6.9[3]	1.4-2.	7.5	3.74
6.2	4.2	8.0	3.74
	changed recorders		
2.5	3.0	5.5	3.74
	3.1	5.25	3.74
2.5	1.6	5.4	3.74
4.8	3.2	5.45	3.74
3.2	3.8	5.5	3.74

Notes: The LSDBN/TS arrangement was used. The coil was 2.5 mm above the top of the heat shield, and the thermocouple was .64 cm above the bottom of the crucible.

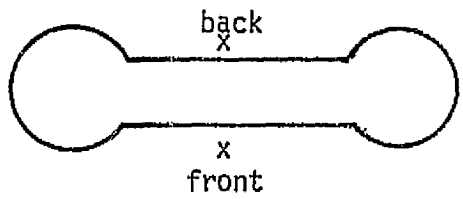

1. Location of measurement shown on sketch.
2. F-B, front to back; L-R, left to right. Relative Temperatures (°C).
3. Changed scale from the readings above.

* Relative Temperatures (°C).

The effect that raising and lowering the coil had on the temperature in the center and one end of the slot, and thus the ΔT from end to center for the NSS, Figure C-8,LSDBN, Figure C-7, and NBT,Figure C-7heat shield are given in Table 18 for the TS susceptor. This data may be compared for the same heat shields on the TSP susceptor given in Table 19. For measurements involving moving the coil in the z direction, i.e., coil position (CP) changes to observe temperature changes or time constants, the thermocouples are left at one place and readings taken until all of the planned CP changes have been made. Then the thermocouples are moved to other spots in sequence and CP changes carried out. Extensive time constant data was taken for vertical shifts in the coil for the three heat shields NSS, LSDBN, and NBT. The data is given in Table 20 for the TS susceptor and in Table 21 for the TSP susceptor. Comparing this data, one can see that the time constants for the furnace under automatic control is from 1 min to 1 min 30 sec., and under manual control from 2 min to 4 min.

At the start of the last phase, Section 3.2.1.4, a 10 turn potentiometer was installed in series with our controller. Twenty-six turns on the pot gave us a 1° change in temperature. With this set-up, we were able to "call for" temperature changes of a fraction of a degree. There is no question that this helped us immeasurably; what we did not know with any certainty was (a) how faithful was the setting, i.e., when we called for a 1/4° change, did we actually get 1/4°? and (b) how reproducible was the setting, i.e., if we increased the temperature 10° (260 turns) using only the pot and then decreased it back to the original setting, would it come back to the exact

temperature? With our TC set-up, we studied this by placing a TC in the center of the melt. The measurements were made at 15° above the melting point - a necessary precaution to insure that growth does not take place on the quartz protective tubing. Temperatures were varied 1/4, 1/2, 3/4, 1,2, and 7° as if we were pulling web. The output of the TC was put onto the strip chart recorder, and whenever a change was made, a time notation was marked on the chart. The final resulting temperature and the time it took to reach that temperature were read off of the strip chart. The data is given in Table 22. One can see that the temperature that we actually obtained and that which we "called for" are within 1/4° for changes up to 2° and better than 1/2° for a change of 7°. The response times run around 1.3 minutes as we had measured earlier. Numerous other data showed that by using only the 10 turn pot - to make a change we could always come back to the same temperature within 1/4°. Several times long term stability of the temperature was investigated by leaving everything set on automatic control and continuously monitoring the TC output on the strip chart recorder. Table 23 reports a 15 min run in which the temperature variation was $\pm$ .6° with a total of .5° noise in the TC. Other runs showed a stability within $\pm$ .6° for up to 2 hours. This data, in Table 22, was taken for the NSS/TS arrangement. Other pertinent data in noise, long runs, also manual control are given in Table 23. For example it can be seen that it takes 15 - 30 sec. before the TC responds to a 2-3° temp. change.

Table 18. THE TEMPERATURE CHANGE BY VERTICAL SHIFT OF COIL FOR TAPER SIDED SUSCEPTOR

Heat shield	Top of Coil above top of heat shield (mm).	Relative Temperatures (°C)		ΔT
		Center	End	
NSS[2]	4.5	11.84	5.6	6.24
	3.5	10.56	4.16	6.4
	2.5	9.28	2.56	6.72
	1.5	8.32	2.24	6.08
	.5	7.36	1.76	5.6
LSDBN	3.5	6.24	12.48	6.24
	2.5	4.00	8.48	4.48
	1.5	8.32	14.4	6.08
	.5	8.80	14.08	5.28
NBT	4.5	14.64	8.32	6.32
	3.5	12.96	7.04	5.92
	2.5	10.56	5.28	5.28
	1.5	9.44	4.00	5.44
	.5	8.80	1.60	7.2

Notes: 1. Thermocouple was .44 cm above the bottom of the crucible.
2. Heat shields: NSS, Fig. C-8 LSDBN, Fig. C-7 NBT, Fig. C-9.

Table 19. The Temperature Change by Vertical Shift of Coil for Taper Sided Susceptor with Ports

Heat Shield Heat Shield	Top of coil above top of heat shield in mm.	Relative Temperatures in °C		ΔT
		Center (3)	End (1)	
NBT	4.5	5.76	8.56	2.8
	3.5	4.4	6.64	2.24
	2.5	3.6	5.84	2.24
	1.5	2.24	4.4	2.16
	.5	.88	3.84	2.96
LSDBN	4.5	12.6	17.3	4.7
	3.5	10.7	16.3	5.6
	2.5	9.3	14.4	5.1
	1.5	8.2	13.0	4.8
	.5	6.7	11.2	4.5
NSS	4.5	6.7	12.4	5.7
	3.5	5.5	11.0	5.5
	2.5	4.4	10.0	5.6
	1.5	3.4	9.0	5.6
	.5	2.3	7.5	5.2

Notes: 1. Thermocouple was .44 cm above the bottom of the crucible.

2. Heat shields: NSS, Fig. C-8, LSDBN, Fig. C-7; NBT, Fig. C-9.

Table 20. TIME CONSTANTS FOR VERTICAL SHIFTS OF COIL FOR TAPER SIDED SUSCEPTOR

Heat Shield	Coil Shift (mm)	Temperature Change (°C)	Time (min. and sec.)
NSS	2.5-4.5	2.4	36"
	4.5-3.5	2.2	1' 6"
	4.5-3.5	1.3	1'
	3.5-2.5	1.3	1'
	2.5-1.5	1.3	1' 12"
	1.5- .5	.8	1' 12"
	12.5-7.5	scale change	3' 30"
LSDBN	7.5-2.5	3.3	2' 30"
	2.5-1.5	1.5	1' 30"
	1.5- .5	1.5	1' 30"
	.5-2.5	2.3	1' 12"
	2.5-3.5	1.5	1'
	12.5-2.5	8.0	1' 30"
	2.5-12.5	scale change	1' 48"
NBT	12.5-2.5	14.4	1' 6"
	2.5-12.5	14.4	2' 48"
	12.5-2.5	13.2	1' 42"
	2.5-4.5	2.8	1' 50"
	4.5-3.5	1.7	2' 15"
	3.5-2.5	2.4	1' 25"
	2.5-1.5	1.1	1' 12"
	1.5-.5	.8	1' 24"
	4.5-3.5	1.7	1' 18"
	3.5-2.5	2.4	1' 48"
	2.5-1.5	1.1	1' 18"
	1.5- .5	.6	1' 12"

Note: Heat shield designations are given in Table 19.

Table 21. TIME CONSTANTS FOR VERTICAL SHIFTS OF COIL FOR TAPER SIDED SUSCEPTOR WITH PORTS.

Heat Shield	Coil Shift	Temp. Change in °C	Time in min. & sec.
LSDBN	2.5 - 1.5	1	1' 24"
	1.5 - 2.4	3.1	4' 0"
	2.5 - 1.5	2.6	4' 30"
	1.5 - 3.5	4.1 - 6.1	4' 0"
	2.5 - 4.5	3.6	1' 42"
	4.5 - 3.5	1.9	1' 48"
	3.5 - 2.5	1.4	1' 48"
	2.5 - 1.5	1.3	1' 42"
	1.5 - .5	1.6	1' 30"
	4.5 - 3.5	.4	1' 12"
	3.5 - 2.5	1.9	1' 54"
	2.5 - 1.5	1.6	1' 36"
	1.5 - .5	1.6	1' 36"
NBT	2.5 - 4.5	2.0	1' 36"
	4.5 - 3.5	1.4	36" - 1' 24"
	3.5 - 2.5	1.0	1' 18"
	2.5 - 1.5	1.7	54"
	1.5 - .5	1.7	1' 6"
	.5 - 1.5	.6	36"
	1.5 - 2.5	1.4	1' 24"
	2.5 - 3.5	.8	1' 6"
	3.5 - 4.5	1.9	1' 0'
	4.5 - 2.5	2.1	1' 24"
NSS	4.5 - 3.5	1.2	1' 12"
	3.5 - 2.5	1.1	42"
	2.5 - 1.5	1.0	1' 30"
	1.5 - .5	1.1	1'
	4.5 - 3.5	1.4	1' 30"
	3.5 - 2.5	1.0	1' 24"
	2.5 - 1.5	1.0	1' 30"
	1.5 - .5	1.5	1' 48"

Table 22. TEMPERATURE AND TIME RESPONSE TO PROGRAMMED TEMPERATURE CHANGE WITH THE NSS/TS[1] ASSEMBLY

Programmed Temperature Change (°C)	Time to reach temperature(Min.)	Temperature for change on thermocouple (°C)
up 1	1.3	1.2
down 1	1.0	.6
up 1	1.4	1.2
down 1	1.4	1.2
up 1/4	1.2	.25
down 3/4	1.2	.6
up 2	1.2	1.8
down 2	1.0	1.75
down 7[2]	1.3	7.2
down 7[2]	1.5	6.5
up 7[2]	1.3	7.5

Notes: Thermocouple in the center, .44 cm above the bottom of the crucible.

1. NSS/TS is narrow straight sided, Fig. 25, heat shield on the taper sided susceptor. The top of the heat shield is 45 mm below top of coil.
2. For this data the heat shield was changed to the NBT, Fig. 49. Top of heat shield was 2.5 mm below top of coil.

Table 23. OTHER DATA

With coil at 9.1 and temp. 1450 over a 15 min. period, T. C. varied ± .6°. Noise was .5° total.

Ends noisier than center but time const. is same.

Response time of TC is 15 - 30 sec. for a 2 - 3° temp. change.

Manual control - 90.3v was 1461°. We went up to 92.6v, this gave 1479° a change of 18°. (15.2° on T.C.) to change 2 min. 40 sec. We dropped to 90.8v - 1464° (down 15°) (15.2° on TC)in 3 min. 20 sec. The coil was .44 cm above the top of the heat shield.

Temperature changes across the slot as a result of changes in the vertical position of the coil such as those given in Tables 18 and 19 are plotted in the Figures 50 through 56 for the various heat shield/susceptor combination given in Table 24. These can be compared with earlier data - see Figure 34, Figure 40, and Figure 41. Some of the data is plotted in a different way in Figures 57 and 58 namely as temperature versus depth below the surface of the melt at the center, and at one extremity of the heat shield opening. As one can see, the vertical gradients are of the type making it the coolest at the surface, intermediate at half, and hottest at the bottom - rather than one of the inverse or inversion type discussed in Section 4.2.3. A careful comparison of the curves in these figures shows that for each heat shield the ports in the susceptor, TSP, have a slight cooling effect in the melt causing the T to be a few tenths of a degree below that for the susceptor with no ports, TS - see Table 24. The cooling effect of the ports is seen more strikingly in the curves themselves (compare Figures 50, 51, 53, and 54, and 55 and 56). The flattening out of the curves at the outer edges for the TSP is quite evident.

Besides the difference in the curves caused by the different susceptors or a given heat shield, one can also see a difference between the heat shields. Referring again to Table 24, it is seen that the long straight, narrow dog-bone (LSDBN) heat shield gives the smallest temperature gradient across the slot (with the TS and TSP susceptors) while the NSS heat shield gives the largest gradient. It should also be noticed that the straight sided susceptor (SS) gave a much higher temperature gradient across the LSDBN heat shield than was found for either the TS or TSP susceptor. This larger gradient definitely suggests that the SS susceptor is not as favorable as the tapered ones, contrary to the suggestion in the thermal modeling section 3.2.3 that the SS susceptor should give wider web. We have at present no answer to this apparent conflict.

Detailed probing of the melt was carried out for the three heat shields on the TSP susceptor. In addition the LSDBN shield was used with the SS susceptor. We also included data we had taken previously for the LDBeW/SS combination. The data was taken by rigidly holding the TC at one level with a rubber "O" ring (11/64" thick). The TC was moved horizontally to each station until all data at one level was taken, then another spacer was put on and the process repeated until the entire melt had been probed. The data was then plotted on a drawing of a crucible. The data for LDBeW/SS is found in Appendix C in Figure C-10; LSDBN/SS, Figure C-11; LSDBN/TSP, Figure C-12; NBT/TSP, Figure C-12; NSS/TSP, Figure C-14; and a more detailed probing of NSS/TSP in Figure C-15. In reality very little can be said of Figure C-10. This was data taken earlier by reading the output of a TC on a digital voltmeter; it was included here to show the difference between the two techniques.

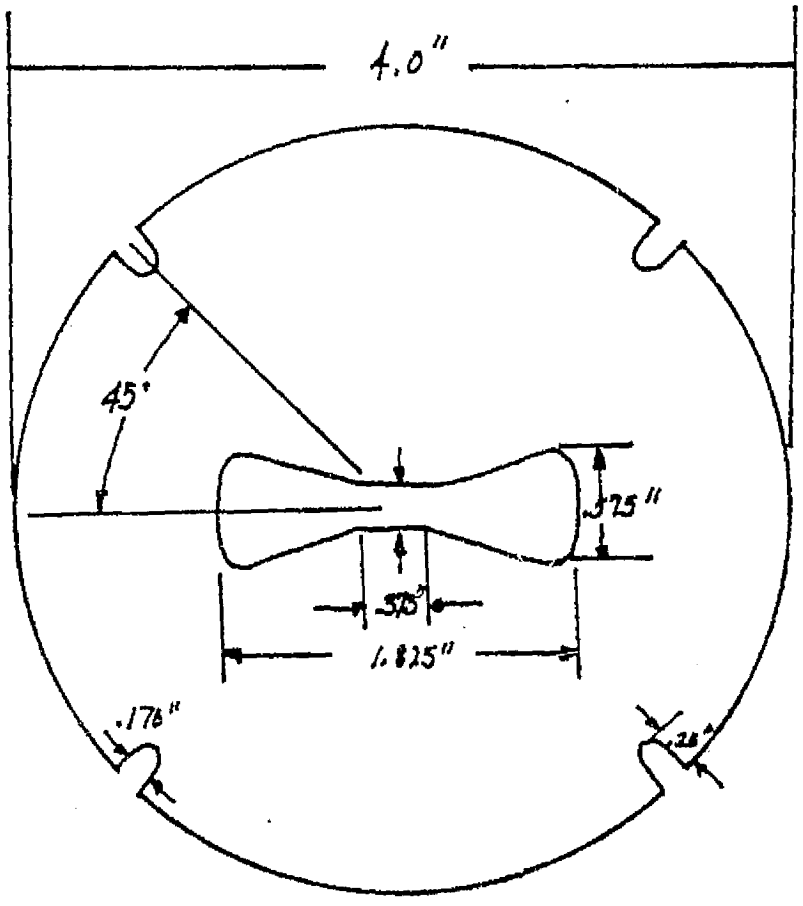

Figure 49. Narrow bow-tie (NBT) heat shield.

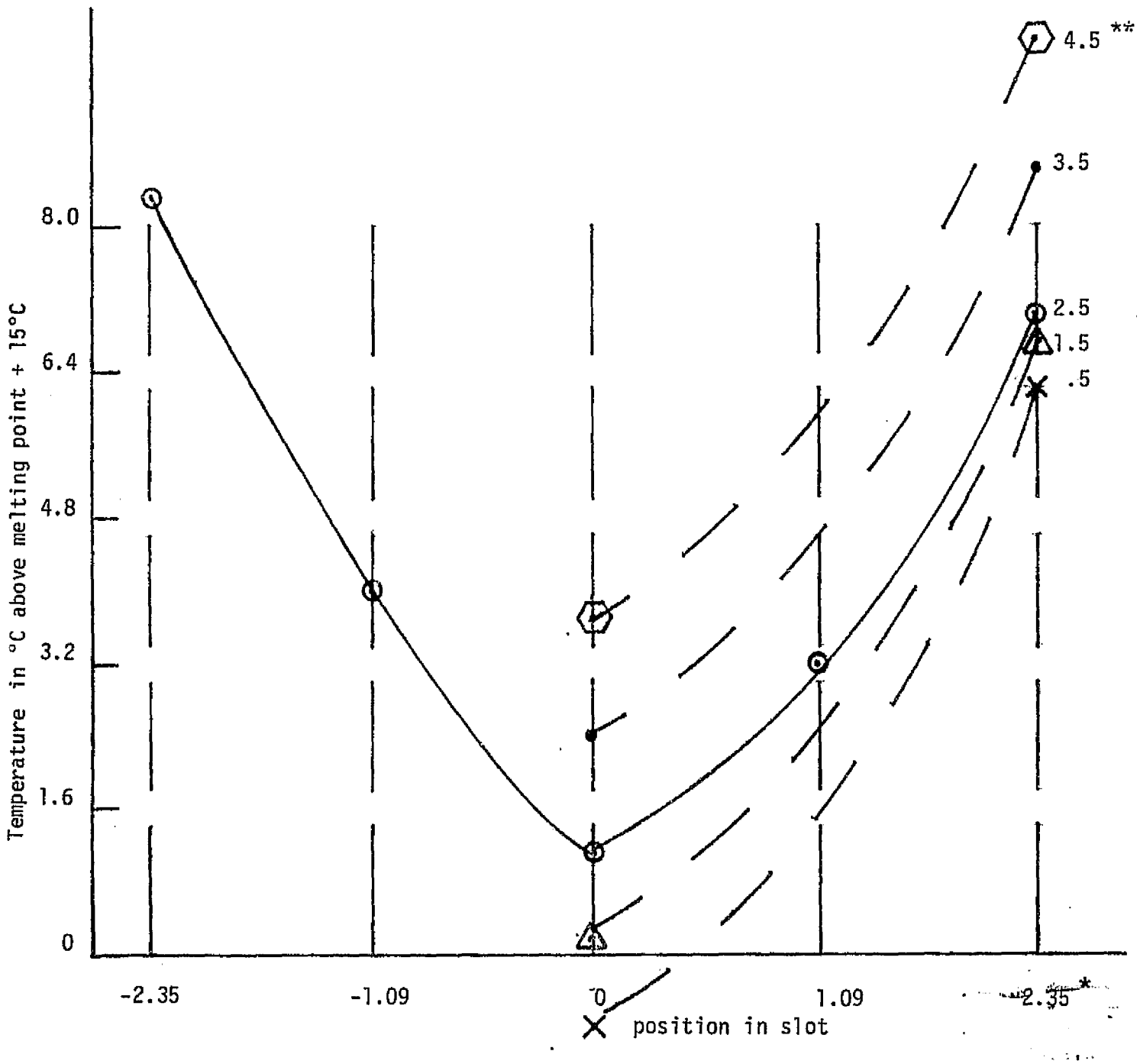

Figure 50. Temperature across slot for straight slot. Tapered susceptor with no ports. T.C. 11/64" from bottom of crucible.

* Numbers indicate position in slot given in cns. from center.

** Top of coil above top of heat shield in mms.

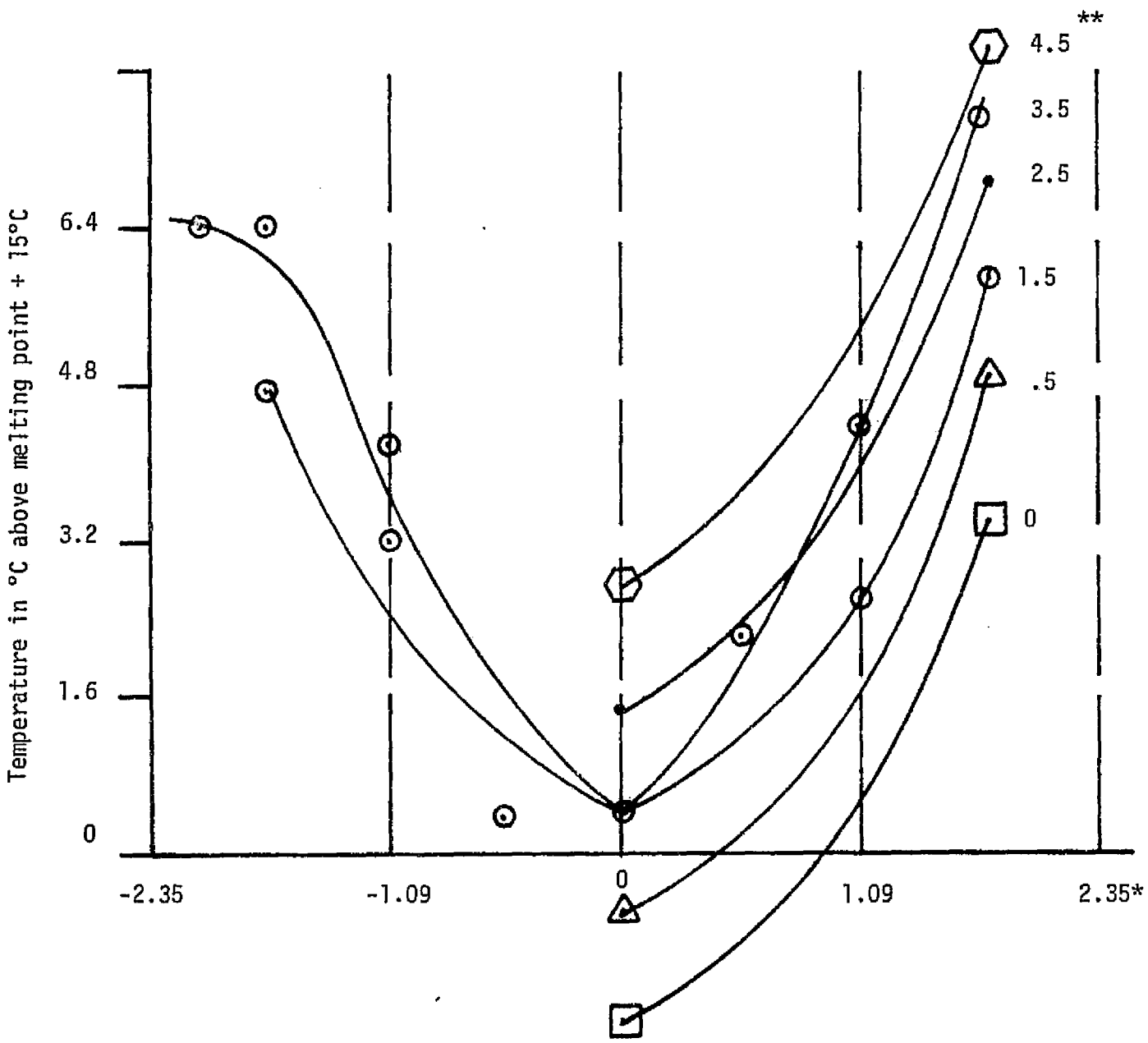

Figure 51. Temperature across slot for narrow straight slot and tapered susceptor with ports.

* Numbers indicate position in slot given in cms from center.

** Top of coil above top of heat shield in mms.

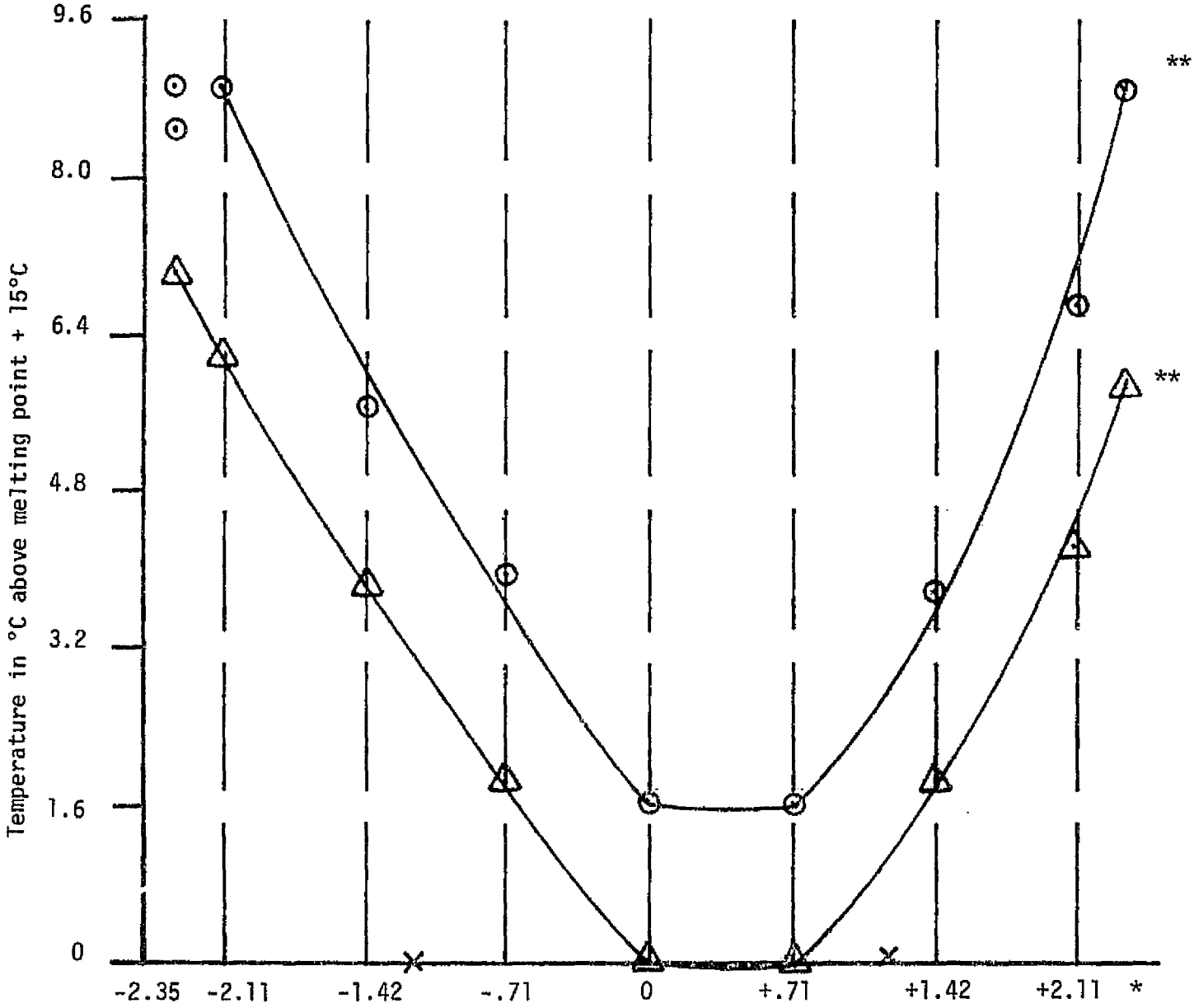

Figure 52. Temperature across dog-bone slot LSDBN/SS. T.C. 11/64" from bottom of crucible.

* Numbers indicate position in slot given in cms from center.

** Curves for two coil positions. The top curve is for the higher coil position.

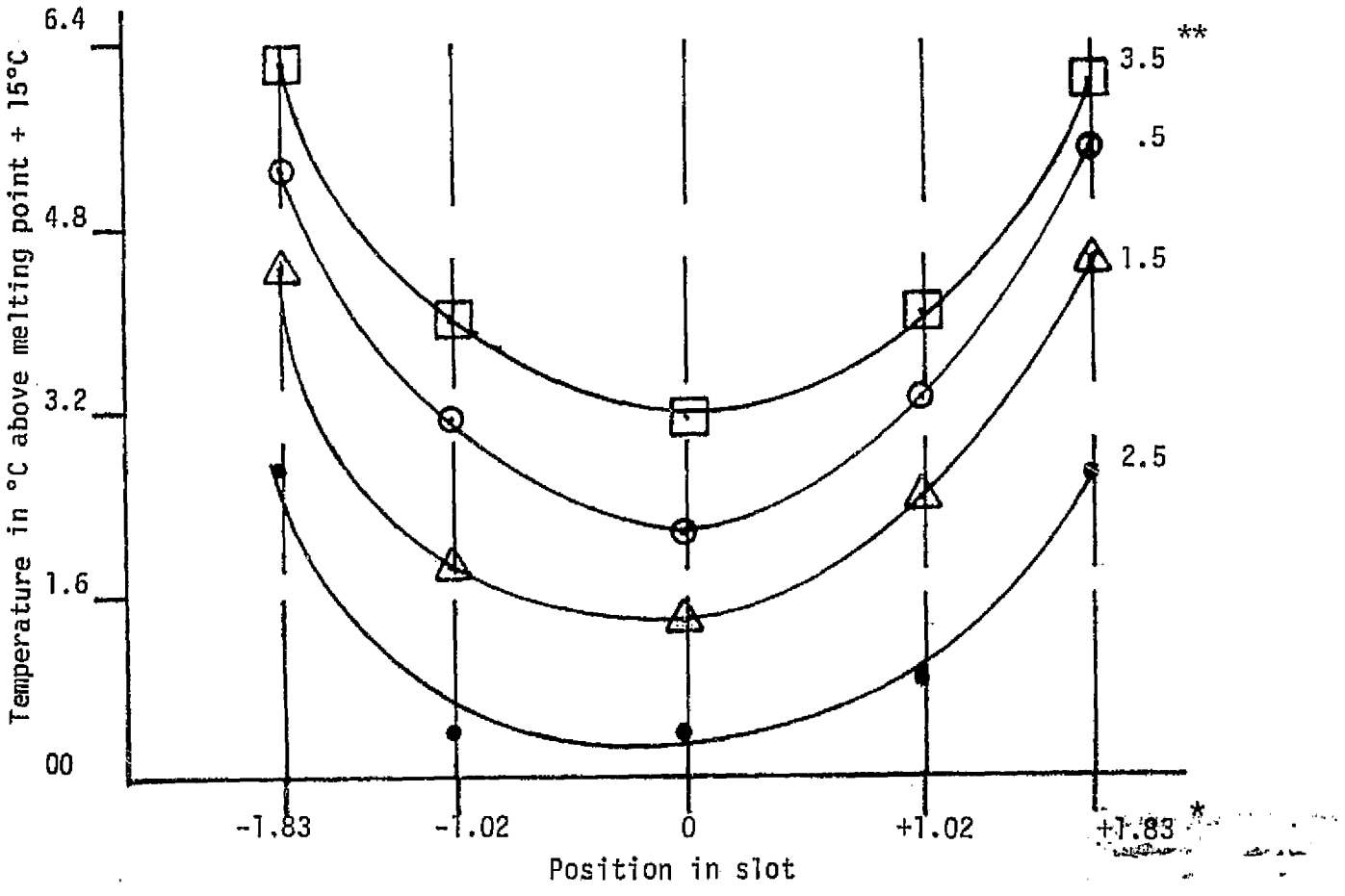

Figure 53. Temperature across dog-bone slot . LSDBN/TS T.C. 11/64" from bottom of crucible.

* Numbers indicate position in slot given in cms. from center.

** Top of coil above top of heat shild in mms.

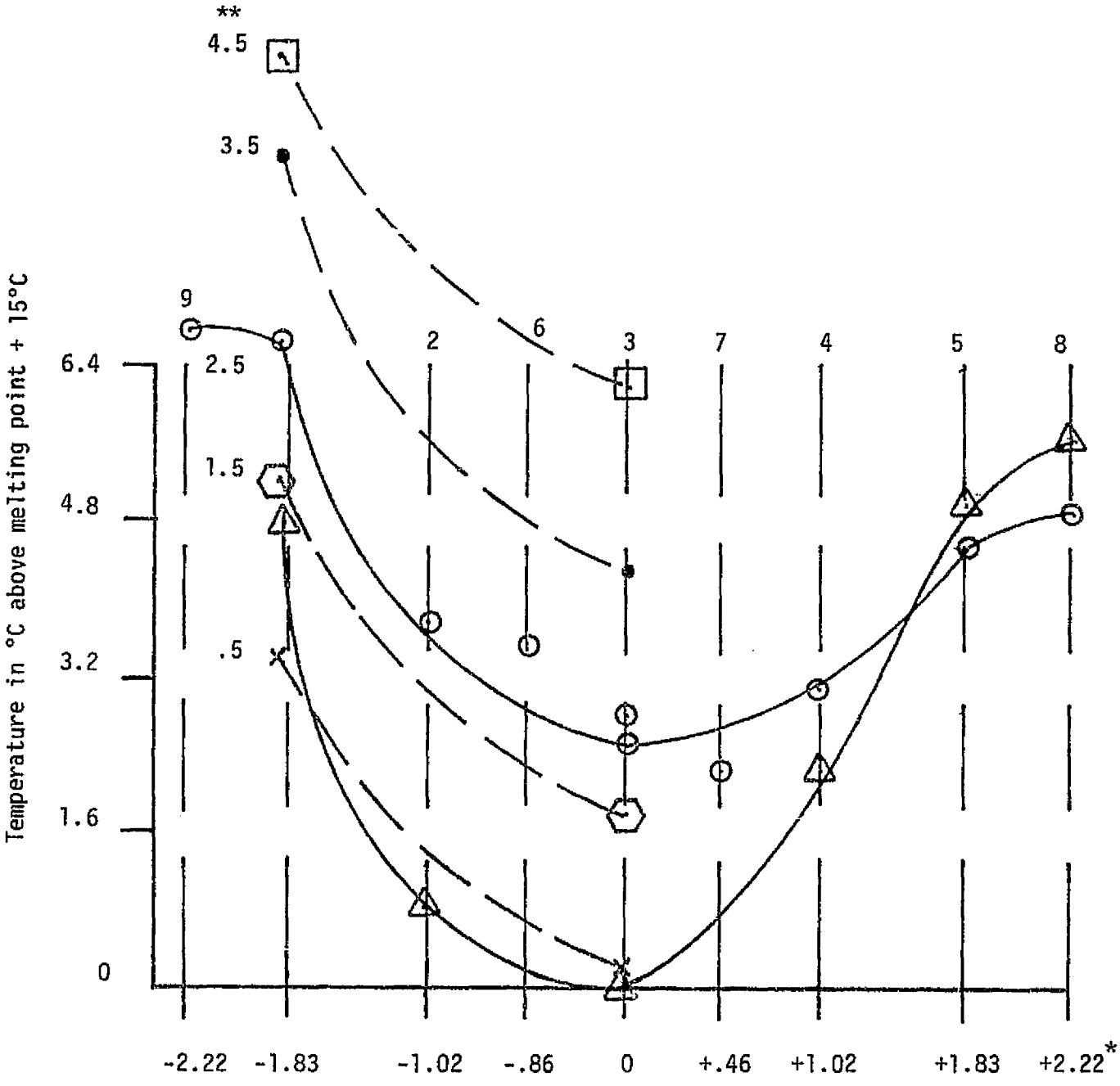

Figure 54. Temperature across dog-bone slot LSDBN/TSP.
T. C. 11/64" from bottom of crucible.

* Numbers indicate position in slot given in cms. from center.

** Top of coil above top of heat shield in mms.

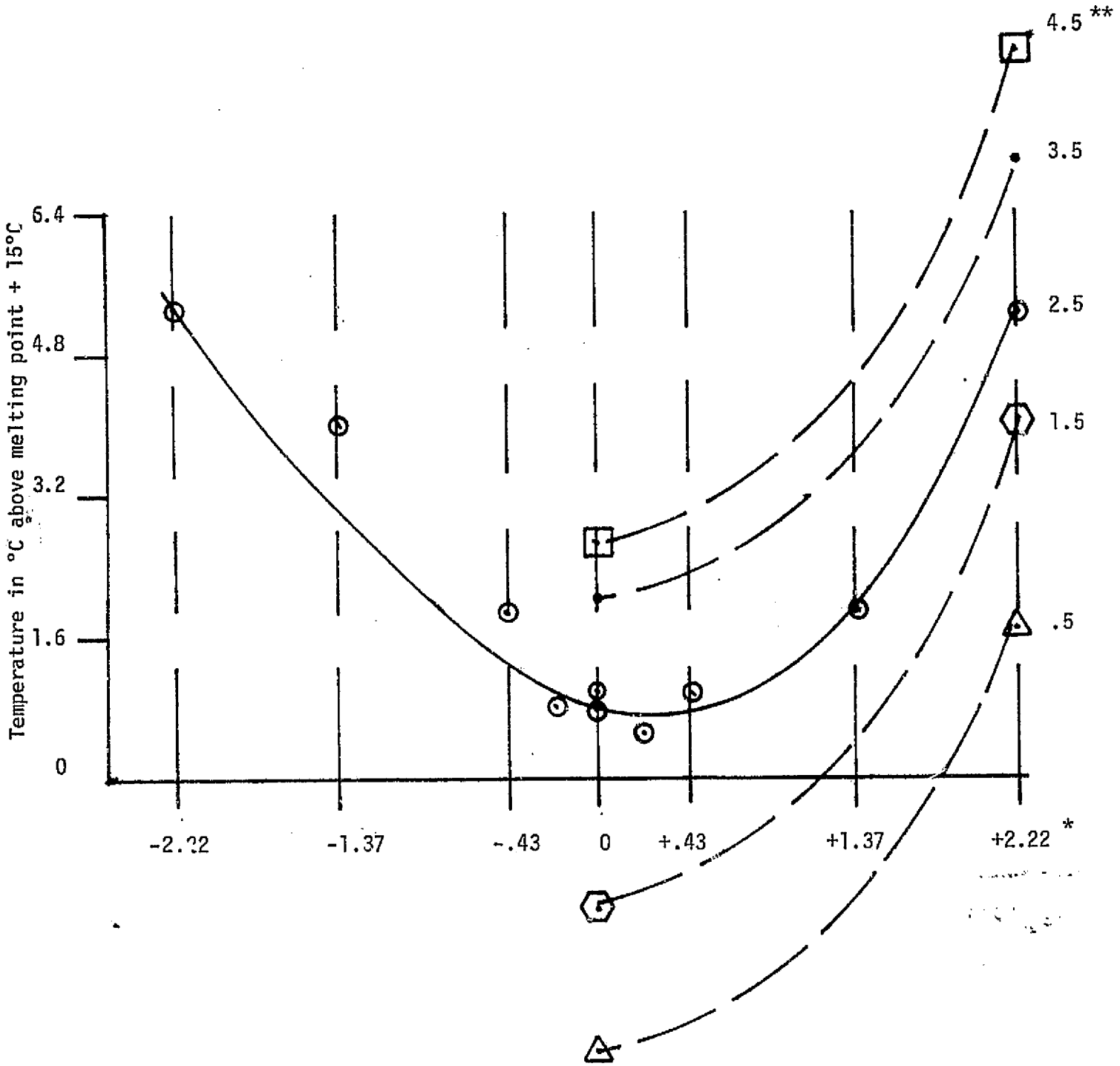

Figure 55: Temperature across bow-tie slot NBT/TS
T.C. 11/64" from bottom of crucible.

* Numbers indicate position in slot given in cms. from center.

** Top of coil above top of heat shield in mms.

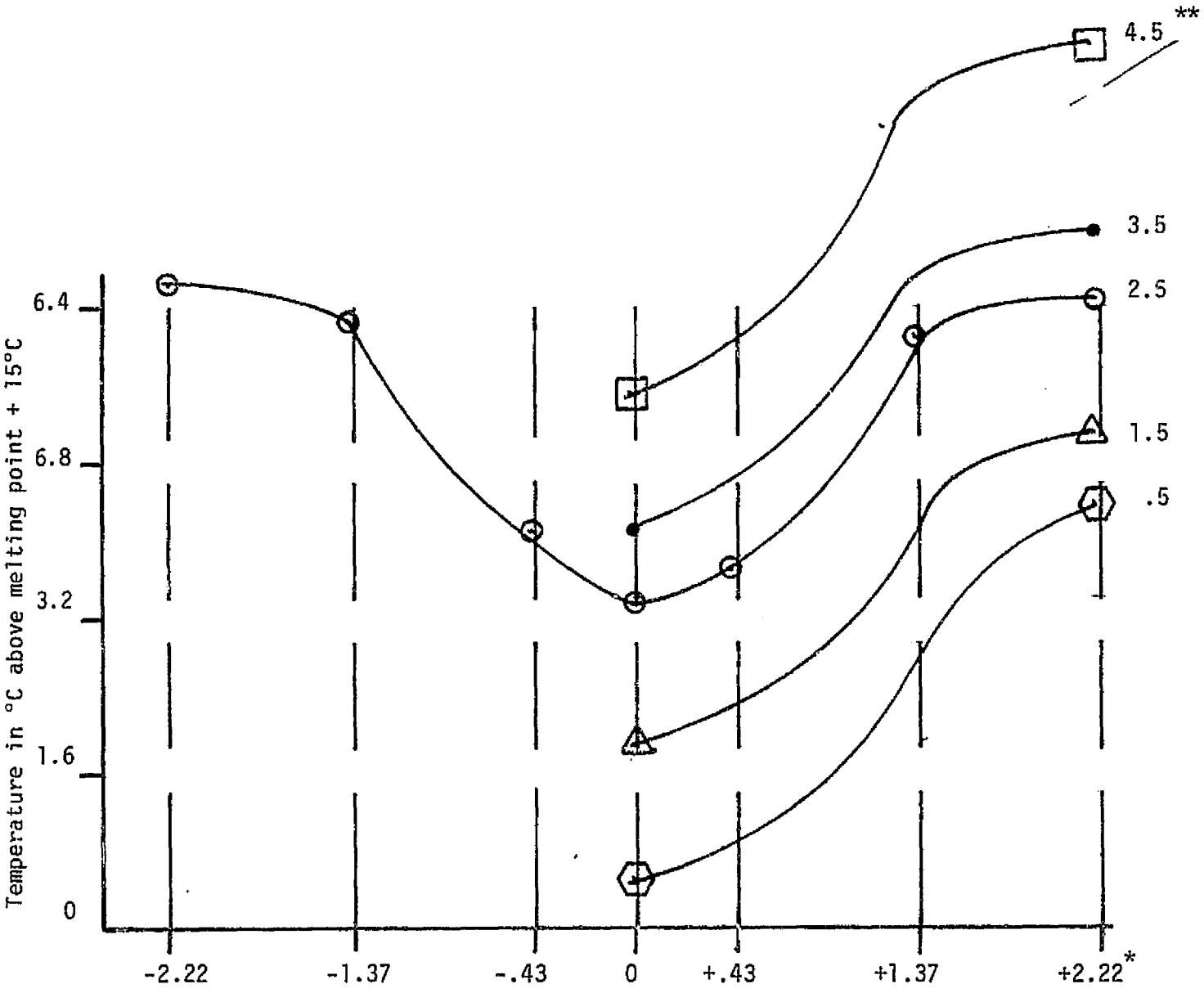

Figure 56. Temperature across dog-bone slot NBT/TSP. T. C. 11/64" from bottom of crucible.

* Numbers indicate position in slot given in cms. from center.

** Top of coil above top of heat shield in mms.

Table 24. TEMPERATURE DIFFERENCES (ΔT) BETWEEN THE CENTER AND THE RIGHT SIDE OF THE SLOT AS READ FROM FIGURES 50-56

Susceptor[1]	Heat Shield[2]		
	NSS	LSDBN	NBT
SS		6.0 (52)[3]	
TS	5.6[4] (50)	2.3 (53)	4.6 (55)
TSP	5.4 (51)	2.0 (54)	3.3 (56)

Notes:
1. Susceptor: SS, straight sided; TS, taper sided; TSP, taper sided with ports.
2. Heat Shield: NSS, Fig. 25; LSDBN, Fig.C-7; NBT, Fig. 49.
3. Number in paremphases refer to the Figure number from which ΔT was read.
4. ΔT (°C).

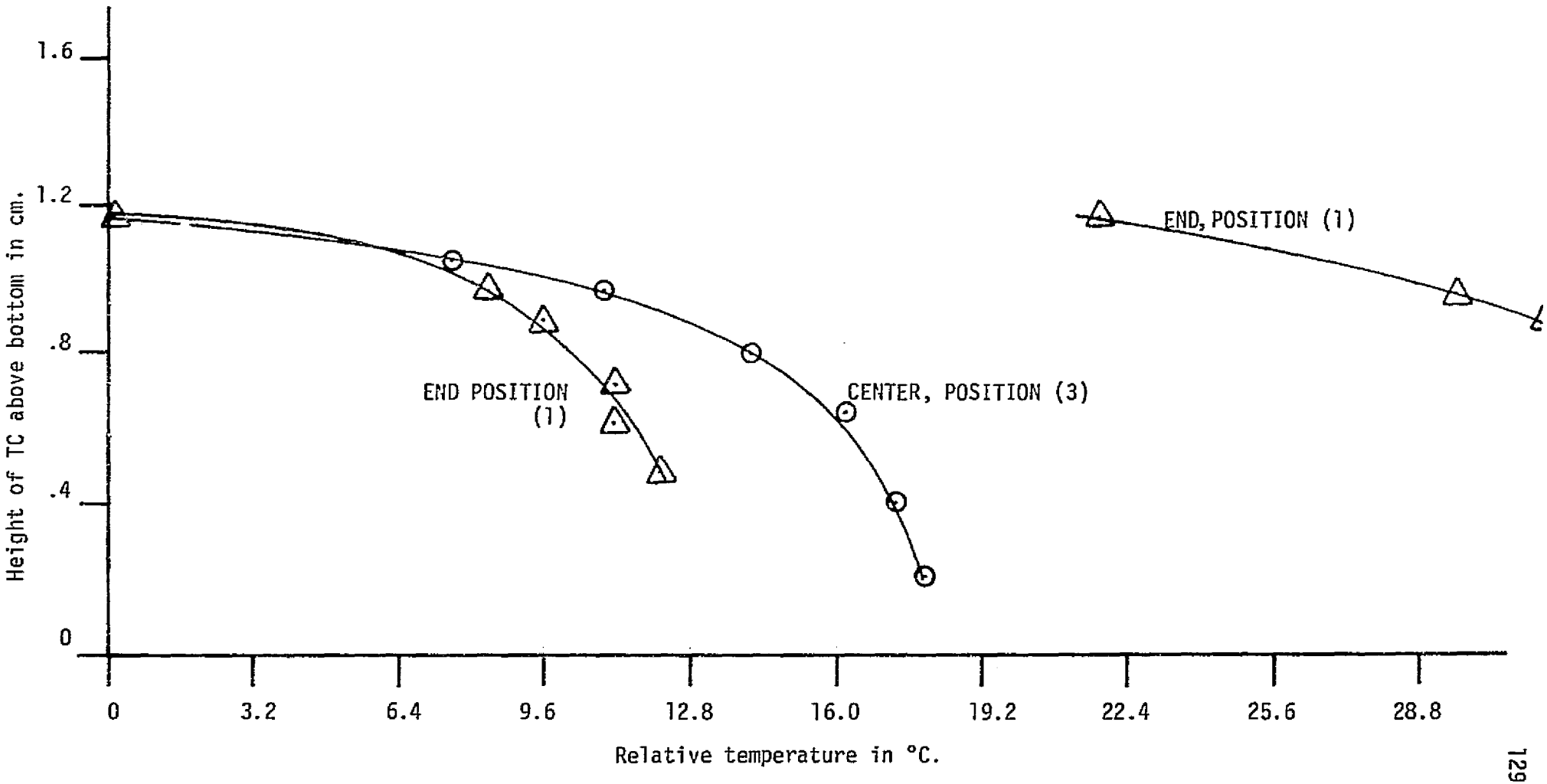

Figure 57. Temperature as a function of depth in melt.
NSS/TS
Top of coil 2.5 mm above top of heat shield.

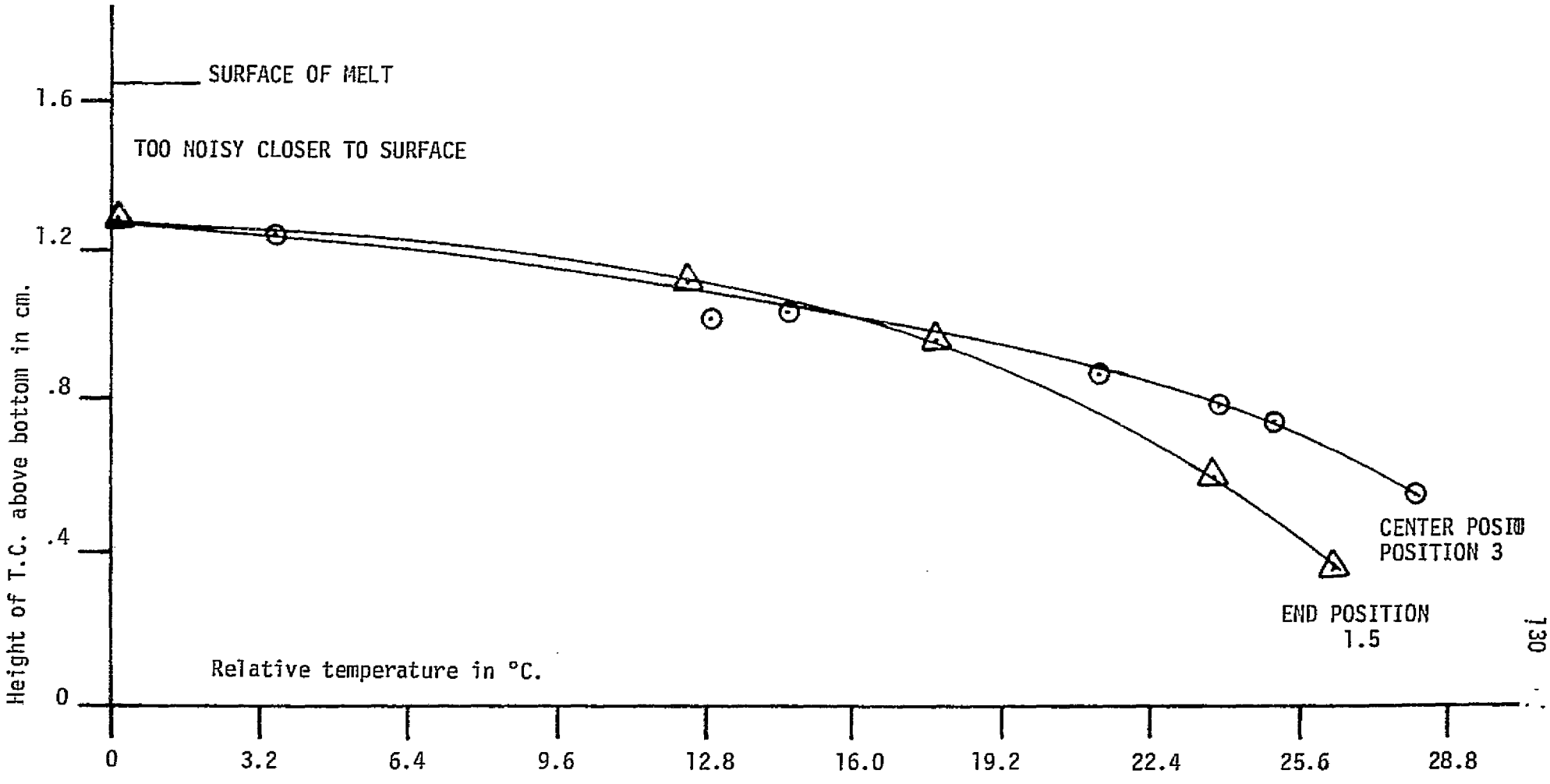

Figure 58. Temperature as a function of depth in melt. NBT/TS
Top of coil 2.5 mm above top of heat shield.

Examining Figures C-12, C-13, C-14, and C-15, one can see - by laying over the figure a piece of transparent paper upon which a curve has been drawn that has the shape of the bottom of the crucible - that the isotherms fairly well follow the shape of the crucible except in the vicinity of the ports where they appear to flatten out indicating again the cooling effect of the ports. The LSDBN heat shield was used in conjunction with the SS susceptor to compare it with the TSP data and to see what the detailed TC probing could show. Figure C-11 shows that the isotherms in the bottom half of the melt are almost flat - a situation that we reported to be the case earlier from other studies. At the time that we standardized on the TS susceptor for the final phase (see Section 4.2.4), we made the choice on our studies that indicated we did not want isothermal conditions on the bottom of the melt.

5. Web Characterization

5.1 Development of sampling strategy, prototype technique.

While the key to crystal growth studies is characterization of the material, the key to material characterization is careful sampling. Because of the uniformity of the material from the web growth process, one is not trying to get a scheme for truly random sampling with a large enough number of samples to have statistical significance. Instead what is desired is to take enough samples along the strip to catch any deviation or anamolous changes in the structural and electrical properties of the material, but not so many samples that material, time, and money are wasted.

A strategy based on past experience with webs and solar cells, and in keeping with the requirements of this contract was worked out in the first quarter. The growth button (or, in the case of direct seeding from a web, the region of seeding) are separated from the seed and the rest of the length of web, by careful scribing and fracturing perpendicular to the growth direction. A twelve inch length followed by two one inch lengths were separated by fracturing. This was repeated down the entire length of the pull. Each piece was carefully identified as to its position from the seed. The twelve inch pieces were stored. One of each of the one inch pieces along with the seed sample were used for the structural characterization, and the other one inch piece for electrical characterization and test solar cell fabrication. In case of pulls less than two feet, the longer lengths were reduced from twelve inches accordingly.

The graduate students had all been trained in the characterization techniques in their course work, and some of them had done these measurements on previous contracts.

During the first quarter, no web was grown. The time was spent in designing and building special equipment necessary for holding and preparing web samples for measurements involving optical microscopy and transmission electron microscopy.

Measurement of twin spacings, thickness, density of dislocations running down the web paralled to the two main faces, and spacing of twin lamellae between the main faces necessitate viewing the sample "end on" under an optical microscope. This requires very exacting alignment. Often it is desired to tilt the sample approximately 20° to examine one of the {111} planes on the fracture cross-section. The sample holder itself shown in Appendix C, Figure C-16, was fabricated from a 1/4 inch diameter steel rod with one end machined flat and a wire spring attached so that the sample is held firmly against the flat. The rod is placed in a V cut in a small block of steel that is afixed on one side of a steel plate cut to the size of a microscope slide. A knob allows rotation of the sample.

Transmission electron microscopy required samples one-eighth (1/8) inch in diameter to fit on the standard electron microscope sample grids. The samples must then be thinned to less than 2000 Å. A tool was designed and made for the ultrasonic cutter to cut 1/8 inch diameter samples.

Thinning of such small samples for TEM requires jet etching. Jet etchers for Si and Ge require special materials that can withstand HNO_3 and HF and also not introduce contamination. A jet etching apparatus was designed and constructed somewhat along the lines of several already reported in the literature. The first design proved to be too critical in adjustment and gave very uneven etching. A second one was built.

With the new instrument and practice an operator can repeatedly produce successfully etched samples. The active nature of the etchant is a constant worry, but immediate clean-up of the etcher after use minimizes part wear. Parts that wear are the tip and the bottom cap of the nozzle which are made of quartz.

The following is a description of the etcher; a detailed etching operation procedure is given in Appendix D, Table D-7.

As depicted in Figure C-17 the nozzle body is made of teflon instead of quartz. Since the CP4 etchant does not react with teflon, the problem of erosion is eliminated. The tip is made of a piece of quartz capillary with an inside diameter of 1 mm. It is sealed to a holder which screws into the nozzle body. The holder is also made of teflon. The etchant does erode the tip and the bottom cap. If care is taken in thoroughly cleaning the nozzle after each etching operation, the tip and the bottom cap can last for many operations.

Examination of the twin spacing using optical microscopy on fractured surfaces showed the twin spacing to be very narrow. Measurements were made but the resolution of the optical microscope is about .5 μm; thus for one of the lamellae the narrower spacing could only be estimated. The SEM was used on the fractured surfaces because of its higher resolution and great depth of field. A special holder had to be made for these samples. The SEM method is slower than OM, but is essential for narrow spacings. Attempts were made to measure the twin spacing by REM (replica electron microscopy) using a direct carbon replica. The technique, however, provided no saving of time and was not as versatile.

The studies using the SEM showed for approximately a dozen different dendrites and webs that were grown in the first 6 weeks, that instead of three twin planes we had 5. The spacing of the lamellae between the twin planes is 0.5, 0.2, 0.2 and 3 microns on the average as seen in Table 25. Two samples did not show the 3 micron lamella; this, however, was presumably due to poor fracturing. Two samples from a piece of web that was grown at Westinghouse prior to 1967 were examined by this technique. The results were the same which is not too surprising since a piece of this material was used as the initial seed.

Table 13 shows the results of twin spacings measured on primitive dendrites grown during this contract to evaluate the roll of the twin spacing in web growth; while Table 26 gives the twin spaicng os some of our seeds used in the later phases.

In addition to the structural work, the electrical resistivities, from four-probe measurements, were recorded on a number of the early dendritic-web samples. This data along with the other physical characteristics of typical samples produced during this contract are shown in Appendix D, Table D-8.

6. Discussion of Experimental Findings as Related to Theory

6.1. Web-dendritic ribbon growth

Detailed comparisons of the analytical results of web-dendritic ribbon growth with the experimental results were not performed since the experimental data was of insufficient detail to make the comparisons realistically possible. General agreement was found, however, as for example. satisfactory pull rates for web growth was determined to be, both theoretically and experimentally, in the range of 3-5 cm/min. See Figures 8, 9, and 10 for comparison with experimental results given in Section 4.2.4.1.

Table 25. TWIN SPACING DATA

Sample Number	Twin Lamella (μm)			
	A	B	C	D
1-26-67-0	0.57	0.22	0.16	-
1-28-19	0.63	0.31	0.22	
1-28-19	0.60	0.24	0.15	2.7
2-2-76-6	-	0.21	0.22	1.98
2-2-76-6	0.66	0.21	0.22	2.1
2-2-76-7	-	0.21	0.22	2.1
2-2-76-16	(A + B + C = 2.6)			2.95
2-4-76-14	0.42	0.22	0.17	2.2
2-11-76-B-17	0.52	0.22	0.16	2.63
2-11-76-A	0.52	0.21	0.21	3.1
2-11-76-A	0.42	0.33	0.1	2.4
Sample from earlier work	0.52	0.22	0.16	3.1
Sample from earlier work	0.62	0.33	0.21	3.1

Note: WEB CROSS-SECTION

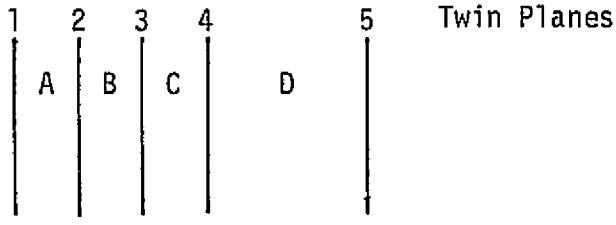

Table 26. TWIN SPACINGS IN DENDRITIC-WEB SAMPLES

SAMPLE: 7-6-76-C-3

SEED: 5 Twins
Spacings: 1.6μ, .45μ, .10μ, .45μ.

3 Regions
a) 5 Twins 2μ, 2μ (4 Twins)
b) 3 Twins 27μ, 0.15μ.
c) 4 Twins 27μ, 2.μ (3 Twins)

SAMPLE: 7-6-76-C-2

SEED: 5 Twins
Spacings 1.6μ, .45μ , .10μ, .45μ.

5 Regions
a) Web, no Twin
b) 1 Twin
c) 2 Twins 26μ
d) 6 Twins 26μ, 1.8μ, 0.1μ, 0.1μ, 1.8μ.
e) 2 Twins 26μ.

SAMPLE: 6-28-76-D-4

SEED: 5 Twins
1.6 μ .45 μ, .10 μ, .45μ

5 Twins Run through the entire sample, some spacing as seed.

SAMPLE: 6-25-76-F-2

SEED: 5 Twins 1.6 μ, .45 μ, .10 μ, .45 μ
Sample has only 3 Twins 1.7 μ and 0.2 μ.

SAMPLE: 6-28-76-D-2 #2

SEED: 5 Twins
1.6μ, .45μ, .10μ, .45μ.

2 Regions 5 Twins in both regions
Spacings 1.6μ, 45μ, .10μ, .45μ.
The twins from two regions do not meet.

SAMPLE; 6-28-76-D-1

Twin structure is the same as 6-28-D-2 #2.

SAMPLE: 6-28-76-D-2 #1

SEED: 5 Twins
1.6μ, .45μ, 10μ, .45μ.

Twin in web is the same as in seed.

SAMPLE: 7-7-76-

SEED 3 Twins
8μ, 2μ.

3 Twins run across the entire sample. Spacing measures 6μ, 1.75μ.

SAMPLE: 6-17-76-A 5.6

SEED	5 Twins 2μ, 1μ(4 Twins)
5 Regions	a) 5 Twins: 2μ, .8μ, (4 Twins) b) 3 Twins: 1.2μ, .8μ. c) 3 Twins: .25μ, 1.75μ. d) 7 Twins: .25μ, 1.75μ, 2μ, .9μ(4 Twins) e) 5 Twins: 2μ, .9μ(4 Twins)

SAMPLE: 6-17-76-C-4

SEED	5 Twins 2μ, 1μ (4 Twins)
4 Regions	a) 5 Twins 2μ, 1μ (4 Twins) b) 3 Twins c) 1 Twin Too small for optical measurement d) 4 Twins

6.2. Susceptor Geometry and Radial Temperature Gradients in the Melt.

The analytical treatment discussed in Section 3.2.3 indicates that between the two types of susceptor used, straight sided (SS) and tapered (TS), the tapered susceptor should give the greater radial temperature gradient. Experimental data (See Figures 52 and 53) taken with the two types of susceptors and using a long straight narrow dog-bone (LSDBN) slotted top heat shield failed to support this however; and,in fact,the data gives the opposite result. The discrepancy here is most probably due to the inadequacy of the analytical technique for handling the actual real thermal problem. The thermal analysis was limited to two dimensions and was incapable of including the effects of a slot in the top heat shield. It is apparent from this that completely misleading results can occur from an oversimplified analytical model.

The same type of discrepancy is seen to arise when one compares the effects of radiation ports on the temperature distribution within the melt. The theoretical analysis, based on a model which does not include, adequately, the effects of the slot in the top heat shield, gives results directly opposite to those obtained from experimental measurements. Compare Figures 18 with Figures 53 and 54.

For the analytical treatments which included the slot geometry, agreement with the experimental data was quite reasonable, see Figure 45 and Tables 7 and 8.

7. GENERAL CONCLUSIONS AND RECOMMENDATIONS

A. Web Growth

For web, or any sheet process, to be cost competitive with Czochralaski, it was pointed out that the process must have the following capabilities (a) pull rate in excess of 5 cm/min, (b) yield wide sheets (at least 5 cm wide), (c) pull several sheets simultaneously from the same crucible, and (d) continuous growth (i.e., replenish the Si). It was shown that (a) appears to be obtainable although no value can be set as to how fast. No new definitive information was obtained on (b); however, from the information obtained on thermal gradients and the length of opening in the top shield, it appears that 5 cm width is possible. There may, however, be a real problem in attaining both the width and pull rate goals together. More work must be done on the interaction between the pull rate and the width.

It was found in this investigation that the requirements on the mechanical and thermal stability were much stricter than had previously been thought. Great care must be taken in the mechanical design and operation of a furnace for pilot plants or production. All internal and external sources of vibration or jarring must be eliminated. Furthermore, the r.f. coil must be rigidly mounted not only to cut out vibration for the sake of mechanical stability but also to help eliminate small temperature fluctuations which can cause premature pull-out. Exceedingly tight tolerance on the crucible specifications must be used - far tighter than usually given for quartz. These plus the data on the isotherms make it very doubtful if multiple webs can be pulled from the same pot, (c).

The thermal probing data showed that it was possible to shape isotherms in the melt to a variety of shapes. Thus it is possible to shape the isotherms in a manner that would allow continuous feeding to keep the melt level constant, required by (d). Great care must be exercised in the construction of the feed mechanism, however, to be sure that it can not become a source of vibration.

The studies on other twin spacings, showed that the 2μ - 3μ spacing was difficult to seed, although once formed the dendrites and web gave no problem in continued growth. The 2μ - 8μ spacing seeded and grew well but had an upper limit of 4 cm/min on the pull rate; while the .9μ - 2μ spacing showed no upper limit (i.e., up to at least 10 cm/min). More work will be needed before one can say what the true optimum spacing is.

Widening rates were found to be a function of ΔT(1/2 slot length) rather than ΔT alone. High widening rates were found to be detrimental to good crystal perfection. Thus it is recommended that widening rates be kept moderate.

Several thermal and mechanical changes made during this work helped greatly in obtaining our goal of getting two dendrite webs to grow from buttons that were grown on the seeds. Three of these changes in procedure should be mainly credited with the attainment of our goal.

1. Changes in temperature and pull rate: We found that abrupt changes of 1° or more in the temperature during pulling invariably led to the web falling free at the start or to the web and edge dendrites pulling free at any time after the web had solidified. This was especially true when we were using the transient seeding technique. In a like manner abrupt increases in the pull rate led to the formation of "third" dendrites in the web portion or to the outside of either edge dendrite. The latter effect was enhanced if the web was growing in an asymmetric temperature gradient.

2. Seeding technique: We had been using the "Transient Seeding" technique as described in Section 4.2.1. This technique had given us problems in overshooting the temperature as we have already mentioned. The interface allows us to control the temperature automatically so that the "Stationary Seeding" technique could be used. The procedure for the technique consists of:

   (a) Find melting point of melt. This is accomplished by dipping a seed into the melt and adjusting the temperature until the seed neither melts nor grows. A seed etched to a point gives a more accurate melting point. Note: Be sure that the seed is clean. Once the m.p. has been found, it is best to check it by etching the seed and lowering it into the melt again.

   (b) Set desired ΔT on the temperature controller (can be anywhere from 2-25°. Actually we used 5 - 10°).

   (c) As the melt temperature drops to the new value, a button begins to grow. When wings just first appear pulling is commenced at 70% of speed controller (this corresponds to 5 cm/min). As the button reaches the surface of the melt, the speed controller is reduced almost to zero and the temperature is raised to give a ΔT of from 2 -5°.

   (d) After the web has solidified the pull rate is slowly increased to the desired velocity for web growth (2 -5 cm/min.).

   Temperature and pull speeds are adjusted during the pull as needed. Note: Changes should be small at any one time.

3. Pull rate: When we first used the stationary seeding technique, the pull rate after the button cleared the surface of the melt had been reduced to 10% rather than the "almost zero" given in (c) above. This proved to be too fast, and it was not until we went to this "almost zero" rate until the web solidified did we get reproducable web from the initial seed.

The 10-turn potentiometer to give fine control on setting temperatures was vital in our case. Any equipment set up by others must have similar capabilities. Furthermore sudden changes in temperature or pull rate must be avoided. Temperature changes during growth should not exceed 1° in 1 1/2 min; pull speed changes should not exceed .5 cm/min in a similar time. Also the pulling set-up must have a clutch that gives instant start and stop.

It is strongly recommended that a thermocouple with a suitable recorder and bucking voltage be used to determine (and correct for) the center of thermal symmetry at the start of each melt. It was found that the symmetry of the button technique does not give the very fine positioning required for long pulls.

Of numerous heat shield/susceptor combinations that we investigated, the best resulted from using the long straight dog-bone slot with the narrow opening and the ported, tapered susceptor. More work should be done with this especially with the inclusion of after heaters.

B. Thermal Modeling

(1) Furnace design parameters predicted to have a major role in determining the web pull rate are (1) thermal shield temperature, (2) spacing between the thermal shield and melt surface, and (3) thickness of the growing web. A decrease in the thermal shield temperature or a decrease in the spacing between the thermal shield and melt surface result in an increase in the pull rate. In addition, the pull rate is predicted to increase as the thickness of the web decreases.

These studies indicate that growth is stable over a wide range of conditions. For example, after a small increase in pull rate, equilibrium conditions will again be reached with a thinner web. If the silicon is not replinished during growth it will be necessary to decrease the growth rate as the level is decreased because of the increase in the spacing between the thermal shield and the melt surface.

Predicted growth rates are approximately equal to experimental values. However, detailed comparison between analytical and experimental results were not made because experimental data is limited.

(2) Temperature distributions calculated in the melt indicate that the slot geometry has a significant effect on the temperature distribution in the melt. A more uniform temperature is predicted for the dog-bone slot which is advantageous for web-dendritic growth.

Temperature distributions were obtained for two susceptor designs: a cylindrical shaped design and a tapered design with a lip at the top edge. Results show that the temperature gradients are smaller with the cylindrical shaped susceptor than with the tapered design. The temperature is predicted to decrease with depth with the tapered susceptor which should enhance growth of the dendrites.

The effect of the radiation ports on the temperature distribution yielded unexpected results. The model predicted that the radiation ports have an extremely small effect on the temperature distribution. In addition, it was predicted that the temperature of the melt in the region of the ports increases rather than decreases as had been anticipated. Temperature measurements taken in the melt apparently contradict the analytical results however. The analytical model is subject to inaccurcies which may have resulted in the discrepancy.

Recommendation

Further analytical and experimental work is recommended to understand the heat and mass transport in the region of the liquid-solid interface. Methods of increasing the heat loss from the interface should be investigated. The use of externally cooled radiation shields to reduce the radiation received by the web and meniscus from the thermal shield and melt surface is one conceivable means of obtaining increased pull rate.

8. REFERENCES

1. Faust, Jr, J.W. and H. F. John, J. Electrochemical Society, 108 (1961) 855.

2. Harrill, M.D., M.S. Thesis, University of South Carolina (1976).

3. Batchelor, G. K., An Introduction to Fluid Dynamics (Cambridge Univ. Press, London, 1967) p. 63.

4. IBM Continuous System Modeling Program III, Program Reference Manual SH19-7001-2 (1972).

5. Touloukian, Y. S. and D. P. DeWitt, Thermophysical Properties of Matter, Vol. , (IFI)/Plenum, New York, 1970) p. 376.

6. Surek T., and B. Chalmers, J. of Crystal Growth, 29, (1975) 1.

7. Schmid, J. R., Lechliter, G. L., Fischer, W. W., "Lion: Temperature Distribution for Arbitrary Shapes and Complicated Boundary Conditions", Report No. KAPL-M-6532 General Electric Corp. Knolls Atomic Power Laboratory, July 27, 1966.

APPENDIX A

IRRADIATION OF THE WEB BY THERMAL RADIATION EMITTED BY THE SURFACE OF THE THERMAL SHIELD

In the web-dendritic ribbon growth furnace, the web is extracted from the furnace through a slot in the thermal shield as shown in Figure I-1. The thermal shield is a circular molybdenum disk and is maintained near the silicon melt temperature by radiation exchanged with the melt and susceptor and by induction heating. Thermal radiation is emitted from the top surface of the thermal shield to the surroundings. Some of this radiation strikes the web surface where a portion is absorbed. The irradiation of the web by the thermal shield is the only significant source of radiation because other surrounding surfaces are at relatively low temperature. Thus, the irradiation, H, of the web surface area above the thermal shield is due to radiation exchange with the thermal shield.

Each side of the web receives radiation from a semi-circular section of the thermal shield. The thermal shield and web surfaces are assumed gray and diffuse and radiation received from the surrounding surfaces is neglected. Only the radiation emitted by the thermal shield and reaching web surface is included; thus, radiation which reaches the web surface by reflection between the two surfaces is neglected.

The irradiation H of the web surface is the thermal radiation emitted by the thermal shield which strikes the web. It is apparent from an examination of Figure I-1 that the irradiation of the web surface is higher near the thermal shield than at distances above the thermal shield.

Figure I-2 shows an element of area dA_2 on the web surface which receives radiation from an element dA_1 on the thermal shield. From Gebhart[1] the radiation heat transfer rate from dA_1 and dA_2 is given by

$$dq_{dA_1 - dA_2} = W_1 dA_1 dF_{dA_1 - dA_2} \qquad (1)$$

where W_1 is the emissive power of dA_1 and $dF_{dA_1 - dA_2}$ is the fraction of the radiation emission from dA_1 which strikes dA_2 or the angle factor.

The area dA_2 is located on the centerline of the web at a distance X above the thermal shield surface. The irradiation of the web surface is slightly higher along the centerline of the web than at its edges. The irradiation

1. Gebhart, B., Heat Transfer, McGraw-Hill, N. Y., 2nd Ed., 1971, pp 133-165.

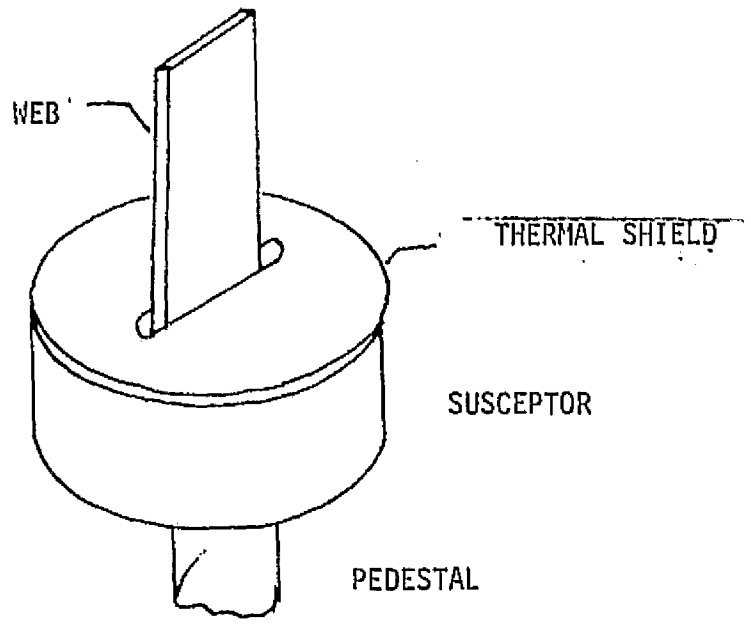

Figure A-1. Radiation from thermal shield irradiates the web surface. The intensity of the radiation decreases with elevation above thermal shield.

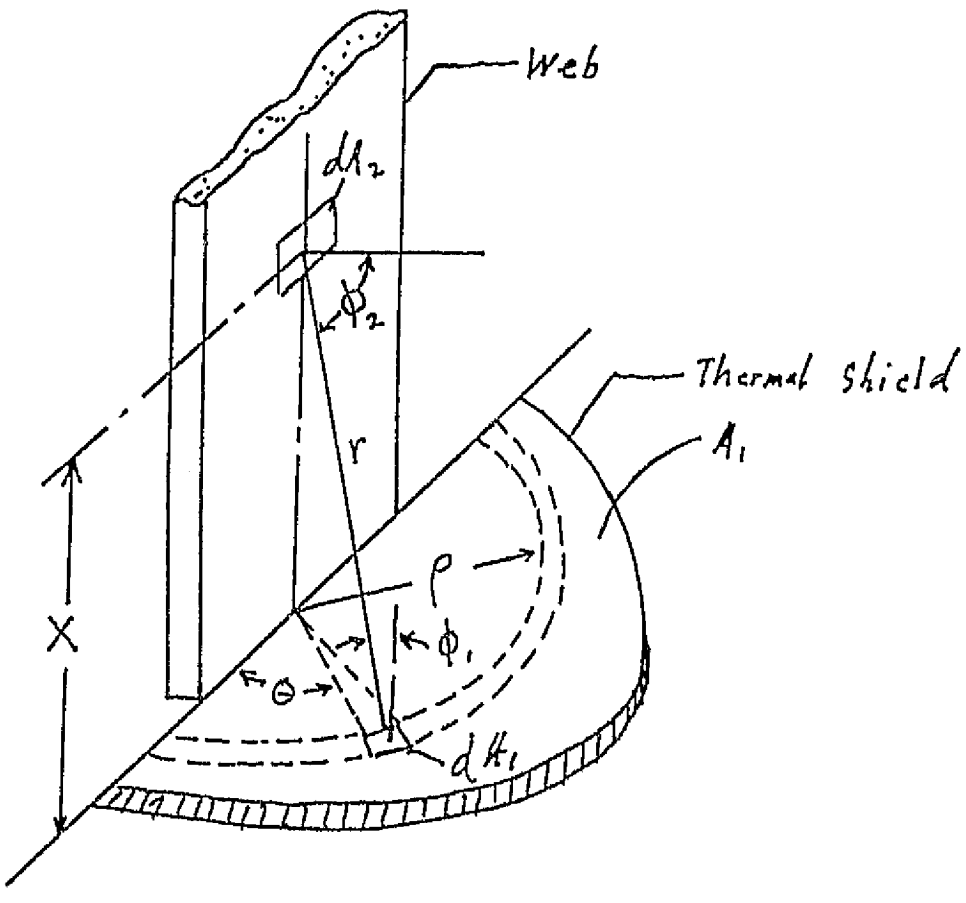

Figure A-2 A fraction of the thermal radiation emitted from dA_1 on thermal shield striker dA_2. The web area dA_2 is irradiated by one-half of thermal shield.

will be determined for dA_2 located at the centerline to obtain the maximum H.

From reciprocity,

$$dA_1 dF_{dA_1-dA_2} = dA_2 dF_{dA_2-dA_1} \tag{2}$$

Substituting Equation (1) in (2) and dividing left and right sides by dA_2 yields,

$$\frac{dq_{dA_1-dA_2}}{dA_2} = W_1 \, dF_{dA_2-dA_1} \tag{3}$$

The left side of Equation (3) is the heat transfer rate per unit area. By integrating Equation (3) over A_1 we obtain the irradiation, H_1 for dA_2 which is the value sought. The thermal shield is normally approximately uniform in temperature and therefore W_1 is approximately constant. Integrating Equation (3) over A_1 we obtain,

$$H - W_1 \int_{A_1} dF_{dA_2-dA_1} \tag{4}$$

The right hand side of Equation (4) is the fraction of radiation emitted by dA_2 that strikes A_1 and is denoted by $F_{dA_2-A_1}$ and can be written [1],

$$d_{dA_2-A_1} = \int_{A_1} dF_{dA_2-dA_1} = \int_{A_1} \frac{\cos \phi_1 \cos \phi_2}{r^2} \, dA_1 \tag{5}$$

where the variables contained in Equation (5) are shown in Figure I-2. the angles ϕ_1 and ϕ_2 are the angles between the normal to the areas dA_1 and dA_2 and the line joining the two areas and r is the distance between the areas.

Equation (5) can be integrated by substituting the polar coordinates (ρ, θ) in the plane of A_1 as shown in Figure I-2. The radius is the distance from the center of the thermal shield to dA_1 and θ is the angle measured from the plane of the ribbon. Area dA_1 in terms of these coordinates becomes

$$dA_1 = \rho d\theta d\rho \tag{6}$$

1. Ibid

The following additional relations can be obtained,

$$r^2 = \rho^2 + X^2 \tag{7}$$

$$\cos \phi_1 = \frac{X}{\sqrt{\rho^2+X^2}} \tag{8}$$

$$\cos \phi_2 = \frac{\sin}{\sqrt{\rho^2+X^2}} \tag{9}$$

Substituting Equations (6) - (9) into Equations (5) and introducing the proper integration limits, we obtain

$$F_{dA_2-A_1} = \frac{X}{\pi} \int_0^R \int_0^{\pi} \frac{\rho \sin\theta d\theta d\rho}{(\rho^2+X^2)^2} \tag{10}$$

where R is the radius of the thermal shield. Integrating Equation (1) with respect to and given the relations,

$$F_{dA_2-A_1} = \frac{1}{\pi}[- \frac{XR}{X^2+R^2} + \tan^{-1}(\frac{R}{X})] \tag{110}$$

Finally substituting Equation (11) into Equation (4), H is given by

$$H = \frac{W_1}{\pi} [- \frac{XR}{X^2+R^2} + \tan^{-1} \frac{R}{X}] \tag{12}$$

It is of interest to consider the value of $F_{dA_2-A_1}$ at X=0 and X→∞. When dA_2 is adjacent to the thermal shield, it is seen in Figure I-2 that one-half its solid angle is thermal shield while the remainder is the surroundings. It would seem that the value of $F_{dA_2-A_1}$ should be 0.5 at X=0 which is the value obtained from Equation (11). Thus, it is seen that Equation (11) yields correct values at these two points.

Appendix B. CALCULATION OF Si CHARGE

Calculations based on 20 feet of web at the goal dimensions of 5 cm wide and 4 mils thick using a density of Si of 2.33 gms/cm^3.

Web

20 ft = 610 cm
4 mils thickness = 0.01 cm
volume - 610 cm X 5 cm X 0.01 cm = 30.5 cm^3

Edge dendrites (estimates)

20 mils = 0.051 cm
volume - 2 X 610 cm X $(0.051\ cm)^2$ = 3.2 cm^3
total volume = 33.7 cm^3
weight Si = 78.5 gms
leave in about 20.5 gms

99.0 gms charge

The charge for the same length of web on 1965 requirements (i.e., 2 cm wide and 8 mils thick)

web vol.	24.4 cm^3
dend. vol.	3.2 cm^3
total	27.6 cm^3
weight Si	64.3 gms
leave	14.7 gms
	79.0 gms charge

Appendix C

Miscellaneous Figures

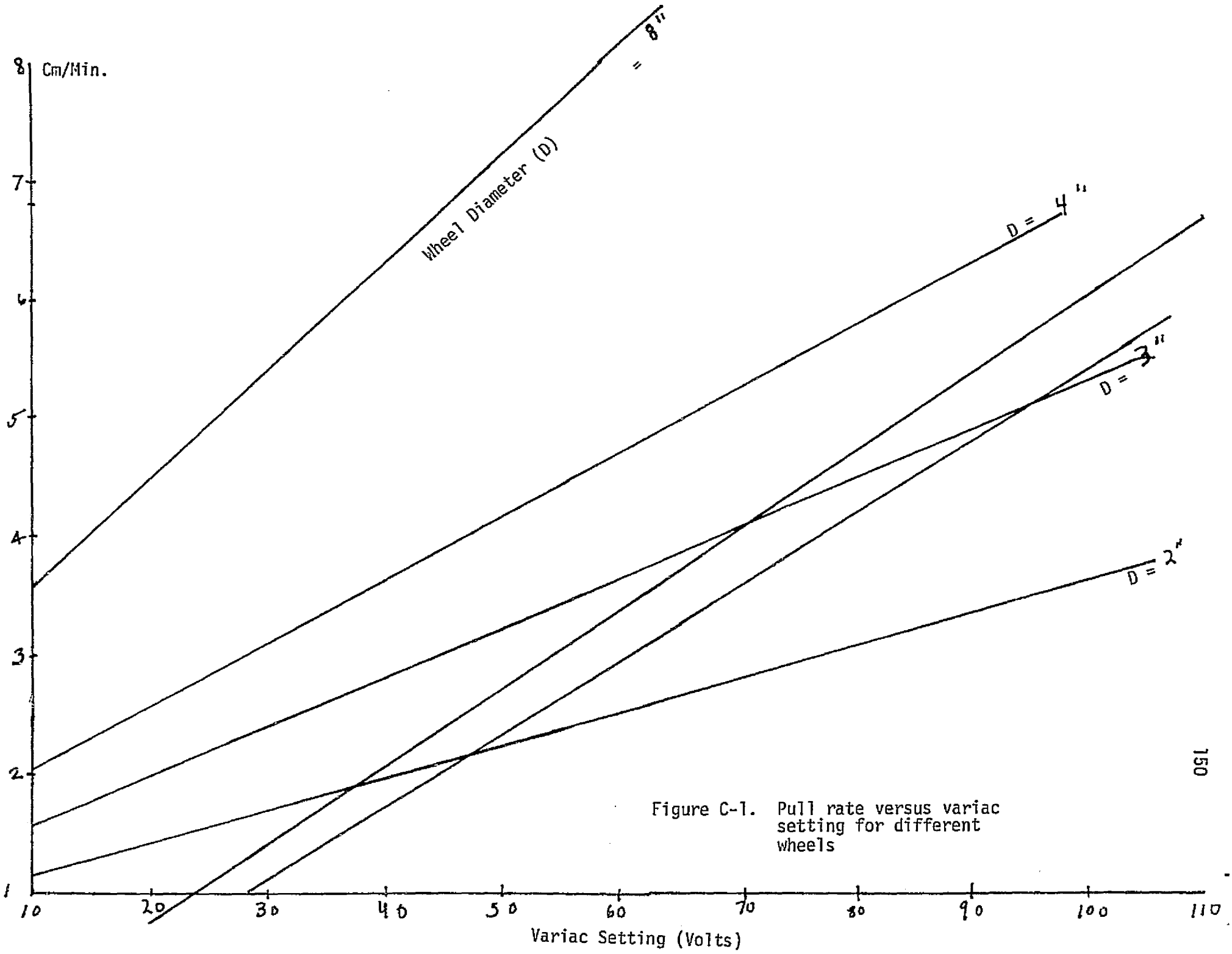

Figure C-1. Pull rate versus variac setting for different wheels

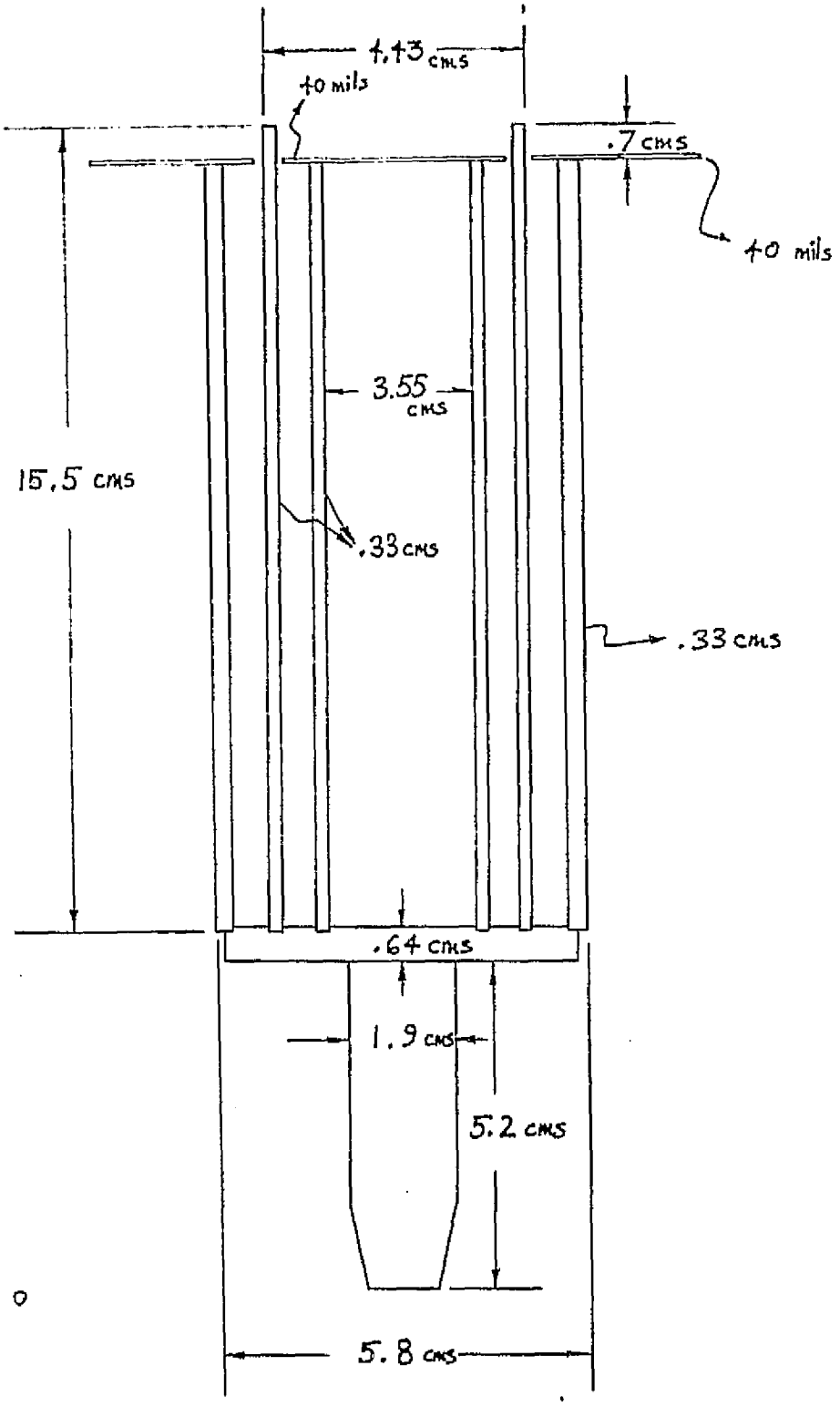

Figure C-2. Al_2O_3 pedestal arrangement.

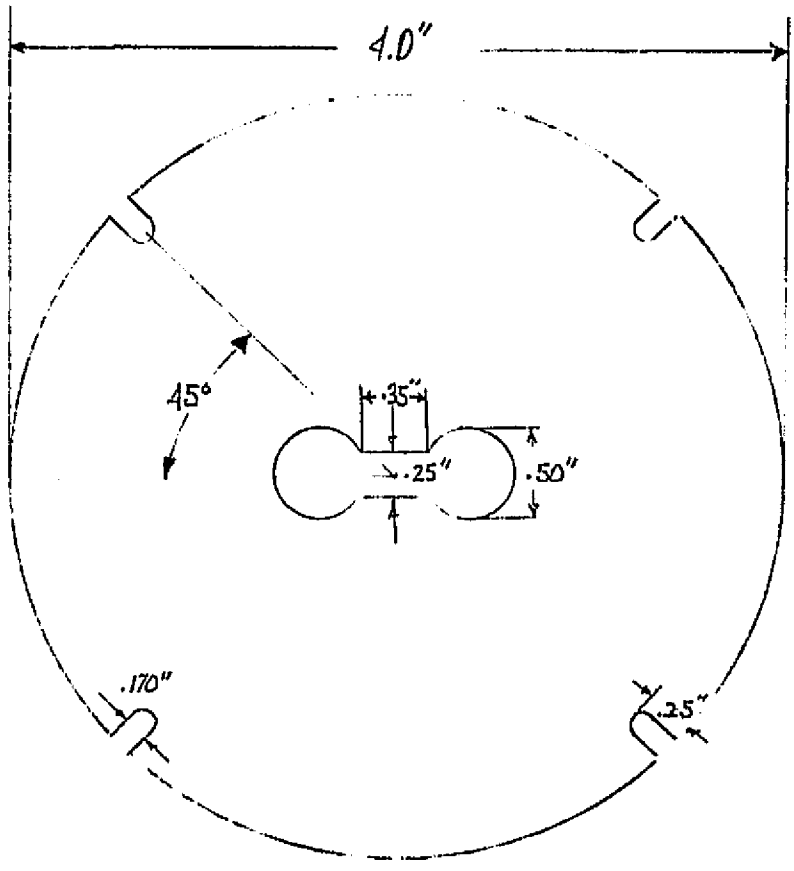

Figure C-3. Short straight dog-bone (SSDB) heat shield.

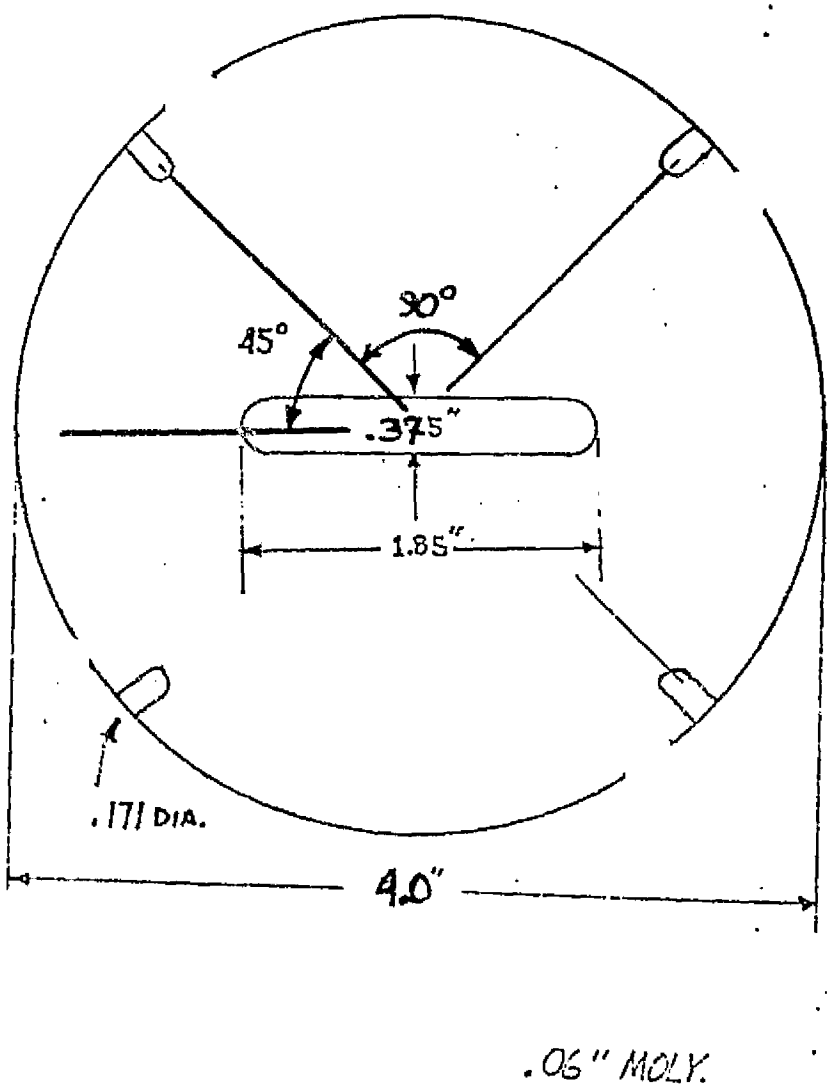

Figure C-4. Medium straight slot (MSS) heat shield.

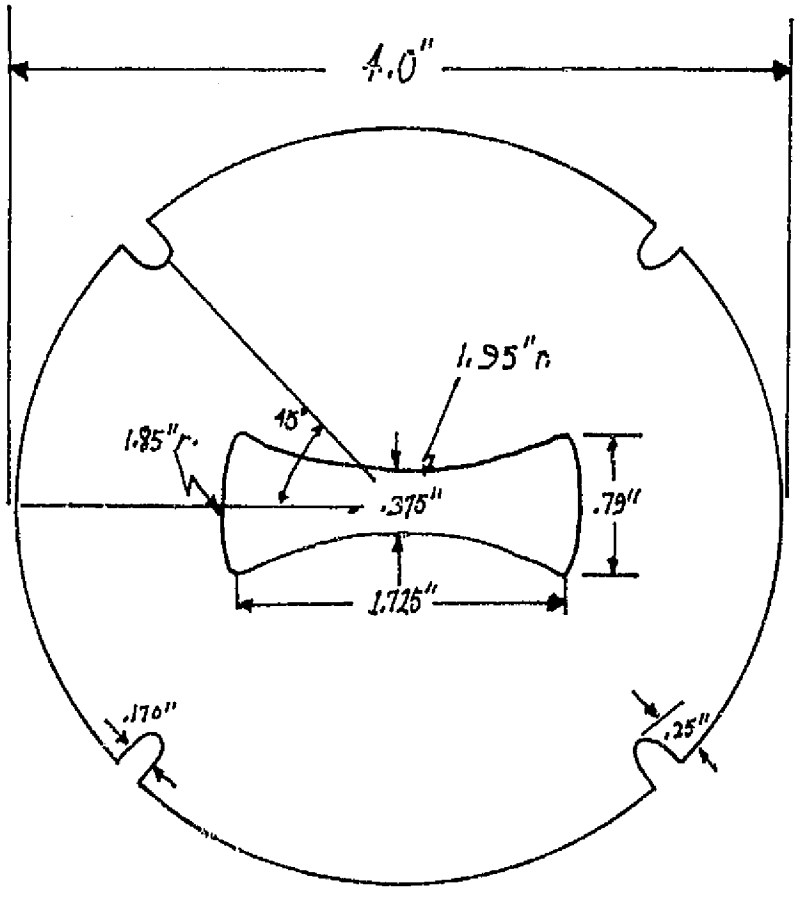

Figure C-5. Bow tie (BT) heat shield.

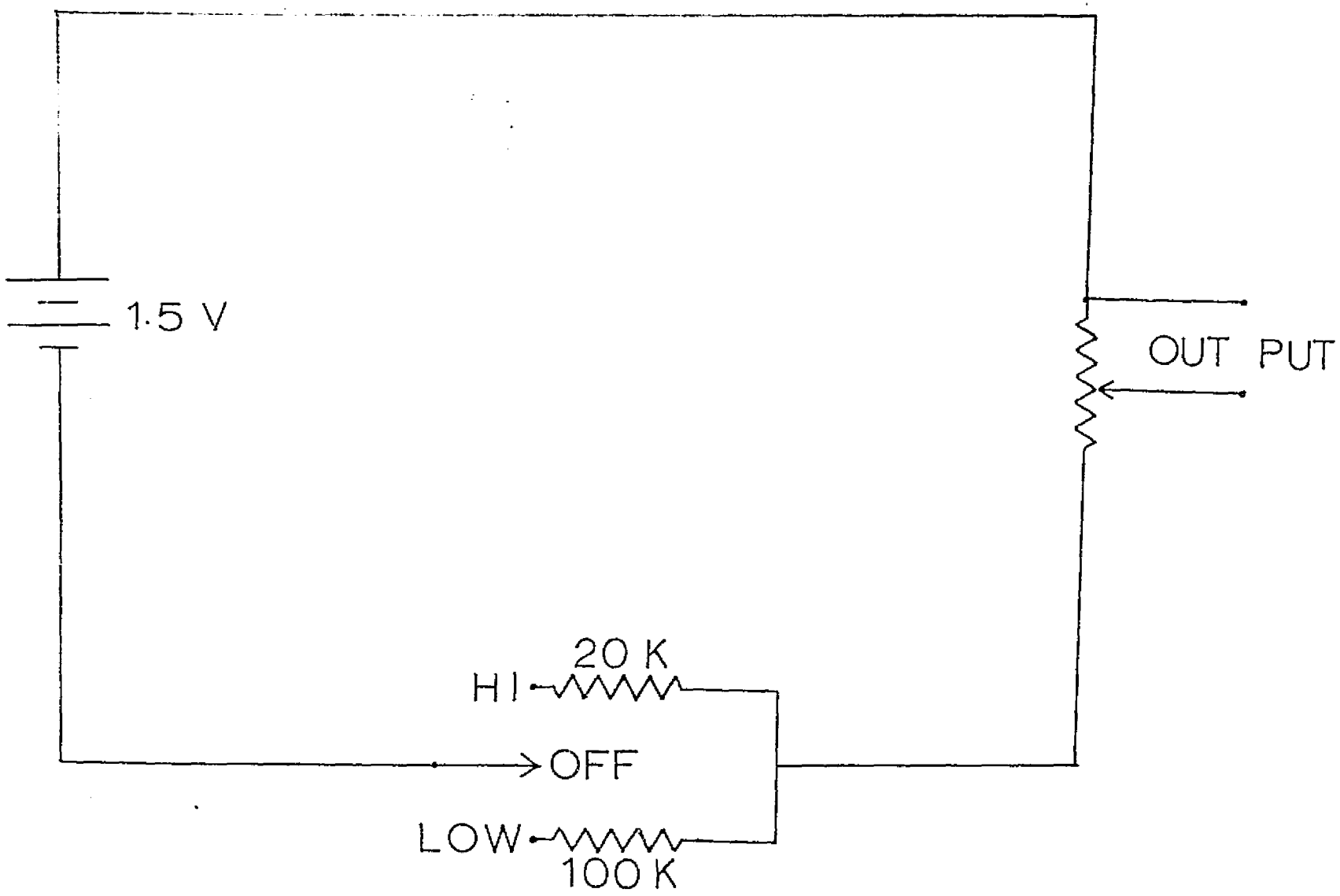

Figure C-6. Bucking voltage power supply.

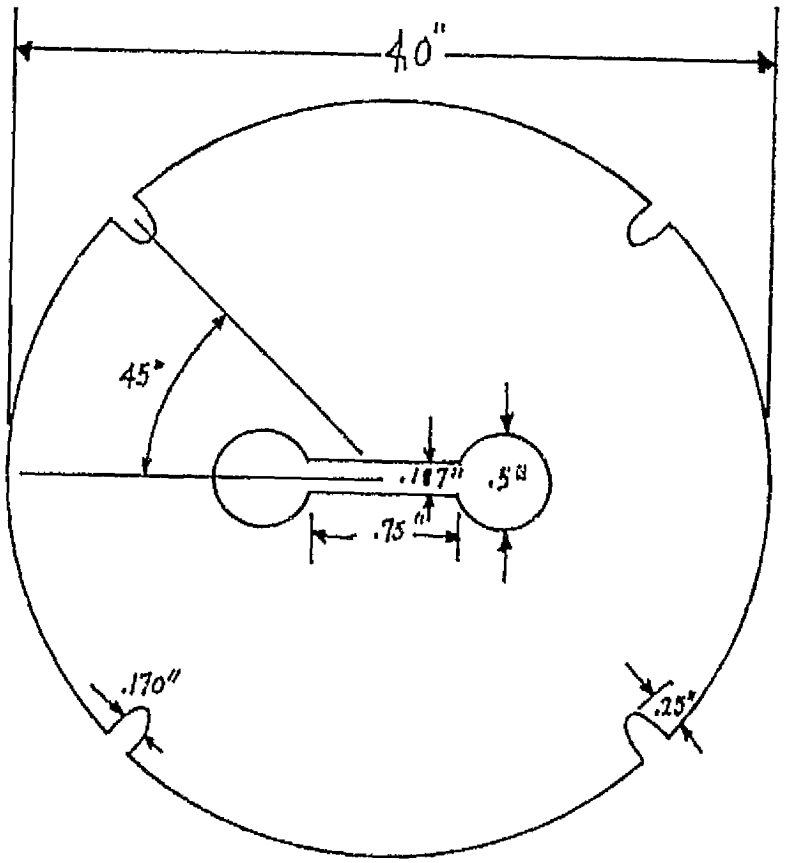

Figure C-7. Long straight narrow dog-bone (LSDBN) heat shield.

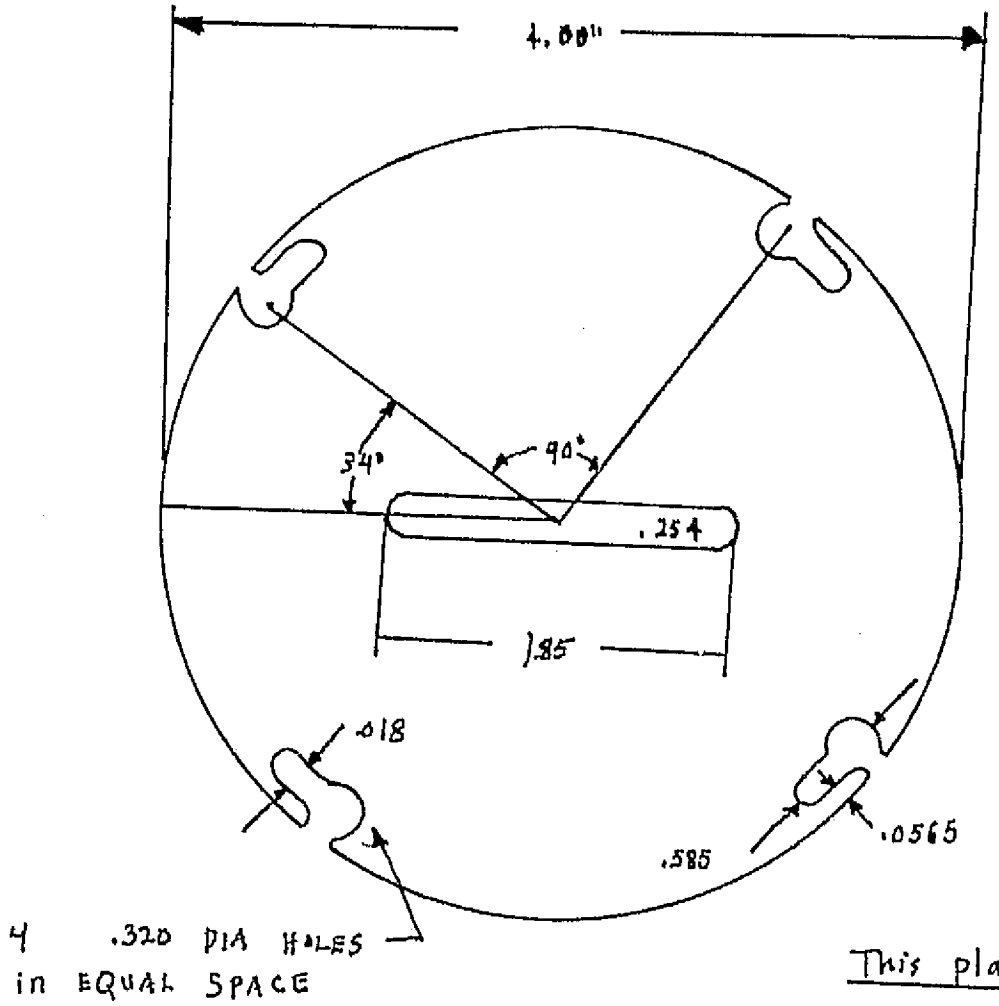

Figure C-8. Narrow straight slot (NSS) heat shield.

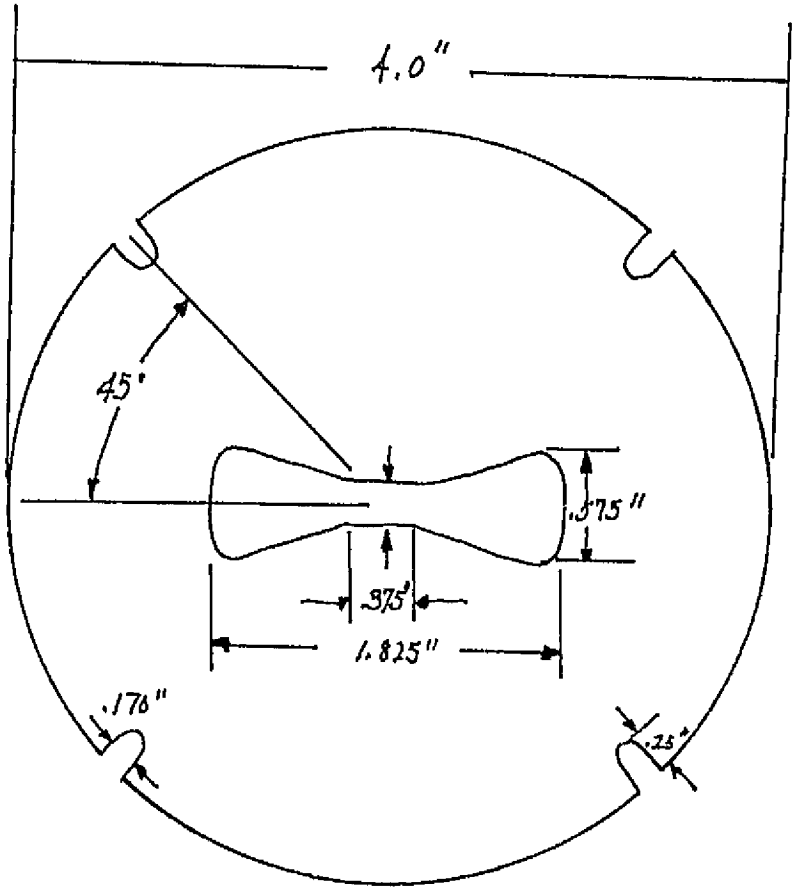

Figure C-9. Narrow bow-tie (NBT) heat shield.

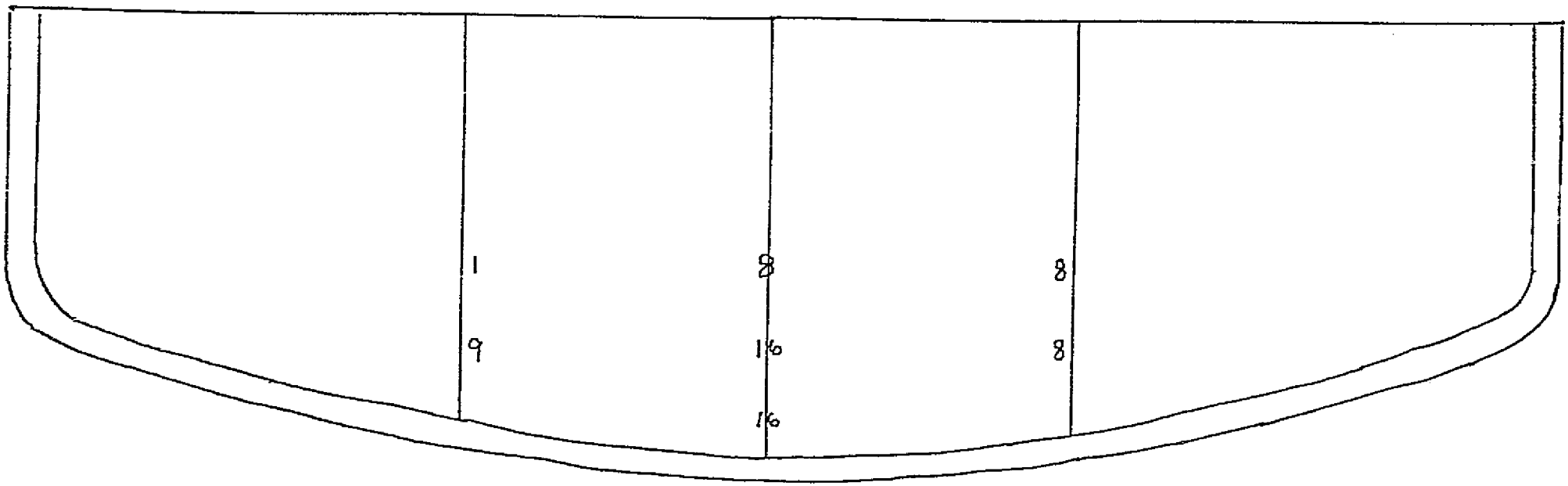

Figure C-10. Temperatures in melt for LDBeW/SS. Numbers represent °C above an arbitrary reference temperature near top of melt.

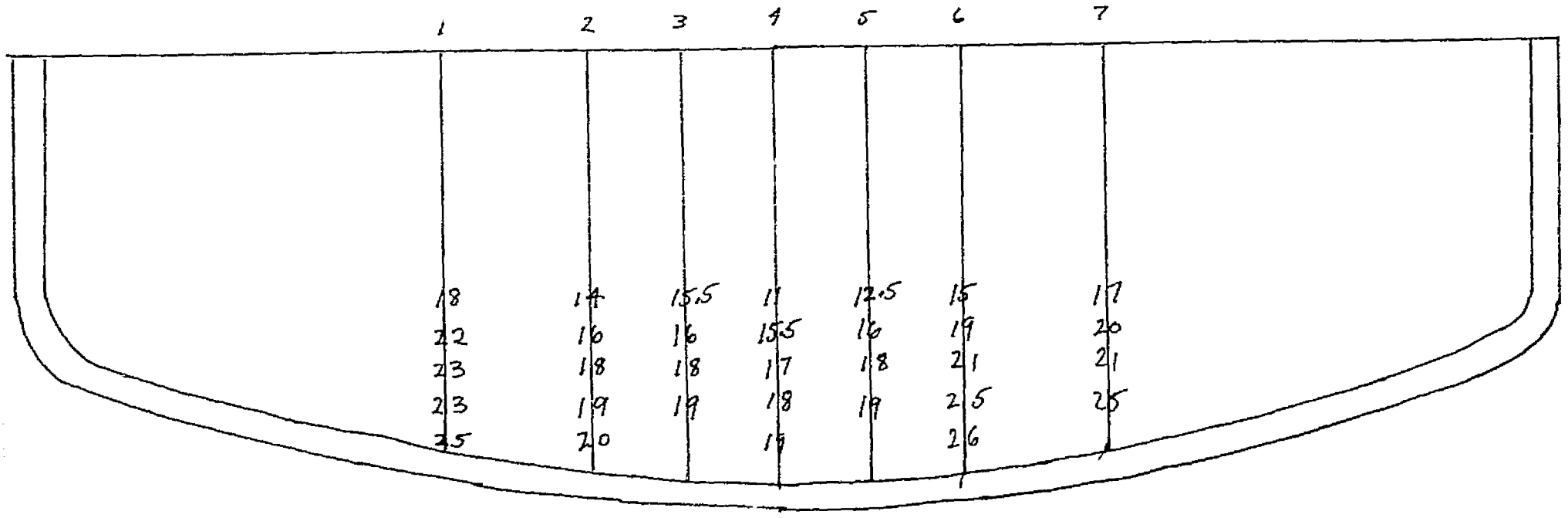

Figure C-11. Temperatures in melt for LSDBN/SS. Numbers represent °C above an arbitrary reference temperature near the top of the melt.

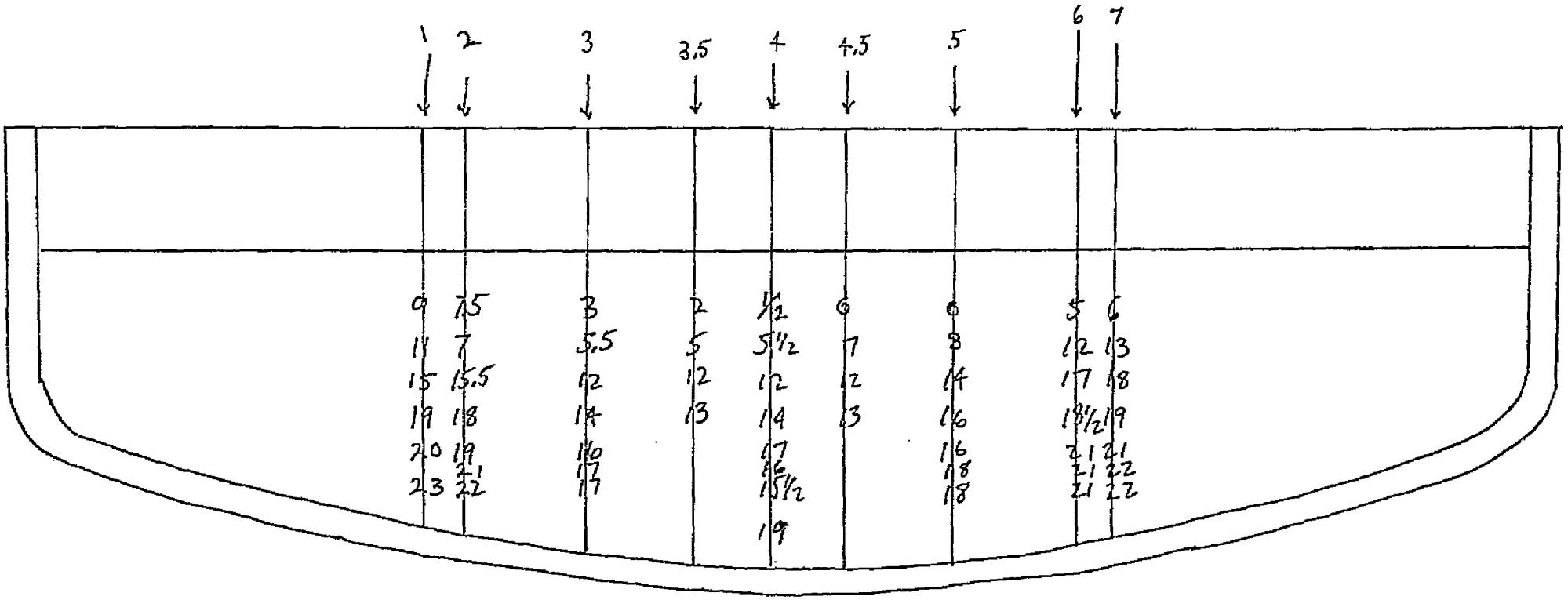

Figure C-12. Temperatures in melt for LSDBN/TSP. Numbers represent °C above an arbitrary reference temperature near the top of the melt.

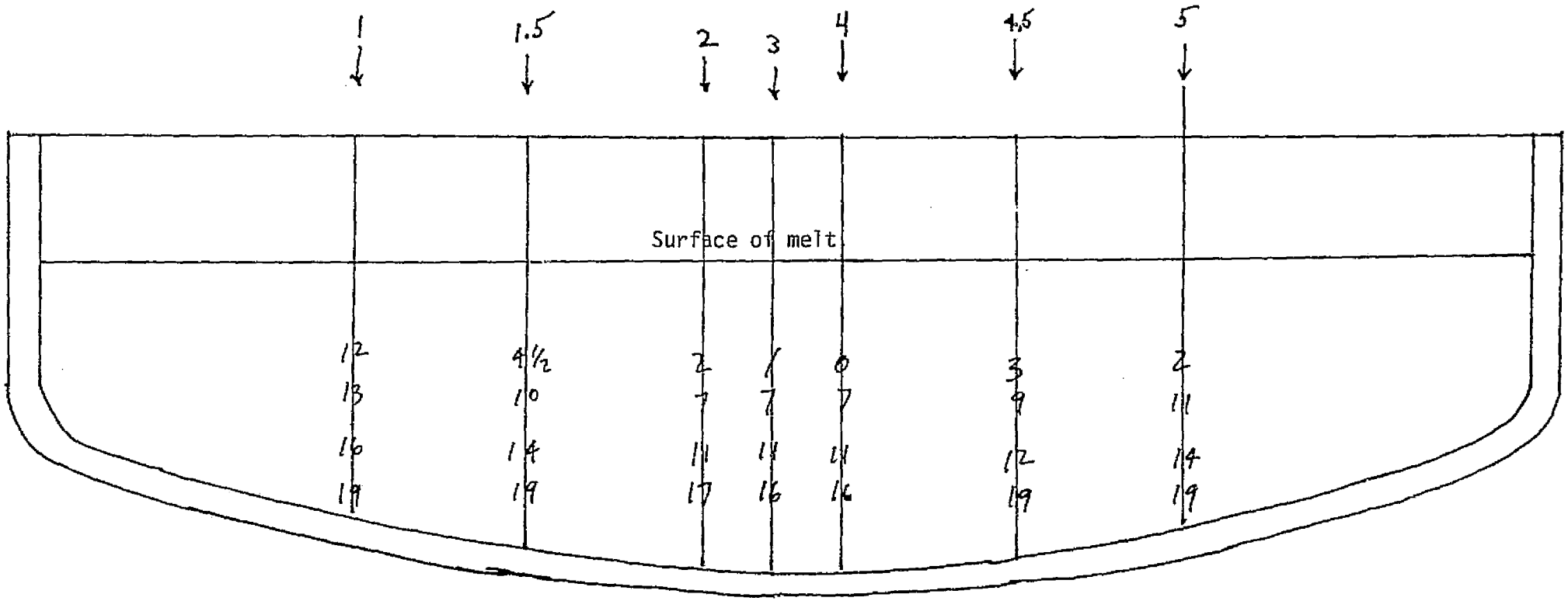

Figure C-13. Temperatures in melt for NTB/TSP. Numbers represent °C above an arbitrary reference temperature near the top of the melt.

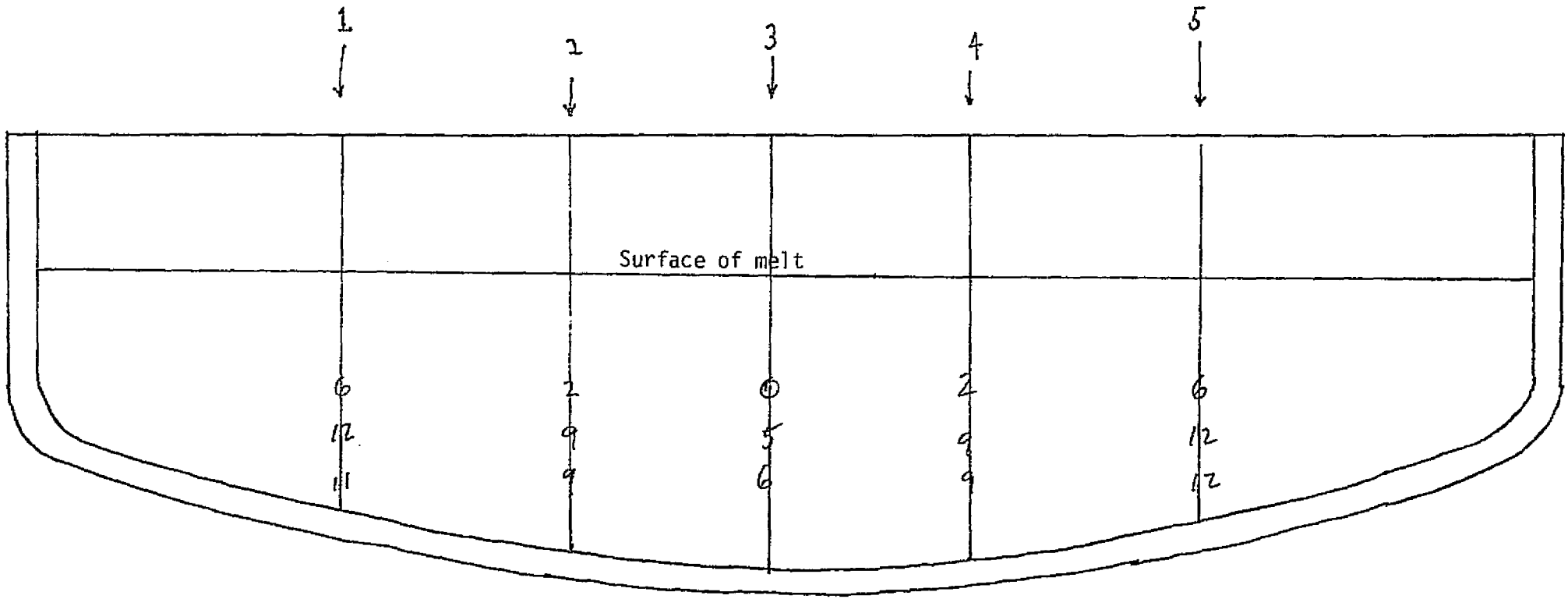

Figure C-14. Temperatures in melt for NSS/TSP. Numbers represent °C above an arbitrary reference temperature near the top of the melt.

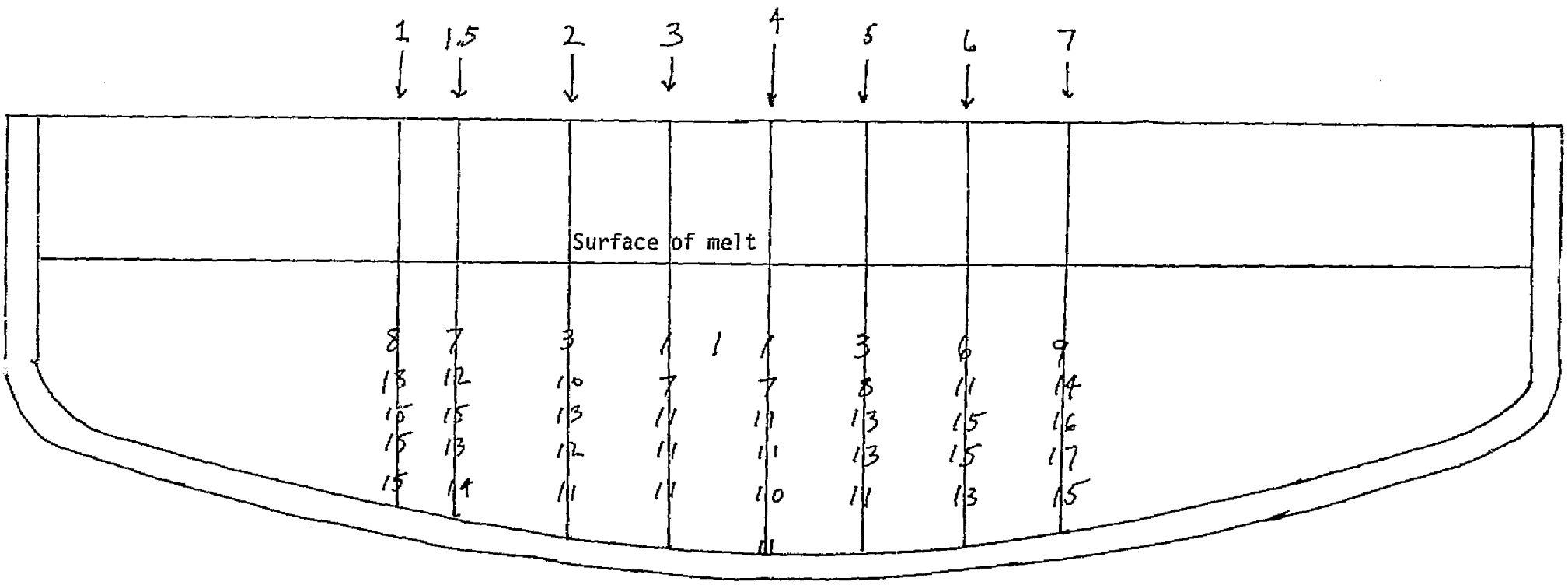

Figure C-15. Temperatures in melt for NSS/TSP. Numbers represent °C above an arbitrary reference temperature near the top of the melt.

Rotating
Sample Holder
for

Metallurgical Microscope

11/12/75

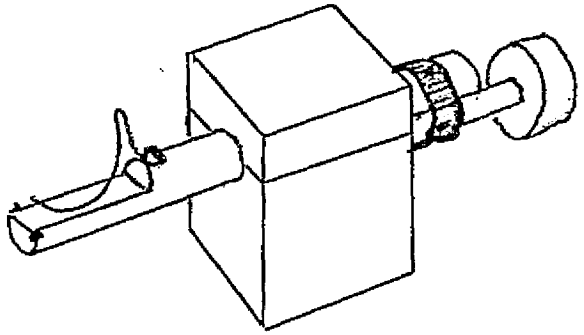

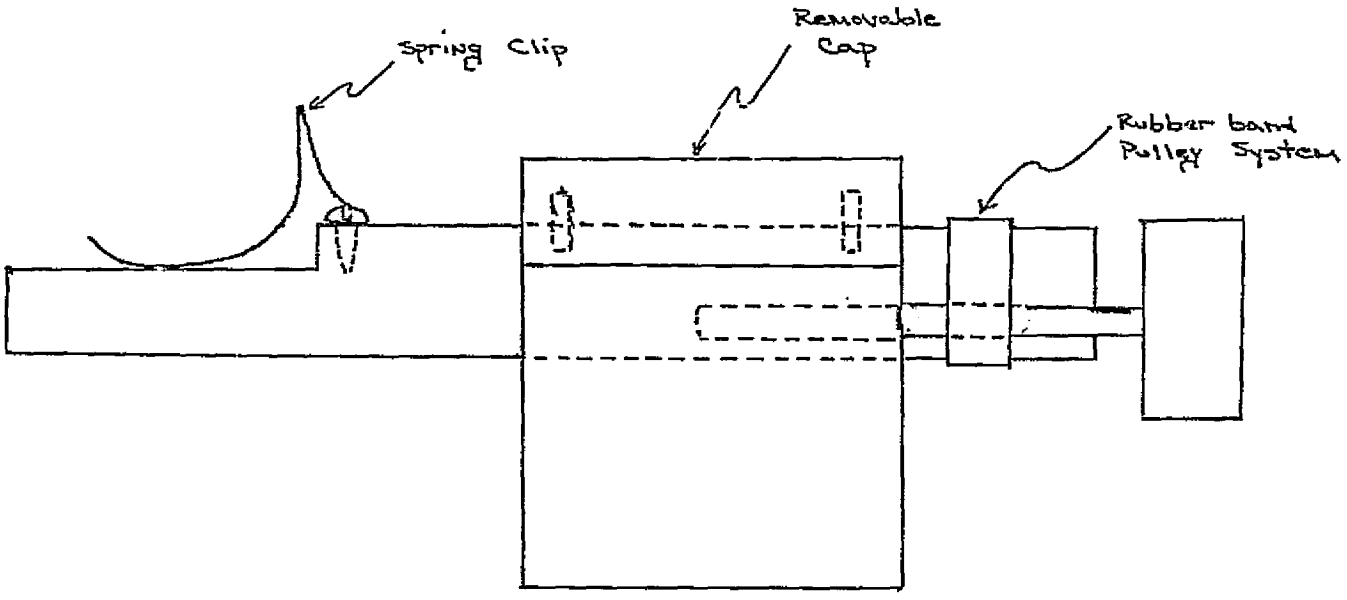

Side View

Scale: 2:1

Figure C-16. Rotating sample holder for metallurgical microscope.

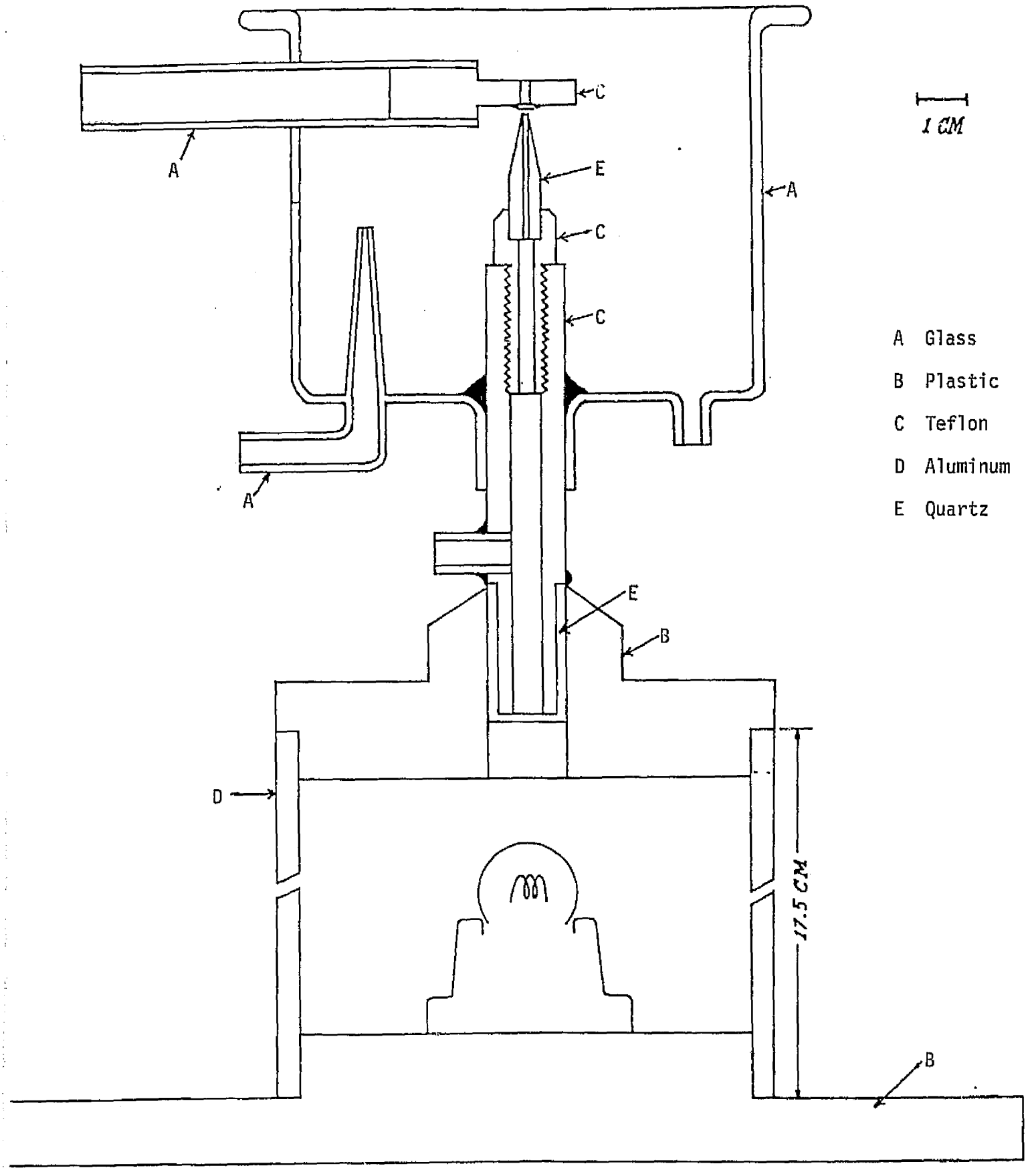

Figure C-17. Jet Etcher.

Appendix D.

Miscellaneous Tables.

Table D-1. OPERATING INSTRUCTIONS FOR WEB FURNACE

Prestart-up

1. Check generator off button on generator.
2. Check filament off button on generator.
3. Check main breaker on rear of generator.

Start-up

Load and assemble the furance. After this is complete, proceed as follows:

1. Check cooling water on furnace. Turn on both valves - one to furnace and other to generator.
2. Turn on argon flow to 50 cfh.
3. Turn on filament button on generator.
   Note: After the above three items have been accomplished, wait 15 minutes. This will allow the chamber to be purged with argon, and the vacuum tube filaments in the generator to warm up.
4. Check controller Auto-Manual switch. Put it in manual position and have temperature control on zero.
5. Turn on power button on the generator.
   Caution: Work coil is now HOT!
6. Adjust power to 5 kilovolts until susceptor glows (approximately a minute). Increase power to 6 kilovolts until out gassing stops (approximately 5 minutes). Increase to 8 kilovolts for 2 minutes to let the temperature stabilize. Then increase to 10.5 kilovolts until complete melting is obtained.
7. Decrease argon flow to 35 cfh.
8. Lower temperature to growth value. After the temperature has stabilized it is ready for web growth.

Furnace Shut Down

1. Flip the Auto-Manual switch to Manual.
2. Cut furnace temperature.
3. Turn the generator power button to off.
4. Wait 30 minutes for cool-down and proceed as follows.
5. Turn filament button off.
6. Turn off main breaker.
7. Turn off argon.
8. Turn off water valves.

Table D-2. TEMPERATURE DATA ACROSS THE SLOT IN LDBeWM2 HEAT SHIELDS AND THE TEMPERATURE DIFFERENCE BETWEEN THE SHIELD AND THE SURFACE OF THE MELT COMPARING NUMBER AND THICKNESS OF HEAT SHIELDS. THE SS SUSCEPTOR WAS USED AND THE Al_2O_3 PEDESTAL.

	Heat Shield		Temp. across slot in °C				Temp. Diff. (°C)
Run	Top[1]	Bottom[2]	CP[3]	LS[4]	M[4]	RS[4]	heat shield to melt
10-21-76[a]	2	1M	3.55	1401	1397		77
			3.05	1393	1390		142
			2.55	1397	1390		139
10-22-76[b]	2	1M	3.55	1385	1381		110
			3.05	1394	1388		200
			2.55	1389	1389		204
10-25-76[c]	2	1M	3.05	1393	1388		149
10-27-76[d]	2	1M	2.30	1385	1397		214
11-1-76	1	1M	4.05	1396	1389	1394	
			3.70	1401	1384	1396	
			3.55	1399	1389	1397	
11-5-76	1(1/4")	1M	3.55	1396	1396	1398	
			2.55	1396	1395	1398	111
12-20-76	1(1/4")	1A	2.47	1405	1399	1403	113
			.97	1409	1403	1407	233
			1.47	1411	1407	1412	211
			1.97	1405	1402	1404	200
11-8-76	1	1M	3.55	1395	1388	1386	106
			2.55	1403	1402	1399	139
			2.30	1408	1400	1409	161
11-9-76	1	1M	2.55	1395	1397	1392	134
			2.30	1386	1380	1389	94
			2.05	1398	1392	1397	81
11-24-76	1	1A	2.47				167
			.97				172
			.47				178
12-9-76	1	1A	1.47	1374	1373.5	1373	170
			.97	1397	1397	1397	
			.47	1397	1401	1400	197
12-22-76	2	1A	2.47	1406	1400	1398	178
			1.97	1401	1397	1399	150
			1.47	1404	1400	1399	239
			.97	1404	1399	1400	327
			.47	1402	1401	1400	339
12-27-76	1	1A	2.60	1407	1404	1403	106
			2.10	1407	1407	1403	82
			1.60	1399	1393	1393	150
			1.10	1404	1401	1401	290
			60				197

Notes:

1. 1 means only one shield was used.
   " in column refers to the thickness - if no thickness is given the shields were 60 mils thick.

Table D-2 (CONTINUED)

2 means 1 60 mil thick shield was placed above a 1/4" thick shield.

2. M - molybdenum shield; A - Al_2O_3 shield.
3. CP is the height of the top of the coil above the top of the susceptor.
4. LS - left side of slot,; M = middle; RS = right side.

a. 100 GM melt
b. 168 GM. melt
c. 165 GM melt
d. Remaining data for 150 GM melt.

Table D-3. MELT TEMPERATURE ACROSS SLOT IN THE HEAT SHIELD FOR A 50 GM SI MELT USING A STRAIGHT-TIPPED THERMOCOUPLE.

Position in Melt	Temperatures (°C) for Slot Positions[1]						
	1	2	3	4	5	6	7
0.4 cm below surface	1279	1271	1279	1254	1262	1271	1279
Repeat of above	1271	1287	1295	1271	1262	1274	1279
Near surface	1213						
At bottom	1321						

Note: Slot positions for shield LDBeWM2 (Figure 36).

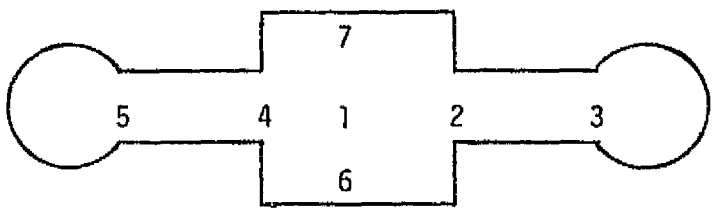

Table D-4. THERMAL PROFILE OF MOLTEN 100 GM CHARGE OF SI USING LDBeW2' HEAT SHIELD.

Distance Below Surface (cm)	Horizontal distance from center of crucible (cm)						
	-2.44	-1.65	-.64	0	+.64	+1.65	+2.44
.0				1227			
.32				1290			
.48	1338	1332	1325	1298	1298	1317	1365
.64				1397			
.79				1406			
.95				1410			
1.11(bottom)	1416	1416	1415	1414	1416	1418	1419

Notes: 1. Fig. 36.
2. Temperatures (°C).

Table D-5. SURFACE TEMPERATURES OF MELT ACROSS LDBeW2' HEAT SHIELD.

Position on Surface of Melt[2]									
1	2	3	4	5	6	7	8	9	10
1423[3]	1415	1415	1406	1415	1423	1440	1423	1423	1431

Notes: 1. Fig. 36.

2. As in sketch.

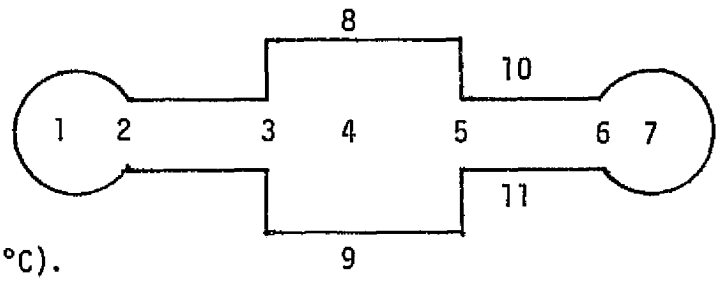

3. Temperatures (°C).

Table D-6. SELECTED WIDENING RATES

Run	Heat Shield	Susceptor	Thickness (mils)	Widening Rates (cm/m)
12-27-76	LDBeW	SS	40	23
12-28-76	LDBeW	SS	28	8
1-3-77	LDBeW 1/4	SS	44	11
	LDBeW 6	SS		
1-28-77	KDBeW	TS	35	16
			22	5
3-3-77	SDBN	TSP	25	.95
			14.8	1.10
			2.8	.50
			3.2	.30
			4.0	.61
3-4-77			7.4	.81
			10.5	.75
			26.5	1.04
3-13-77	LSDBN	TSP	15.2	.50
			14.0	1.43
			13.0	.57
3-16-77	SDBN	TSPO	11.8	1.4
			10.6	.77
			7.1	.69
3-17-77	SDBN+AH	TSP	4.9	.15
			2.3	.60
3-18-77			3.9	.76
3-21-77	LSDBN+AH	TSP	9.2	.54
			7.5	.80
			3.3	.54
			8.0	82
3-22-77			14.5	1.08
			12.6	1.35
			9.8	.96
			7.2	.76
3-23-77	LDBN+AH	TSP	9.3	1.02
			5.0	.40
			4.8	.20
3-27-77			15.0	1.83
			5.3	.61
			7.6	.26
3-30-77			22.	1.51
			5.5	.69
			5.5	.70
			7.1	.64

Note: The heat shield and susceptor designations are the same as those given in Table 1.

Table D-7. OPERATION PROCEDURES FOR THE JET ETCHER

PRECAUTION: Protective gloves should be worn during entire operation procedure.

1. Insure that drain reservoir is properly connected to the drain and charged with the necessary $CaCO_3$ + $CaCl_2$ + H_2O acid neutralizer.
2. Mount the sample to the holder with black wax. (Use toluene as solvent.)
3. Position the sample above the nozzle tip. The distance between the sample and the tip should be approximately 3 mm.
4. Place the top on the etcher. Assure that the sample can be observed from the viewing mirror.
5. Adjust the bottom of the etchant reservoir to a level approximately 5 cm above the nozzle tip.
6. Mix CP4 etchant. (To etch a 10 mil silicon sample, use 27 cc. HF + 123 c.c. HNO_3).
7. Turn on rinse jet water.
8. Turn on the etcher light.
9. Turn off the room light.
10. Pour etchant into the reservoir.
11. When a dim red light is observed in the viewing mirro, reposition the sample holder so that the sample is directly above the rinse jet.
12. Turn on the room light.
13. Decant the residual etchant from the reservior into a plastic beaker.
14. Disconnect the tubing from the reservoir to release the remaining etchant into the beaker.
15. Stop the rinse jet water.
16. Remove the sample holder and rinse it in water.
17. Disconnect tubing from the rinse jet.
18. Remove tubing from the drain reservoir.
19. Rinse the etcher with tap water.
20. Unscrew the nozzle tip holder from the nozzle body and rinse both parts thoroughly with water.
21. Remove the sample from the holder. (Dissolve wax in toluene.)
22. Rinse the sample in acetone.

Table D-8. PHYSICAL DATA ON SELECTED DENDRITE-WEBS

Web number	Length (cm)	Width (mm)	Thickness (mills)	Widening Rate (cm/m)	Resist. (sm)
1-28-77-A	2.2	7.0	27.8	3.6	
1-28-77-C	3.2	7.7	32.5	2.2	
2-3-77-A	1.1	4.8	29.2	.9	
2-3-77-F	2.1	5.4	23.0	5.7	
2-4-77-B	3.2	4.1	20.0	.94	
2-4-77-C	2.9	4.8	21.8	2.8	
2-4-77-D	1.7	6.8	11.0	.67	
2-11-77-A	4.4	4.6	11.3	.23	
2-15-77-K	49.5	11.0	20.7	1.01	24
3-4-77-D	48.5	8.9	8.7	.56	5
3-3-77-I	49.5	7.7	3.8	.30	
3-3-77-K	37.5	7.4	7.8	.61	
3-8-77-F	20.8	7.0	10.0	.55	
3-9-77-D	49.3	7.0	9.2	.83	
3-9-77-H	42.5	6.8	4.8	.45	3
3-13-77-J	28.5	6.1	3.4	1.02	
3-13-77-L	22	6.5	3.8	.93	
3-17-77-B	11.7	5.5	2.3	. 6	
3-21-77-G	22.0	6.4	9.7	.54	.9
3-14-77-E	40	6.8	6.4	.55	
3-17-77-G	65	8.4	9.0	.53	75
3-18-77-D	81.3	12.1	8.0	.88	1.5
3-21-77-A	23.7	7.4	7.5	.8	
3-18-77-H	14.	11.5	25.0	1.86	
3-21-77-C	81	8.5	4.0	.57	
3-21-77-E	43.2	6.4	4.0	.34	
3-21-77-H	35.3	5.5	4.0	.13	2.5
3-22-77-A	24.0	6.6	9.8	.96	
3-22-77-E	30.5	7.4	14.5	1.08	
3-22-77-H	63.5	9.0	7.2	.76	
3-23-77-C	10.0	6.6	6.0	.4	
3-25-77-B	39.0	8.4	5.8	.85	
3-26-77-F	69.5	9.1	10.5	.44	
3-27-77-H	31.2	7.0	8.3	.54	
3-28-77-H	60.3	8.4	7.0	.48	
3-29-77-B	13.7	6.8	12.5	1.06	
3-30-77-A	10.8	5.2	4.9	.69	
3-30-77-B	4.3	6.5	22.0	1.51	
3-30-77-C	22.5	6.4	8.2	.64	
3-30-77-E	37.5	7.1	4.5	.59	
3-31-77-B	17.5	6.2	5.0	.69	